FINAL REPORT

FRACTURE MECHANICS LIFE ANALYTICAL METHODS VERIFICATION TESTING

(VERIFICATION AND VALIDATION OF NASCRAC™)

NAS8-38103

Prepared For:

George C. Marshall Space Flight Center
National Aeronautics and Space Administration
Marshall Space Flight Center, Alabama 35812

Prepared By:

Nichols Research Corporation
Cornell University
Fracture Analysis Consultants

16 September 1994

Nichols Research Corporation
4040 S. Memorial Parkway
P.O. Box 400002
Huntsville, AL 35815-1502

EXECUTIVE SUMMARY

The objective of this project was to evaluate NASCRAC™ version 2.0, a second generation fracture analysis code, for verification and validity. This report represents the achievement of this objective. NASCRAC™ was evaluated for verification and validity using a combination of comparisons to the literature, closed-form solutions, numerical analyses, and tests. Several limitations and minor errors were detected. Additionally, a number of major flaws were discovered. These major flaws were generally due to application of a specific method or theory, not due to programming logic.

Verification in this project was defined as meeting one of two criteria: 1) agreement of NASCRAC™ with the equations and algorithms of the source specified by NASCRAC™, or 2) agreement within engineering accuracy between NASCRAC™ results and results from a lesser known source not necessarily employing the same method. An example of the first type of verification is a comparison of NASCRAC™ and NASA/FLAGRO source codes for a solution that NASCRAC™ adapted from FLAGRO. An example of the second type of verification is agreement between NASCRAC™ results and results computed by FRANC2D, a fracture and fatigue numerical analysis program.

Validation was also defined using one of two criteria: 1) agreement within engineering accuracy between NASCRAC™ results and results from a well-known source, or 2) favorable comparison between NASCRAC™ results and results from the tests completed for this project. The first validation criterion referenced such sources as *The Stress Analysis of Cracks Handbook* by Tada, Paris, and Irwin or *ASTM E399*.

Eleven different capabilities were identified in NASCRAC™. Although certain capabilities depended on other capabilities (e.g., fatigue crack growth depended on K solutions), the independent features of each capability were evaluated separately for verification and validity. Section 4 details the verification and validation results; however, the following list provides succinct general conclusions about the validity of each capability:

- *K vs a*: majority of solutions valid. NASCRAC™ performs RMS averaging of K's for multi-dimensional cracks. This approach leads to errors in surface crack (quarter-elliptical, semi-elliptical) calculations when high stress gradients are present.

- *J vs a*: generally valid; limited number of configurations encoded.

- *Crack opening area*: generally valid; limited number of configurations encoded.

- *Life calculation due to fatigue crack growth*: modified Forman and Hopkins-Rau equations not valid. Paris equation valid; Walker and Collipriest equations verified.

- *Tolerable crack size*: valid and verified to the extent that fatigue crack growth is valid and verified. Sensitive to inputs (number of cycles per block, threshold value of ΔK).

- *Proof test logic*: not valid. Observed failure loads were significantly higher than those predicted by NASCRAC™. This difference in failure loads resulted in discrepancies between NASCRAC™'s remaining life predictions and observed life.

- *Tearing instability*: Implemented algorithm is not equivalent to the algorithm discussed in the NASCRAC™ Users Manual. Two-dimensional configurations validated analytically. Proved analytically that none of the three-dimensional configurations available in NASCRAC™ will exhibit stable tearing.

- *Creep crack growth*: In general, the C* model implemented in NASCRAC™ does not correlate with creep crack growth rates in aluminum. Experimentally-observed and NASCRAC™-predicted creep crack growth rates in 304 stainless steel fell within the range reported in the literature. Since this range was broad, the evaluation of NASCRAC™'s creep crack growth validity was inconclusive.

- *Crack transitioning*: Invalid because the transitioning factor f_t does not capture the load cycles required to transition a crack from one configuration (e.g., a surface crack) to another configuration (e.g., a corner crack). Although this capability was invalid in comparison to test results, the NASCRAC™ results were conservative, i.e., NASCRAC™ predicts failure at a fewer number of cycles compared to test observations.

- *Crack retardation due to due to overloads*: The implementations of the Wheeler and Willenborg retardation models in NASCRAC™ were verified. However, these models are very simplistic and do a poor job of capturing the physics of crack retardation; therefore, in general, the models can only be considered marginally valid compared to tests. These models should only be used for quick and easy first order estimations of crack retardation.

- *Elastic-plastic stress redistribution*: The sensitivity of this NASCRAC™ capability to material property values renders this feature impractical for engineering analyses.

Exceptions accompany each of the above general conclusions from the verification and validity evaluations; however, these conclusions are intended to provide NASA/MSFC management with the following generalization about NASCRAC™: *the code is an acceptable fracture tool for K solutions of simplified geometries, for a limited number of J and crack opening area solutions, and for fatigue crack propagation with the Paris equation and constant amplitude loads when the Paris equation is applicable.*

The successful completion of the evaluation of NASCRAC™ for verification and validity provides NASA with two benefits beyond the scope of the funded effort. These added benefits are:

- a large database of experimental results in fatigue, tearing, and creep fracture which can serve as a validation base for other NASA projects and for future software simulators. Much of this data was obtained on structural configurations which are not typical of the simple geometries often used in laboratory experiments.

- a refined verification and validation methodology which can be applied to future fracture simulators.

These added benefits are now available to the NASA Fracture Control Board to evaluate current and future fracture mechanics tools for verification and validity.

TABLE OF CONTENTS

TABLE OF CONTENTS (CONTINUED)

SECTION **PAGE**

TABLE OF CONTENTS (CONTINUED)

TABLE OF CONTENTS (CONTINUED)

TABLE OF CONTENTS

TABLE OF CONTENTS

TABLE OF CONTENTS (CONCLUDED)

LIST OF FIGURES

LIST OF FIGURES (CONTINUED)

LIST OF FIGURES (CONTINUED)

LIST OF FIGURES (CONTINUED)

LIST OF FIGURES (CONTINUED)

LIST OF FIGURES (CONTINUED)

LIST OF FIGURES (CONTINUED)

LIST OF FIGURES (CONTINUED)

LIST OF FIGURES (CONTINUED)

LIST OF TABLES

LIST OF TABLES (CONTINUED)

LIST OF TABLES (CONTINUED)

LIST OF TABLES (CONTINUED)

LIST OF TABLES (CONTINUED)

LIST OF SYMBOLS

ai	crack length (2D or elliptical crack)
A	crack surface area
b1	Test geometry parameters, depth or width
b2	Test geometry parameters, thickness
b3	Test geometry parameters, moment arm or diameter
B	NASCRAC™ geometric parameter (thickness), (other)
B	Creep Strain Rate Coefficient
c	NASCRAC™ geometric parameter (r + B, #208)
C	Paris Law Coefficient, Modified Forman Coefficient
C_1	Coefficient for J resistance equation
Cp	Wheeler Retardation Parameter
C0	Modified Forman Coefficient
C3	Creep Crack Growth Rate Equation Coefficient
C*	Creep J-integral
C(t)	Riedel Creep Parameter
CT	Saxena Creep Parameter
d	Modified Forman exponent
d	NASCRAC™ geometric parameter (2r, #208)
D	Ramberg-Osgood Coefficient
D	NASCRAC™ geometric parameter (diameter)
E	Young's Modulus
E'	E plane stress or $E / (1-\nu^2)$ plane strain
f	
G	Energy release rate
h	NASCRAC™ geometric parameter (thickness #301)
h1,2,3,4	Influence function for DOF 1, 2, 3 or 4
i	typical index
J	J-integral
J_e	Linear elastic value of J
J_p	fully plastic value of J
j	typical index

LIST OF SYMBOLS

K_{max}	maximum applied K during a load cycle to a point on the crack front
K_{min}	minimum applied K during a load cycle to a point on the crack front
ΔK	$K_{max} = K_{min}$
ΔK_{th}	threshold value of ΔK below which da / dn = 0
$K_{I, II, III}$	Stress Intensity Factor, corresponding to mode I, II or III
$\bar{K}$ (1, 2, 3)	RMS Stress Intensity Factor, corresponding to DOF 1, 2 or 3
Kc	Critical Stress Intensity Factor
KIc	Kmax required to overcome plastic zone created
$K_{max, req}$	by overload (Willenborg)
k	typical index
li	NASCRAC™ geometric parameter
L	Paris law exponent, Modified Forman exponent
m	Creep Crack Growth rate equation exponent
m_{creep}	Ramberg-Osgood exponent, Modified Forman exponent
n	shaping parameter (Wheeler model)
n	fatigue cycles
n	Creep strain rate exponent
n_{creep}	
o	Modified Forman exponent
p	exponent for J resistance equation
p	NASCRAC™ pin load
p	Modified Forman exponent
q	Extent of yield zone (Wheeler model)
rp	NASCRAC™ geometric parameter (#302)
R	ratio of K_{min} to K_{max} in a fatigue cycle
R	effective R ratio for Willenborg retardation model
R_{eff}	NASCRAC™ geometric parameter (radius)
r	crack front
s	NASCRAC™ geometric parameter (thickness)
t	

t	time
u	displacement in x direction
v	displacement in y direction
w	displacement in z direction
W	NASCRAC™ geometric parameter
W_1	NASCRAC™ geometric parameter
W_2	NASCRAC™ geometric parameter
W_3	NASCRAC™ geometric parameter
W_4	NASCRAC™ geometric parameter
x	coordinate axis
x	NASCRAC™ geometric parameter (#502, 605, 702)
x_c	NASCRAC™ geometric parameter
y	coordinate axis
y_c	NASCRAC™ geometric parameter (#502, 605, 702)
z	coordinate axis
α	NASCRAC™ geometric parameter (a/W), (a/D, #404) (a1/W, #702)
β	NASCRAC™ geometric parameter (2a1/ (a2+a3) #702)
ε	strain
$\dot{\epsilon}$	strain rate
ϕ	NASCRAC™ geometric parameter (angle #502)
γ	NASCRAC™ geometric parameter (r/W), (r/r+t #403)
λ	NASCRAC™ geometric parameter (a / $\sqrt{}$rh, #301)
μ	NASCRAC™ geometric parameter (1-a / r, #402)
ν	poisson's ratio
σ	stress
σ_b	extreme fiber bending stress
σ_t	uniform stress
σ_e	Von Mise's effective stress
ν_1	Retardation
ν_2	Retardation
ς	NASCRAC™ geometric parameter (x / W)

1.0 INTRODUCTION

NASCRAC™ (NASA Crack Analysis Code - Version 2.0) is a second generation fracture analysis code developed for NASA/Marshall Space Flight Center (MSFC). The code uses a weight function approach to solve traditional fracture problems such as stress intensity factors and life calculation due to fatigue. NASCRAC™ also contains capabilities for advanced fracture analysis, e.g., crack retardation, life calculation due to creep, and elastic-plastic stress redistribution near the crack tip. Since NASCRAC™ includes the computationally efficient weight function approach and a broad spectrum of advanced capabilities, NASA/MSFC expects to employ NASCRAC™ as an integral component of the NASA Fracture Control Program for validating flight hardware. This critical role of NASCRAC™ in future NASA analyses dictates both a complete and objective independent verification and validation (V/V) of the code to ascertain the restrictions and ranges of applicability for each NASCRAC™ solution and capability. Nichols Research Corporation (NRC) and its subcontractor, Cornell University, and consultant, Fracture Analysis Consultants (FAC), were contracted by NASA/MSFC to perform such a V/V. This report presents the results of the NASCRAC™ verification and validation.

The V/V effort focused on verification and validation of solutions embedded in NASCRAC™. No attempts were made to correct solutions or to develop new solutions. In the case of minor programming errors, corrected versions were run offline to determine the extent of the problem.

The V/V process was based on categorization of the NASCRAC™ solutions and capabilities into three groups: *basic information (BI), synthesized results (SR), and advanced capabilities (AC).* The BI group consisted of *K vs a*, *J vs a*, and *crack opening area (COA) vs a.* The SR group included *life calculation by fatigue crack growth, tolerable crack size, proof test logic, tearing instability*, and *life calculation by creep crack growth.* The AC group included crack transitioning, retardation due to overloads, and elastic plastic stress redistribution. Section 2 of this report provides a succinct description of the theory behind NASCRAC™. Section 3 focuses on the V/V methods and decision process used to verify and validate NASCRAC™. Results and solution specific discussion are presented in Section 4. Conclusions and recommendations are provided in Section 5. Finally, Appendix A contains a listing of recommended ranges for the K solutions. References are included at the end of each section.

2.0 TECHNICAL BACKGROUND

NASCRAC™ is a fracture analysis code capable of performing linear elastic and elastic-plastic fracture analyses. NASCRAC™ is restricted to mode I, or opening mode, fracture. Capabilities incorporated into NASCRAC™ include computation of *K vs a, J vs a, COA vs a, fatigue crack growth, tolerable crack size, creep crack growth, proof test logic, tearing instability*, and *localized elastic-plastic stress redistribution.* NASCRAC™ can accept cyclical, steady-state, and random load spectrum definitions. Eleven material libraries are available: two miscellaneous steel libraries, stainless steel, AL-2024, AL-6061, AL- 7075, two miscellaneous aluminum libraries, cast aluminum, inconel, and titanium. Users may also define a material interactively or create a material library. Currently twenty-eight crack configurations are incorporated in the code. Crack retardation is possible using either the Wheeler or Willenborg models.

K solutions in NASCRAC™ are computed using encoded closed form solutions for uniform tensile loads and weight function formulations for arbitrary loads. Robust integration routines incorporating Gaussian integration and a broad library of weight functions provide an extensive computational capability for calculating K solutions of various loadings and geometries. In the weight function approach, a K solution of a specific geometry can be calculated for an arbitrary loading by integrating a point load solution over the crack face. This approach can be expressed as:

$$K = \int_0^a \sigma(x)\, h(x,a)\, dx \qquad \text{eq. 2.0-1}$$

where a = crack length
$\sigma(x)$ = crack plane stress derived from the uncracked geometry
h(x,a) = weight function from a known solution

Weight functions can be determined from simple load cases and applied to unique, complex load cases. Figures 2.0-1 and 2.0-2 illustrate the weight function approach to fracture analysis. As shown in Figure 2.0-1, K solutions can be obtained for an arbitrary loading by employing superposition to reduce the arbitrary loading to two simpler loadings: a cracked geometry with external tractions (the problem of interest) and an identical cracked geometry with tractions only along the crack face. Since these two loadings are reduced from an uncracked problem, their K solutions sum to zero, i.e., $K_d = -K_e$.

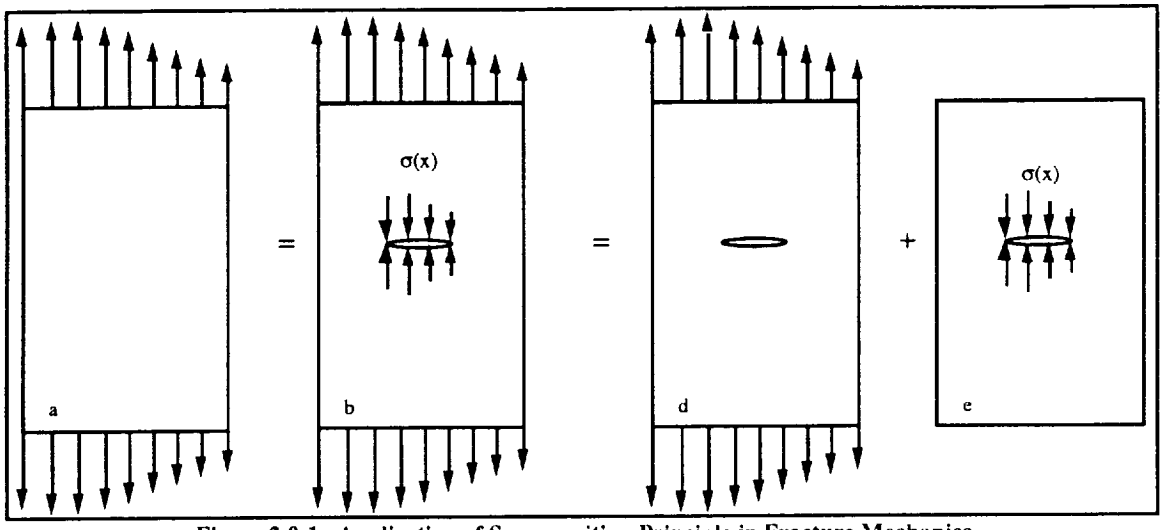

Figure 2.0-1. Application of Superposition Principle in Fracture Mechanics

As depicted in Figure 2.0-2, $-K_e$ can be calculated from a weight function formulation. The weight function solution is calculated by integrating the product of the crack face stress distribution $\sigma(x)$ and the weight function $h(x,a)$ along the crack face.

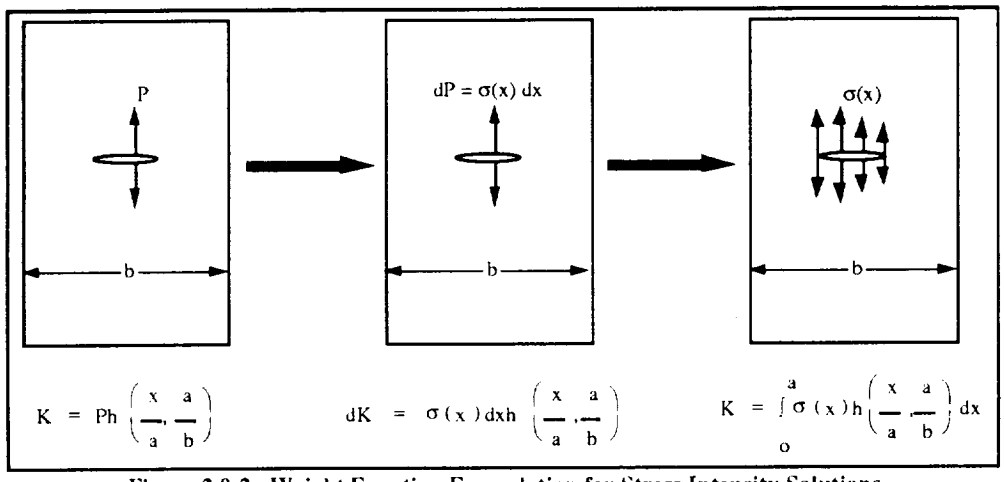

Figure 2.0-2. Weight Function Formulation for Stress Intensity Solutions

J-integral solutions in NASCRAC™ are computed by assuming J to be a summation of elastic and fully plastic components:

$$J = J_e + J_p \qquad \text{eq. 2.0-2}$$

where J is the total J integral, J_e is the elastic component of the J integral, and J_p is the plastic component of the J integral.

The elastic component is computed by using an effective crack length with a standard K solution and the plastic component is computed from a limit load concept using a calibration factor obtained from handbook solutions. A Ramberg-Osgood constitutive relationship is used to

define plasticity. J_p values generally require interpolation because the handbook solutions are limited in range. The general equation for J_p is given as:

$$J_p = \alpha \sigma_y \varepsilon_y c \frac{a}{b} h_1 (\frac{P}{P_0})^{n+1} \qquad \text{eq. 2.0-3}$$

In this equation α is a material property; σ_y and ε_y are the yield stress and strain of the material; a, b, and c are geometric dimensions with a being the crack length; P and P_0 are the applied load and limit load of the structure, h_1 is a correction factor related to geometry and strain hardening of the material, and n is the strain hardening exponent from the Ramberg-Osgood model.

In NASCRAC™, five configurations have an option for calculating crack opening area. For each configuration, the crack opening area is calculated according to closed form solutions found in references.

Seven of NASCRAC™'s configurations include a variable thickness option for calculating a K solution and life due to fatigue crack growth. The option is a discrete variable thickness with the thickness being defined at specified points along the crack plane. During calculation of K, the stress is distributed along the crack in proportion to the thickness at the discrete points.

Three types of load spectrums can be input into NASCRAC™: cyclic, steady-state, and random. For the cyclic spectrum, load transients are defined with a specified number of cycles. Transients are arranged into blocks to form the spectrum. To define a load, the user must input two of the following five variables: maximum stress, minimum stress, stress range, stress mean, and R ratio.

NASCRAC™ provides five coded equations for fatigue crack growth and tolerable crack size analysis: Paris, Walker, modified Forman, Collipriest, and Hopkins-Rau. The NASCRAC™ material libraries include crack growth constants for the modified Forman equation only. The user is required to input material properties values when using one of the other growth equations. Using the da/dN computed from the selected equation, cracks are grown by one of three integration schemes: cycle-by-cycle, transient-by-transient, or piecewise-linear.

NASCRAC™'s tearing instability capability provides the analyst with an automated means of determining the stress level at which a crack in a plane stress specimen will grow catastrophically to failure. Prior to this critical stress level, tearing of the specimen will occur in a stable manner and will be arrested due to the increased tearing resistance of the material caused by plasticity at the crack tip.

In the NASCRAC™ theory manual, the criteria for tearing instability are given as:

$$K_{applied} > K_R \textit{ and } \quad dK_{applied}/da > dK_R/da \qquad \text{eq. 2.0-4, eq. 2.0-5}$$

where $K_{applied}$ is the stress intensity factor due to the applied stress; K_R is the crack growth resistance K corresponding to the initial load and crack length; $dK_{applied}/da$ is the slope of the $K_{applied}$ curve (where the $K_{applied}$ curve is linear from (0, 0) to (a, $K_{applied}$)); and dK_R/da is the slope of the crack growth resistance curve at K_R. The tearing instability option in NASCRAC requires input of a crack growth resistance curve (K-R curve) in tabular format or as a power law function ($K_R = C_1 (\Delta a)^p$).

Figure 2.0-3 illustrates a typical tearing resistance analysis. The K_R-Δa curve is superimposed on the graph such that Δa = zero coincides with the initial crack length, a_o. Four $K_{applied}$-a curves corresponding to increasing loads P_1 through P_4 are shown. For initial crack size, a_o, the load P_1 does not result in $K > K_{Ic}$. Therefore, no crack propagation occurs. Crack propagation begins at load P_2, when $K_{applied} = K_{Ic}$. At load P_3, the crack has propagated a length Δa_3. After this propagation increment $K_{applied} = K_R$. The result is a stable crack of length, $a_o + \Delta a_3$. At load P_4, the tangents of the $K_{applied}$-a and the K_R-Δa curves are equal. Therefore, crack propagation is unstable.

Proof test logic in NASCRAC™ is a two-step analysis. First, NASCRAC™ predicts the largest crack which will survive a given proof test. This prediction is done iteratively. This predicted crack is then used as an initial crack length for a life calculation due to fatigue crack growth under a typical service load spectrum.

NASCRAC™ calculates life due to creep crack growth using the C* crack growth model. In the C* model stress, strain, and strain rate are described in a relationship

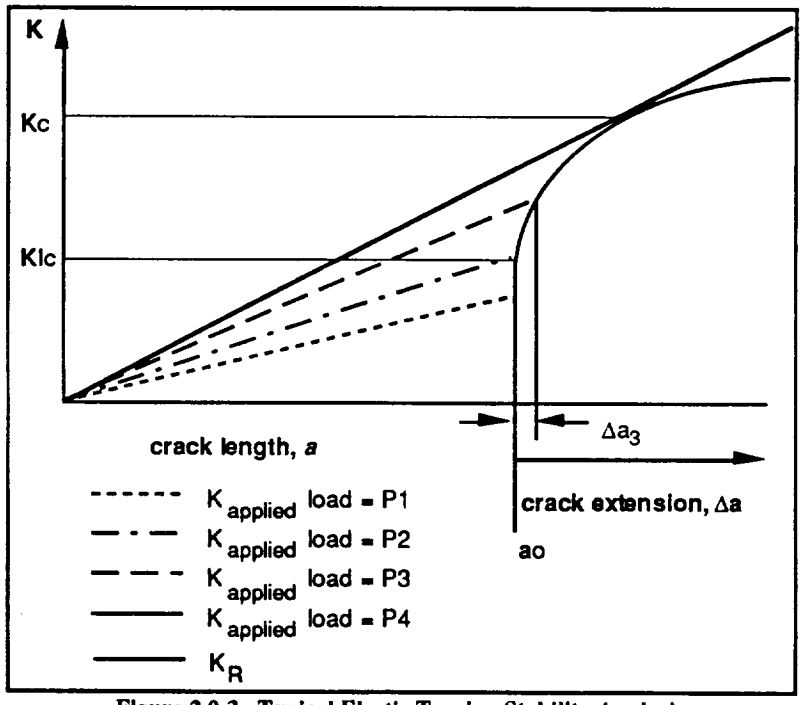

Figure 2.0-3. Typical Elastic Tearing Stability Analysis

similar to the Ramberg-Osgood stress-strain model. The stress tensor is a function of C*. C* is a path independent integral defined by the following equation,

$$C^* = \int_r \dot{W}_\varepsilon dx_2 - \sigma_{ij} n_i \frac{\dot{u}_j}{x_1} ds \qquad \text{eq. 2.0-6}$$

where

$$\dot{W}_\varepsilon = \int_o^{\dot{\varepsilon}_{ij}} \sigma_{ij} \, d\dot{\varepsilon}_{ij}$$

The equation for C* is analogous to the plastic term in the J-integral, with strain rate replacing strain. Given C*, NASCRAC™ predicts creep crack growth rate based on the following relationship,

$$\frac{da}{dt} = C_3 (C^*)^{n_{creep}} \qquad \text{eq. 2.0-7}$$

At the onset of loading, the creep strains will be zero and crack growth will be dependent on the stress intensity factor K and the K field. However, long term, the creep strains will be much larger than the elastic strains, and the C* field will dominate. This long term effect, defined as steady state creep crack growth, is the creep crack growth calculated in NASCRAC™. Loading for this capability is restricted to uniform tension.

3.0 VERIFICATION AND VALIDATION METHODOLOGY

The NASCRAC™ verification and validation plan was a comparative approach using three different types of reference solutions: 1) documented solutions from the literature, including closed form and graphical solutions, 2) finite element and boundary element solutions, and 3) testing. NASCRAC™ solutions were categorized into three areas: *Basic Information (BI), Synthesized Results (SR), and Advanced Capabilities (AC).* The *BI* category consisted of *K vs a, J vs a,* and *crack opening area (COA) vs a.* The *SR* category included *life calculations due to fatigue and creep, tolerable crack size, proof test logic,* and *tearing instability.* The *AC* category included *elastic-plastic stress redistribution, crack transitioning,* and *crack retardation due to overloads.*

NASCRAC™ contains 422 solutions and capabilities. This quantity was calculated by summing the number of crack topologies available for each NASCRAC™ capability. Variations in loading conditions were not included in the tabulation. Each NASCRAC™ group, i.e., *BI*, *SR*, and *AC*, required a different V/V approach. *BI* solutions are dependent on analytical, numerical, and experimental results external to NASCRAC™ plus the weight function feature of NASCRAC™. Solutions in the *SR* category use a number of programmed theoretical or empirical crack growth rate and stability models (e.g., Paris's equation) plus data calculated or interpolated from *BI* results to synthesize or compute results. An accurate *SR* depends on the accuracy of the *BI* and also on the proper choice of a theoretical or empirical model for the physical problem. Thus, verification of *BI* solutions were accomplished with literature and numerical analyses whereas verification of an *SR* solution required verifying the *BI* and determining the applicability of the chosen empirical or theoretical model using experimental and numerical techniques. *AC* solutions (overloads, elastic-plastic stress redistribution, crack transitioning) required *BI* results and advanced theoretical formulations. Accurate *AC* solutions are strongly dependent on understanding the range for which the formulation is applicable.

Verification in this project was defined as meeting one of two criteria: 1) agreement of NASCRAC™ with the equations and algorithms of the source specified by NASCRAC™; or 2) agreement within engineering accuracy between NASCRAC™ results and results from a lesser known source not necessarily employing the same method. An example of the first type of verification is a comparison of NASCRAC™ and NASA/FLAGRO source codes for a solution that NASCRAC™ adapted from FLAGRO. An example of the second type of verification is agreement between NASCRAC™ results and results computed by FRANC2D, a fracture and fatigue numerical analysis program.

Validation for this project was also defined using one of two criteria: 1) agreement within engineering accuracy between NASCRAC™ results and results from a well-known source; or 2) favorable comparison between NASCRAC™ results and results from the tests completed for this project. The first validation criterion referenced such sources as *The Stress Analysis of Cracks Handbook* by Tada, Paris, and Irwin or *ASTM E399.*

A sequence of comparisons was set up to evaluate validity. In the first step, NASCRAC™ and a literature source or closed form solution were compared. If reasonable agreement was found, the solution or capability was consider valid. If reasonable agreement was not found, a second solution from the literature was compared. Agreement between the original literature source and the second source indicated an error in NASCRAC™. Agreement between NASCRAC™ and the second source suggested a problem with the literature source. If this second comparison was not conclusive or not available, testing was performed. Results from testing were considered to be ground zero results within experimental variation. If NASCRAC™ results did not fall within the statistical variation of the experiment, the NASCRAC™ solution was determined to be invalid.

Independent integration external to NASCRAC™ was used to check the NASCRAC™ integration routines. The external routines were based on a Romberg integration algorithm which differed from the Gaussian quadrature algorithms in NASCRAC™.

The accuracy of NASCRAC™'s ability to estimate K solutions for variable thickness planar bodies using weight function solutions was determined by comparing NASCRAC™ results with finite element results. The finite element models included up to third order polynomial variation in global thickness.

Several references were used extensively for the V/V process. For *K vs a* solutions and uniform or bending loads, [1] and [2] provided graphical, curve fit, and closed form solutions. [2] also contained closed form point load solutions for certain NASCRAC™ configurations. These point load solutions were integrated numerically to verify the NASCRAC™ weight function solutions. [3] was also a primary reference for weight function solution V/V. For several of the non-through crack *K vs a* solutions, [4] was a critical resource.

[5] and [6] were the primary V/V sources for NASCRAC™'s seven *J vs a* configurations. These two references listed the coefficient tables coded into NASCRAC™ in addition to the coded equations.

Three different NASCRAC™ solution groups were verified by direct comparison of coded equations with literature sources. In the 100 series configurations (ASTM standard fracture toughness specimens), the coded equations were compared to [7]. For the J-integral capabilities, the coded limit load (P_0) equations were compared to [5]. Finally, for the five *COA vs a* configurations, the coded equations were compared to equations listed in references [2] and [3].

FRANC, a fracture specific finite element and boundary element tool described in [8] and [9], was employed in the *K vs a* V/V efforts. This workstation based code allows an analyst to compute stress intensity factors for arbitrary cracks in arbitrary bodies. Menu-driven post-processing routines provide both numerical and graphical results.

3.1 REFERENCES FOR SECTION 3.0

1. Rooke, D.P., and Cartwright, D.J., Compendium of Stress Intensity Factors, Her Majesty's Stationery Office, London, 1976.
2. Tada, H., Paris, P.C., and Irwin, G.R., The Stress Analysis of Cracks Handbook, 2nd ed, Paris Productions, St. Louis, Paris Productions, 1985.
3. Wu, X.R. and Carlsson, A.J., Weight Functions and Stress Intensity Factor Solutions, Pergamon Press, New York, 1991.
4. Newman, J.C., and Raju, I.S., "Stress Intensity Factor Equations for Cracks in Three-Dimensional Finite Bodies," in Fracture Mechanics 14th Symposium Volume I: Theory and Analysis ASTM STP 791, Philadelphia, American Society for Testing and Materials, 1983, pp. I-238 - I-265.
5. Kumar, V., German, M.D., and Shih, C.F., An Engineering Approach for Elastic-Plastic Fracture Analysis, NP-1931, Research Project 1237-1, prepared by General Electric Company for Electric Power Research Institute, July, 1981.
6. Kumar, V., et al, Advances in Elastic-Plastic Fracture Analysis, NP-3607, Research Project 1237-1, Final Report, prepared by General Electric Company for Electric Power Research Institute, July, 1984.
7. "E 399 (Standard Test Method of Plane-Strain Fracture Toughness of Metallic Materials" in 1992 Annual Book of ASTM Standards, American Society for Testing and Materials, Philadelphia, 1992, pp 506-536.
8. Wawrzynek, P. FRacture ANalysis Code (FRANC) Primer for Version 2.5, Cornell University, Ithaca, NY, 1991.
9. Wawrzynek, P. FRacture ANalysis Code (FRANC) Version 2.3+ Release Notes, Cornell University, Ithaca, NY, 1990.

4.0 RESULTS AND DISCUSSION

The techniques described in the previous section were used to verify and validate NASCRAC™. Results ranged from identical and acceptable solutions versus references to coding errors, documentation errors, and unacceptable solutions. This section presents the V/V results of each NASCRAC™ solution and capability.

4.1 *K vs a* CALCULATION: UNIFORM THICKNESS

The uniformly thick K solutions in NASCRAC™ form the foundation of the code. There are twenty-eight uniformly thick K solutions. These solutions permit static checks of K versus K_{Ic} and also drive the fatigue crack growth, tolerable crack size, tearing instability, and proof test logic capabilities.

4.1.1 100 SERIES RESULTS

The 100 series K solutions in NASCRAC™ simulate the four standard test specimens specified by ASTM E399 [1]. These solutions were verified and validated using two comparisons: a comparison of the coded mathematical expression versus the equations listed in ASTM E399-90 and a comparison of NASCRAC™ results versus results calculated from the ASTM E399-90 equations. Results from these comparisons prove the general validity of the coded NASCRAC™ solutions. Specific exceptions to this conclusion are discussed in the following subsections.

4.1.1.1 Configuration 101 (Compact Tension Specimen)

The geometry for configuration 101, the ASTM E399 *compact tension specimen*, is shown in Figure 4.1.1.1-1. A subset of comparative results is presented in Table 4.1.1.1-1. Although the results shown in the table appear acceptable, the comparison of the NASCRAC™ code with the ASTM E399 equation revealed a minor coding error. The error, shown in Figure 4.1.1.1-2, is a typographical error in the first coefficient of the FAOW equation. The coefficient should be 0.886 but the NASCRAC™ value is 0.866.

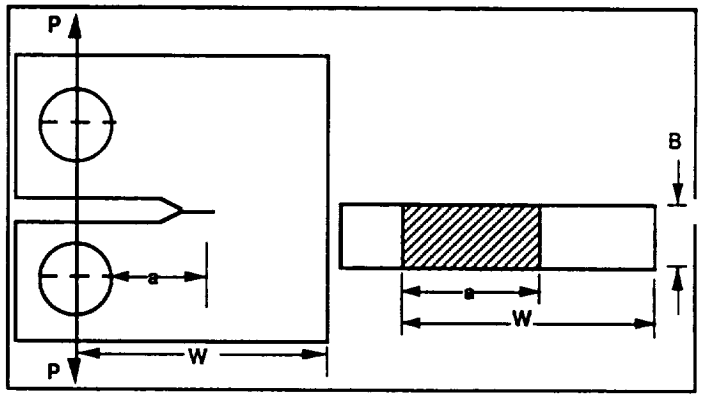

Figure 4.1.1.1-1. Geometry for Configuration 101, *Compact Tension Specimen*

Table 4.1.1.1-1 Representative Results for Configuration 101

W	B	a	P	K -- ASTM	K - NASCRAC™
5.0"	1.0"	1.0"	1,000 lb	1,883 psi - $in^{1/2}$	1,884 psi - $in^{1/2}$
10.0"	5.0"	5.0"	1,000 lb	602 psi - $in^{1/2}$	602 psi - $in^{1/2}$
10.0"	3.3"	5.0"	1,000 lb	903 psi - $in^{1/2}$	903 psi - $in^{1/2}$
10.0"	2.5"	5.0"	1,000 lb	1,204 psi - $in^{1/2}$	1,204 psi - $in^{1/2}$
10.0"	2.5"	1.0"	1,000 lb	754 psi - $in^{1/2}$	754 psi - $in^{1/2}$
10.0"	2.5"	2.0"	1,000 lb	1,284 psi - $in^{1/2}$	1,284 psi - $in^{1/2}$

```
      SUBROUTINE K100
C-----------------------------------------------------------------------C
C-----------------------------------------------------------------------C
      AOW=ANOW(1)/WIDTHS(1)
      SIGZ=EQPARS(ITRANS,IDEF,1)
C
      GOTO (101,102,103,104) (KRKTYP-100)
C
C    COMPACT TENSION SPECIMEN , KRKTYP=101
C
 101  FAOW=0.866 +AOW*(4.64 +AOW*(-13.32 +AOW*(14.72 +AOW*(-5.6))))
      FAOW=FAOW*(2.+AOW)/((1.-AOW)**1.5)
      XK(IDEF,1)=FAOW*SIGZ / (WIDTHS(2) * SQRT(WIDTHS(1)))
```

Figure 4.1.1.1-2. Coefficient Error for Configuration 101

ASTM E399 limits the validity of this solution to $2 \leq W/B \leq 4$. This limitation needs to be documented clearly on screen and in the user's manual.

4.1.1.2 Configuration 102 (Disk Shaped Compact Type Specimen)

Figure 4.1.1.2-1 displays the geometry of configuration 102, the ASTM E399 *disk-shaped compact type specimen* . The K solution coded in NASCRAC™ compared identically to the equation listed in ASTM E399. Additionally, for three different thicknesses, NASCRAC™ results were identical to analytical results computed using the E399 equation. These comparative results are listed in Table 4.1.1.2-1. This NASCRAC™ solution is valid based on the consistency in these two sets of comparisons. ASTM E399 limits the validity of this solution to $2 \leq W/B \leq 4$. This limitation needs to be documented clearly on screen and in the user's manual.

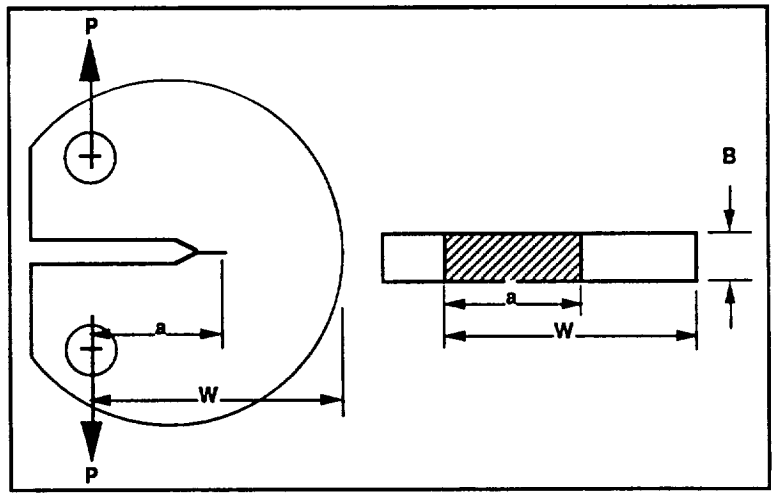

Figure 4.1.1.2-1. Geometry for Configuration 102, *Disk Shaped Compact Type Specimen*

Table 4.1.1.2-1. Representative Results for Configuration 102

SAMPLE WIDTH	SAMPLE THICKNESS	CRACK LENGTH	LOAD	ASTM RESULT	NASCRAC™ RESULT
5.0"	2.0"	1.0"	1000 lb_f	922 psi - $in^{1/2}$	922 psi - $in^{1/2}$
5.0"	1.25"	1.0"	1000 lb_f	1476 psi - $in^{1/2}$	1476 psi - $in^{1/2}$
5.0"	1.0"	1.0"	1000 lb_f	1845 psi - $in^{1/2}$	1845 psi - $in^{1/2}$

4.1.1.3 Configuration 103 (Arc Shaped Specimen)

Figure 4.1.1.3-1 displays the geometry for configuration 103, the ASTM E399 *arc shaped specimen* . Comparative results computed by parameterizing specimen thickness are listed in Table 4.1.1.3-1. These results plus agreement between the NASCRAC™ coded equations and the ASTM E399 equation validate this model. The comment of dimension limits discussed for configurations 101 and 102 is also applicable to this configuration: ASTM E399 limits the validity of this solution to $2 \leq W/B \leq 4$. This limitation needs to be documented clearly on screen and in the user's manual.

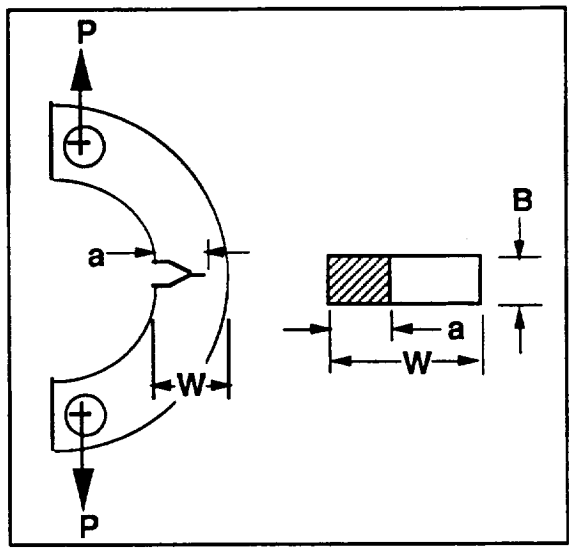

Figure 4.1.1.3-1. Geometry for Configuration 103, *Arc Shaped Specimen*

Table 4.1.1.3-1. Representative Results for Configuration 103

SAMPLE WIDTH	CURVATURE DESCRIPTION	SAMPLE THICKNESS	LOAD OFFSET	CRACK LENGTH	LOAD	ASTM RESULT	NASCRAC™ RESULT
3.0"	3.0"	1.5"	2.5"	1.0"	1,000 lb	3,656 psi - $in^{1/2}$	3,656 psi - $in^{1/2}$
3.0"	3.0"	1.0"	2.5"	1.0"	1,000 lb	5,484 psi - $in^{1/2}$	5,484 psi - $in^{1/2}$
3.0"	3.0"	0.75"	2.5"	1.0"	1,000 lb	7,311 psi - $in^{1/2}$	7,311 psi - $in^{1/2}$
3.0"	3.0"	0.5"	2.5"	1.0"	1,000 lb	10,967 psi - $in^{1/2}$	10,967 psi - $in^{1/2}$

4.1.1.4 Configuration 104 (Standard Three-Point Bend Specimen)

Figure 4.1.1.4-1 shows the geometry for configuration 104, the ASTM E399 *standard three-point bend specimen.* Table 4.1.1.4-1 presents comparative results for this solution. The K solution for configuration 104 is coded correctly but an onscreen message is misleading to the user. The onscreen message occurs during definition of the specimen geometry as shown in Figure 4.1.1.4-2. The message should read *Please Note: For K solution, L is set equal to 2W, no matter what value of L is entered.* In NASCRAC™, *4W* in the message should be replaced by *2W*, or, alternatively, eliminate *L* as input.

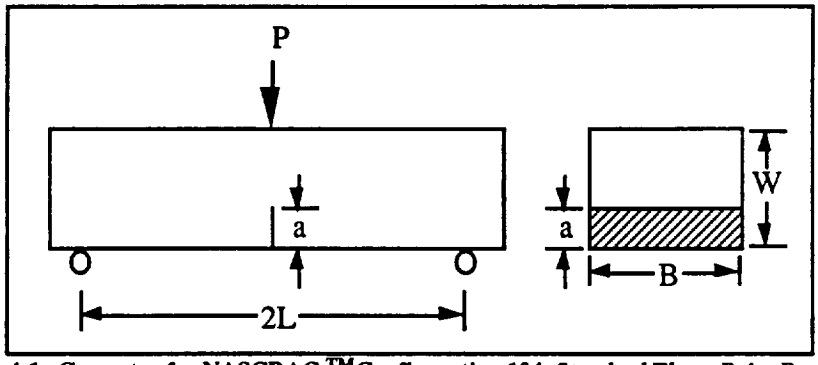

Figure 4.1.1.4-1. Geometry for NASCRAC ™Configuration 104, *Standard Three-Point Bend Specimen*

Table 4.1.1.4-1. Representative Results for Configuration 104

a (in)	W (in)	B (in)	L* (in)	P (lbf)	K (psi - $in^{1/2}$)		
					ROOKE & CARTWRIGHT	ASTM	NASCRAC™
0.1	1.5	2	6	1000	2325	2317	1158
0.1	1.5	1	6	1000	4651	4634	2317
0.2	2.0	1	4	1000	2345	2396	2396

* NASCRAC™ automatically sets L to 2W

```
STANDARD 3-POINT BEND SPECIMEN        [104]
-------------------------------------------------
Variable Thickness:  Not Available
Crack Position  Xc:  Not Used
                Yc:  Not Used
Crack Orientation Phi:  Not Used
Stress Input Options :  Pin Load only; Use Equation Type 6
J-Integral Solutions :  Available for plane stress and plane strain
                        0.125 =< a/W =< 0.875        1 =< n =< 20
-------------------------------------------------
```

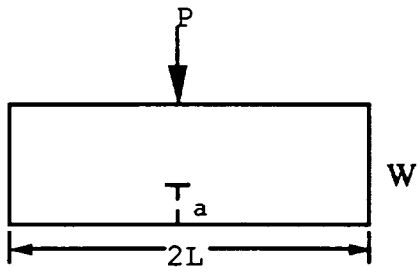


```
Please Note:  For K
Solution, L is set
equal to 4W, no matter
what value of L is
entered.

Inputs Required:  a = Crack depth; W = Width in direction of crack
                  B = Specimen thickness; L = Specimen half length
-------------------------------------------------
Enter a, W, L, and B
```

Figure 4.1.1.4-2. Error in Onscreen Note for Configuration 104

4.1.2 200 SERIES RESULTS

The nine 200 series K solutions modeling various through cracks configurations were verified and validated using three approaches: comparison to literature, independent numerical integration of weight functions, and finite element analysis with FRANC. No significant model or implementation errors were discovered. Several inconsistencies in the documentation were discovered.

Several 200 series configurations were analyzed to determine if the integration schemes in NASCRAC™ were acceptable. Table 4.1.2-1 lists representative results from NASCRAC™ and from direct integration of weight functions for configurations 201, 203, and 204, i.e., crack in an infinite plate, single edge crack in a plate, double edge cracks in a plate. The weight functions were obtained from [3]. The integrations were performed for non-uniform stress distributions as listed and were accomplished in FORTRAN using Romberg integration since the weight functions were singular at the crack tip. The results listed in Table 4.1.2-1 indicate that the Gaussian integration schemes used in NASCRAC™ are acceptable.

Table 4.1.2-1. NASCRAC™ Versus Romberg Integration of Selected Weight Functions

CONFIGURATION	GEOMETRY	STRESS DISTRIBUTION	NASCRAC™ RESULT	ROMBERG INTEGRATION
201	a =0.1"	$1000-200x+10x^2$	567 psi $\sqrt{in}$	566 psi $\sqrt{in}$
203	a =0.1", W =10"	$4000-800x+40x^2$	2513 psi $\sqrt{in}$	2524 psi $\sqrt{in}$
204	a =0.1", W =10"	500 + 50x	319 psi $\sqrt{in}$	316 psi $\sqrt{in}$
204	a =0.1", W =10"	$4000-800x+40x^2$	2509 psi $\sqrt{in}$	2483 psi $\sqrt{in}$

4.1.2.1 Configuration 201 (Crack in An Infinite Plate)

Figure 4.1.2.1-1 displays the geometry for configuration 201, *crack in an infinite plate*. NASCRAC™ results for uniform tension showed exact agreement with multiple literature sources. Additionally, the coded equation in NASCRAC™ was identical to the well-known solution for a crack in an infinite plate subjected to uniform tension: $K = \sigma\sqrt{\pi a}$. For non-uniform loading types, NASCRAC™ uses an influence function. Comparative, representative results for both uniform loading and non-uniform loads are shown in Table 4.1.2.1-1.

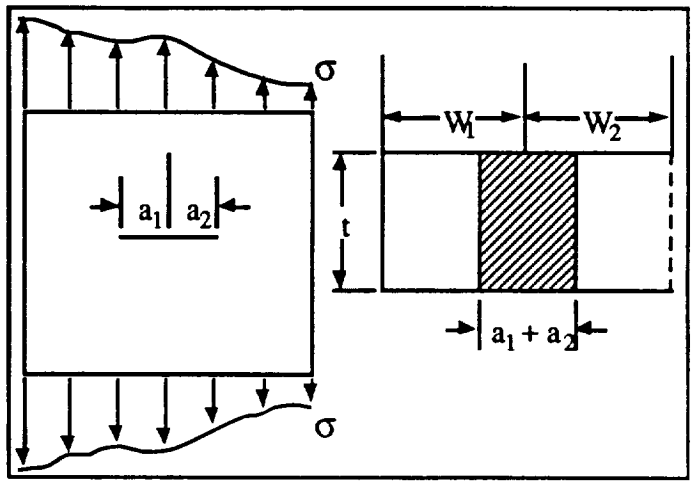

Figure 4.1.2.1-1. Geometry for Configuration 201, *Crack in an Infinite Plate*

This K solution is valid for a uniformly thick plate of unit thickness based on the studies represented by the results in Table 4.1.2.1-1 and the equivalency between the coded equation and the known solution for a crack in an infinite plate. An inconsistency does occur in this solution for uniformly thick specimens not equal to unit thickness when the variable thickness option is activated. This inconsistency is discussed in Section 4.2.

Table 4.1.2.2-1. Representative Results for Configuration 201

a (in)	σ (psi)	K	
		NASCRAC™	REFERENCE
0.10	1000	560.5 psi √in	560.5 psi √in [2,4]
0.10	1000 + 50x	562.4 psi √in	561.9 psi √in [3][1]
0.10	1000 - 50x	559.6 psi √in	559.1 psi √in [3][1]
0.10	$1000 - 200x + 10x^2$	566.6 psi √in	566.2 psi √in [3][1]

1 computed using Romberg integration and the weight function from [3]

4.1.2.2 Configuration 202 (Center Cracked Panel)

The geometry for configuration 202, *center cracked panel*, is shown in Figure 4.1.2.2-1. This K solution in NASCRAC™ uses a curve fit for uniform stresses and a weight function for non-uniform stresses. The formulation assumes that stresses are symmetric about the panel centerline. This assumption explains the results in Table 4.1.2.2-2 where two sets of K values are listed. One set corresponds to a symmetric load about the panel centerline, i.e., the stress function varies linearly from zero at the left edge to 10 at the centerline and back to zero at the right edge. The second set corresponds to an antisymmetric load about the panel , i.e., the stress is 20 at the left and decreases linearly to 10 at the centerline and to zero at the right edge.

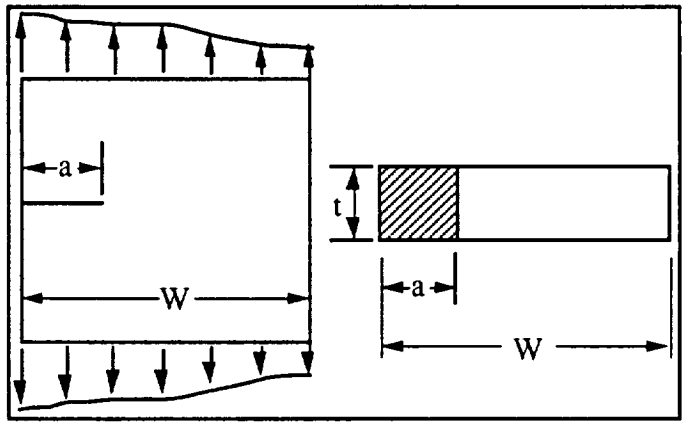

Figure 4.1.2.2-1. Geometry for Configuration 202, *Center Cracked Panel*

Table 4.1.2.2-2. Comparison of 202 K Values for Symmetric and Antisymmetric Loads

a	W	K : SYMMETRIC LOAD	K : ANTISYMMETRIC LOAD
1"	10"	16.7	16.7
2"	10"	22.5	22.5
3"	10"	26.5	26.5
4"	10"	29.8	29.8
5"	10"	33.0	33.0

Comparative results from a broad range of geometries are presented in Table 4.1.2.2-3. The studies represented by these results validated this NASCRAC™ solution for uniformly thick plates of unit thickness. An inconsistency does occur in this solution for uniformly thick specimens not equal to unit thickness when the variable thickness option is activated. This inconsistency is discussed in Section 4.2.

Table 4.1.2.2-3. Representative Results for Configuration 202

a (in)	W_1 (in)	W_2 (in)	s (psi)	K	
				NASCRAC™	REFERENCE
0.05	5	5	1000	396.4 psi √in	396.4 psi √in [2,4]
0.10	5	5	1000 + 100x	564.2 psi √in	563.3 psi √in [4]
0.10	5	5	1000 - 100x	557.0 psi √in	557.7 psi √in [4]
0.10	5	5	$1000 - 400x + 40x^2$	546.4 psi √in	548.0 psi √in [3][1]

1 computed using Romberg integration and the weight function from [3]

Misinterpretation of results from this K solution is possible if the symmetry assumption is neglected. This assumption needs to be more apparent in the user's manual, printed output, and onscreen.

4.1.2.3 Configuration 203 (Single Edge Crack in a Plate)

Figure 4.1.2.3-1 presents the geometry for NASCRAC™ configuration 203, *single edge crack in a plate*. This K solution in NASCRAC™ uses a curve fit function for uniform tension loads and a weight function for general loads. Representative results from comparative studies are presented in Table 4.1.2.3-1. These studies validated this configuration for uniformly thick plates.

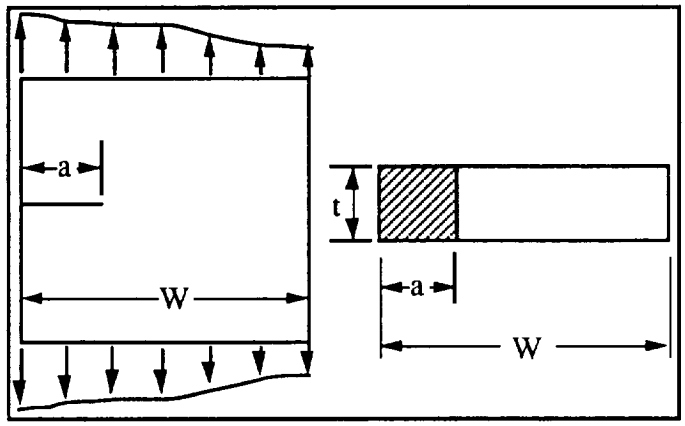

Figure 4.1.2.3-1. Geometry for Configuration 203, *Single Edge Crack in a Plate*

Table 4.1.2.3-1. Representative Results for Configuration 203

a (in)	W (in)	σ (psi)	K	
			NASCRAC™	REFERENCE
1.0	10	1000	2119 psi √in	2103 psi √in [4]
0.1	10	500 + 100x	321.8 psi √in	315.8 psi √in [3]
0.1	10	1500 - 100x	950.1 psi √in	947.5 psi √in [3]
0.1	10	$4000 - 800x + 40x^2$	2513.2 psi √in	2523.6 psi √in [3][1]

1 computed using Romberg integration and the weight function from [3]

4.1.2.4 Configuration 204 (Double Edge Cracks in a Plate)

The geometry for configuration 204, *double edge cracks in a plate*, is shown in Figure 4.1.2.4-1. The formulation of this K solution in NASCRAC™ is similar to that of configuration 202. Both formulations use a curve fit for uniform stresses and a weight function for non-uniform stresses and both formulations assume that stresses are symmetric about the plate centerline.

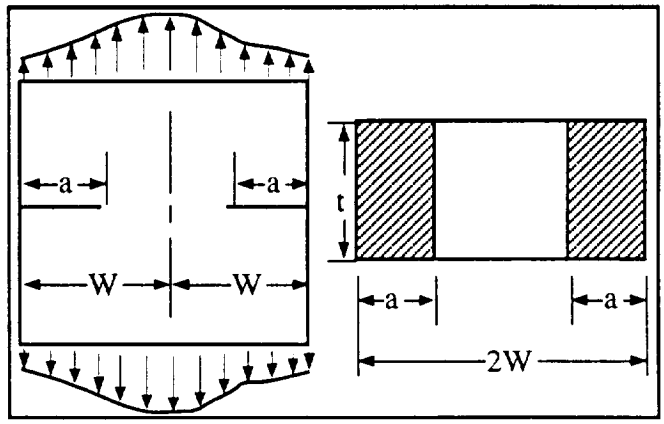

Figure 4.1.2.4-1. Geometry for Configuration 204, *Double Edge Cracks in a Plate*

Table 4.1.2.4-1 lists comparative results for this solution. These results indicate that this solution is valid for uniformly thick specimens of unit thickness.

Table 4.1.2.4-1. Representative Results for Configuration 204

a (in)	W (in)	σ (psi)	K	
			NASCRAC™	REFERENCE
0.1	10.0	1000	628.9 psi √in	630.9 psi √in [3]
0.1	10.0	500 + 50x	319.4 psi √in	316.2 psi √in [3]
0.1	10.0	1500 - 50x	950.5 psi √in	949.5 psi √in [3]
0.1	10.0	$4000 - 800x + 40x^2$	2509 psi √in	2497 psi √in [3][1]

1 computed using Romberg integration and the weight function from [3]

As in configuration 202, an inconsistency does occur in this solution for uniformly thick specimens not equal to unit thickness when the variable thickness option is activated. This inconsistency is discussed in Section 4.2, *K vs a* CALCULATION: VARIABLE THICKNESS.

Misinterpretation of results from this K solution is possible if the symmetry assumption is neglected. Therefore, this assumption needs to be more visible in the user's manual, printed output, and onscreen.

4.1.2.5 Configuration 205 (Axial (id) Crack in a Hollow Cylinder)

The geometry for configuration 205, *axial (inner diameter) crack in a hollow cylinder*, is shown in Figure 4.1.2.5-1. The K formulation for this configuration includes a uniform tension solution and a weight function solution for general loadings. The weight function solution is available for a limited number of r/W ratios where r is the inner radius of the cylinder and W is the wall thickness of the cylinder.

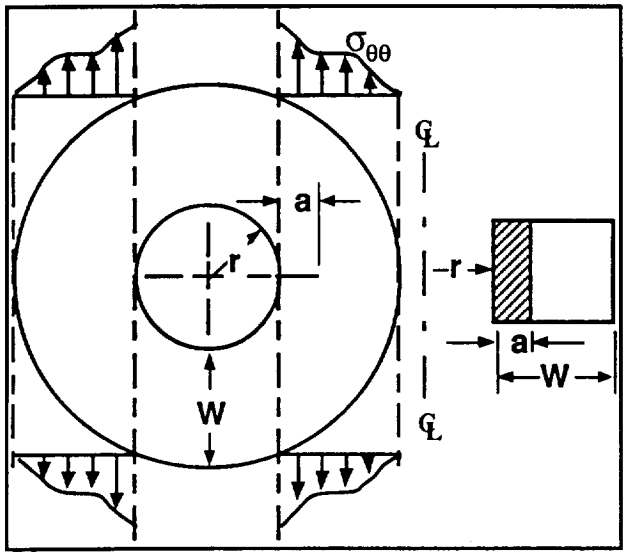

Figure 4.1.2.5-1. Geometry for Configuration 205, *Axial (id) Crack in a Hollow Cylinder*

Uniform tension results for 205 compared well to a number of reference results. Representative uniform tension results are shown in Table 4.1.2.5-1. For a majority of the cases NASCRAC™ was conservative by as much as 10%. In cases 4 and 5, NASCRAC™ is less than but within 2% of the FRANC value. Case 3 shows uniform tension results from NASCRAC™ using the weight function option. A comparison of case 3 and case 2 shows that the uniform tension solution is more conservative than the weight function solution for uniform tension. In case 6 the large difference between NASCRAC™ and FRANC may be due to the fidelity of the finite element mesh.

Table 4.1.2.5-1. Representative Uniform Tension Results for Configuration 205

CASE	a	r	W	σ	K		
					NASCRAC™	REFERENCE	FRANC
1	0.2	2	2	1.0	0.91	0.87 [5][1]	0.84
2	0.7	2	2	1.0	1.97	1.93 [7][2]	1.81
3	0.7	2	2	1000 + 0.0x	1893	n/a	1806
4	1.0	4	2	1000	2978	n/a	3027
5	1.0	10	2	1.0	3.65	n/a	3.73
6	1.0	20	2	1.0	4.32	3.92 [7][2]	3.07

1 computed using Romberg integration and the weight function from [5]
2 computed using Romberg integration and the weight function from [7]

The 205 weight function solution is available for a limited number of inner radius to wall thickness ratios: r/W = 1,5,10 . Selected results from weight function solutions are shown in Table 4.1.2.5-2.

Table 4.1.2.5-2. 205 Representative Results for Non-Uniform Loads

CASE	a	r	W	σ	K		
					NASCRAC™	[5][2]	FRANC
1	0.2	2	2	800 + 800x	786	782	750
2	0.2	2	2	960 - 800x	755	750	722
3	1.5	4	3	1000 - 500x	1806[1]	n/a	2401
4	0.2	2	2	1200 - 12000x + 30000x^2	261	258	n/a
5	1.0	10	2	x	1.98	n/a	1.72
6	1.0	10	2	1 - x	2.00	n/a	2.00
7	1.0	20	2	x	2.13	n/a	1.14
8	1.0	20	2	1 - x	2.26	n/a	1.94

1 NASCRAC™ used solution for r/W = 1
2 computed using Romberg integration and the weight function fro m [5]

NASCRAC™ does allow 205 geometries in which the r/W ratio is not equal to one of the three coded ratios. If an uncoded ratio is specified NASCRAC™ automatically uses one of its coded ratios to compute results and prints a warning on the geometry page of the output file that the analysis was completed for a coded ratio, not the ratio specified by the user. This approach is not erroneous but, since NASCRAC™ is designed to be an engineering tool, such logic increases the chances of human error.

Table 4.1.2.5-3. Comparison of NASCRAC™ 205 Output for Various r/W Ratios

a	r/W						
	0.5	1.0	2.0	3.0	3.25	4.75	5.25
	K						
0.5	1.26	1.26	1.26	1.26	1.53	1.53	1.53
1.0	1.83	1.83	1.83	1.83	3.00	3.00	3.00
1.5	2.32	2.32	2.32	2.32	5.34	5.34	5.34

To illustrate the potential problem, a 205 configuration was analyzed with r/W = 0.5, 1.0, 2.0, 3.0, 3.25, 4.75, and 5.25. For each r/W ratio, the cylinder wall thickness, the crack length, and the stresses on the crack plane were identical. The only variable was the inner radius of the cylinder. Results of the analysis are presented in Table 4.1.2.5-3; identical results were observed for r/W = 0.5, 1.0, 2.0, and 3.0 and also for r/W = 3.25, 4.75 and 5.25. The first set of identical results corresponds to r/W = 1.0 and the second set corresponds to r/W = 5.0. Figure 4.1.2.5-2 shows a condensed version of the output file for r/W = 2.0 with the r/W warning listed on the geometry page. The calculated results in this output are reasonable for the coded r/W ratio (r/W = 1.0) but are not necessarily reasonable for the specified r/W ratio (r/W = 2.0), which could mislead an analyst. This conclusion is supported by Table 4.1.2.5-3 as the crack length increases. From Table

4.1.2.5-3, if the geometry of interest were r/W = 3.0 with W = 2.0, NASCRAC™ would calculate K = 2.32 for a = 1.5; however, if the cylinder radius increased slightly such that r/W = 3.25 with W = 2.0, then NASCRAC™ would calculate K = 5.34 for a = 1.5. Again this discrepancy arises because NASCRAC™ is using its r/W = 1 solution in the first case and its r/W = 5 solution in the second case.

```
   PROBLEM TITLE : g205ratioc2

  ->    Axial(ID) crack in a hollow cylinder                205

** WARNING : Ri/h =       2.0000
   For stresses defined by Equation 1, K solution for
   Ri/h =   2.00 will be used

   IF solution for Ri/h = 1 will be used otherwise.

         Initial Crack Dimension(1) =   0.50000
         Final Crack Size           =   1.50000
         Crack Size Increment       =   0.10000
                     BODY WIDTHS(1) =   2.00000
                     BODY WIDTHS(2) =   4.00000
   .
   .
   .
MAXIMUM STRESS DEFINED BY EQUATION TYPE :  2 WHICH IS ...
STRESS= A0 + A1*X, A0=  1.0000E+00
                   A1= -5.0000E-01
                   MULTIPLICATION FACTOR =     1.00000E+00

K VS. A SUMMARY  FOR TRANSIENT #   1
     A1         KMAX1       KMIN1
    0.5000      1.2608      0.0000
    1.0000      1.8327      0.0000
    1.5000      2.3249      0.0000
```

Figure 4.1.2.5-2. Typical Output for Configuration 205 Including r/W Warning

In future NASCRAC™ releases, a minimum update to this solution should include this r/W warning on the *K vs a* results page as well as the geometry page. The best resolution of this potential problem is to prevent an analyst from specifying an uncoded r/W configuration by including a geometry error flag. This error checking approach will force the analyst to bound or extrapolate his configuration using the coded solutions and will also force the analyst to recognize the assumptions and limitations of the K solution.

4.1.2.6 Configuration 206 (Edge Crack in a Solid Disk)

Figure 4.1.2.6-1 displays the geometry of configuration 206, *edge crack in a solid disk.* This solution consists of a uniform tension solution and a weight function solution. Closed form solutions from [3] and FRANC were used to verify and validate this solution. Two types of loads were applied to FRANC models: a traction and a crack face pressure. These load types, which were designed to be equivalent load systems, resulted in similar K values as expected. Representative results from the V/V studies are shown in Table 4.1.2.6-1.

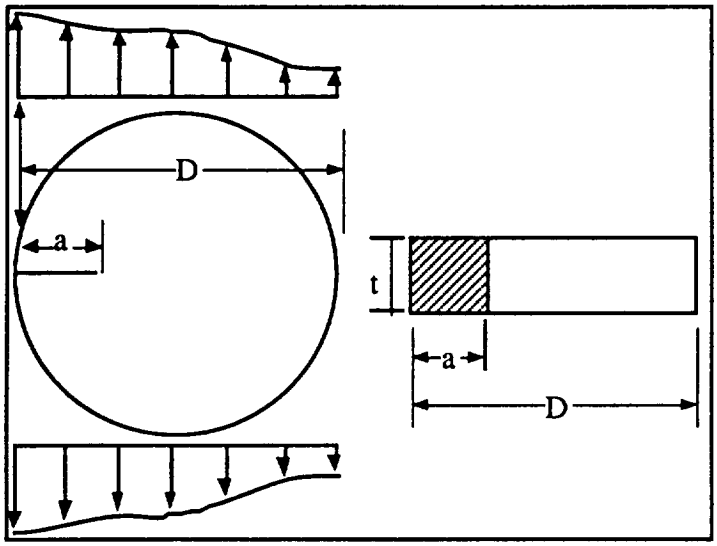

Figure 4.1.2.6-1. Geometry for Configuration 206, *Edge Crack in a Solid Disk*

Table 4.1.2.6-1. Representative Results for Configuration 206

CASE	a	D	σ	K		
				NASCRAC™	[3]	FRANC
1	0.5	5	1000	1660	1660	TRACTION: 1628 PRESSURE: 1613
2	0.5	5	500 + 200x	945	N/A	TRACTION: 910
3	0.5	5	1500 - 200x	2449	N/A	TRACTION: 2349
4	0.5	5	$2000 - 800x + 80x^2$	3021	N/A	TRACTION: 2760 PRESSURE: 2755

Results from NASCRAC™ and [3] were identical for the case of uniform tension (case 1 in Table 4.1.2.5-1). NASCRAC™ and FRANC agreed within 10% for the variety of loads listed in Table 4.1.2.5-1. In all 206 comparisons with FRANC, NASCRAC™ was conservative, i.e., the NASCRAC™ K value was larger than either FRANC value. The studies represented by the tabulated comparisons in Table 4.1.2.6-1 verify the 206 *K vs a* solution in NASCRAC™.

4.1.2.7 Configuration 207 (Axial (od) Diameter Crack in a Hollow Cylinder)

The geometry for configuration 207, *axial (outer diameter) crack in a hollow cylinder*, is shown in Figure 4.1.2.7-1. The K formulation for this configuration is similar to configuration 205. It includes a uniform tension solution and a weight function solution for general loadings. The weight function solution is available for only a single r/W ratio, i.e., r/W = 1. Table 4.1.2.7-1 lists representative K results for this configuration.

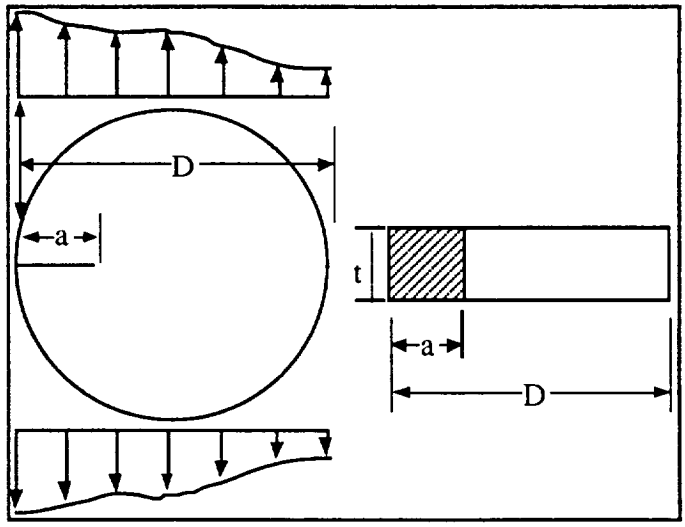

Figure 4.1.2.7-1. Geometry for Configuration 207, *Axial (od) Crack in a Hollow Cylinder*

Table 4.1.2.7-1. Representative Results for Configuration 207

CASE	a	r	W	σ	K		
					NASCRAC™	[5][1]	FRANC
1	0.2	2	2	1000	938	913	914
2	1	2	2	1.0	3.17		3.08
3	2	4	4	1.0	4.48		4.35
4	5	5	5	1.0	7.09		6.87
5	10	4	2	1000	3169		3374
6	0.2	2	2	800 + 800x	840	818	816
7	0.2	2	2	960 - 800x	811	789	793
8	0.2	2	2	1200-12000x+30000x^2	295	287	

1 computed using Romberg integration and the weight function from [5]

As with configuration 205, NASCRAC™ does not prevent the user from analyzing geometries with r/W ratios different from the coded solution of r/W = 1. If an uncoded ratio is specified NASCRAC™ automatically uses one of its coded ratios to compute results and prints a warning on the geometry page of the output file that the analysis was completed for r/W = 1, not the ratio specified by the user. This approach is not erroneous but, since NASCRAC™ is designed to be an engineering tool, such logic increases the chances of human error.

In future NASCRAC™ releases, a minimum update to this solution should include the r/W warning on the *K vs a* results page as well as the geometry page. The best resolution of this potential problem is to include in error path in the code which would prevent an analyst from specifying a configuration with r/W ≠ 1. This approach will force the analyst to extrapolate his configuration from the coded solution and will also force recognition of the assumptions used to formulate the analysis.

4.1.2.8 Configuration 208 (Through Crack from a Hole in a Finite Plate)

The geometry for configuration 208, *through crack from a hole in a plate*, is shown in Figure 4.1.2.8-1. This solution was adapted from NASA/FLAGRO and does not feature a weight function solution. The loading in this K solution is restricted to uniform tension and/or a pin load at the hole. Table 4.1.2.8-1 lists selected results from the 208 V/V studies.

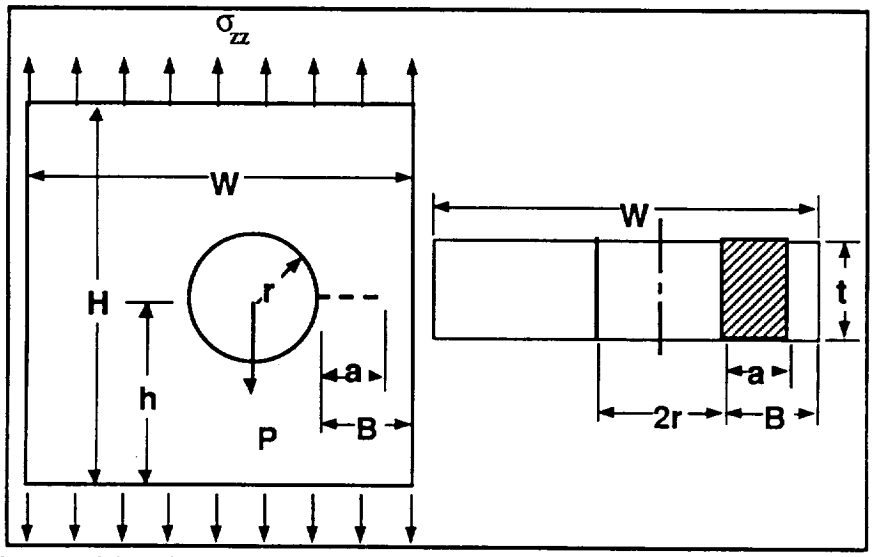

Figure 4.1.2.8-1. Geometry for Configuration 208, *Through Crack from a Hole in a Plate*

Table 4.1.2.8-1. Representative Results for Configuration 208

CASE	GEOMETRY	LOAD	a	NASCRAC™	FLAGRO	LITERATURE	FRANC
1	R = 0.5 B = 11.5 W = 24 H = 24 h = 12	σ = 1.0	1.0 2.0 4.0 8.625	1.840 2.229 2.938 5.243	1.838 2.227 2.936 5.241	1.87[2]	1.819 2.220 2.788 4.782
2	R = 0.5 B = 11.5 W = 24 H = 24 h = 12	σ = 1.042 P = 1.0	1.0 2.0 4.0 8.625	2.129 2.478 3.187 5.617	2.127 2.476 3.185 5.616		2.057 2.392 2.936 4.945
3	R = 0.5 B = 6.0 W = 24 H = 24 h = 12	σ = 1.0	1.0 2.0 4.5	1.862 2.309 4.077	1.860 2.308 4.075	1.87[2]	1.832 2.268 3.829
4	R = 0.5 B = 6.0 W = 24 H = 24 h = 12	σ = 1.077 P = 1.0	1.0 2.0 4.5	2.221 2.648 4.554	2.218 2.646 4.554		2.145 2.478 4.087
5	R = 0.5 B = 3.0 W = 24 H = 24 h = 12	σ = 1.0	1.0 2.25	1.961 3.307	1.958 3.305	1.87[2]	1.905 2.932
6	R = 0.5 B = 3.0 W = 24 H = 24 h = 12	σ = 1.143 P = 1.0	1.0 2.25	2.468 3.991	2.465 3.988		2.235 3.304
7	R = 0.5 B = 11.5 W = 24 H = 24 h = 6	σ = 1.0	1.0 2.0 8.625	1.840 2.229 5.243	1.873 2.227 5.241	1.87[2]	1.853 2.282 5.816
8	R = 0.5 B = 11.5 W = 24 H = 24 h = 6	σ = 1.042 P = 1.0	1.0 2.0 8.625	2.129 2.478 5.617	2.127 2.476 5.616		2.118 2.499 6.001
9	R = 0.5 B = 6.0 W = 24 H = 24 h = 6	σ = 1.0	1.0 2.0	1.862 2.309	1.860 2.308	1.87[2]	1.883 2.330
10	R = 0.5 B = 6.0 W = 24 H = 24 h = 6	σ = 1.077 P = 1.0	1.0 2.0	2.221 2.648	2.218 2.646		2.166 2.571

Table 4.1.2.8-1. Representative Results for Configuration 208 (Continued)

CASE	GEOMETRY	LOAD	a	NASCRAC™	FLAGRO	LITERATURE	FRANC
11	R = 0.5 B = 3.0 W = 24 H = 24 h = 6	σ = 1.0	1.0 2.25	1.961 3.307	1.958 3.305	1.87[2]	1.919 3.004
12	R = 0.5 B = 3.0 W = 24 H = 24 h = 6	σ = 1.143 P = 1.0	1.0 2.25	2.468 3.991	2.465 3.988		2.253 3.381
13	R = 1.0 B = 11.0 W = 24 H = 24 h = 12	σ = 1.0	1.0 2.0 8.25	 2.643 5.598	2.342 2.640 5.595	2.42[2] 2.65[2]	2.342 2.674 5.523
14	R = 1.0 B = 11.0 W = 24 H = 24 h = 12	σ = 1.042 P = 1.0	1.0 2.0 8.25	 2.935 6.008	2.896 3.112 6.182		2.619 2.878 5.525
15	R = 1.0 B = 5.0 W = 24 H = 24 h = 12	σ = 1.0	1.0 2.0 3.75	 2.872 4.501	2.424 2.869 4.497	2.42[2] 2.65[2]	2.382 2.806 4.172
16	R = 1.0 B = 5.0 W = 24 H = 24 h = 12	σ = 1.083 P = 1.0	1.0 2.0 3.75	 3.307 5.087	3.096 4.499 5.293		2.679 3.084 4.509
17	R = 2.0 B = 5.0 W = 24 H = 24 h = 12	σ = 1.0	1.0 2.0 3.75	3.377 3.885 5.882	3.372 3.879 5.875	3.07[2] 3.41[2] 3.73[2]	
18	R = 2.0 B = 5.0 W = 24 H = 24 h = 12	σ = 1.0 P = 1.0	1.0 2.0 3.75	3.903 4.437 6.641	4.354 4.794 6.952		
19	R = 5.0 B = 5.0 W = 20 H = 40 h = 12	σ = 1.0	0.5 1.0 2.0 3.0 3.5	4.29 5.41 6.72 8.32 9.45		3.91[7] 5.16[7] 6.92[7] 8.84[7] 10.15[7]	

NASCRAC™ results compares favorably with the results from NASA/FLAGRO, FRANC, [2], and [7] listed in Table 4.1.2.8-1. The comparison between NASCRAC™ and [2] is better for cases where the remaining ligament is large compared to the crack length (cases 1, 3, 7,

9, 13) because [2] does not account for edge effects. Differences between NASCRAC™ and [2] occur for shorter ligaments (cases 5, 11, 15, and 17). In these cases NASCRAC™ appears to correctly model the edge effect based on comparisons with FRANC. Results from [7] were developed by assuming a 3/x stress distribution along the crack plane where x = 1 at the crack mouth and x = 2 at the plate edge. This distribution approximates the analytical solution for stress concentration at a circular hole in a plate subjected to uniform tension. Case 19 provides a comparison between NASCRAC™ and [7], a weight function solution for a 3/x stress distribution. The results from case 19 show reasonable agreement between NASCRAC™ and [7] even though the stress distribution in [7] only approximated the stress on the crack plane in NASCRAC™.

The minor differences between NASCRAC™ and FLAGRO results in Table 4.1.2.8-1 were unexpected since the NASCRAC™ solution was taken from FLAGRO. A comparison of the source codes revealed a minor coding difference: a transposition of digits in the assignment statement for *FOZ* in *FUNCTION FCT208* (*G0* in *SUBROUTINE SITC03* in FLAGRO).

References [7] and [10] plus FRANC results indicated a dependency of K on plate height to width ratio. Table 4.1.2.8-2 lists selected results from [10] and FRANC which confirm this dependency. These results and discussion in the [7] suggest that K is independent of plate height for plate to width ratios (H/W) ≥ 2. NASCRAC™, which does not require H as input, is in good agreement with [10] and FRANC for such ratios. However, for H/W < 2, NASCRAC™ differs from the reference solutions by 10-30%. These results suggest that the NASCRAC™ solution is **valid for H/W ≥ 2, reasonable for 1 < H/W < 2, and non-conservative (and therefore not valid) for H/W ≤ 1.** Warnings in the documentation, onscreen, and in printouts should inform users that use of the solution for cases where H/W < 2 is marginally acceptable and should be used with caution. The results in Table 4.1.2.8-1 generally did not reflect this dependency because the plate dimensions were large compared to the hole and crack dimensions.

Table 4.1.2.8-2. Representative 208 Results Showing Dependency on Height to Width Ratio (H/W)

H/W	GEOMETRY	a	NASCRAC™	[10]	FRANC
0.5	R = 2.0	1.0	3.31		5.05
	B = 6.0	2.0	3.71		6.33
	W = 16	3.0	4.26		7.75
		4.0	5.18		9.16
1.0	R = 2.0	1.0	3.31	3.76	3.72
	B = 6.0	1.6	3.55	4.20	4.18
	W = 16	2.0	3.71	5.47	5.46
		2.8	4.13		
		4.0	5.18		
2.0	R = 2.0	1.0	3.31	3.34	3.34
	B = 6.0	1.6	3.55	3.56	3.56
	W = 16	2.0	3.71	3.71	3.74
		2.8	4.13	4.10	4.14
		4.0	5.18	5.13	5.18
3.0	R = 2.0	1.0	3.31	3.34	3.33
	B = 6.0	2.0	3.71	3.69	3.71
	W = 16	4.0	5.18	5.07	5.17

The NASCRAC™ user's manual and theory manual indicate only pin and uniform tension loads are available for this solution. This is in agreement with the formulation adapted from FLAGRO. Additionally, if a user attempts to use another type load, NASCRAC™ flags the input as a fatal error and will not execute. However, in the source code, a weight function solution for general loadings is included. A future release of NASCRAC™ should permit the user to access this function if it is valid.

4.1.2.9 Configuration 209 (Through Crack from a Hole in a Lug)

Figure 4.1.2.9-1 displays the geometry of NASCRAC™ configuration 209, *through crack from a hole in a lug*. This solution was adapted from NASA/FLAGRO and does not feature a weight function solution. The loading in this K solution is restricted to a pin load at the hole. Table 4.1.2.9-1 lists selected results for configuration 209.

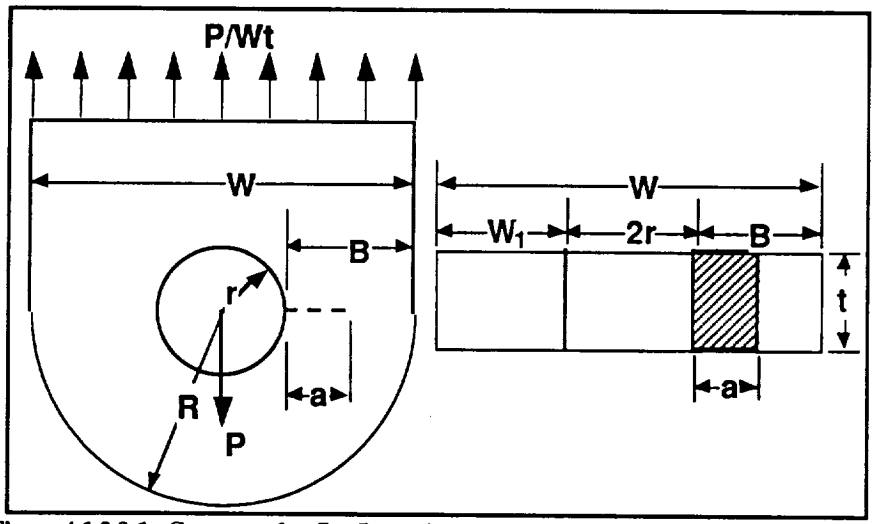

Figure 4.1.2.9-1. Geometry for Configuration 209, *Through Crack from a Hole in a Lug*

NASCRAC™ compared favorably with [12] and FRANC, and identically matched the results from FLAGRO. Figure 4.1.2.9-2 shows results of NASCRAC™ and [12]. The trends in the results are identical although NASCRAC™ was consistently conservative by as much as 20%. For the FRANC calculations, two different loadings were applied to finite element model: a point load at the center of the hole and a distributed load along the surface of the hole. In each case, the total load was equal to 1 lb_f. The results, which are tabulated in Table 4.1.2.9-1, show little difference between the two load configurations and a maximum difference of 8% between NASCRAC™ and FRANC. Table 4.1.2.9-1 also lists the selected FLAGRO results. Based on the identical agreement between NASCRAC™ and FLAGRO, this solution is coded correctly. Furthermore, the favorable comparison between NASCRAC™, FRANC, and [12] verifies this NASCRAC™ solution.

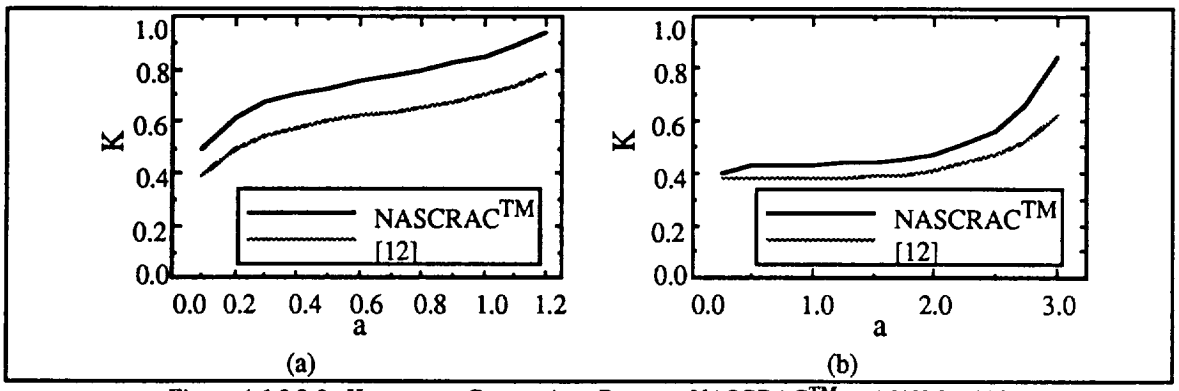

Figure 4-1.2.9-2. K versus *a* Comparison Between NASCRAC™ and [12] for 209
(a) r = 1.125", R = 2.8125" (b) r= 1.125", R = 4.5

Table 4.1.2.9-1. Representative Results for Configuration 209 with r = 1.125", R = 3.375"

CASE	a	σ	P	NASCRAC™	FLAGRO	FRANC
1	1.0		1.0	0.6161	0.6161	0.6678
	1.5			0.7035	0.7035	0.7093
2	1.0	1.0		0.6161		0.6569
	1.5			0.7035		0.6976

4.1.3 300 SERIES RESULTS

There are three 300 series K solutions in NASCRAC™. These solutions model through cracks in cylinders and spheres. All three solutions were found to be valid. Representative V/V results and suggestions to improve the NASCRAC™ range checking capabilities and clarify the documentation are described in the following subsections.

4.1.3.1 Configuration 301 (Through Crack in a Sphere)

Figure 4.1.3.1-1 shows the geometry of configuration 301, *through crack in a sphere*. This solution is formulated as a uniform tension solution; therefore, this formulation is only applicable to a thin walled pressure vessel subjected to internal pressures. Table 4.1.3.1-1 shows comparative results from representative V/V cases. In this table R represents the outer radius of the sphere and λ is a function of a, t (thickness), and R. In addition to the tabulated results in Table 4.1.3.2-1, a spreadsheet of f(λ) results computed with the equation coded in NASCRAC™ compared favorably to an f(λ) plot in [2]. f(λ) is the β function for this solution such that $K = f(\lambda)\sigma\sqrt{\pi a}$.

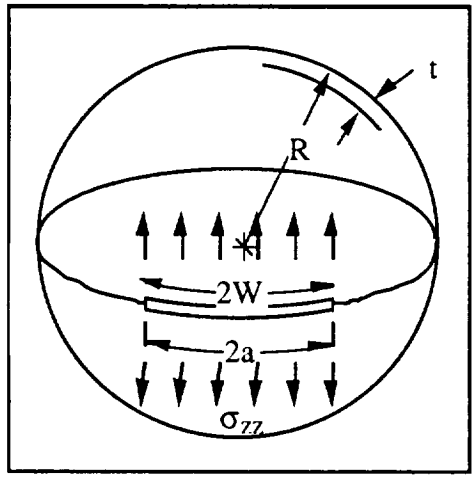

Figure 4.1.3.1-1. Geometry for Configuration 301, *Through Crack in a Sphere.*

Table 4.1.3.1-1. Representative Results for Configuration 301

a	R	t	σ	λ = a/√(t R)	f(λ)	K NASCRAC™	K [2]
0.1	2	0.2	1.0	0.158	1.02	0.57	0.57
0.5	2	0.2	1.0	0.791	1.38	1.71	1.73
1.0	2	0.2	1.0	1.58	2.18	3.76	3.86
1.5	2	0.2	1.0	2.37	3.08	6.53	6.69
1.0	10	0.1	1.0	1.00	1.57	2.77	2.78
2.0	10	0.1	1.0	2.00	2.63	6.60	6.59
3.0	10	0.1	1.0	3.00	3.88	11.77	11.91

No errors were found in the K solution for this configuration; however, the NASCRAC™ documentation does not clearly define the radius to be input. Figures in the NASCRAC™ documentation (user's and theory manuals) and in [2] indicate that the required radius is the outer radius of the sphere; however, in the NASCRAC™ source code the solution has been coded for a midsurface radius input. The outer radius R is then calculated from the input radius by adding one-half the sphere wall thickness. This discrepancy is insignificant for thin shell inputs, i.e., $t \leq 0.1R$. For the extreme case, i.e., $t = 0.1R$, the discrepancy in $\lambda = a/\sqrt{(t\ R_{mid})}$ and $\lambda = a/\sqrt{(t\ R)}$ is less than 3% and the corresponding change in the correction factor $f(\lambda)$ of the solution is less than 0.0013.

Three minor changes would improve the usability of this solution. First, a note should be included in the user's manual and onscreen stating that thin shell theory is assumed and no bending effects are considered. Secondly, the user's manual should clearly identify which radius (midsurface radius) is required for input. Finally, an error flag should be included in the code to detect specified geometries which do not meet thin shell requirements.

4.1.3.2 Configuration 302 (Axial Through Crack in a Cylinder)

Figure 4.1.3.2-1 shows the geometry of configuration 302, *axial through crack in a cylinder*. This solution is formulated as a uniform tension solution. Table 4.1.3.2-1 shows comparative results of $f(\lambda)$ and K for representative V/V cases. In this table R represents the outer radius of the cylinder and λ is a function of a, t (thickness), and R. $f(\lambda)$ is the β function for this solution such that $K = f(\lambda)\sigma\sqrt{\pi a}$.

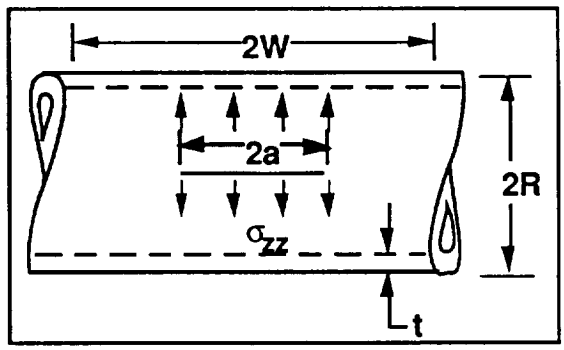

Figure 4.1.3.2-1. Geometry for Configuration 302, *Axial Through Crack in a Cylinder*

Table 4.1.3.2-1. Representative Results for Configuration 302

CASE	a	$\lambda = a/\sqrt{(t\,R)}$	$f(\lambda)_{[2]}$	$f(\lambda)_{NASCRAC^{TM}}$	$K_{[2]}$	$K_{NASCRAC^{TM}}$
R = 2	0.1	0.158	1.02	1.06	0.572	0.593
t = 0.2	0.5	0.791	1.38	1.48	1.730	1.872
σ = 1.0	1.0	1.58	2.02	2.18	3.580	3.932
	1.5	2.37	2.75	2.92	5.970	6.453
	2.0	3.16	3.42	3.63	8.573	9.291
	4.0	6.32		6.10		21.988
	6.0	9.49		7.67		33.640
R = 10	1.0	1.0	1.55	1.65	2.747	2.936
t = 0.1	2.0	2.0	2.42	2.57	6.066	6.455
σ = 1.0	5.0	5.0		5.16		20.479
	10.0	10.0		7.82		43.885

NASCRAC™ and [2] are in reasonable agreement for 302 *K vs a* calculations. From Table 4.1.3.2-1, the differences between the two solutions are due to differences in $f(\lambda)$. NASCRAC™ uses a curve fit to compute these values whereas the [2] results were obtained from a graph. The higher values of $f(\lambda)$ in NASCRAC™ are reflected in the calculated stress intensity factor. The $f(\lambda)$ curve fit equation in the NASCRAC™ source does identically match the equation listed in the FLAGRO manual [13], which was the source for this solution. [13] adapted the solution from [14] and lists the valid range as $0 < \lambda \leq 10$. [2], however, lists the valid range as $0 < \lambda \leq 5$. This range is supported by [3], which uses a different $f(\lambda)$ curve fit from [13]. The equivalency of $f(\lambda)$ in NASCRAC™ and FLAGRO verifies this solution. This solution is valid based on the reasonable agreement of K between NASCRAC™ and [2] in addition to reasonable agreement of $f(\lambda)$ among NASCRAC™, [2], and [3].

The definition of the required input radius is not clear in the NASCRAC™ documentation. Figures in the NASCRAC™ documentation (user's and theory manuals) indicate that the required radius is the inner radius of the cylinder; however, in [2] an outer radius is depicted. Additionally, NASCRAC™ has been coded such that one-half the cylinder wall thickness is added to the input radius to obtain the radius used in the λ calculation.

Three minor changes would improve the usability of this solution. First, a note should be included in the user's manual and onscreen stating that thin shell theory is assumed and no bending effects are considered. Secondly, the user's manual should clearly identify which radius (midsurface radius) is required for input. Finally, an error flag should be included in the code to detect specified geometries which do not meet thin shell requirements.

4.1.3.3 Configuration 303 (Circumferential Through Crack in a Cylinder)

The geometry for configuration 303, *circumferential through crack in a cylinder*, is shown in Figure 4.1.3.3-1. Table 4.1.3.3-1 presents V/V results from this configuration. This solution was formulated for uniform tension and bending loads using superposition. In Table 4.1.3.3-1, R_i is the inner radius of the cylinder, t is the cylinder wall thickness, σ_t is the uniform tensile stress, and σ_b is the bending stress.

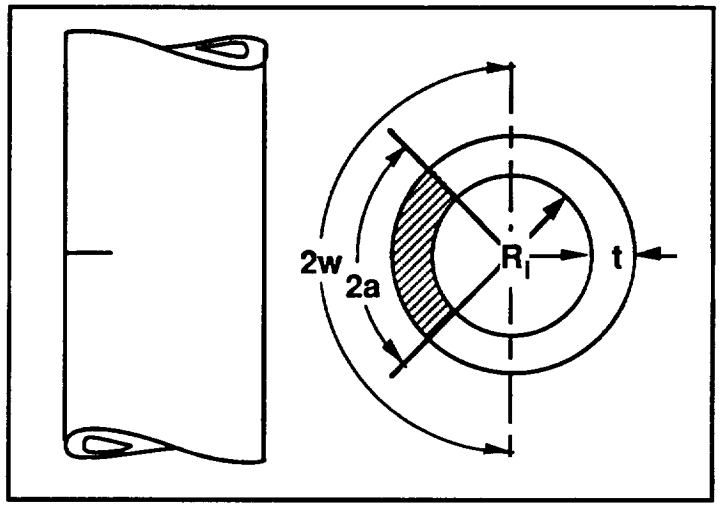

Figure 4.1.3.3-1. Geometry for Configuration 303, *Circumferential Through Crack in a Cylinder*

Table 4.1.3.3-1. Representative Results for Configuration 303

a	R_i	t	$\sigma_t + \sigma_b$	$K_{NASCRAC^{TM}}$	$K_{[16]}$	$K_{[2]}$	$K_{[15]}$
1.0	5.0	0.5	1.0 + 0.0	1.878	1.878	1.88	1.87
1.5	5.0	0.5	1.0 + 0.0	2.458	2.458		
1.9	5.0	0.5	1.0 + 0.0	2.948	2.948		
1.0	5.0	0.5	1.0 + 1.0	3.752	3.752		
1.5	5.0	0.5	1.0 + 1.0	4.895	4.895		
1.9	5.0	0.5	1.0 + 1.0	5.853	5.853		

The 303 *K vs a* solution in NASCRAC™ was adapted from [16]. The identical agreement between NASCRAC™ and [16] results in Table 4.1.3.3-1 verifies and validates this solution. [2] and [15] provided a spot check of [16].

The NASCRAC™ documentation for this solution did contain several oversights. First, the documentation needs to clearly state that the computed K value corresponds to the midsurface of the cylinder wall. Thus, no local bending of the pressure vessel is computed. In reality, a higher K will occur at the inner or outer surface of the cylinder wall although the discrepancy should be minor for a thin-walled cylinder. This local bending occurs even in the uniform tension case (see [2] and [15]) and therefore is not due to the input bending stress. Second, the NASCRAC™ solution is hardwired for a Poisson's ratio of 0.3. This value is included in the shell parameter ε where $\varepsilon = (\sqrt{t}/R_{mid})\,(12(1-\nu^2))^{-0.25}$. For ν between 0.1 and 0.33 ε does not vary much and therefore the hardwired value should be acceptable. This assumption should be documented. Finally, the NASCRAC™ documentation in the theory manual contains at least three typographical mistakes which are misleading. The mistakes and the corrections are listed in Table 4.1.3.3-2. The corrections were obtained from [16].

Table 4.1.3.3-2. Documentation Errors for Configuration 303

$$I_0 = \alpha^2 [g(\alpha) + \frac{\pi C^2}{\lambda} - 2^{1.5}] \text{ -----> } I_0 = \frac{\alpha^2}{\varepsilon} [g(\alpha) + \frac{\pi C^2}{\lambda} - 2^{1.5}]$$

$$C = 1 + \frac{\pi}{16}\lambda^2 - 0.0293\,\lambda^2 \text{ -----> } C = 1 + \frac{\pi}{16}\lambda^2 - 0.0293\,\lambda^3$$

$$\lambda = \frac{a}{\sqrt{rt}} \text{ -----> } \lambda \sim \frac{a}{\sqrt{rt}};\ \lambda = \frac{\alpha}{2\varepsilon}$$

4.1.4 400 SERIES RESULTS

The four 400 series K solutions in NASCRAC™ model specific surface crack configurations in hollow and solid cylinders. These solutions were verified and validated using published results and direct integration of weight functions from the literature. In addition, for configuration 404, *edge crack in a solid circular bar*, NASCRAC™ results were checked versus FLAGRO and FRANC computations. Configuration 404 was the only solution from this series which could not be validated unequivocally.

4.1.4.1 Configuration 401 (Circumferential Crack (id) in a Hollow Cylinder)

Figure 4.1.4.1-1 shows the geometry of configuration 401, *circumferential crack (id) in a hollow cylinder*. The K formulation for this configuration includes a uniform tension solution and a weight function solution for general loadings. Representative V/V results are presented in Table 4.1.4.1-1.

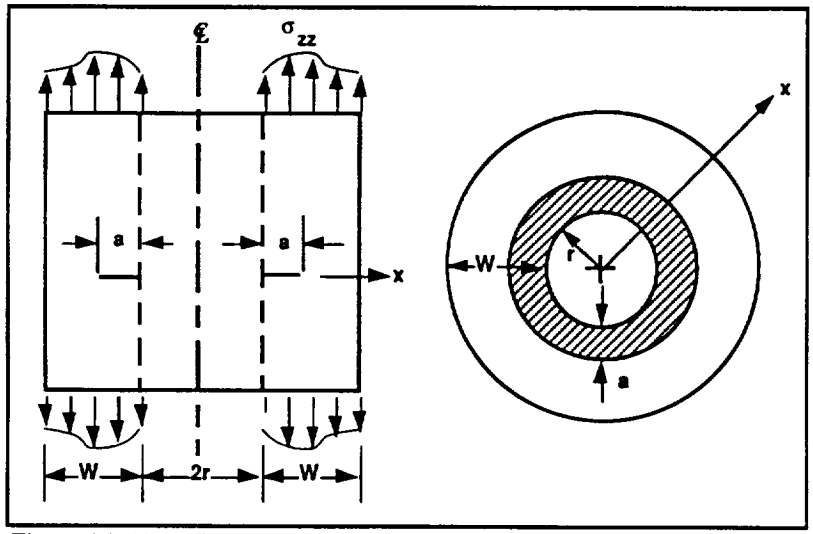

Figure 4.1.4.1-1. Geometry for Configuration 401, *Circumferential Crack (id) in a Hollow Cylinder*

Table 4.1.4.1-1. Representative Results for Configuration 401

PARAMETERS	a	$K_{NASCRAC^{TM}}$	$K_{reference}$
r = 3.5	0.015	0.2435	0.243[7]
t = 1.5	0.60	1.7387	1.76[7]
σ = 1.0	0.90	2.4231	2.51[7]
r = 4.0	0.01	0.223	0.225[7]
t = 1.0	0.30	1.190	1.191[7]
σ = 1.0	0.60	39.630	39.630[7]
r = 4.5	0.005	0.1406	0.14[7]
t = 0.5	0.15	0.9649	0.96[7]
σ = 1.0	0.30	1.9404	1.97[7]
r = 5.0	0.125	0.7331	0.727[17]
t = 1.0	0.250	1.1181	1.117[17]
σ = 1.0	0.500	1.9406	2.018[17]
	0.750	3.1937	3.300[17]
r = 5.0	0.0625	0.5297	0.527[17]
t = 0.5	0.125	0.8451	0.827[17]
σ = 1.0	0.250	1.6031	1.613[17]
	0.375	2.7541	2.703[17]
r = 5.0	0.03125	0.3843	0.382[17]
t = 0.25	0.0625	0.6461	0.603[17]
σ = 1.0	0.1250	1.3419	1.272[17]
	0.1875	2.3896	2.218[17]

The coded uniform tension algorithm was developed by curve fitting the data in [3]. This data is valid for $0.1 \leq r/(r+t) \leq 0.9$. NASCRAC™ does not prevent the user from analyzing r/(r+t) ratios outside this range, which is an oversight in the code that should be corrected using an error check on the input values. Validation of this uniform tension solution was based on comparison with [7] and [17]; therefore, the solution is valid to the extent that [7] and [17] are valid.

The 401 weight function solution was formulated for two r/t ratios: r/t = 5 and r/t = 10. The code permits all r/t ratios to be analyzed. For $r/t \leq 7.5$, the weight function solution for r/t = 5 is used and if r/t > 7.5, the solution for r/t = 10 is used to calculate K. NASCRAC™ does issue a warning in the output file informing the user of the weight function employed. Validation of the 401 weight function solution was not completed because a reference was not found. The bending solution in [3] could not be used as a reference for comparison with a linear stress distribution and the weight function solution because NASCRAC™ requires axisymmetric loads.

4.1.4.2 Configuration 402 (Circumferential Crack in a Solid Cylinder)

Figure 4.1.4.2-1 displays the geometry of configuration 402, *circumferential crack in a solid cylinder*. This solution was adapted from FLAGRO and is programmed for uniform tension loads only. The FLAGRO solution, which is based on [3], also includes only uniform tension loads although [3] presents a K solution for bending. A fatal error occurs during NASCRAC™ execution if a bending load is applied.

Representative V/V results are presented in Table 4.1.4.2-1. A comparison of the source code to equations in [3] indicated a very minor typographical error in cubed term of the G equation in the NASCRAC™ function *S402U*. The programmed coefficient is -0.1875 but should be -0.1815. This difference is not significant and thus the NASCRAC™ results listed in Table 4.1.4.2-1 are almost identical to the reference results. The reasonable agreement between NASCRAC™ and [3] validates this solution to the extent that [3] is valid.

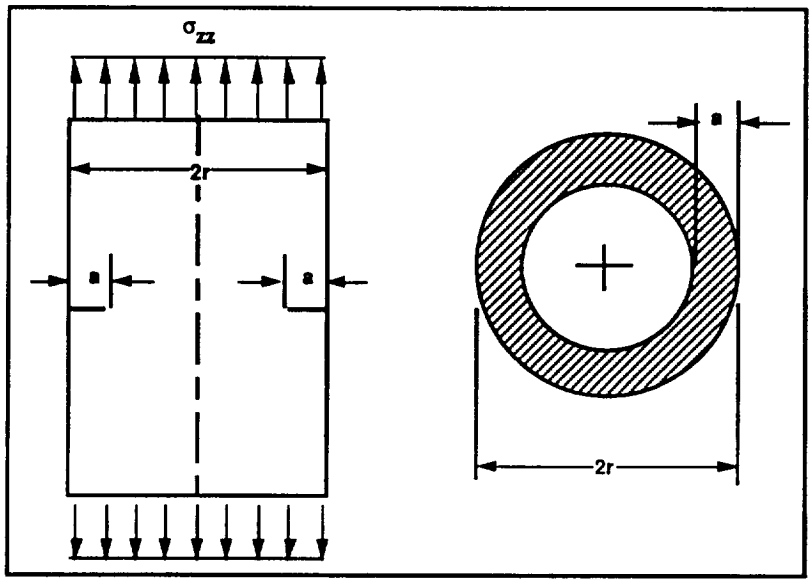

Figure 4.1.4.2-1. Geometry for Configuration 402, *Circumferential Crack in a Solid Cylinder*

Table 4.1.4.2-1. Representative Results for Configuration 402

PARAMETERS	a	$K_{NASCRAC^{TM}}$	$K_{[3]}$	K_{FLAGRO}
r = 1.0	0.05	0.142	0.143	0.143
σ = 0.3183	0.50	0.758	0.758	0.758
	0.95	25.229	25.230	25.229
r = 1.0	0.05	0.223	0.224	0.225
σ = 0.5	0.50	1.190	1.191	1.191
	0.95	39.630	39.631	39.630

4.1.4.3 Configuration 403 (Circumferential Crack (od) in a Hollow Cylinder)

The geometry for configuration 403, *circumferential crack (od) in a hollow cylinder*, is shown in Figure 4.1.4.3-1. The coded solution, which is based on a curve fit to the graphical solution of [3], is limited to $0.05 \le R_i/R_o \le 0.95$; however, the solution in [3] only contains results for $0.1 \le R_i/R_o \le 0.9$. NASCRAC™ permits other configurations (outside the $0.05 \le R_i/R_o \le 0.95$) to be input but issues a warning in the output file on the configuration page. This NASCRAC™ K solution, like 402, is only valid for uniform

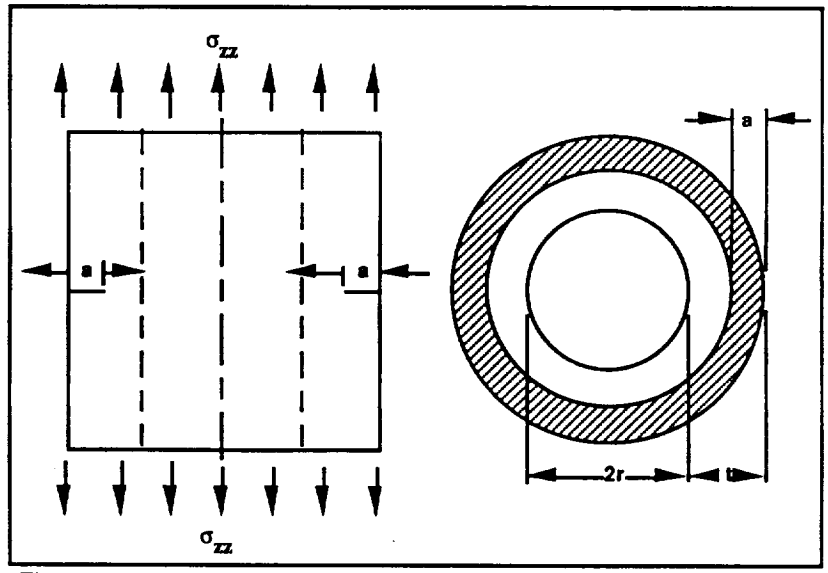

Figure 4.1.4.3-1. Geometry for Configuration 403, *Circumferential Crack (od) in a Hollow Cylinder*

tension even though [3] contains both a uniform tension and a bending solution. Comparative results from V/V simulations for 403 are shown in Table 4.1.4.3-1.

Table 4.1.4.3-1. Representative Results for Configuration 403

PARAMETER	a	$K_{NASCRAC^{TM}}$	$K_{[2]}$	$K_{[7]}$	$K_{[3]}$	K_{FLAGRO}
r = 2.0	0.25	1.018	0.978			0.978
t = 3.0	0.50	1.503	1.400		1.52	1.399
σ = 1.0	0.75	1.937	1.771			1.771
	1.00	2.374	2.156		2.39	2.156
	1.25	2.848	2.593			2.593
	1.50	3.399	3.123		3.45	3.123
	1.75	4.087	3.807			3.807
	2.00	5.010	4.753		5.01	4.753
	2.25	6.361	6.181			6.181
	2.50	8.611				8.661
r = 4.5	0.05	0.462	0.454	0.47		0.454
t = 0.5	0.10	0.714	0.666	0.72	0.71	0.666
σ = 1.0	0.15	0.980	0.857	1.00		0.857
	0.20	1.285	1.053	1.30	1.30	1.053
	0.25	1.646	1.276	1.67		1.277
	0.30	2.079	1.552	2.09	2.10	1.552
	0.35	2.613	1.929			1.929
	0.40	3.328	2.524		3.34	2.524
r = 4.0	0.1	0.650	0.636	0.66		0.636
t = 1.0	0.2	0.993	0.928	1.00	1.00	0.928
σ = 1.0	0.3	1.339	1.192	1.34		1.192
	0.4	1.721	1.468	1.70	1.70	1.468
	0.5	2.158	1.788	2.14		1.788
	0.6	2.670	2.191	2.64	2.64	2.191
	0.8	3.304	2.751			2.751
	0.9	4.189	3.652		4.17	3.652

The results in Table 4.1.4.3-1 verify and validate this solution. NASCRAC™ appears to be a more conservative solution compared to the graphical solution of [2] and NASA/FLAGRO. The validity of the solution is dependent on the validity of [2], [3], and [7]. Since [2] and [3] are well-known fracture references, the validity of this solution includes a high level of confidence. [7] provides additional support of validity. The NASCRAC™ 403 solution should be restricted to $0.1 \leq R_i/R_o \leq 0.9$ since it was obtained from [3], which was restricted to this range. Additionally, since the solution is only valid for uniform tension, an error check should be included in NASCRAC™ which would prevent non-uniform loads from being input.

4.1.4.4 Configuration 404 (Edge Crack in a Solid Circular Bar)

The NASCRAC™ K solution for configuration 404, *edge crack in a solid circular bar*, is a FLAGRO solution developed in [18]. The solution is a curve fit based on test results and a hypothetical crack front. The crack front model assumes that the crack is perpendicular to the bar at the free surface. This crack front, which results in higher K values when compared to a circular crack front whose center is at the surface of the bar, allows the crack to be specified

using the crack length at the crack centerline and the radius of the bar. Figure 4.1.4.4-1 displays this crack front definition. The crack front equations listed in this figure indicate that this geometry is mathematically undefined for a/D ≥ 0.5; however, test results in [18] included cracks with a/D ≤ 0.6 and the curve fit in FLAGRO was calculated for a/D ≤ 0.6. Thus, as a minimum, the NASCRAC™ 404 K solution needs to be limited to a/D ≤ 0.6. Preferably the limit should be set to a/D < 0.5. To impose this limitation, an error flag should be included in the code to detect a/D > 0.5 and the crack geometry should be clearly defined in the user's manual and onscreen during execution.

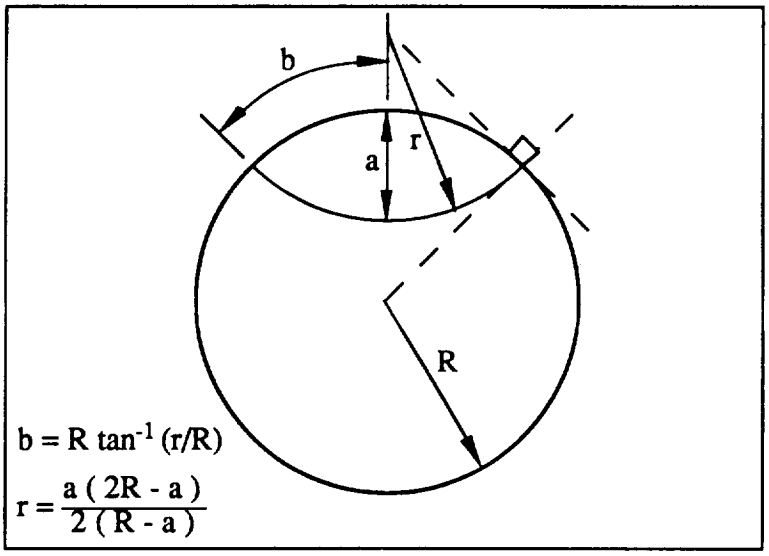

Figure 4.1.4.4-1. Geometry for Configuration 404, *Edge Crack in a Solid Circular Bar*

In configuration 404, K varies symmetrically along the crack front. Figure 4.1.4.4-2 depicts this varation, which is about 10%. In this figure, NASCRAC™ results are identical to the results in [18]. The NASCRAC™ results correspond to K on the centerline of the crack front. The NASCRAC™ documentation should discuss this variation and clarify that NASCRAC™ only calculates K at the midpoint of the crack, which is the minimum K along the crack front.

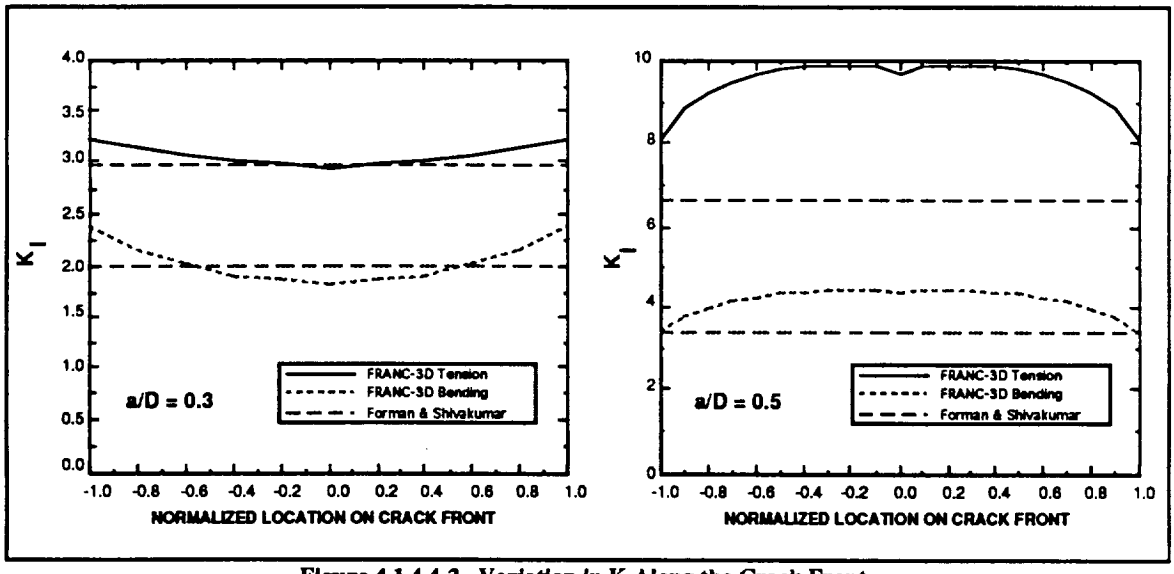

Figure 4.1.4.4-2. Variation in K Along the Crack Front

The case where a/D = 0.5 deserves special attention. From the crack front equations listed in Figure 4.1.4.4-1, the NASCRAC™ crack front would be straight for this case since a = R and therefore r = ∞. Several literature sources were available for straight front cracks; in particular, NASCRAC™ results for a/D = 0.5 were compared to [19], [20] and FRANC results. Table 4.1.4.4-1 lists results of these comparisons. [19] assumes a straight front crack whereas reference [20] assumes an elliptical crack front for small a/D ratios but gradually permits the crack front to become straight as the a/D ratio increases to 0.5. From Table 4.1.4.4-1 it is apparent that NASCRAC™ agrees well with [20] and FRANC for small a/D ratios (< 0.3) but diverges for larger a/D ratios. Compared to [19] (straight front crack) the NASCRAC™ computed K is consistently lower for all values of a/D. Additionally, FRANC results match [19] and [20] when a/D = 0.5 (straight edge cracks). These results suggest that NASCRAC™ may underestimate K by as much as 50% when a/D = 0.5, i.e., when a = R.

Table 4.1.4.4-1. Representative Results for Configuration 404

PARAMETERS	a	$K_{NASCRAC^{TM}}$	$K_{[20]}$	$K_{[19]}$	K_{FRANC}
D = 2R = 10.0	1.0	2.322	2.481		
$\sigma_t + \sigma_b$ = 1.0 + 1.0	2.0	3.527	3.835		
	3.0	4.950	5.793		4.77
	4.0	6.940	9.086		
	5.0	9.986	14.169		13.88
	6.0	15.108	22.537		
D = 2R = 5.0	0.5	0.878	0.940		
$\sigma_t + \sigma_b$ = 1.0 + 0.0	1.0	1.419	1.631	2.11	
	1.5	2.104	2.562		
	2.0	3.095	4.169	3.86	
	2.5	4.640	6.796		
	3.0	7.270	11.331	11.24	
D = 2R = 10.0	1.0	1.241	1.329		
$\sigma_t + \sigma_b$ = 1.0 + 0.0	2.0	2.006	2.306	2.98	
	3.0	2.976	3.623		2.95
	4.0	4.377	5.895	5.46	
	5.0	6.561	9.611		9.58
	6.0	10.281	16.025	15.90	

The variation of K along the crack front and the inability of NASCRAC™ to account for this variation will lead to errors during fatigue crack growth. The calculated K value in NASCRAC™ is frequently the minimum K along the crack front. Thus, during fatigue crack growth, the crack front at the free surface will have a higher rate of crack growth due to a higher K value. This variation in crack growth rate would lead to a change in crack front shape until K is uniform along the crack front. The uniform K crack front is bounded by the NASCRAC™ model and a straight front crack.

In summary, the 404 K solution in NASCRAC™ is valid for static checks of K where a/D < 0.5 if the crack front of interest adheres to the condition of intersecting the free surface perpendicularly. The geometry on which the NASCRAC™ curve fit model is based should be fully identified in the NASCRAC™ user's manual and a corresponding explanation of the geometry should be included onscreen. Warnings should be given when applying the model to fatigue crack growth and for a/D ≥ 0.5. Results suggest that for a/D ≥ 0.5, NASCRAC™ is nonconservative by as much as 50% compared to reference results for straight crack fronts. The V/V results did show that K values for a propagated crack front whose initial shape matched the NASCRAC™ model were bounded by the NASCRAC™ model and a straight crack front model.

4.1.5 500 SERIES RESULTS

The 500 series in NASCRAC™ represent buried, four degree-of-freedom cracks. Only one solution, configuration 502, *buried elliptical crack*, is available in this series. The geometry for configuration 502 is shown in Figure 4.1.5-1. Representative results from V/V studies are shown in Table 4.1.5-1. The FRANC results for larger geometries ($W_1 = 5.0$, $W_3 = 10.0$) in Table 4.1.5-1 compared well with the Irwin solution (see [4]) for a buried elliptical crack in an infinite body.

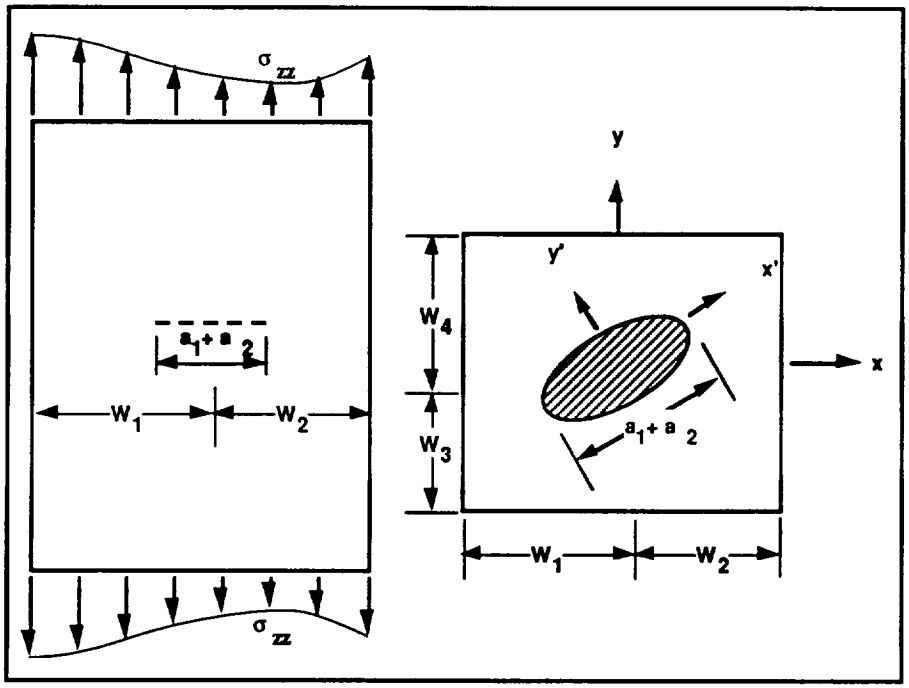

Figure 4.1.5-1. Geometry for Configuration 502, *Buried Elliptical Crack*

NASCRAC™ *K vs a* capability for configuration 502 is valid based on the comparisons with FRANC shown in Table 4.1.5-1. Differences do exist between NASCRAC™ and FRANC results but the general trends are the same and the differences are within 20%. Differences between NASCRAC™ and FRANC generally were more pronounced for the crack tips along the major axes of the ellipse (a_3 and a_4). For each of these cases, and especially for the non-uniform loadings, NASCRAC™ remained conservative with respect to FRANC. One minor mistake in the user's interface was observed: During the definition of the crack geometry, the program requests the final a_2 to a_1 ratio as input when, in fact, the final a_3 to a_1 ratio is required.

Table 4.1.5-1. Representative Results from Configuration 502

PARAMETERS	a_1	a_3	σ	$K_{NASCRAC^{TM}}$		K_{FRANC}	
	INCHES	INCHES	psi	K @ a_1	K @ a_3	K @ a_1	K @ a_3
$W_1 = W_2 = 5.0$ $W_3 = W_4 = 10.0$ $\theta = 0$ deg	1.0 1.25 1.5	2.0 2.5 3.0	UNIFORM 1.0	1.39 1.56 1.72	1.18 1.32 1.45	1.44 1.63 1.80	1.02 1.16 1.28
$W_1 = W_2 = 3.0$ $W_3 = W_4 = 4.0$ $\theta = 0$ deg	1.0 1.25 1.5	2.0 2.5 3.0	UNIFORM 1.0	1.41 1.61 1.82	1.21 1.39 1.63	1.45 1.66 1.89	1.03 1.18 1.34
$W_1 = W_2 = 3.0$ $W_3 = W_4 = 4.0$ $\theta = 120$ deg	1.0 1.25 1.5	2.0 2.5 3.0	UNIFORM 1.0	1.41 1.61 1.82	1.21 1.39 1.63	1.45 1.66 1.89	1.03 1.18 1.35
$W_1 = W_2 = 5.0$ $W_3 = W_4 = 10.0$ $\theta = 0$ deg	1.0	2.0	LINEAR 0.0-1.0	0.69, 0.69[1]	0.68, 0.50[2]	0.71, 0.71[1]	0.58, 0.43[2]
$W_1 = W_2 = 3.0$ $W_3 = W_4 = 4.0$ $\theta = 0$ deg	1.0	2.0	LINEAR 0.0-1.0	0.71 0.71[1]	0.84 0.37[2]	0.73, 0.73[1]	0.71, 0.32[2]
$W_1 = W_2 = 3.0$ $W_3 = W_4 = 4.0$ $\theta = 0$ deg	1.0	2.0	BI-LINEAR 0.0-1.0	0.64 0.77[1]	0.72 0.48[2]	0.66, 0.79[1]	0.61, 0.42[2]
$W_1 = W_2 = 3.0$ $W_3 = W_4 = 4.0$ $\theta = 120$ deg	1.0	2.0	LINEAR 0.0-1.0	0.65, 0.75[1]	0.81, 0.40[2]	0.69, 0.78[1]	0.69, 0.35[2]

1: K @ a_2 2: K @ a_4

4.1.6 600 SERIES RESULTS

NASCRAC™ includes three corner crack configurations in the 600 series: configurations 601, 602, and 605. These cracks each have two crack tips initially and hence two degrees-of-freedom.

The NASCRAC™ models for configurations 601 *corner crack from a hole in a plate*, and 602, *corner crack from a hole in a lug*, are similar. Both were derived from FLAGRO and neither incorporates a weight function. For each model, only simple loads may be applied (uniform tension and/or pin load for 601 and a pin load for 602). The V/V process for each of these models included literature sources and numerical analysis using FRANC and FLAGRO. V/V results from these configurations indicate that results from NASCRAC™ and the references (FRANC, FLAGRO, literature) are the same order of magnitude; however, NASCRAC™ differs non-conservatively from the references by 20-40%.

NASCRAC™'s *K vs a* capability for configuration 605, *corner crack in a plate*, was verified and validated using the literature and FRANC. The literature included references from Newman and Raju and from Kobayashi and Enetanya for uniform tension loads. The Kobayashi paper also included linear crack pressure loads. FRANC analyses were completed for both uniform and linear loads where the linear loads were a superposition of uniform tension and

bending loads across the thickness (W_2 dimension of the plate). The Kobayashi linear crack pressure load configuration and the FRANC linear load configuration are not equivalent load systems and hence cannot be compared.

4.1.6.1 Configuration 601 (Corner Crack from a Hole in a Plate)

The geometry for configuration 601, *corner crack from a hole in a plate*, is shown in Figure 4.1.6.1-1. A corresponding FRANC3D boundary element model is shown in Figure 4.1.6.1-2. Figures 4.1.6.1-3 through 4.1.6.1-7 show results from the 601 computations. In each of these figures K's are plotted versus the corresponding crack length. Figures 4.1.6.1-3 and 4.1.6.1-5 indicate that NASCRAC™ does not agree with FLAGRO or FRANC when the applied load consists of a uniform stress. When the load is a pin load and the hole diameter is large compared to the crack length, NASCRAC™ is in agreement with the references (see Figures 4.1.6.1-4 and 4.1.6.1-6) for small crack lengths. Figure 4.1.6.1-7 shows results from a pin load case where the hole diameter was small compared to the crack length. These results indicate that NASCRAC™ may have trouble predicting the stress intensity factor along the bore of the hole (crack tip a_2). This result may be indicative of NASCRAC™ handling of the stress concentration caused by the smaller radius hole or, to a lesser degree, the distribution of the load in FRANC

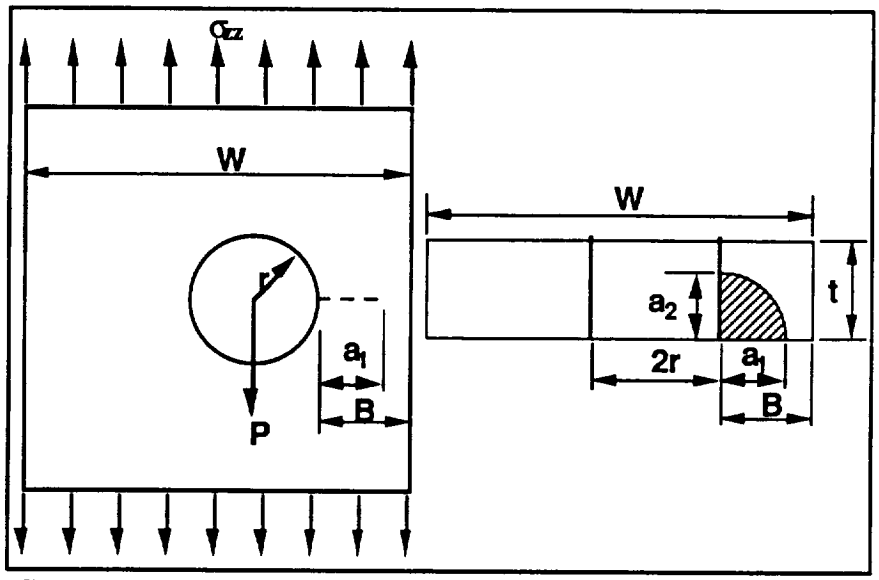

Figure 4.1.6.1-1 Geometry for Configuration 601, *Corner Crack from a Hole in a Plate*.

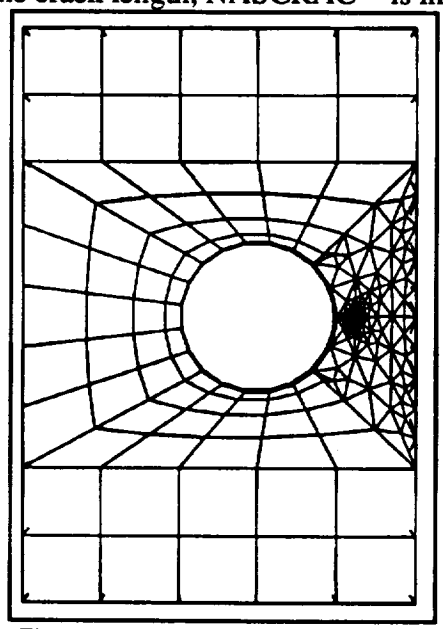

Figure 4.1.6.1-2 Typical FRANC Boundary Element Modelfor Configuration 601

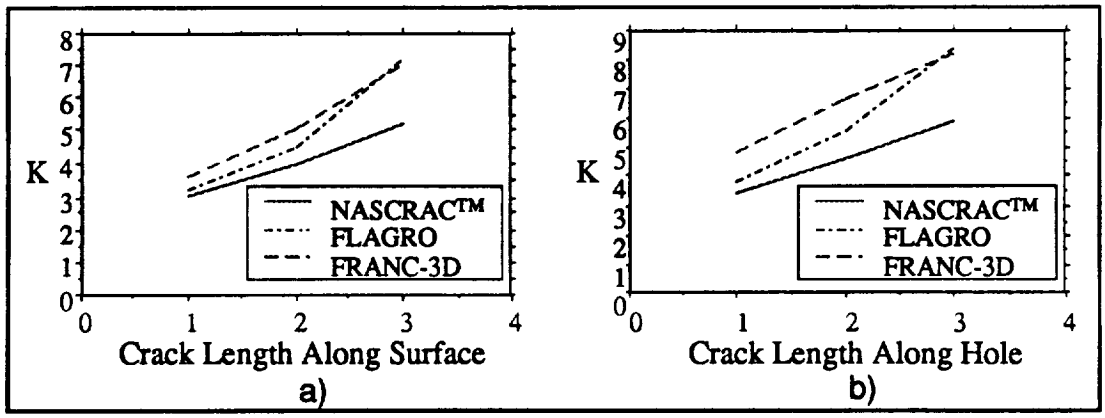

Figure 4.1.6.1-3. Configuration 601 in Uniform Tension, a/c = 1, r = 4
a) K at Crack Tip into Plate, b) K at Crack Tip on Surface

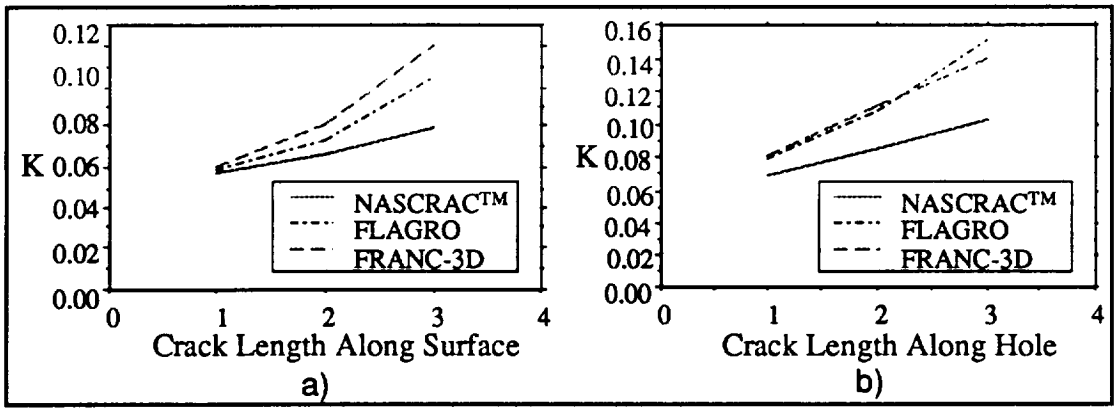

Figure 4.1.6.1-4. Configuration 601 with Pin Load, a/c = 1, r = 4
a) K at Crack Tip into Plate, b) K at Crack Tip on Surface

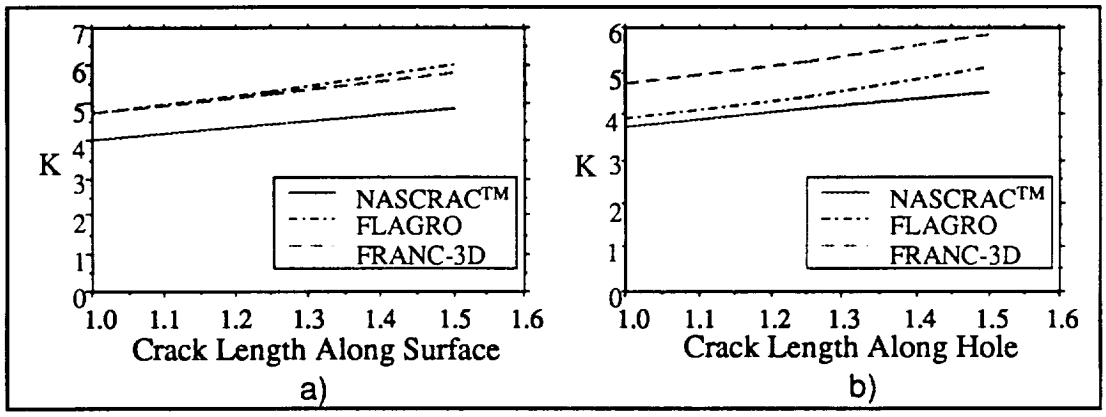

Figure 4.1.6.1-5. Configuration 601 in Uniform Tension, a/c = 0.5, r = 4
a) K at Crack Tip into Plate, b) K at Crack Tip on Surface

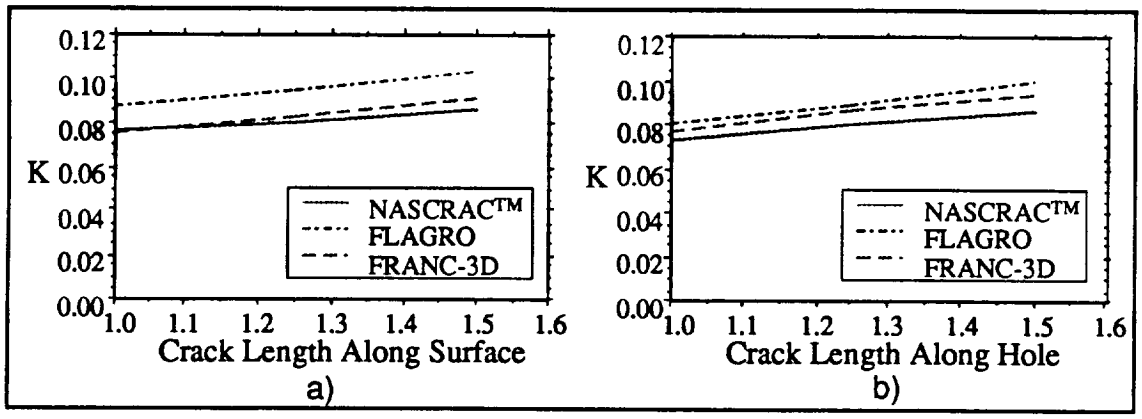

Figure 4.1.6.1-6. Configuration 601 with Pin Load, a/c = 0.5, r = 4
a) K at Crack Tip into Plate, b) K at Crack Tip on Surface

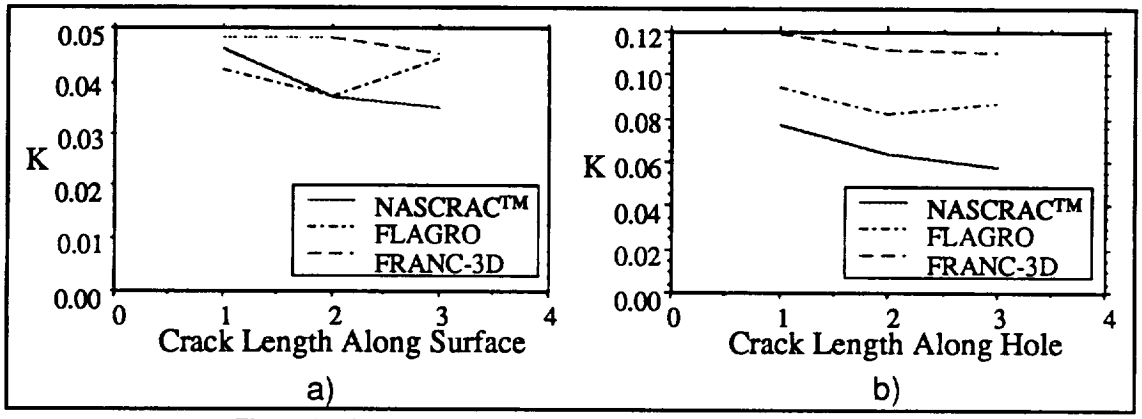

Figure 4.1.6.1-7. Configuration 601 with Pin Load, a/c = 1, r = 0.5
a) K at Crack Tip into Plate, b) K at Crack Tip on Surface

The trends displayed in the NASCRAC™ results appear to agree with FLAGRO and FRANC. For example, in Figure 4.1.6.1-7, K at crack tip a_1 decreases as the crack length increases. This decrease is reflected in all three sets of the plotted results. Another trend reflected in the NASCRAC™ calculations is the percent change in the K values as the crack length increases. This change is reflected in the five figures above. In a majority of the cases, the absolute difference between NASCRAC™ and FRANC is nearly constant as the crack length increases. A final trend of significance is the relative difference between a_1 and a_2. In general, the NASCRAC™ differences are less than those predicted by FRANC. For example, in Figure 4.1.6.1-4 above, the ratio of K at a_2 to K at a_1 in NASCRAC™ varies from 1.11 to 1.16 whereas in FRANC the ratio varies from 1.17 to 1.33.

The differences between NASCRAC™ and FLAGRO were unexpected since the NASCRAC™ model was adapted from FLAGRO. A combination of two factors contribute to these differences. The first factor is a minor error in the NASCRAC™ source code. This error is displayed in the source code listing in Figure 4.1.6.1-8. FLAGRO uses 2B in the denominator of the highlighted line whereas NASCRAC™ uses W. If 2B = W, which is the case for a centered hole, the error disappears. In a trial run, by changing W in NASCRAC™ to 2B, the computed K

at tip a_2 increased from 3.40 to 3.47 and the computed K at tip a_1 increased from 3.05 to 3.12 for B = 8.0 and W = 12.0. The second factor that causes a difference between NASCRAC™ and FLAGRO is NASCRAC™'s calculation of an RMS averaged K at each crack tip using Gaussian quadrature. RMS averaging computes the K of interest by summing weighted values of K from the entire crack surface. FLAGRO, conversely, directly calculates the two K's (one at 0 degrees and one at 80 degrees) using equations identical to those in NASCRAC™ other than the minor error shown in Figure 4.1.6.1-8. Based on the FRANC results, the applicability of the RMS logic in NASCRAC™ may not be valid even though the logic is verified. One final difference can be documented between NASCRAC™ and FLAGRO: FLAGRO accepts bending loads but NASCRAC™, when adapting the solution, omitted bending loads and only permits uniform tension and pin loads.

NASCRAC™

```
FUNCTION CC02(PHI)
   .
Y = D/W
V = A/T
XL=.5*PI*SQRT(V)*(D+C)/(W-C)
FW=SQRT(SIN(BETA)/(BETA*COS(XL)*COS(.5*PI*Y)))
   .
RETURN
END
```

FLAGRO

```
SUBROUTINE SICC02(MODE,LOCN,CREMEN,SMIN4,SMAX4,SYLD1,CAYC1,
&                 A,AOC,NSQUAN,IHDSQ,META,SR,DELTAK,CAYMAX,
&                 F0,F1,F2,F3,Q,NJOB,NETMSG,IACMSG,IYZMSG,*,*)
   .
GWCOEF=(DSIN(BETA)/BETA)/DCOS(PIOVR2*D/W)
GW=DSQRT(GWCOEF/DCOS(PIOVR2*DSQRT(AOT)*(D+C)/(2D0*E-C)))
   .
RETURN
END
```

Figure 4.1.6.1-8. ***CC02*** **Source Code in NASCRAC™ and FLAGRO Highlighting Difference in Codes**

4.1.6.2 Configuration 602 (Corner Crack from a Hole in a Lug)

The geometry for configuration 602, *corner crack from a hole in a lug*, is shown in Figure 4.1.6.2-1. A corresponding FRANC3D boundary element model is shown in Figure 4.1.6.2-2. The NASCRAC™ 602 K solution computes stress intensity factors of the same order of magnitude as FLAGRO and FRANC; however, the NASCRAC™ values are significantly non-conservative (by 20-35% for large diameter holes and 50-100% for small diameter holes) compared to FRANC and slightly less than the FLAGRO results, even though the NASCRAC™ solution was adapted from FLAGRO. This slight discrepancy is caused by two factors: 1) NASCRAC™'s calculation of an RMS averaged K at each crack tip using Gaussian quadrature as compared to FLAGRO's direct calculation of K at specific angles (0 degrees, 80 degrees) along the

crack front, and 2) a typographical error in the equation for G_0 in the function *SICC03*. This error, which is simply a transposition of two digits, is shown in Figure 4.1.6.2-3.

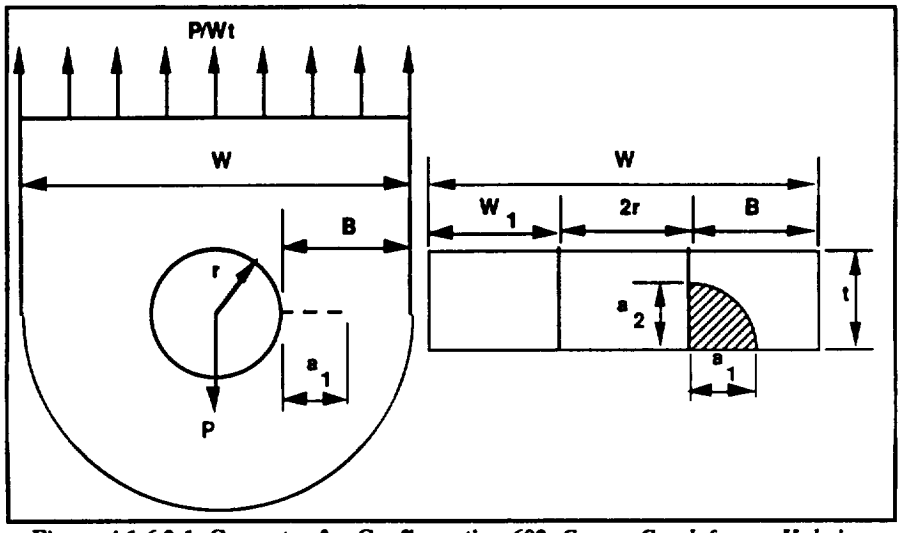

Figure 4.1.6.2-1. Geometry for Configuration 602, *Corner Crack from a Hole in a Lug*

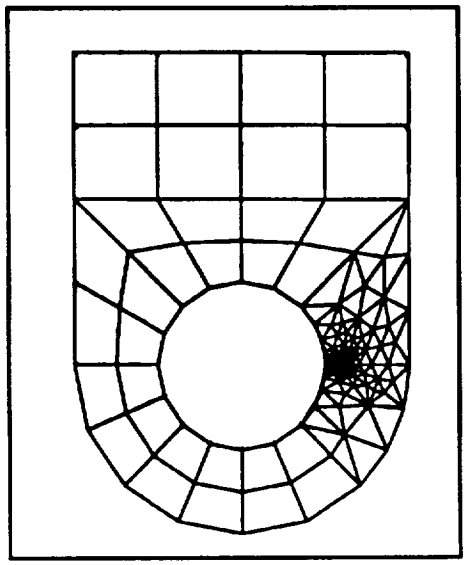

Figure 4.1.6.2-2 Typical FRANC Boundary Element Model for Configuration 602

NASCRAC™

```
FUNCTION CC03(PHI)
   .
F0Z=0.7071+Z*(.7584+Z*(.3415+Z*(.642+.9196*Z)))
F1Z=Z*(.078+Z*(.7588+Z*(-.4293+Z*(.0644+Z*.651))))
G0=F0Z/DS
   .
F0=(0.5*G0*Y + G1)*GW
CC03=F0
   .
RETURN
END
```

FLAGRO

```
SUBROUTINE SICC03(MODE,LOCN,CREMEN,SMIN4,SMAX4,SYLD1,CAYC1,
&                 A,AOC,NSQUAN,IHDSQ,META,SR,DELTAK,CAYMAX,
&                 F0,F1,F2,F3,Q,NJOB,NETMSG,IACMSG,IYZMSG,*,*)
   .
CAPG0  = (.7071D0 + Z*(.7548D0 + Z*(.3415D0 + Z*(.642D0
              + Z*.9196D0 ) ) ) / DENOM
   .
RETURN
END
```

Figure 4.1.6.2-3. ***CC03*** **Source Code in NASCRAC™ and FLAGRO Highlighting Difference in Codes**

Figures 4.1.6.2-4 through 4.1.6.2-6 display plots of K values versus the corresponding crack lengths for configuration 602. In all cases, the applied pin load was 1 lb_f. The figures show that NASCRAC™ and FLAGRO are in better agreement than they were for configuration 601. Only in the case of the small radius hole (Figure 4.1.6.2-6) is there appreciable difference at the crack tip along the bore of the hole (crack tip a_2). This is probably a result of FLAGRO's point solution versus NASCRAC™'s averaged solution.

In all the cases presented in Figures 4.1.6.2-4 through 4.1.6.2-6, NASCRAC™ is non-conservative compared to FRANC. This non-conservativism increases as the crack length increases and is more pronounced at crack tip a_2. Since FRANC is a refined finite element program adept at handling the stress fields around the hole, the FRANC results provide a higher level of confidence.

The 602 results plotted in Figures 4.1.6.2-4 through 4.1.6.2-6 show that relative differences in K for various crack lengths are similar in NASCRAC™ compared to FRANC and FLAGRO. For example, in Figure 4.1.6.2-4a (crack tip a_1) the percent increase in K from $a_1 = 1$ to $a_1 = 2$ is 23% in NASCRAC™ compared to 26% for FLAGRO and 33% for FRANC. Similarly, for crack tip a_2 (Figure 4-.1.6.2-4b), the percent increase in K from $a_2 = 1$ to $a_2 = 2$ for NASCRAC™ is 33% compared to 37% for FLAGRO and 36% for FRANC.

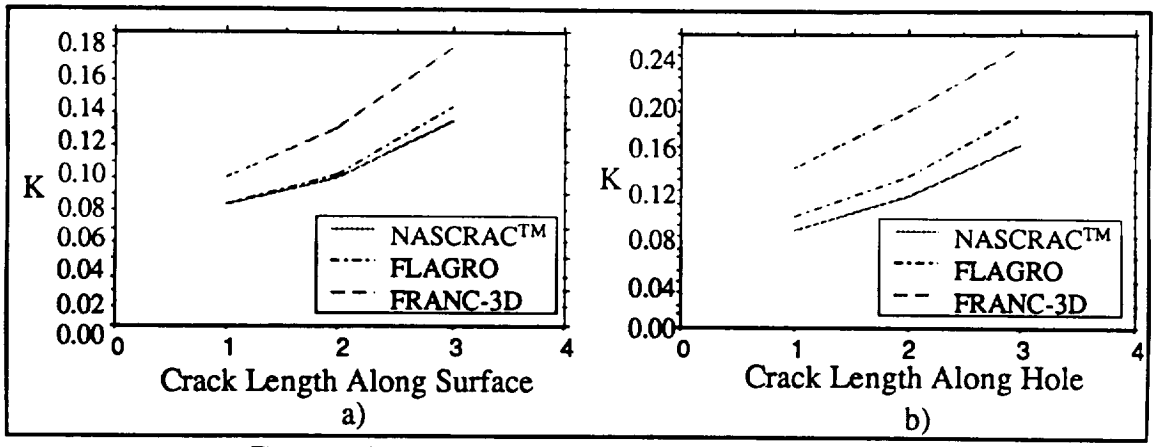

Figure 4.1.6.2-4. Configuration 602 with Pin Load, a/c = 1, r = 4
a) K at Crack Tip into Plate, b) K at Crack Tip on Surface

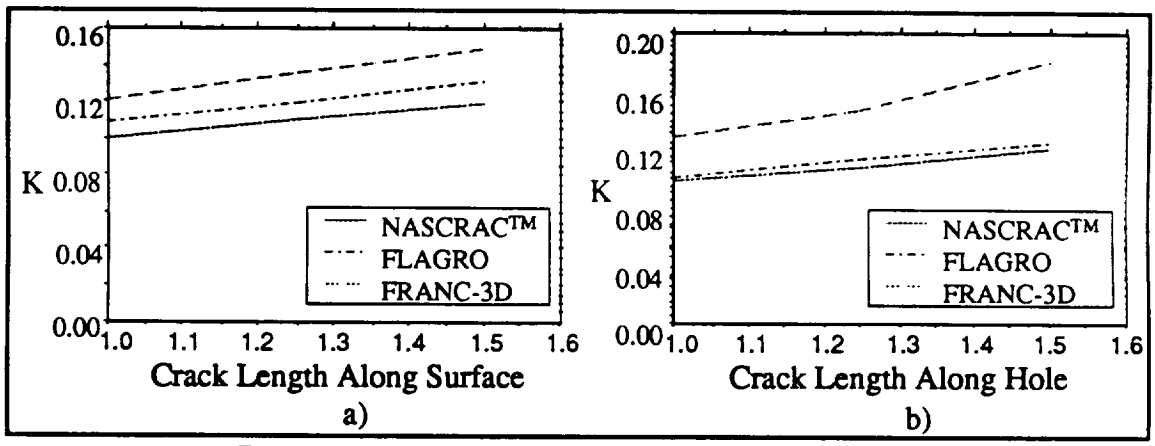

Figure 4.1.6.2-5. Configuration 602 with Pin Load, a/c = 0.5, r = 4
a) K at Crack Tip into Plate, b) K at Crack Tip on Surface

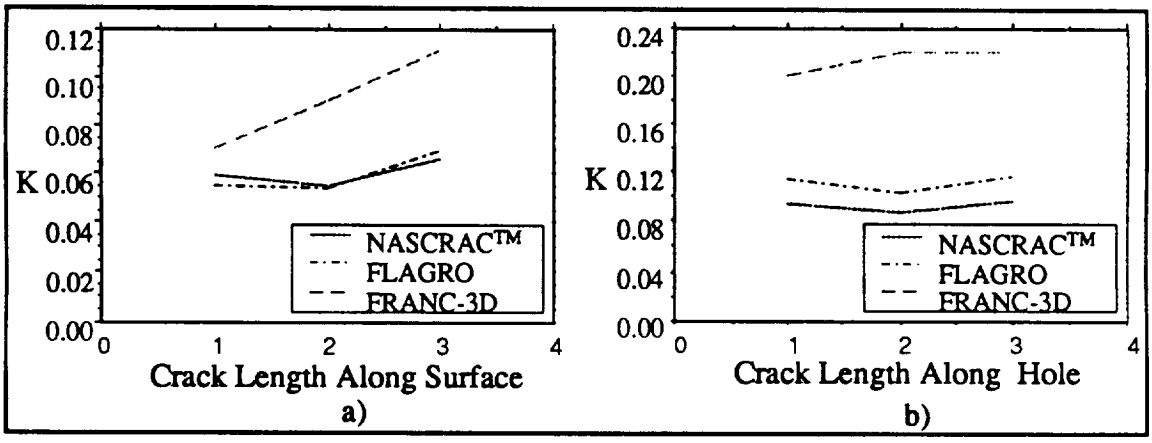

Figure 4.1.6.2-6. Configuration 602 with Pin Load, a/c = 1, r = 0.5
a) K at Crack Tip into Plate, b) K at Crack Tip on Surface

4.1.6.3 Configuration 605 (Quarter Elliptical Corner Crack in a Plate)

Figure 4.1.6-3-1 displays the geometry for configuration 605, *quarter-elliptical corner crack in plate*. 605 V/V results are presented in Figures 4.1.6.3-2 through 4.1.6.3-4. Figures 4.1.6.3-2 and 4.1.6.3-3 present three cases. Case 1 consists of W_1 = 20.0 and W_2 = 2.0. Case 2 consists of W_1= 10.0 and W_2 = 0.8. The final geometry, case 3, consists of W_1 = 10.0 and W_2 = 0.2. Figure 4.1.6-3-1 defines W_1 and W_2. Figure 4.1.6.3-2 displays plots of *K vs a/W* from NASCRAC™, FLAGRO, FRANC, and [21] for three different crack geometries subjected to uniform tension. These results indicate that NASCRAC™ calculates reasonable values of K for uniform tension loads. In case 1 where NASCRAC™'s K value at a_1 is non-conservative, the maximum difference is less than 15%. As the crack becomes smaller (cases 2 and 3), the difference between NASCRAC™ and the references becomes smaller. For K at a_2, NASCRAC is consistently conservative. NASCRAC™ does issue a warning when a_2/W_2 exceeds 0.6 which states that the accuracy limitations of the solution have been exceeded; thus, the non-conservative results for K at a_1 occur beyond the limitations of the solution. The actual warning issued is for a_1/W_1 but this warning is incorrect. The warning should reference a_2/W_2 for the cases studied.

Figure 4.1.6.3-3 presents *K vs a/W* results from NASCRAC™ and [22] for the three crack geometries subjected to a linear crack face pressure. This figure indicates that reasonable agreement between NASCRAC™ and [22] exists for this loading at a_1 but not at a_2. The disagreement at a_2 is due to finite width effects. The solution in [22] is for an semi-infinite plate; hence, the NASCRAC™ a_2 results are more reasonable because K should increase as a_2 approaches the plate edge.

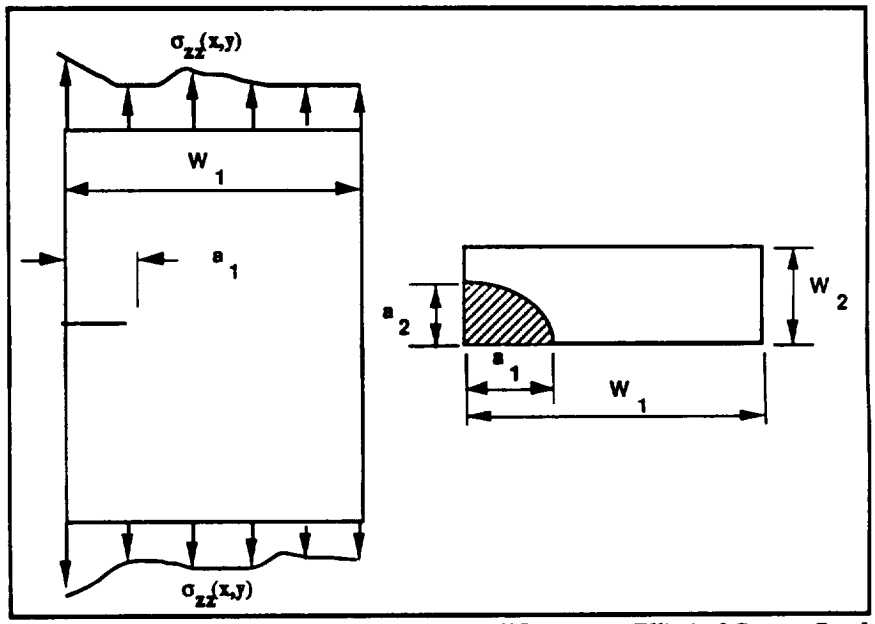

Figure 4.1.6.3-1. Geometry for Configuration 605, *Quarter-Elliptical Corner Crack in a Plate*

A final validation analysis of the 605 K solution was completed for a bending load across the width. This analysis was completed by comparison to FRANC for a plate width W_1 = 10", a plate thickness W_2 = 0.8", and a constant crack aspect ratio a_2/a_1 = 0.4. The load decreased linearly from 1 ksi at the cracked edge to 0. FRANC K results for this geometry are shown in Figure 4.1.6.3-4. In this figure, crack tip a_2 (along the plate thickness) corresponds to 0 on the x-axis and crack tip a_1 (along the plate width) corresponds to 1 on the x-axis. A comparison of these

graphical results and corresponding NASCRAC™ results is tabulated in Table 4.1.6.3-1. These tabulated results indicate that NASCRAC™ and FRANC are in good agreement for bending loads; therefore, these results verify the NASCRAC™ 605 K solution for bending in the plane of the plate (about the y-axis).

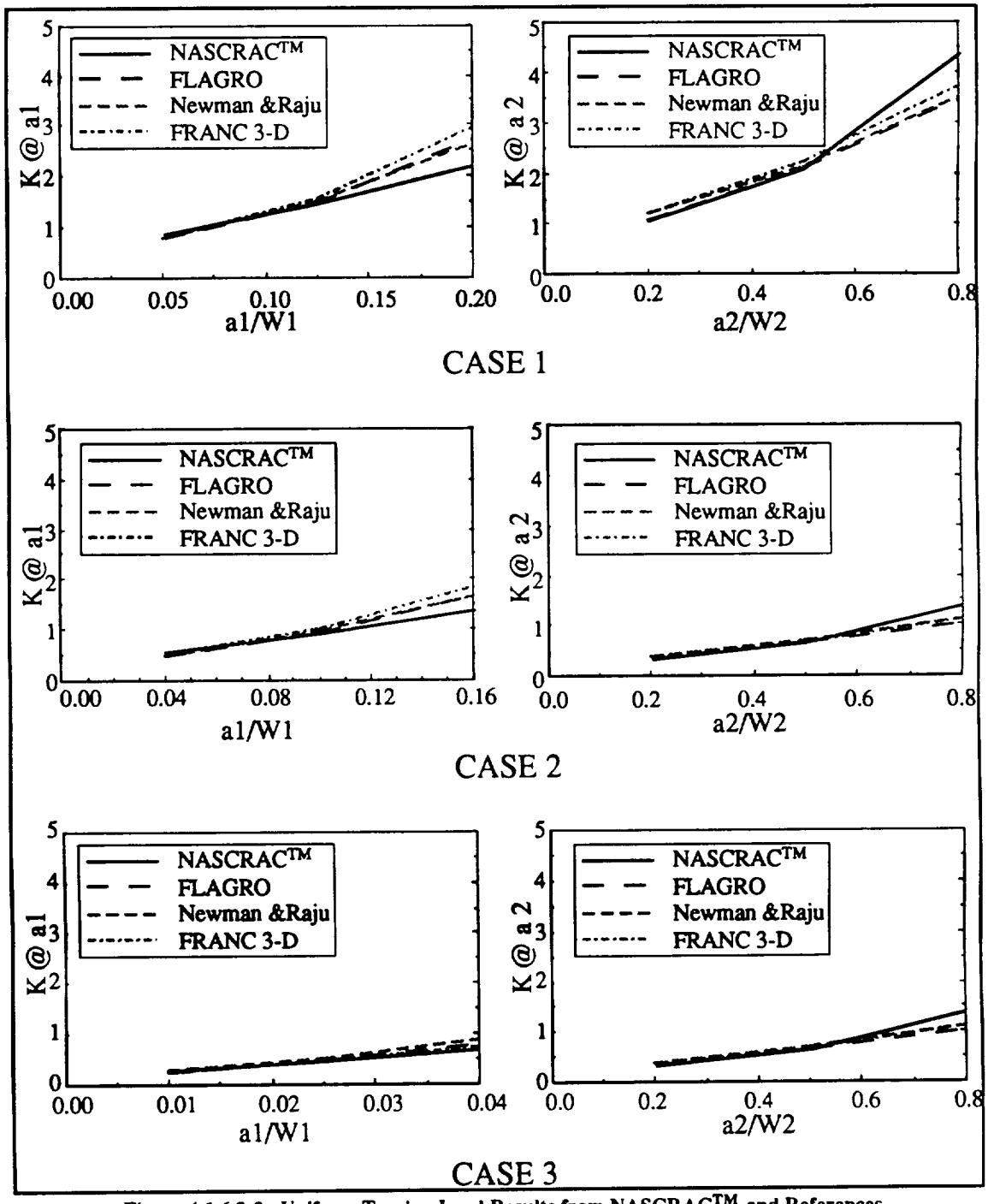

Figure 4.1.6.3-2. Uniform Tension Load Results from NASCRAC™ and References

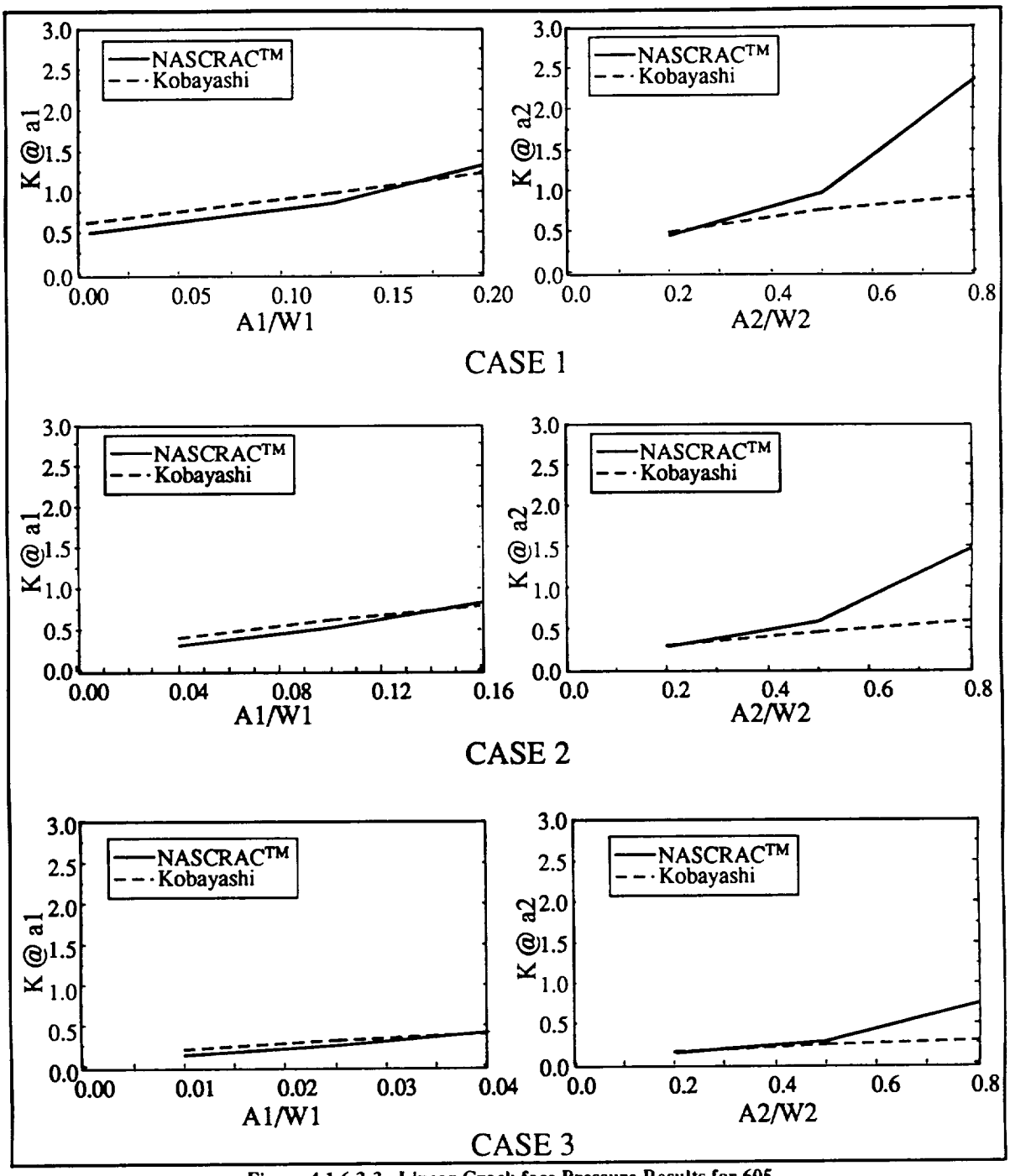

Figure 4.1.6.3-3. Linear Crack face Pressure Results for 605

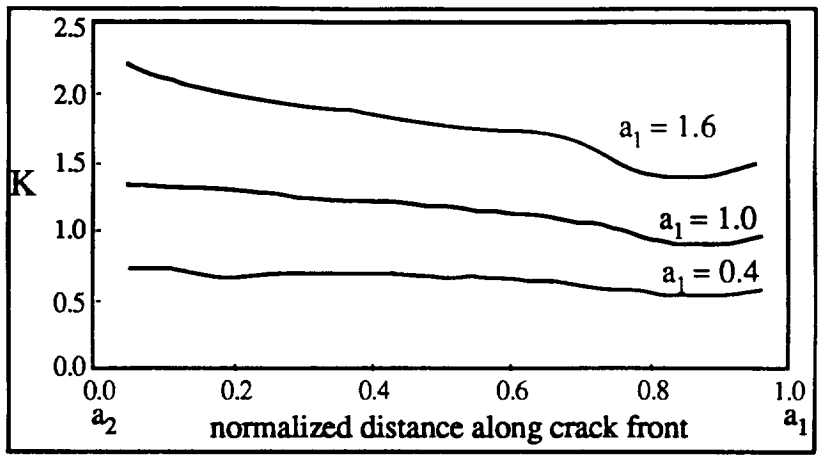

Figure 4.1.6.3-4. FRANC Computed K Distribution for Configuration 605 with $W_1 = 10.0$, $W_2 = 0.8$, $a_2/a_1 = 0.4$ and a Linearly Decreasing Load across W_1 from 1 ksi to 0

Table 4.1.6.3-1. Comparative Results for Configuration 605 Subjected to a Bending Load across the Plate Width

CRACK LENGTH a_1	K @ a_1		CRACK LENGTH a_2	K @ a_2	
	NASCRAC™	FRANC		NASCRAC™	FRANC
0.4	0.53	0.52	0.16	0.67	0.72
1.0	0.87	0.91	0.40	1.28	1.32
1.6	1.25	1.49	0.64	2.61	2.20

In summary, the NASCRAC™ 605 K solution is reasonable for uniform tension loads, crack face pressure loads, and bending loads across the width (W_1) of the plate. The K values at a_1 (along the width of the plate) are consistently in agreement with the references and hence can be used with a higher level of confidence than the values at a_2 (along the plate thickness).

4.1.7 700 SERIES RESULTS

The four 700 series *K vs a* solutions in NASCRAC™ simulate surface cracks using semi-elliptical crack models. These four solutions are based on the same weight function. This function was originally developed for configuration 703, a semi-elliptical (circumferential) surface crack in a cylinder. NASCRAC™ and the references were in agreement for both configurations 703 and 705, a semi-elliptical surface crack in a sphere. The only problem related to these configurations was the potential for a through crack to develop without detection by NASCRAC™. In contrast, the K results for configurations 702 and 704 exhibited differences compared to the references, especially at the surface crack tip (a_2). These differences are apparently due to RMS averaging.

4.1.7.1 Configuration 702 (Semi-Elliptical Surface Crack in a Plate)

Figure 4.1.7.1-1 displays the geometry for configuration 702, *semi-elliptical surface crack in a plate*. Several literature sources were available for the analysis of this configuration. Additionally, unpublished results from a round-robin study conducted by NASA/MSFC were available. The primary literature source was [23], which described an empirical K equation for

surface cracks. The results, shown in Figures 4.1.7.1-2 through 4.1.7.1-9, indicate that the NASCRAC™ K model at the crack tip into the plate (crack tip a_1) is valid for the case of uniform tension (Figure 4.1.7.1-2). Figures 4.1.7.1-3 through 4.1.7.1-5 and Figure 4.1.7.1-9 indicate that the NASCRAC™ model for crack tip a_1 in bending for crack tip to thickness ratios $a_1/t \leq 0.5$. These same figures show that NASCRAC™ differs from [23] at a_1 for bending when $a_1/t > 0.5$. For these cases, the reference values are believable because crack tip a_1 is in a region of compressive stresses and hence a reduced or negative K value is expected. The trends shown by NASCRAC™ for the bending cases appear reasonable. As the crack tip extends into the region of compressive stress, the value of K is less. Additionally, as the crack becomes more circular (a/c increases) the value of K at a_1 decreases. The combined bending and tension curves in Figures 4.1.7.1-6 through 4.1.7.1-8 show similar trends for crack tip a_1, i.e., agreement between NASCRAC™ and [23]is reasonable for small a_1/t ratios but more disagreement occurs as a_1/t approaches 0.8. For crack tip a_2, along the surface of the plate, NASCRAC™ was consistently non-conservative versus the references for both bending and combined bending and tension (Figures 4.1.7.1-6 through 4.1.7.1-8). NASCRAC™ also exhibited an unexpected trend for the cases of linear and non-linear bending, as shown in Figures 4.1.7.1-3 through 4.1.7.1-5 and 4.1.7.1-7. In these figures the K value at a_2 (along the surface) decreased as the crack length increased. This result is unexpected because this region incurs the maximum tensile stress.

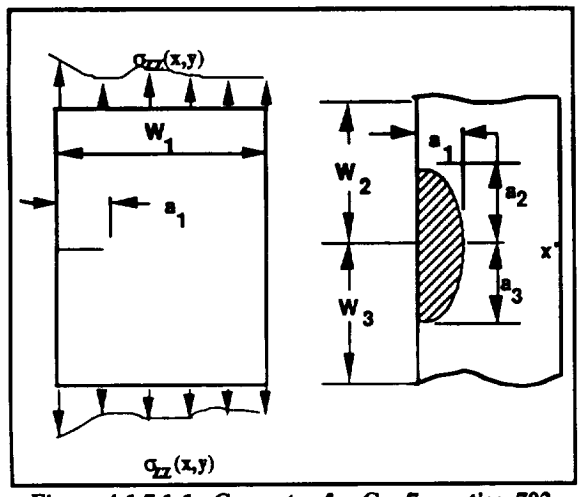

Figure 4.1.7.1-1. Geometry for Configuration 702, *Semi-Elliptical Surface Crack in a Plate*

RMS averaging causes the disagreement between NASCRAC™ and the references. RMS averaging computes K by summing weighted values of K over the entire crack surface. Thus, if part of the crack lies in a region of compressive or reduced tensile stresses, the averaged value of K at the crack tip of interest is less than a point calculation of the same K. This situation occurs in configuration 702 when bending loads are applied. At crack tip a_1, which is the tip into the plate, K should decrease as a_1 becomes large, i.e., as a_1 propagates into the region of compressive stress. This behavior is observed in the [23] results plotted in Figures 4.1.7.1-3 through 4.1.7.1-9. As a_1 propagates into the compressive or reduced tensile (for combined bending and tension) region, NASCRAC™ does a poor job of following the [23] results because the NASCRAC™ computed K value is being influenced by the tensile stresses near the surfaces of the crack. Converse logic applies to crack tip a_2. Here, the crack tip remains in a region of high tensile stress and thus K should increase in value as the crack length increases. This behavior can be seen in the [23] results plotted in Figures 4.1.7.1-3 through 4.1.7.1-9. These same figures show that the NASCRAC™ computed K at a_2 begins to flatten out or decrease with increasing crack length . This unexpected trend in the NASCRAC™ results is caused by the influence of compressive stresses in the a_1 region of the crack surface.

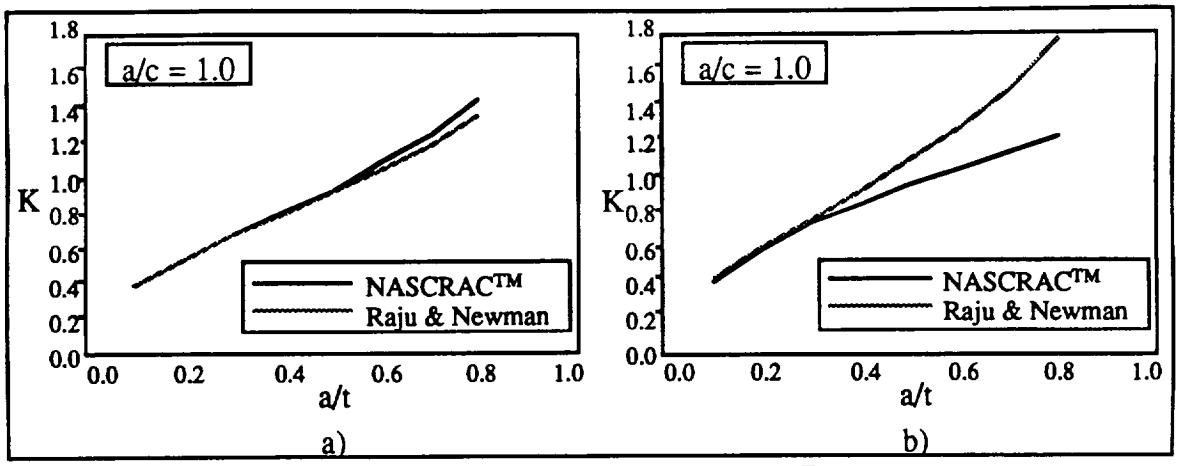

Figure 4.1.7.1-2. Configuration 702 in Uniform Tension
a) K at Crack Tip into Plate b) K at Crack Tip on Surface

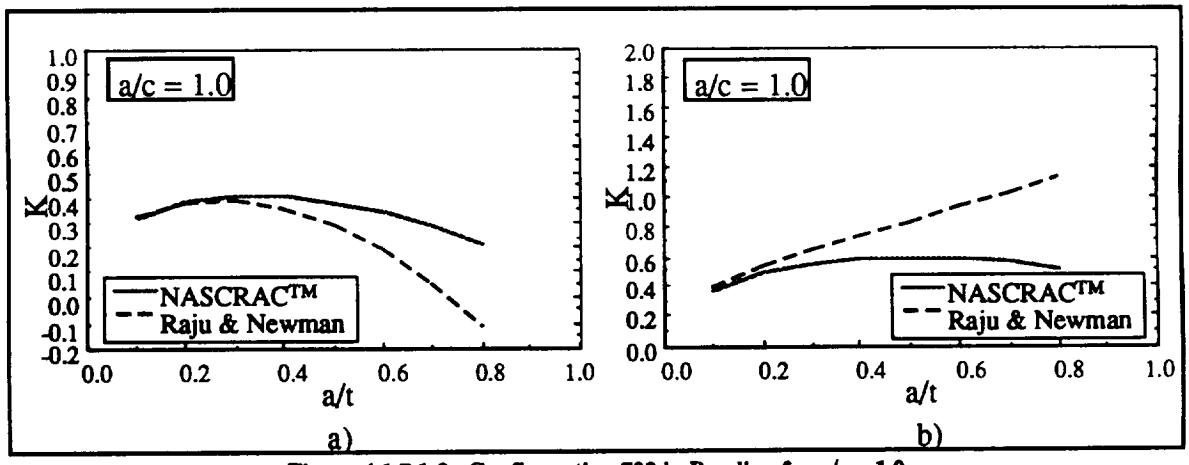

Figure 4.1.7.1-3. Configuration 702 in Bending for a/c = 1.0
a) K at Crack Tip into Plate b) K at Crack Tip on Surface

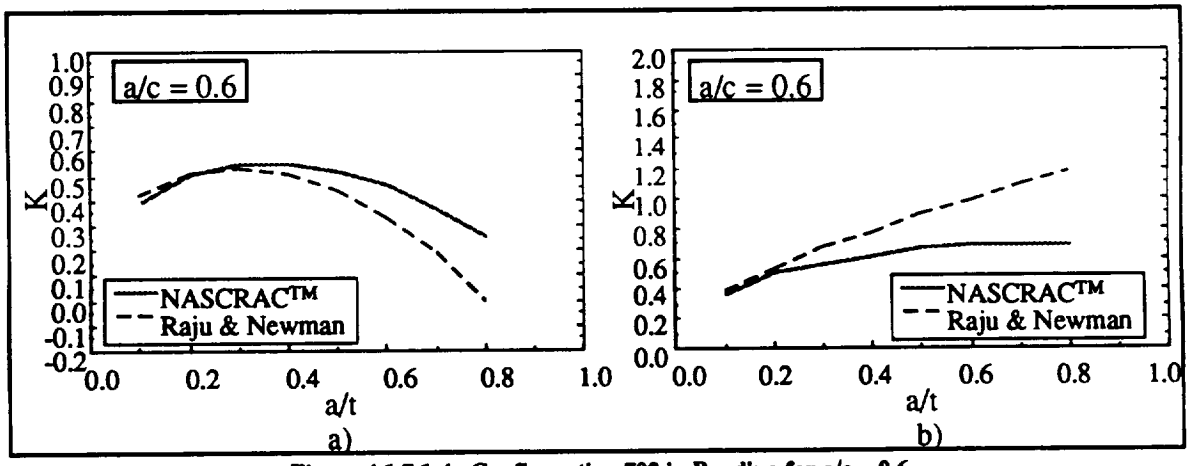

Figure 4.1.7.1-4. Configuration 702 in Bending for a/c = 0.6
a) K at Crack Tip into Plate b) K at Crack Tip on Surface

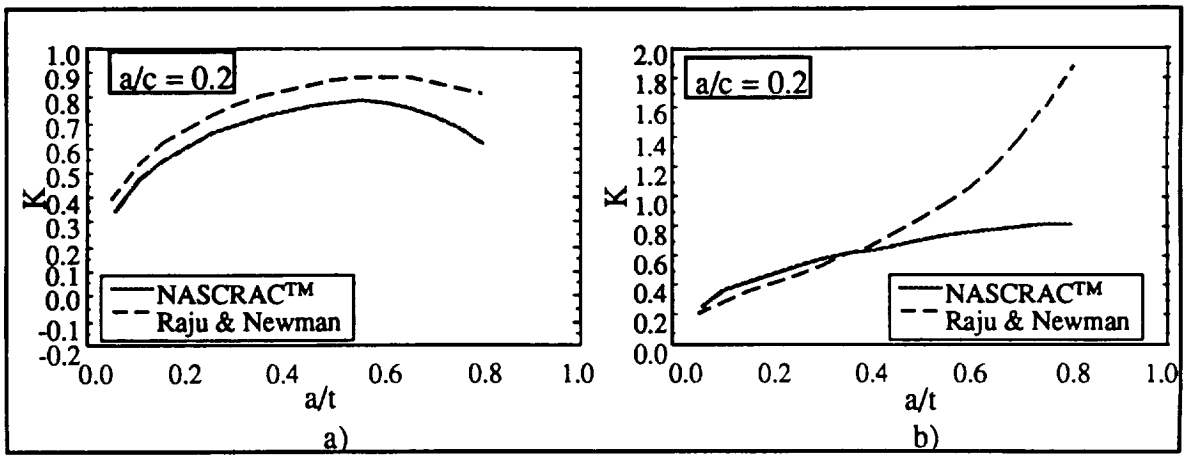

Figure 4.1.7.1-5. Configuration 702 in Bending for a/c = 0.2
a) K at Crack Tip into Plate b) K at Crack Tip on Surface

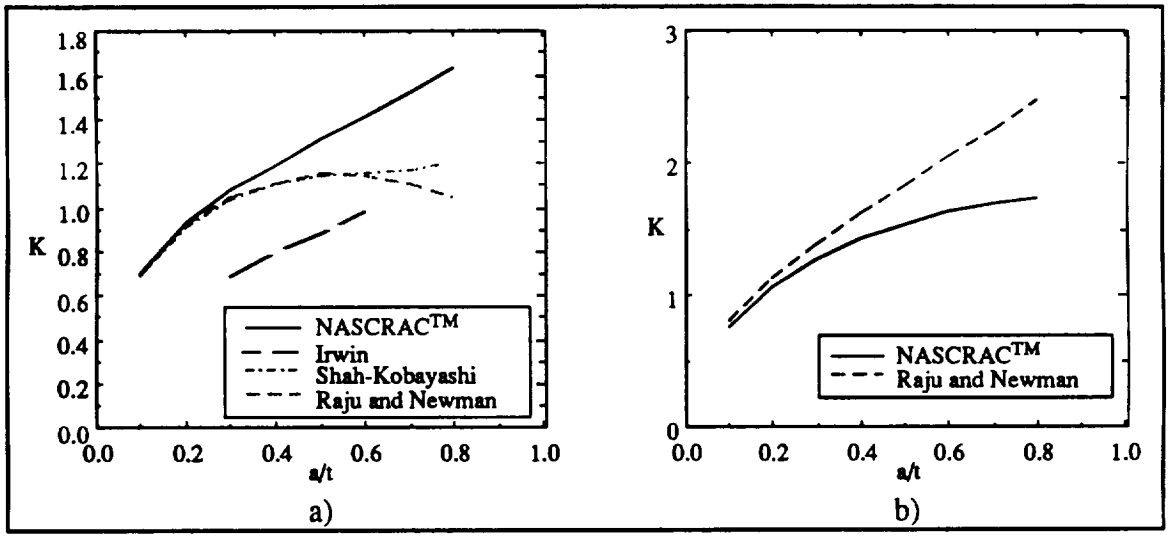

Figure 4.1.7.1-6. Configuration 702 in Combined Bending and Tension for a/c = 1
a) K at Crack Tip into Plate, b) K at Crack Tip on Surface

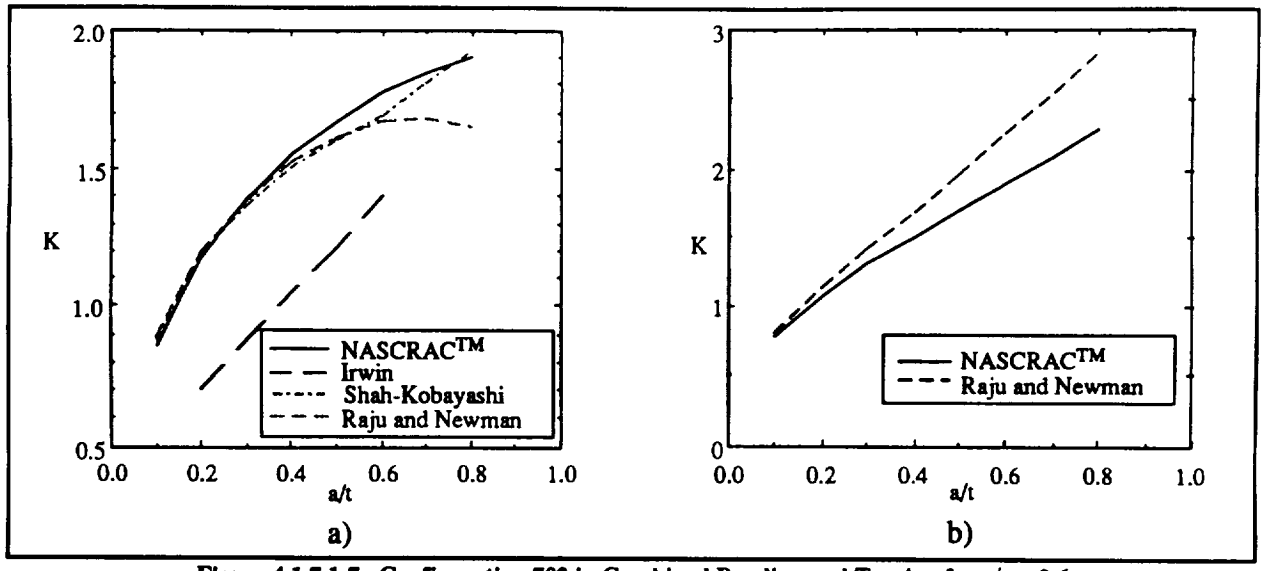

Figure 4.1.7.1-7. Configuration 702 in Combined Bending and Tension for a/c = 0.6
a) K at Crack Tip into Plate, b) K at Crack Tip on Surface

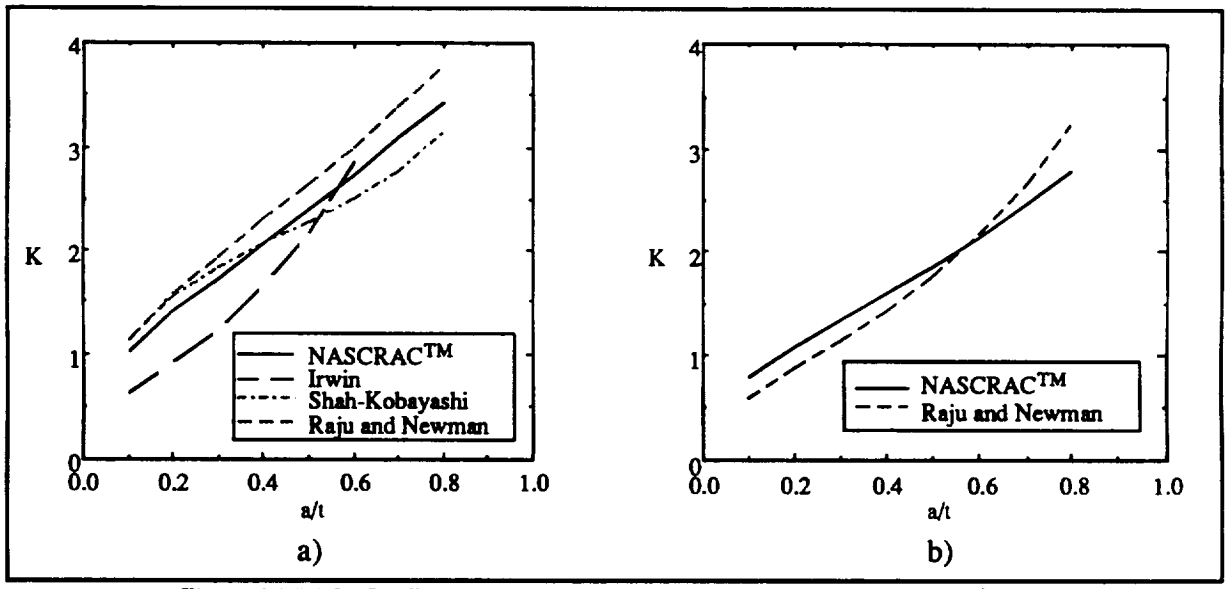

Figure 4.1.7.1-8. Configuration 702 in Combined Bending and Tension for a/c = 0.2
a) K at Crack Tip into Plate, b) K at Crack Tip on Surface

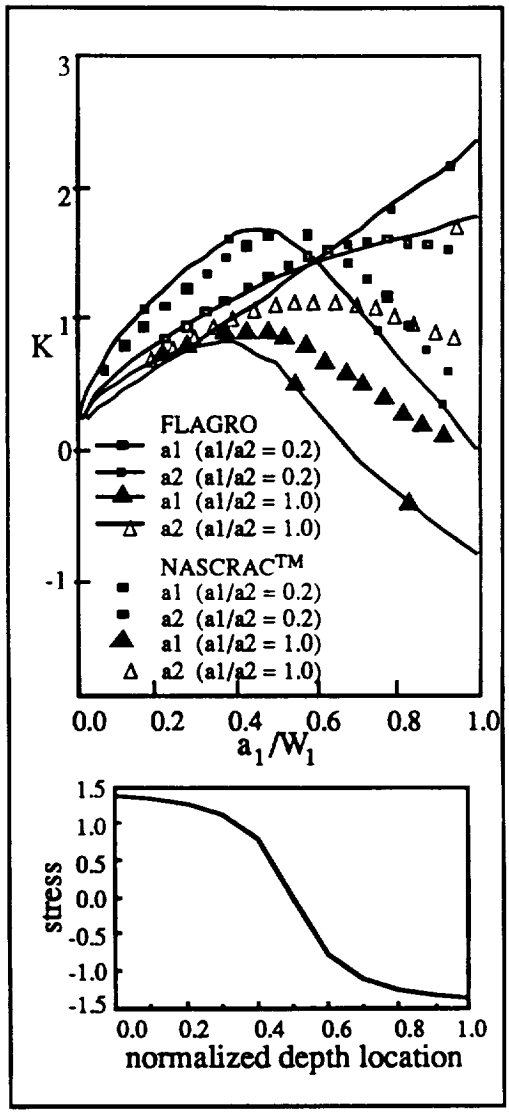

Figure 4.1.7.1-9. Configuration 702 in Non-Linear Bending: Results from a NASA/MSFC Round-Robin Study

4.1.7.2 Configuration 703 (Semi-Elliptical Circumferential Surface Crack in a Cylinder)

Figure 4.1.7.2-1 displays the geometry for configuration 703, *semi-elliptical circumferential surface crack in a cylinder.* Figures 4.1.7.2-2 through 4.1.7.2-10 present comparative 703 results from NASCRAC™ and references. The results in these figures were used to verify the NASCRAC™ 703 solution. Figures 4.1.7.2-11 and 4.1.7.2-12 illustrate specifics to solution 703 which need to be documented for the NASCRAC™ user.

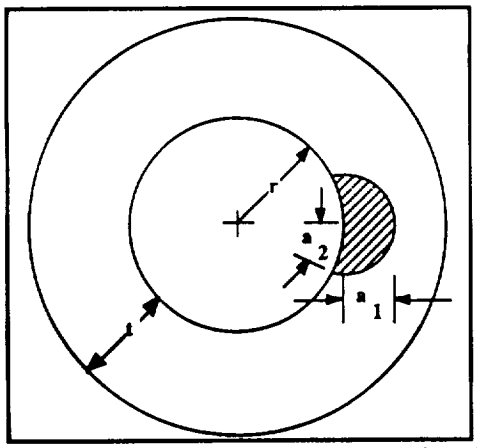

Figure 4.1.7.2-1. Geometry for Configuration 703, *Semi-Elliptical Circumferential Surface Crack in a Cylinder*

From Figures 4.1.7.2-2 through 4.1.7.2-4, it is evident that NASCRAC™ agrees closely with [24] and NASA/FLAGRO for uniform loading and varying inner radii (R_i) and a/c ratios. In each case, NASCRAC™ provides the most conservative estimate as a/t approaches unity. From Figures 4.1.7.2-5 through 4.1.7.2-10, where bending loads have been applied to the cylinder, NASCRAC™ appears reasonable but not conservative compared to [25] and is consistently conservative compared to NASA/FLAGRO. Although NASCRAC™ is generally only about 70% of the [25] value, the trends of NASCRAC™ and [25] are almost identical as a_1/t increases.

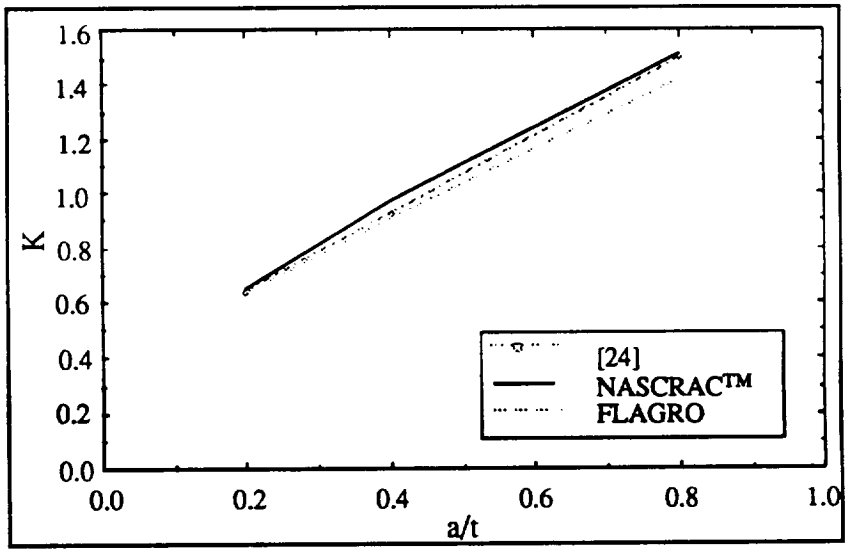

Figure 4.1.7.2-2. 703 K vs a_1/t for r = 5, a_1/a_2 = 0.667, Uniform Stress = 1 psi

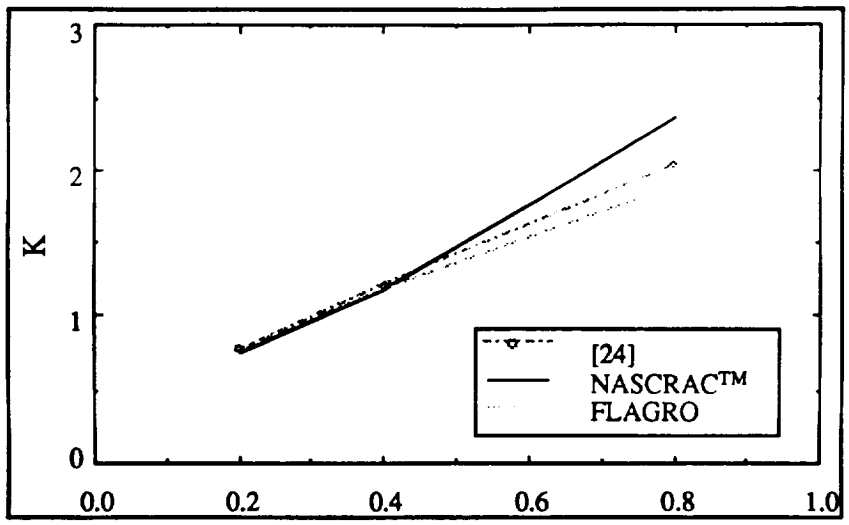

Figure 4.1.7.2-3. 703 K vs a_1/t for r = 10, a_1/a_2 = 0.333, Uniform Stress = 1 psi

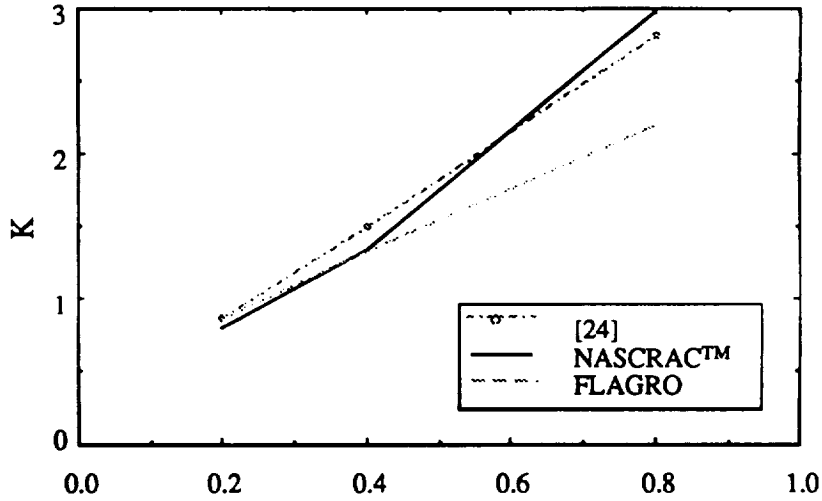

Figure 4.1.7.2-4. 703 K vs a_1/t for r = 20, a_1/a_2 = 0.167, Uniform Stress = 1 psi

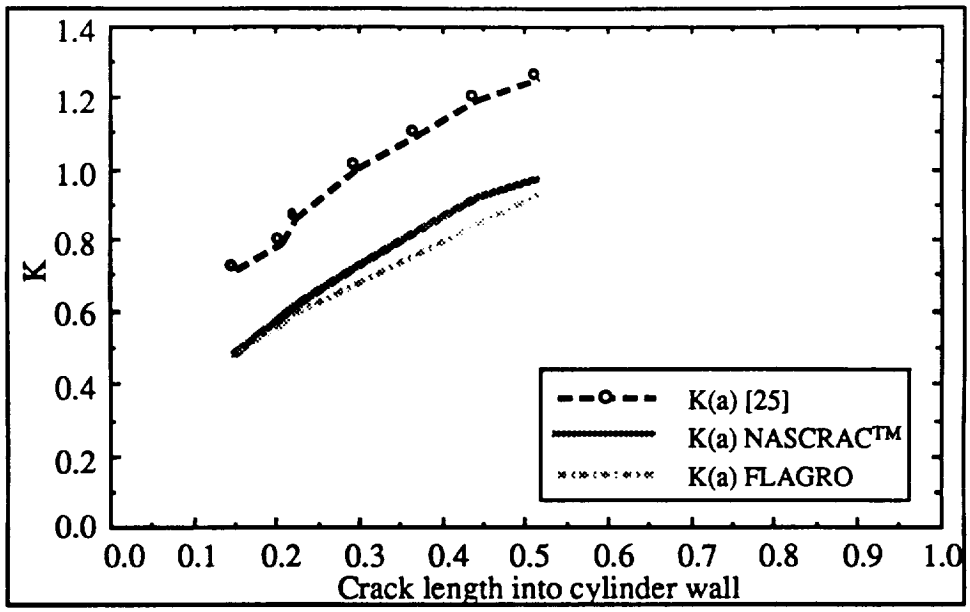

Figure 4.1.7.2-5. 703 K vs a_1 for r = 2.15, t = 0.73, Crack Radius = 0.875, Linear Load σ = 0.348 x + 0.748

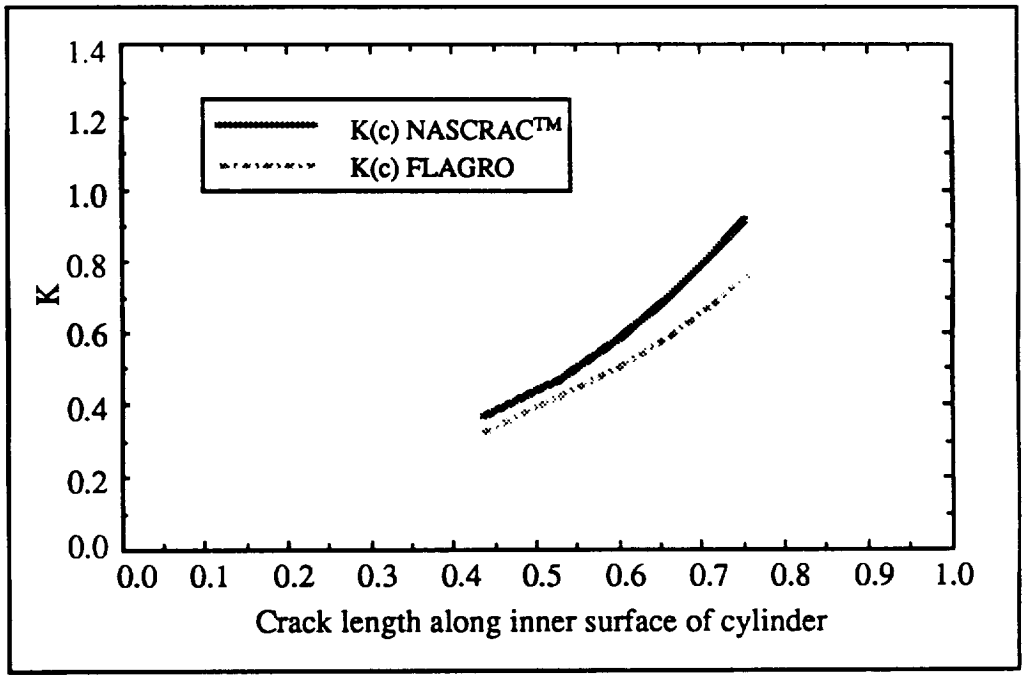

Figure 4.1.7.2-6. 703 K vs a_2 for r = 2.15, t = 0.73, Crack Radius = 0.875, Linear Load σ = 0.348 x + 0.748

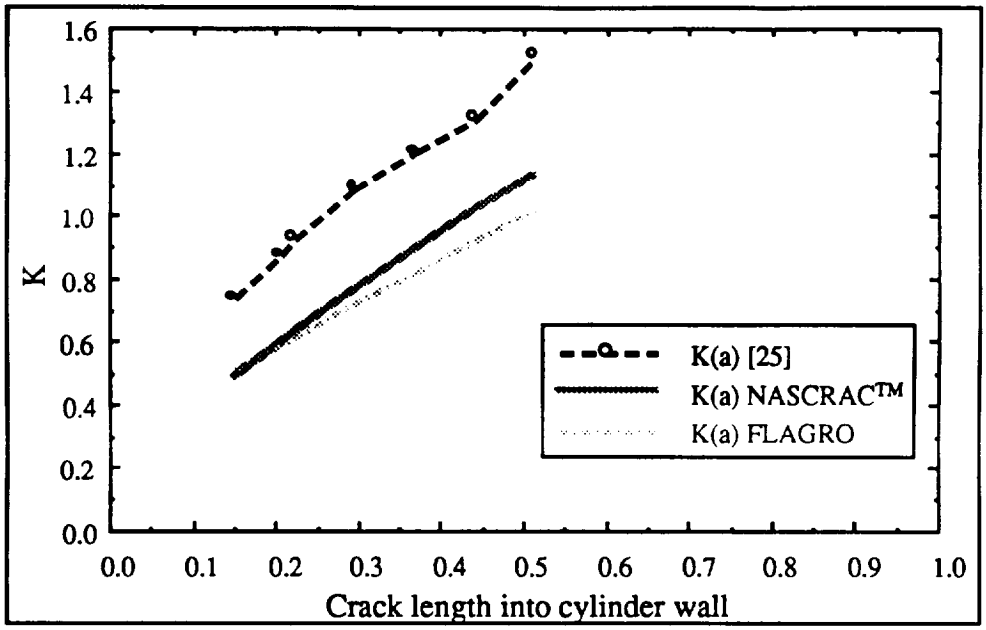

Figure 4.1.7.2-7. 703 K vs a_1 for r = 2.15, t = 0.73, Crack Radius = 1.50, Linear Load σ = 0.348 x + 0.748

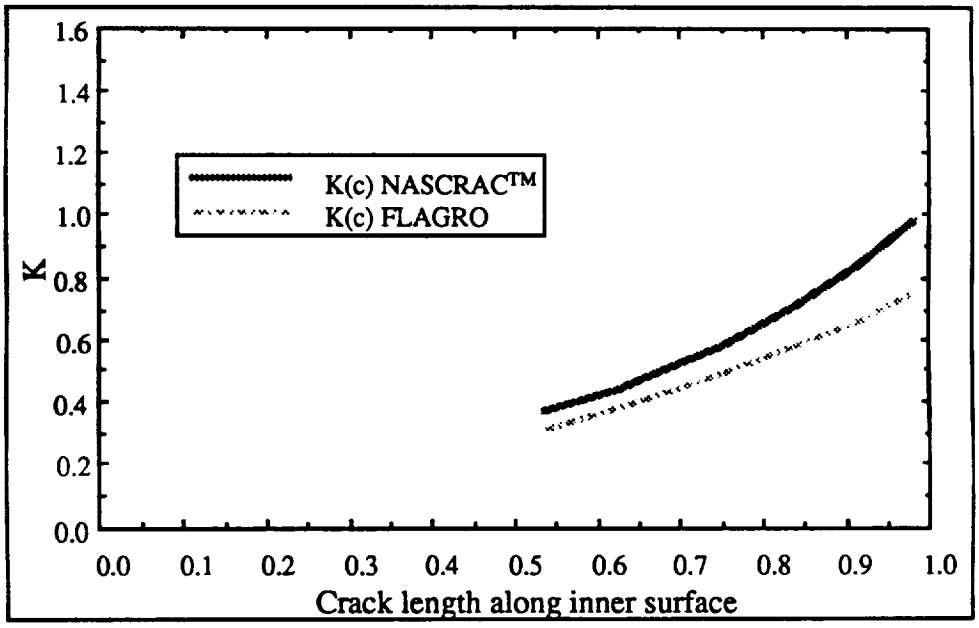

Figure 4.1.7.2-8. 703 K vs a_1 for r = 2.15, t = 0.73, Crack Radius = 1.50, Linear Load σ = 0.348 x + 0.748

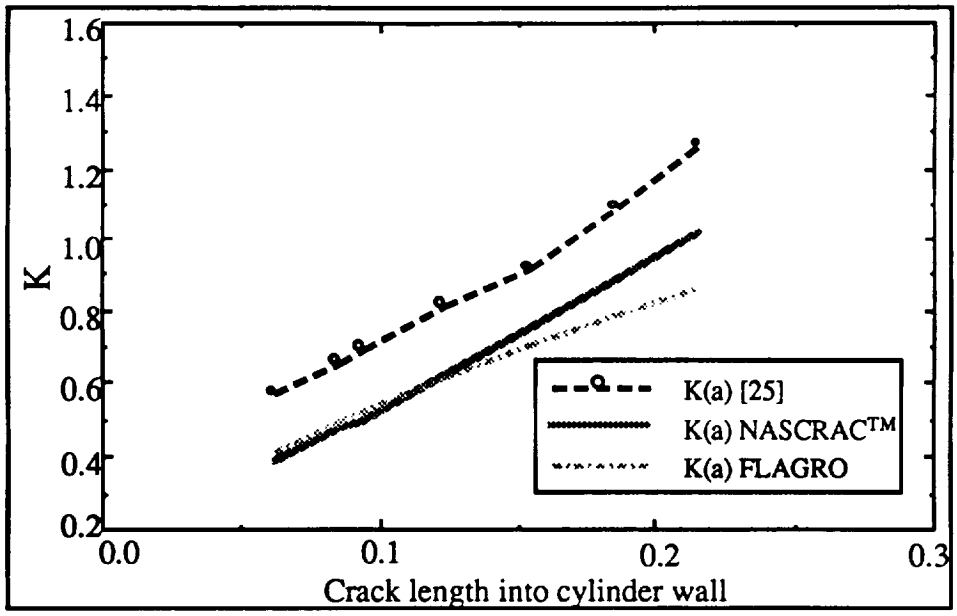

Figure 4.1.7.2-9. 703 K vs a_1 for r = 2.57, t = 0.306, Crack Radius = 1.50, Linear Load σ = 0.348 x + 0.894

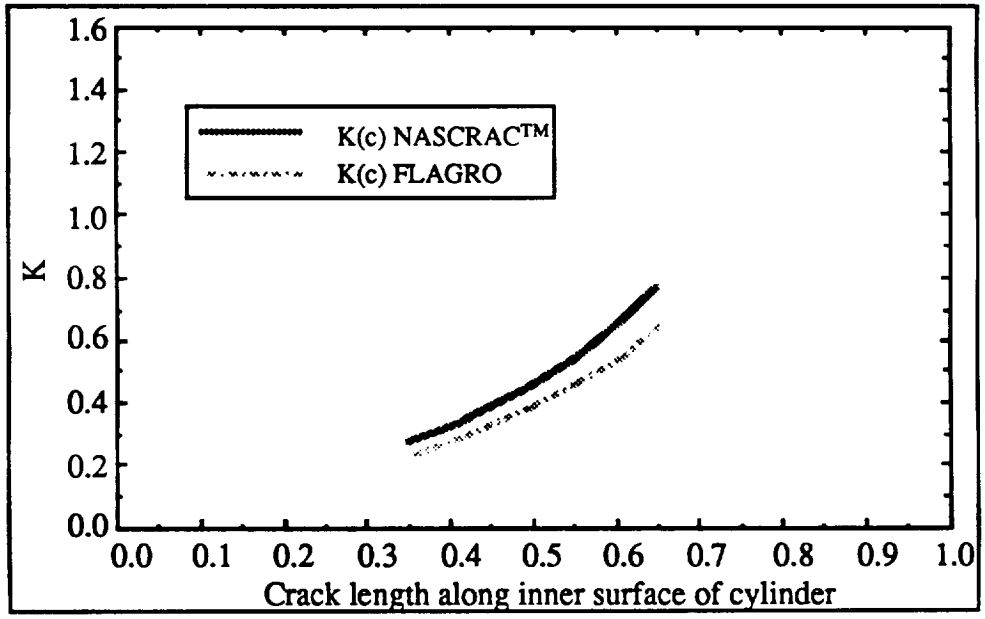

Figure 4.1.7.2-10. 703 K vs a_1 for r = 2.57, t = 0.306, Crack Radius = 1.50, Linear Load σ = 0.348 x + 0.894

Figure 4.1.7.2-11 shows results of a parametric study to determine the sensitivity of the NASCRAC™ 703 solution to the inner radius to wall thickness (r/t) ratio. The parametric study proved that the NASCRAC™ solution is independent of this ratio. Figure 4.1.7.2-11 indicates that K is slightly dependent on this ratio in the reference solutions.

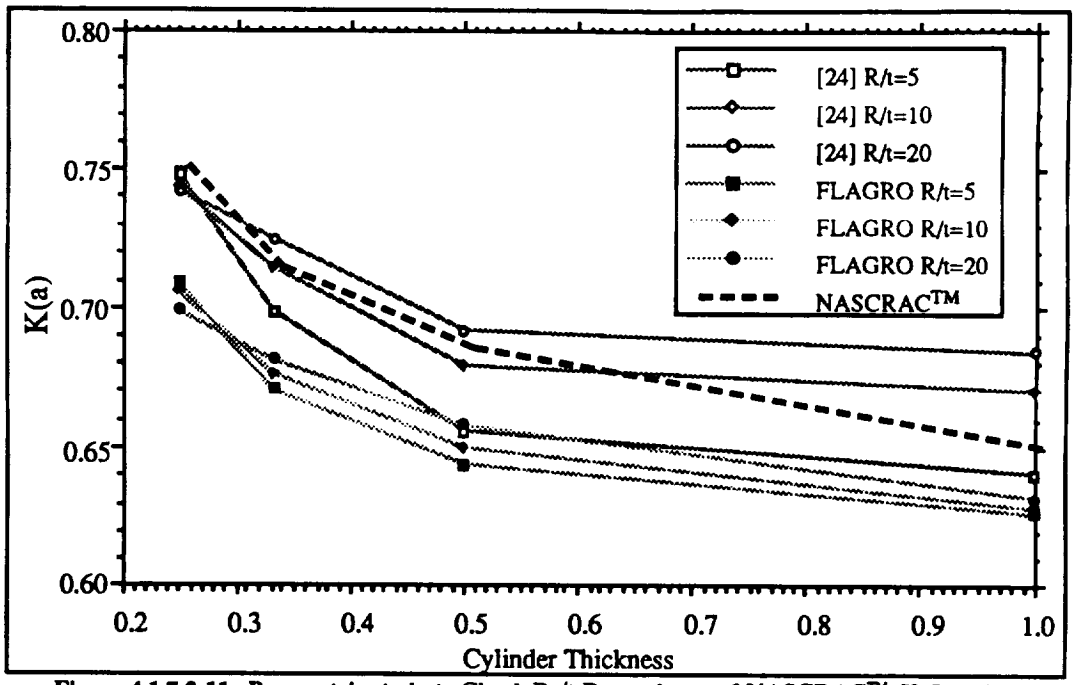

Figure 4.1.7.2-11. Parametric study to Check R_i/t Dependence of NASCRAC™ K Solution a = 0.2, c = 0.3, Uniform Stress = 1 psi

One shortcoming of the NASCRAC™ 703 solution is that pop-through goes undetected. Figure 4.1.7.2-12 shows an example of pop-through. In this figure, for a constant aspect ratio of a_2/a_1 = 2 and a_1 = 1 initially, the crack popped through the cylinder wall when a_1 = 4 but NASCRAC™ continued to calculate K for both a_1 and a_2. This problem may be related to the definition of the semi-ellipse because a_2 is along a curved surface whereas most of the NASCRAC™ configurations (601, 602, 702, 704) define a_2 along a straight surface. In future releases of NASCRAC™ an error check should be included in the code to detect and report the occurrence of pop-through.

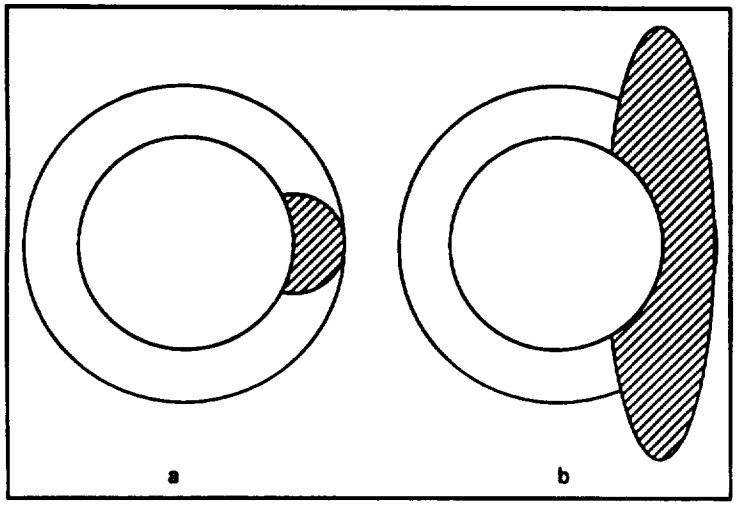

Figure 4.1.7.2-12.

a) a/c = 1.0; no pop through before Crack Axis Reaches back Surface

b) a/c = 0.5; pop through before Crack Axis Reaches the back Surface

The results for the NASCRAC™ 703 K solution indicate that this solution provides reasonable engineering solutions compared to [24], [25], FLAGRO, and FRANC; therefore, these results verified NASCRAC™ 703. However, only a limited number of geometrical configurations were available in the references. Thus, the 703 solution is valid for these reference configurations as well as configurations that are similar in r/t and aspect ratio. For configurations

where the r/t ratio is more similar to a thin walled cylinder, it is more conservative to assume a through crack and use configuration 303, a circumferential through crack in a cylinder.

4.1.7.3 Configuration 704 (Semi-Elliptical Axial Surface Crack in a Cylinder)

Figure 4.1.7.3-1 shows the geometry for configuration 704, *semi-elliptical axial surface crack in a cylinder*. This configuration was verified and validated using [26] - [28] and FLAGRO. The NASCRAC™ model is reasonable for the crack tip extending into the cylinder thickness (crack tip a_1). For this crack tip, differences between NASCRAC™ and the references varied from < 10% for uniform tension (Figure 4.1.7.3-2) and internal pressure induced stresses (Figure 4.1.7.3-3) to < 20% for linearly varying stresses (Figure 4.1.7.3-4) to < 30% for quadratically varying stresses (Figure 4.1.7.3-5). For cases where differences exceeded these limits ($a_1/t = 0.8$, i.e., a crack 80% through the cylinder wall thickness) NASCRAC™ appeared more reasonable than the references because it was more sensitive to the free surface ahead of a_1. One drawback to K at a_1 for 704 is that NASCRAC was generally non-conservative compared to the references (see Figures 4.1.7.3-2 through 4.1.7.3-5). For K at a_2 NASCRAC™ predicted significantly conservative values for the cases of linearly and quadratically varying stresses with differences between NASCRAC™ and the references exceeding 80% for certain geometries. For uniform stresses and internal pressure loadings, NASCRAC™ was reasonable (differences < 20%) compared to the references. The internal pressure case was not too different from a uniform stress case since the ratio of inner radius to wall thickness was 10 and the stresses in the wall varied from 10.52 psi at the inner radius to 9.52 at the outer radius.

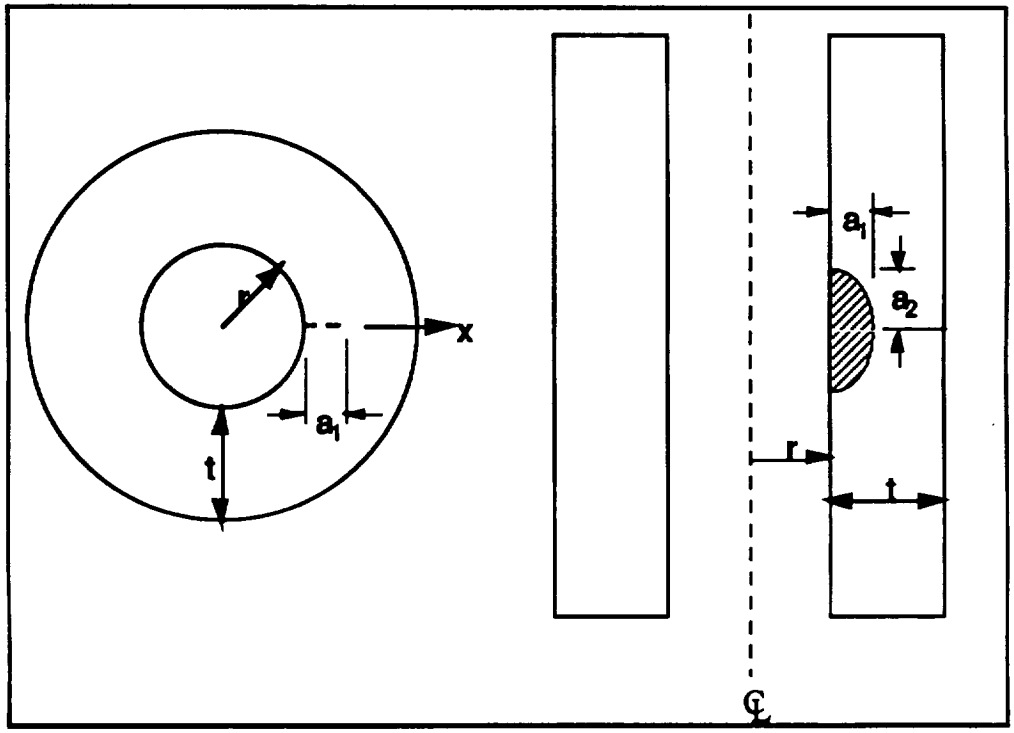

Figure 4.1.7.3-1. Geometry for Configuration 704, *Semi-Elliptical Axial Surface Crack in a Cylinder*

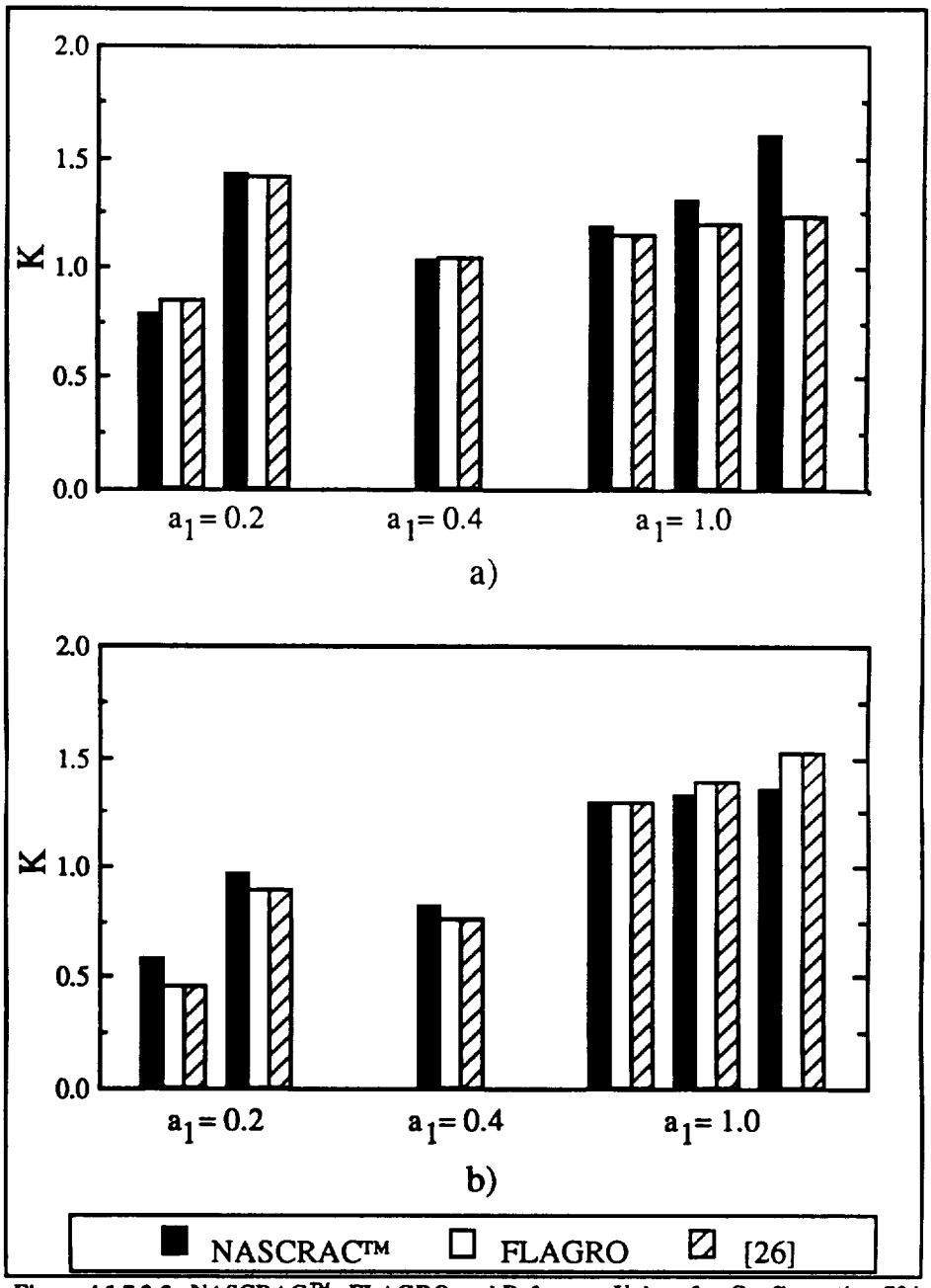

Figure 4.1.7.3-2. NASCRAC™, FLAGRO and Reference Values for Configuration 704
Uniform Stress = 1 psi, t/Ri = 0.10
a) K at Crack Tip into Plate, b) K at Crack Tip on Surface

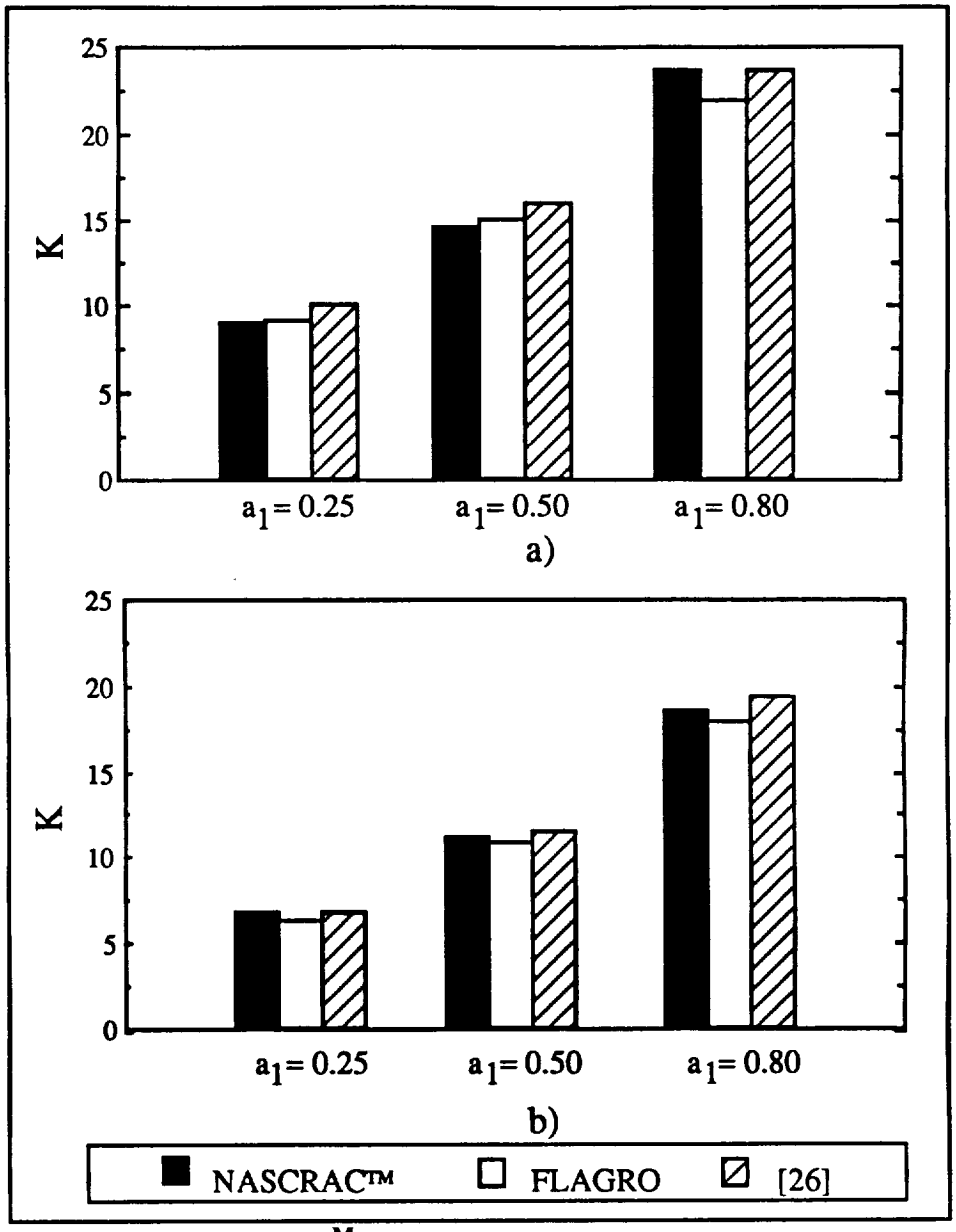

Figure 4.1.7.3-3. NASCRACT^M, FLAGRO and Reference Values for Configuration 704
1 psi Internal Pressure, t/Ri = 0.10
a) K at Crack Tip into Plate, b) K at Crack Tip on Surface

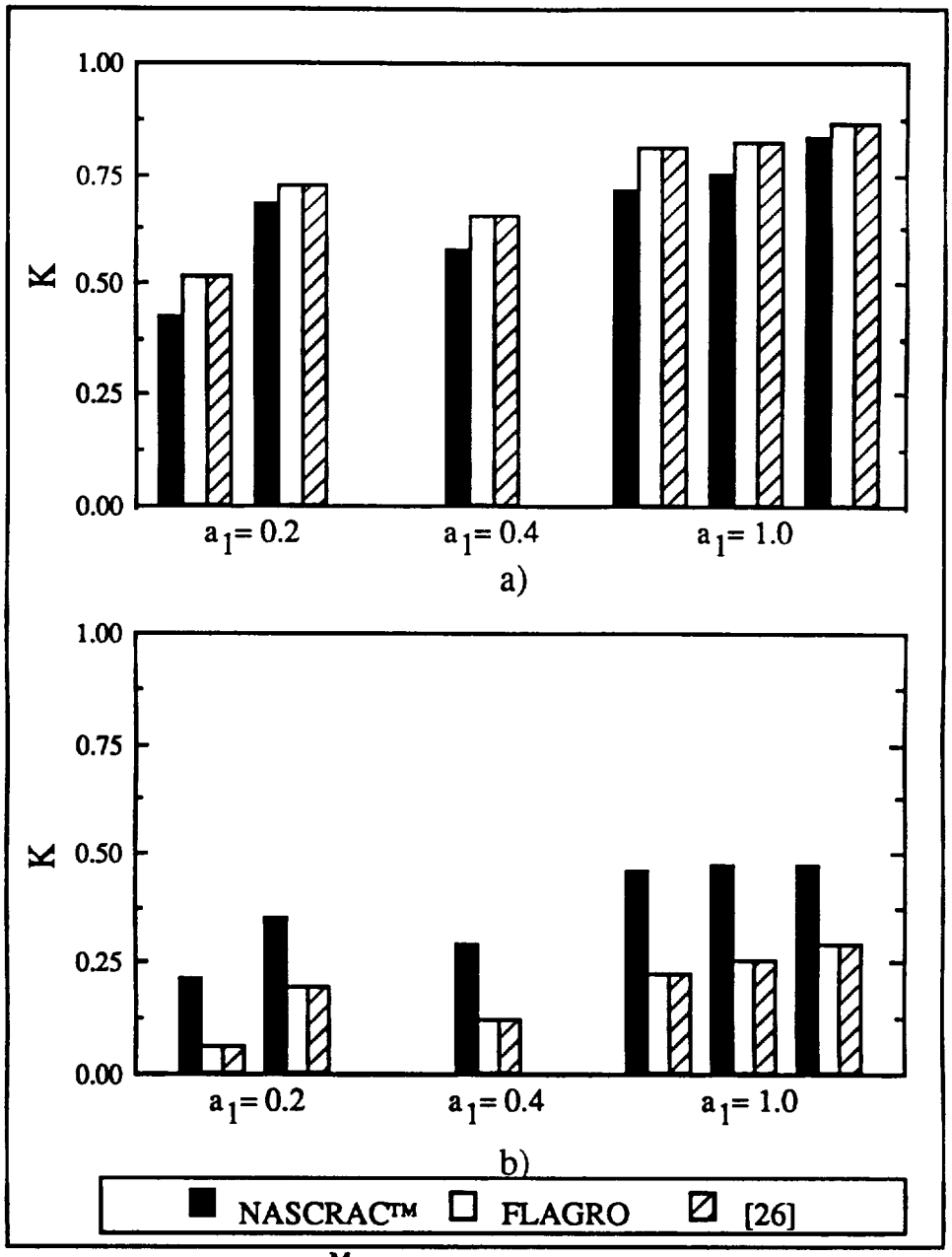

Figure 4.1.7.3-4. NASCRACT^M, FLAGRO and Reference Values for Configuration 704 Linear Stress = 0 psi at Crack Mouth, 1 psi at tip; t/Ri = 0.10
a) K at Crack Tip into Plate, b) K at Crack Tip on Surface

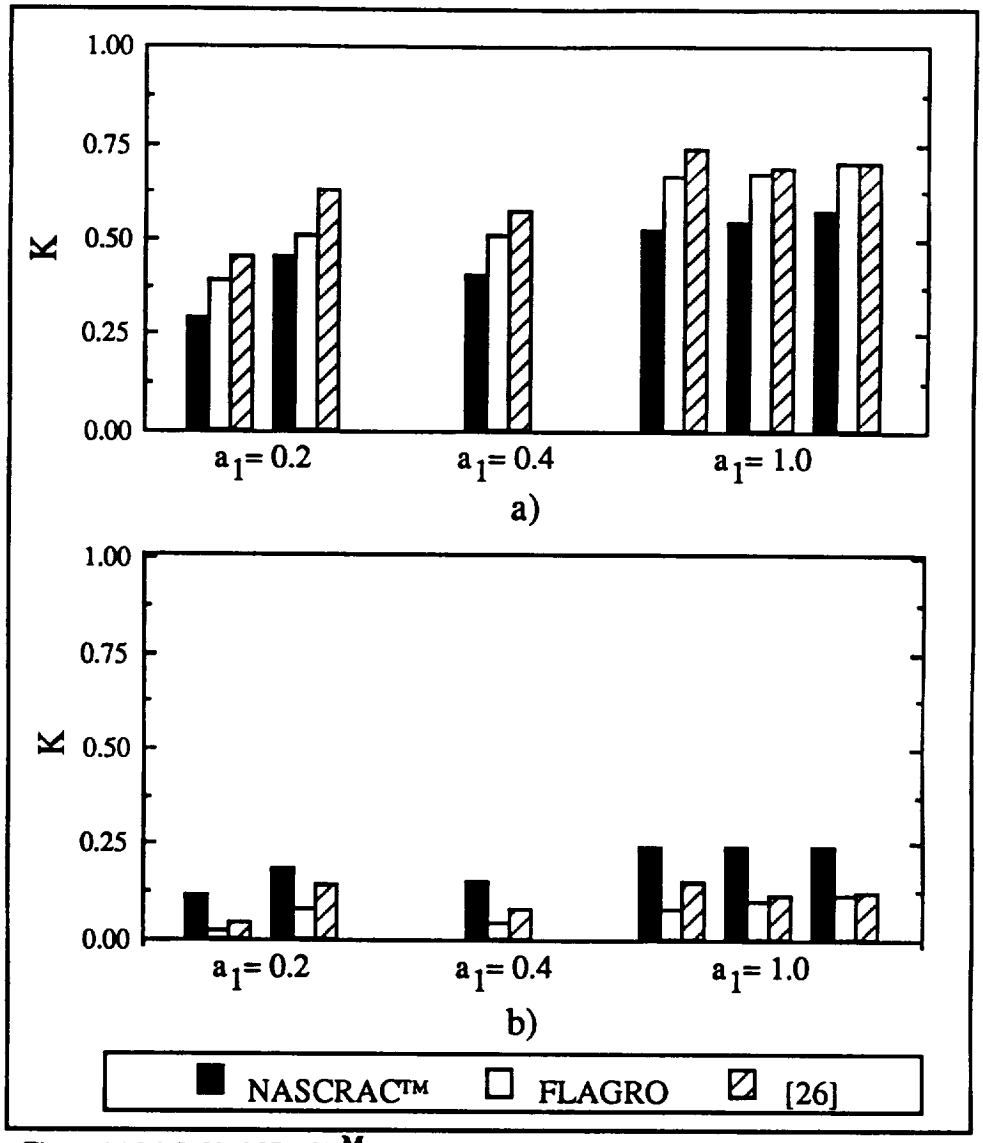

Figure 4.1.7.3-5. NASCRACT^{M,} FLAGRO and Reference Values for Configuration 704 Quadratic Stress = 0 psi at Crack Mouth, 1 psi at tip; t/Ri = 0.10 a) K at Crack Tip into Plate, b) K at Crack Tip on Surface

4.1.7.4 Configuration 705 (Semi-Elliptical Surface Crack in a Sphere)

The geometry of configuration 705, *semi-elliptical surface crack in a sphere*, is shown in Figure 4.1.7.4-1. This configuration was verified for both thin and thick walled spheres. The loading mechanism for verification and validation was internal pressure. For a thin walled pressurized sphere, the membrane stresses in the sphere are $\sigma = pr/2t$. For the thick walled pressurized sphere, the membrane stresses are described by $\sigma = (pR_i^3 (R_o^3 - 2R^3)) / (2R^3 (R_o^3 - 2R_i^3))$. Typical stress profiles for thick walled pressurized spheres are plotted in Figure 4.1.7.4-2.

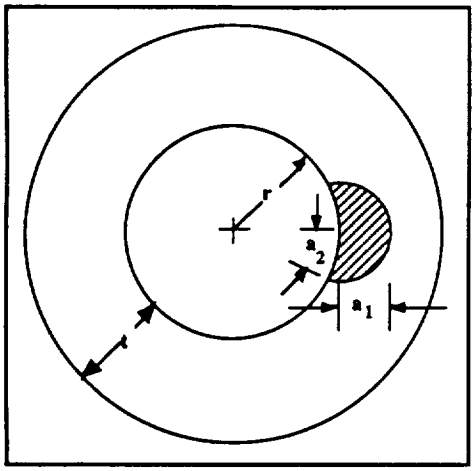

Figure 4.1.7.4-1. Geometry for Configuration 705, *Semi-Elliptical Surface Crack in a Sphere*

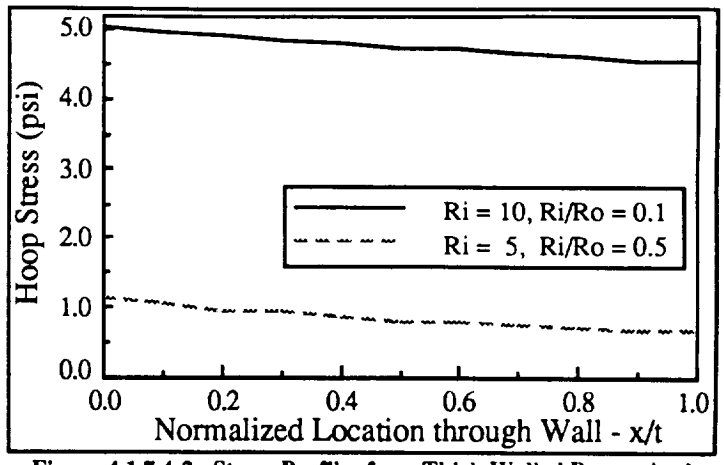

Figure 4.1.7.4-2. Stress Profiles for a Thick Walled Pressurized Sphere

The graphs in Figure 4.1.7.4-3 through 4.1.7.4-7 display *K vs a* curves from NASCRAC™ and FRANC results for five V/V cases. For each case, two graphs are given: 1) *K vs* a_1 where a_1 is the crack depth into the wall thickness of the sphere, and 2) *K vs* a_2 where a_2 is one-half the crack length along the inside surface of the sphere.

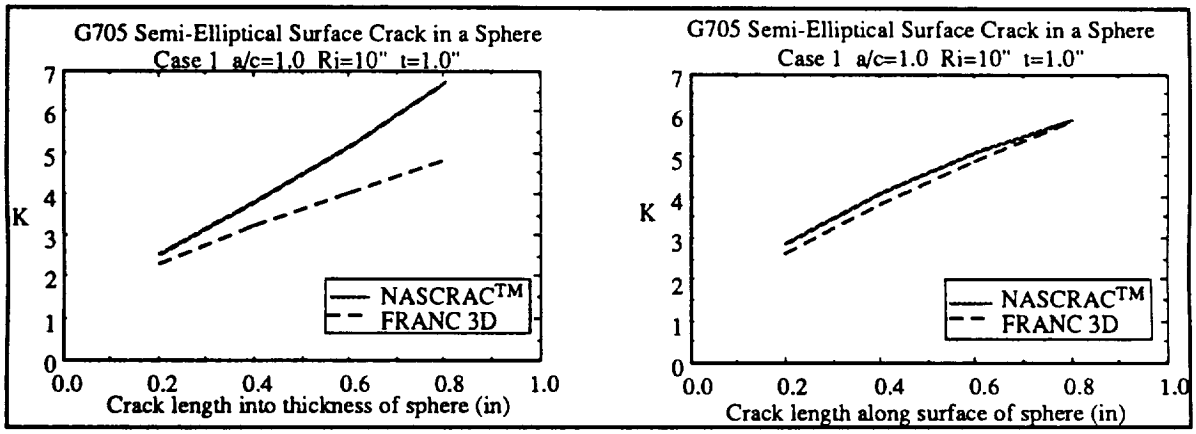

Figure 4.1.7.4-3. Thin-Walled Pressurized Sphere, p = 1 psi, a_1/a_2 = 1.0, r = 10", t = 1"

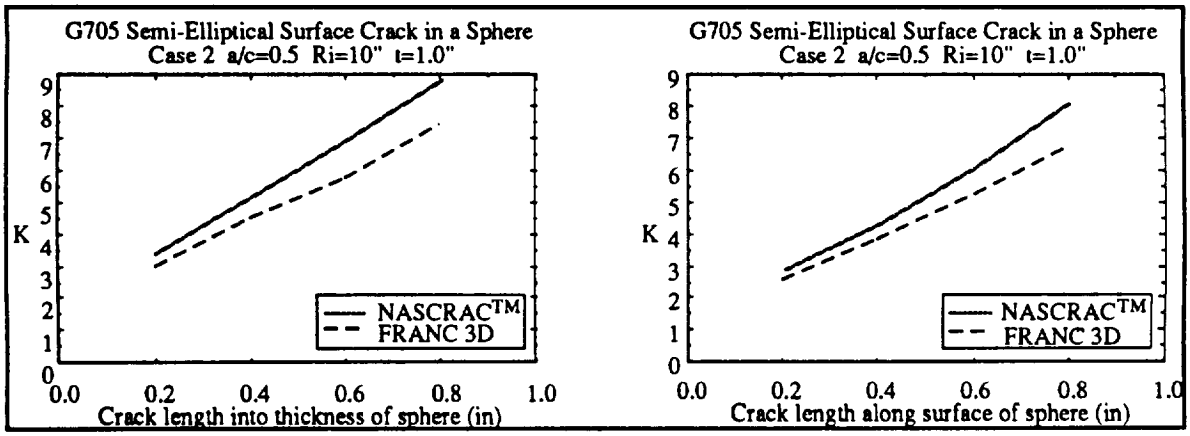

Figure 4.1.7.4-4. Thin-Walled Pressurized Sphere, p = 1 psi, a_1/a_2 = 0.5, r = 10", t = 1"

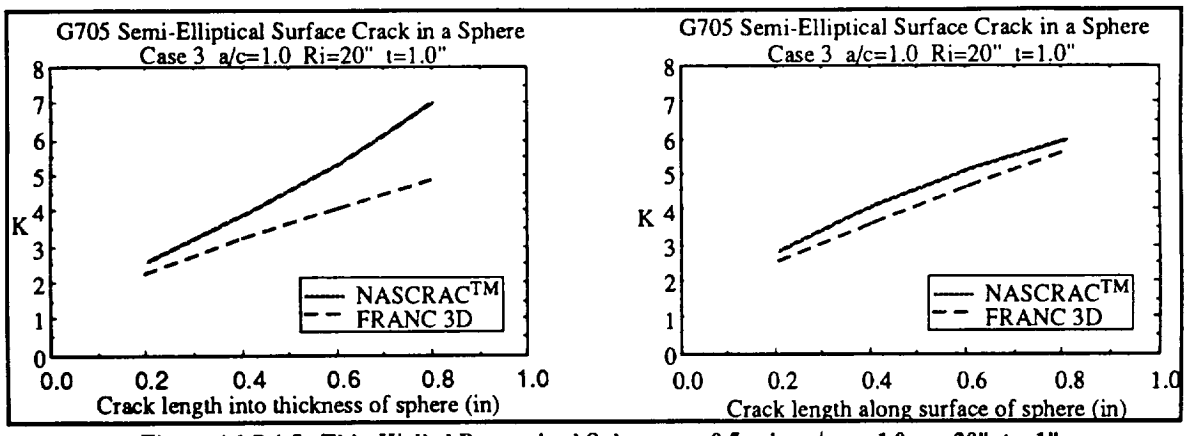

Figure 4.1.7.4-5. Thin-Walled Pressurized Sphere, p = 0.5 psi, a_1/a_2 = 1.0, r = 20", t = 1"

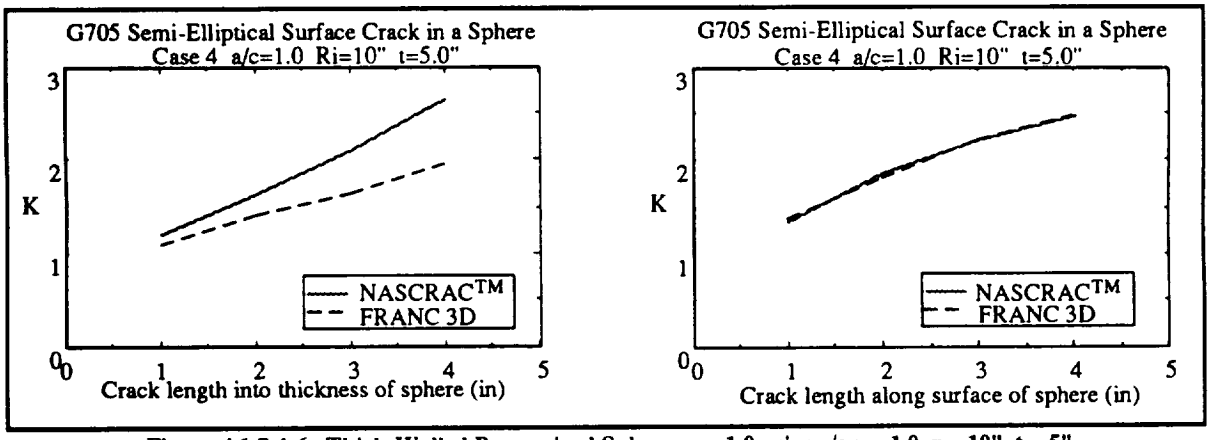

Figure 4.1.7.4-6. Thick-Walled Pressurized Sphere, p = 1.0 psi, a_1/a_2 = 1.0, r = 10", t = 5"

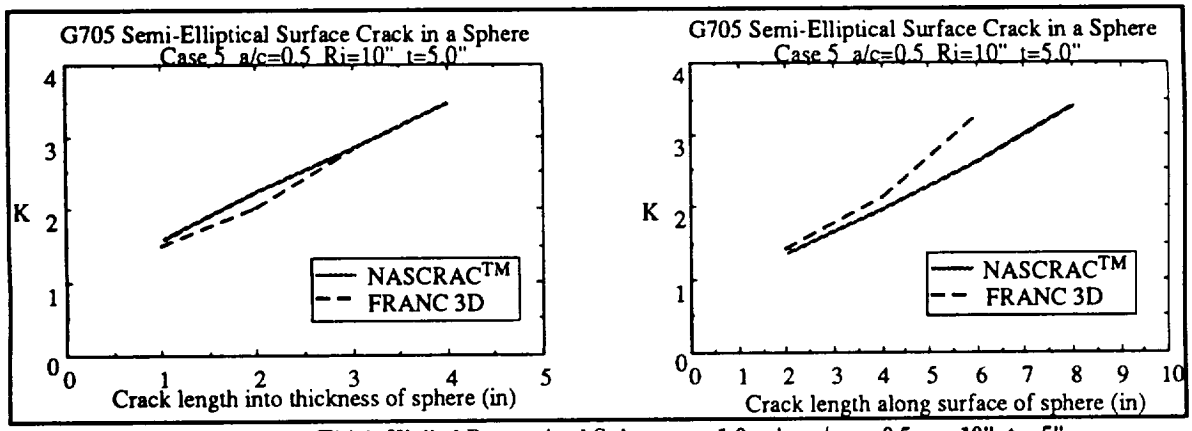

Figure 4.1.7.4-7. Thick-Walled Pressurized Sphere, p = 1.0 psi, a_1/a_2 = 0.5, r = 10", t = 5"

The plotted results above indicate that NASCRAC™ is in good agreement with FRANC for all five cases considered and is conservative for all cases except *K vs* a_2 for case 5, Figure 4.1.7.4-7. This result is expected because case 5 is not physically meaningful as the crack becomes large. As Figure 4.1.7.2-12 and the discussion in Section 4.1.7.2 indicate, this NASCRAC™ solution has the potential to allow undetected crack pop-through. This result was

easily detected in FRANC but was not flagged in the NASCRAC™ results. Other than this minor pop-through flaw, this solution appears valid for both thin- and thick-walled pressurized spheres.

4.1.8 800 SERIES RESULTS

A single configuration, 801 (*user defined K vs a table*), is available in NASCRAC™ under the 800 series. 801 is a solution which accepts a user defined *K vs a* table as input. This configuration is useful when *K vs a* results are available from tests or simulations but the geometry is not one of the standard geometries in NASCRAC™. The solution uses tabular lookup and interpolation/extrapolation.

Table 4.1.8-1 shows three cases used to verify *K vs a* for configuration 801. In the table, the second column displays the *K vs a* tabular values that were input into NASCRAC™. The three cases in the table include a backward linear extrapolation, a linear interpolation, and a forward linear extrapolation.

The data listed in the third and fourth columns of Table 4.1.8-1 indicate an error in the forward extrapolation case. NASCRAC™ does not extrapolate forward correctly because a DO loop counter is used incorrectly to index the user defined data table (see code listing in Figure 4.1.8-1). If the crack length (XA) exceeds all tabulated crack lengths, the DO loop (DO 40) increments its index one final time such that ISTR = MAXDAT + 1. This sets up the interpolation indices such that K = MAXDAT + 1 and J = MAXDAT. Since there is no data for crack length (MAXDAT+1) and K (MAXDAT+1), the linear extrapolation is no longer valid and the NASCRAC™ computed K is simply a ratio of the final K value in the table. To correct this error, an IF/THEN construction should be used to set K=MAXDAT if the crack length (XA) exceeds tabulated values.

Table 4.1.8-1. Representative Results from Configuration 801

a	K USER-DEFINED	K NASCRAC™	K CALCULATED
BACKWARD LINEAR EXTRAPOLATION			
2.0	3.7120		
2.2		3.8075	3.8075
2.4	3.9030		
LINEAR INTERPOLATION			
0.1		2.9300	2.9300
1.0	3.3071		
1.2	3.3909		
FORWARD LINEAR EXTRAPOLATION			
3.8	4.9846		
4.0	5.1786		
4.2		*5.4375*	*5.3726*

```
      SUBROUTINE K801
C-----------------------------------------------------------------
-C
C-----------------------------------------------------------------
-C
C   PURPOSE : CALCULATES K FOR 801 ; A1-K1 TABLE PROVIDED BY THE USER
C
C
C
       XA=ANOW(1)
C
C   INTERPOLATE TO GET K
C
30    DO 40 ISTR=2,MAXDAT
         IF(XA.LT.CRDPTH(ISTR)) GOTO 50
40    CONTINUE
      K=MAXDAT
50    K=ISTR
       J=K-1
         Y=(XA-CRDPTH(J))*XKOSIG(K)-(XA-CRDPTH(K))*XKOSIG(J)
        Y=Y/(CRDPTH(K)-CRDPTH(J))
        SIGZ=EQPARS(ITRANS,IDEF,1)
       XK(IDEF,1)=Y * SIGZ
       RETURN
       END
```

Figure 4.1.8-1. Source Code for Subroutine K801 Showing Error in DO Loop Assignment

4.1.9 900 SERIES RESULTS

A single configuration, 901 *(user defined influence function coefficients)*, is available in NASCRAC™ under the 900 series. This solution allows a NASCRAC™ user to define his or her own weight function solution. The twenty-five weight function coefficients required as input must be generated offline.

Table 4.1.9-1 presents V/V results for this NASCRAC™ capability. These results were calculated by executing the 901 capability using the 203 (single edge crack in a plate) weight function coefficients. The results listed in Table 4.1.9-1 was computed for a 10" wide plate with an initial crack length of 1.0". The load was a linearly decreasing load of σ = 1 psi at the crack mouth and σ = 0 at the free edge of the plate. This load choice forced NASCRAC™ to use the 203 weight function solution during a comparative analysis.

Table 4.1.9-1. Representative Results from Configuration 901

a	K FROM 901	K FROM 203
1	2.023	2.023
1.2	2.235	2.235
1.4	2.441	2.440
1.6	2.644	2.644
1.8	2.849	2.849
2	3.060	3.059
2.2	3.277	3.277
2.4	3.505	3.505
2.6	3.746	3.746
2.8	4.002	4.001
3	4.275	4.274

The analytical results shown in Table 4.1.9-1 show agreement between 203 and 901; therefore, this NASCRAC™ capability can be considered verified and also validated to the extent that the weight function coefficients input into NASCRAC™ are valid. The format of the coefficients file was not identified in the NASCRAC™ user's manual; therefore, this manual should be updated to include an example file.

4.1.10 REFERENCES FOR SECTION 4.1

1. *"E 399 (Standard Test Method of Plane-Strain Fracture Toughness of Metallic Materials" in 1992 Annual Book of ASTM Standards, American Society for Testing and Materials, Philadelphia, 1992, pp 506-536.*
2. *Rooke, D.P., and Cartwright, D.J., Compendium of Stress Intensity Factors, Her Majesty's Stationery Office, London, 1976.*
3. *Tada, H., Paris, P.C., and Irwin, G.R., The Stress Analysis of Cracks Handbook, 2nd ed, Paris Productions, St. Louis, Paris Productions, 1985.*
4. *Broek, D., Elementary Engineering Fracture Mechanics, 4th ed, Martinus Nijhoff, Boston, 1986, pp 80.*
5. *Sha, G.T., and Yang, C.T., "Weight Functions of Radial Cracks in Hollow Disks", Journal of Engineering for Gas Turbines and Power, vol 108 (Apr 1986), pp 403-413.*
6. *Parmerter, R.R., Stress Intensity Factors for 3-D Problems, United Technologies Chemical Systems Division, Sunnyvale, 1976 for Air Force Rocket Propulsion Lab, Edwards AFB, RPL-TR-76-30.*
7. *Wu, X.R. and Carlsson, A.J., Weight Functions and Stress Intensity Factor Solutions, Pergamon Press, New York, 1991.*
8. *Wawrzynek, P. FRacture ANalysis Code (FRANC) Primer for Version 2.5, Cornell University, Ithaca, NY, 1991.*
9. *Wawrzynek, P. FRacture ANalysis Code (FRANC) Version 2.3+ Release Notes, Cornell University, Ithaca, NY, 1990.*
10. *Schijve, J., and Lai, J., "The Stress Intensity Factor of Hole Edge Cracks in a Finite Width Plate," International Journal of Fracture, vol 46, 1990, pp R37-R42.*
11. *Shivakumar, V., and Forman, R.G., "Green's Function for a Crack Emanating from a Circular Hole in an Infinite Sheet," International Journal of Fracture, vol 16, 1980, pp 305-316.*
12. *Zatz, I.J., Eidinoff, H.L., and Armen, H., "An Application of the Energy Release Rate Concept to Crack Growth in Attachment Lugs," 22nd Structures, Structural Dynamics, and Material Conference, American Institute of Aeronautics and Astronautics, Atlanta, 1981, pp 402-415.*
13. *Forman, R.G., et al "Fatigue Crack Growth Computer Program NASA/FLAGRO," JSC-22267, NASA/Johnson Space Flight Center, Houston, 1986.*
14. *Newman, J.C. Jr., "Fracture Analysis of Surface and Through Cracks in Cylindrical Pressure Vessels," NASA TN D-8325, 1976.*
15. *Erdogan, F., and Ratwani, M., "Fatigue and Fracture of Cylindrical Shells Containing a Circumferential Crack," International Journal of Fracture Mechanics, vol 6, 1970, pp 379-392.*

16. *Forman, R.G., et al, "Stress Intensity Factors for Circumferential Through Cracks in Hollow Cylinders Subjected to Combined Tension and Bending Loads," Engineering Fracture Mechanics, vol 21, 1985, pp 563-571.*
17. *Kumar, V., German, M.D., and Shih, C.F., An Engineering Approach for Elastic-Plastic Fracture Analysis, NP-1931, Research Project 1237-1, prepared by General Electric Company for Electric Power Research Institute, July, 1981.*
18. *Forman, R.G., and Shivakumar, V., "Growth Behavior of Surface Cracks in the Circumferential Plane of Solid and Hollow Cylinders," in Fracture Mechanics: Seventeenth Volume, ASTM 905, Underwood, J.H., et al (editors), American Society for Testing and Materials, Philadelphia, 1986, pp 59-74.*
19. *Bush, A.J., "Stress Intensity Factors for Single-Edge-Crack Solid and Hollow Round Bars Loaded in Tension," Journal of Testing and Evaluation, vol 9, no 4 (July 1981), pp 216-223.*
20. *Si, Erjian, "Stress Intensity Factors for Edge Cracks in Round Bars," Engineering Fracture Mechanics, vol 37, no 4, (1990), pp 805-812.*
21. *Newman, J.C., and Raju, I.S., "Stress Intensity Factor Equations for Cracks in Three-Dimensional Finite Bodies," in Fracture Mechanics 14th Symposium Volume I: Theory and Analysis ASTM STP 791, Philadelphia, American Society for Testing and Materials, 1983, pp. I-238 - I-265.*
22. *Kobayashi, A.S., and Enetanya, A.N., "Stress Intensity Factor of a Corner Crack," in Mechanics of Crack Growth 8th Symposium on Fracture Mechanics ASTM STP 590, Philadelphia, American Society for Testing and Materials, 1976, pp. 477 - 495.*
23. *Raju, I.S., and Newman, J.C., "Stress Intensity Factors for a Wide Range of Semi-Elliptical Surface Cracks in Finite Thickness Plates," Engineering Fracture Mechanics, vol 11, no 4, 1979, pp 817-829.*
24. *Kumar, V., et al, Advances in Elastic-Plastic Fracture Analysis, NP-3607, Research Project 1237-1, Final Report, prepared by General Electric Company for Electric Power Research Institute, July, 1984.*
25. *Mullinix, B.R., and Smith, D.G., Fracture Mechanics Design Handbook, United States Army Missile Command, Redstone Arsenal, Alabama, 1976, p.210.*
26. *Raju, I.S., and Newman, J.C., "Stress-Intensity Factors for Internal and External Surface Cracks in Cylindrical Vessels", Journal of Pressure Vessel Technology, vol 104, November 1982, pp 293-298.*
27. *Raju, I.S., and Newman, J.C., "Stress Intensity Factors for Circumferential Surface Cracks in Pipes and Rods under Tension and Bending Loads," in Fracture Mechanics: Seventeenth Volume, ASTM 905, Underwood, J.H., et al (editors), American Society for Testing and Materials, Philadelphia, 1986, pp 789-805.*
28. *Heliot, J., Labbens, R.C., and Pellissier-Tanon, A., "Semi-Elliptical Cracks in a Cylinder Subjected to Stress Gradients", Fracture Mechanics ASTM STP 677, C.W. Smith ,Ed., Philadelphia, American Society for Testing and Materials, 1979, pp 341-364.*

4.2 *K vs a* CALCULATION: VARIABLE THICKNESS

NASCRAC™ includes variable thickness *K vs a* capabilities for seven different configurations in the 200 series (201-207). All of the configurations are through cracks in plate specimens (205 and 207 are considered transverse sections of cylinders.). The variable thickness option allows thickness to be discretized along the plate width. Input is tabular, i.e., a thickness is assigned at a given location along the plate width.

The variable thickness option was verified and validated using two-dimensional finite element models in FRANC [1,2]. FRANC allows thickness variations described by first, second, or third order polynomials.

Comparative results between NASCRAC™ and FRANC revealed an inconsistency in NASCRAC™'s required stress input. For configurations 203, 205, 206, and 207, NASCRAC™ expects stresses on the crack plane to be input. This requirement is consistent with weight function theory. However, for configurations 201, 202, and 204, NASCRAC™ expects crack plane loads/unit plate width. The inconsistency is due to the weight functions coded in NASCRAC™. For configurations 203, 205, 206, and 207, NASCRAC™ uses a generic weight function routine (*GENRIF*). The function coefficients for this routine were generated offline for each crack configuration and hardwired into NASCRAC™. For configurations 201, 202, and 204, NASCRAC™ uses weight functions obtained from [3]. In the literature, these functions are presented in terms of load/unit width. These weight functions are coded into NASCRAC™ exactly as they appear in the literature; thus, a load/unit width input is necessary.

The described inconsistency is illustrated with the source code listed in Figure 4.2-1. This figure lists a skeleton of the typical NASCRAC™ subroutines used to compute K solutions. The first routine, *Kxxx*, calls a Gaussian quadrature integration routine, *QINTxx*, using an external function, *FCTxxx*, as a calling parameter. The x's represent the appropriate configuration number (e.g., 201). The external function *FCTxxx* consists of the weight function for the *Kxxx* configuration. The stress for the analysis is included in the formulation with the variable *SIGMA*. *SIGMA* is obtained by calling the subroutine *STRINT*. NASCRAC™ does not adjust *SIGMA* for thickness but simply obtains the value of *SIGMA* either from a table lookup or functional evaluation. In Figure 4.2-1, near the end of *FUNCTION FCTxxx*, the function value is multiplied by the thickness at x (*TX*) before returning to *Kxxx*. However, after the program returns to *Kxxx*, the thickness at the crack tip a, *THICKX(A)* is divided out. Thus, the thickness operations have zero net effect in terms of changing load to stress but do distribute the load or stress as a function of thickness along the width of the plate. Since the input load or stress is not altered by a factor of thickness, the resulting K value is dependent on whether load or stress is input; therrefore, for 201, 202, and 204, if stresses are input into NASCRAC™ instead of load/unit width, the calculated NASCRAC™ results will be in error by a factor of thickness.

```
      SUBROUTINE Kxxx
C
      EXTERNAL FCTxxx
C
C  INTEGRATION USING THE INFLUENCE FUNCTION
C
      CALL QINTxx(FCTxxx,Y)
C
      IF(IVTHIC.EQ.1) THEN
        XK(IDEF,1)=Y/THICKX(A)
      ELSE
        XK(IDEF,1)=Y
      ENDIF
      RETURN
      END
*****************************************************************
      FUNCTION FCTxxx(XOA)
        .
        .
      CALL STRINT(X,Y,Z,SIGMA)
      FCTxxx= SIGMA * F * A
      IF(IVTHIC.EQ.1) THEN
        TX=THICKX(X)
      ELSE
        TX=1.
      ENDIF
      FCTxxx = FCTxxx*TX
      RETURN
      END
```

Figure 4.2-1. Variable Thickness Operations in *Kxxx* Subroutines

Table 4.2-1 lists comparative results which illustrate the inconsistency described above. In this table three sets of results are listed: FRANC results with a variably thick model, NASCRAC™ results using stress inputs, and NASCRAC™ results using load/unit width inputs. Table 4.2-1 lists results for both configuration 202, which uses a weight function from [3], and configuration 203, which uses a generic weight function generated for NASCRAC™. The results clearly show the inconsistency in the expected inputs for NASCRAC™'s variably thick K solutions. For configuration 202, NASCRAC™ agrees with FRANC when load/unit width values are input to NASCRAC™; conversely, for configuration 203, NASCRAC™ agrees with FRANC when stress values are input. For both configurations, when the variable thickness option is employed but the thickness is uniform with a value of unity (Case 1: $t = 1.0$ in Table 4.2-1) the NASCRAC™ results for stress and load/unit width inputs are identical and agree with FRANC results. Case 2 results, which were also computed with the variable thickness option but with a uniform thickness equal to 2.5, clearly demonstrate the inconsistency. In this case NASCRAC™ 202 load/unit width results agree with FRANC whereas for 203, NASCRAC™ stress results agree with FRANC. This inconsistency is also present in the algorithm of the uniform thickness K solutions (described in Section 4.1) but is not evident in the results because the crack plane

stresses and the crack plane loads/unit width are identical for a thickness of unity. This fact is evident in the subroutines listed in Figure 4.2-1 where the thickness values *TX* and *THICKX(A)* are set to unity (see the highlighted IF-THEN statement) for the constant thickness option.

To correct the inconsistency the required input units for each configuration should be explicitly stated in the documentation and displayed by the user interface. A more rigid resolution of the inconsistency is to recode NASCRAC™ to expect stress values on the crack plane in all situations.

Table 4.2-1 Inconsistency in *K vs a* Variable Thickness Solutions

CASE	a	CONFIGURATION 202			a	CONFIGURATION 203		
		NASCRAC™ (STRESSES)	NASCRAC™ (LOAD / WIDTH)	FRANC		NASCRAC™ (STRESSES)	NASCRAC™ (LOAD / WIDTH)	FRANC
t = 1.0	0.5	0.134	0.134	0.134	1.0	0.206	0.206	0.201
	1.5	0.241	0.241	0.240	3.0	0.495	0.495	0.495
	2.5	0.344	0.344	0.342	5.0	1.117	1.117	1.110
t = 2.5	0.5	0.021	0.053	0.054	1.0	0.083	0.207	0.080
	1.5	0.039	0.097	0.096	3.0	0.199	0.498	0.198
	2.5	0.055	0.138	0.138	5.0	0.448	1.120	0.443

To summarize the variable thickness *K vs a* verification effort, the NASCRAC™ capability was verified for all variably thick configurations (201-207) **if the correct stress input (as discussed above) is applied.** This verification is based on good agreement between NASCRAC™ and FRANC for small cracks and uniform, non-unity thicknesses; linearly varying thicknesses; and quadratically varying thicknesses and reasonable agreement for similar thicknesses and larger cracks.

4.2.1 CONFIGURATION 201 (CRACK IN AN INFINITE PLATE)

Table 4.2.1-1 lists comparative results for 201 variable thickness *K vs a* calculations. These results were computed using a stress field on the crack plane induced by a 1 lb_f point load along the plate centerline. The stresses along the crack plane were determined using FRANC and input into NASCRAC™ as a stress table. Table 4.2.1-2 shows the two variants of input stresses for each case listed in Table 4.2.1-1.

Table 4.2.1-1. Representative Variable Thickness *K vs a* Results for 201

CASE	a	FRANC	NASCRAC™ STRESS INPUT	NASCRAC™ LOAD/UNIT WIDTH INPUT
1. UNIFORM THICKNESS (t = 2.5)	0.5	0.024	0.010	0.024
	1.0	0.034	0.134	0.034
	1.5	0.042	0.016	0.041
	2.0	0.048	0.019	0.047
	2.5	0.054	0.021	0.052
2. LINEARLY VARYING THICKNESS (t = 1.5 + 0.2x)	0.5	0.014	0.003	0.014
	1.0	0.020	0.004	0.019
	1.5	0.024	0.005	0.023
	2.0	0.027	0.006	0.026
	2.5	0.030	0.006	0.028

The K values listed in Table 4.2.1-1 for the two different stress inputs validate the variable thickness *K vs a* solution for configuration 201 **when the stress inputs in NASCRAC™ are load/unit width values on the crack plane**, i.e., stress values on the crack plane multiplied by the corresponding plate thickness at that stress location. This NASCRAC™ solution uses weight function theory in which the weight function is defined in terms of load/unit width [3]. This type input is inconsistent with other NASCRAC™ variable thickness solutions and traditional weight function theory, where the formulation is in terms of stresses on the crack plane. This inconsistency needs to be clearly identified in the documentation. A more consistent approach is to recode the solution to accept stress input.

Table 4.2.1-2 . Stress Inputs for 201 Variable Thickness *K vs a* Calculations

LOADS ON CRACK PLANE				
POSITION	CASE 1		CASE 2	
x	σ	σ* t	σ	σ* t
-20.00	-0.0004	-0.0010	0.0037	-0.0129
-15.92	0.0029	0.0073	0.0050	-0.0133
-11.84	0.0077	0.0191	0.0072	-0.0135
-7.76	0.0129	0.0324	0.0097	-0.0102
-3.67	0.0175	0.0437	0.0113	-0.0027
0.00	0.0192	0.0480	0.0113	0.0057
4.08	0.0175	0.0437	0.0094	0.0124
8.16	0.0129	0.0324	0.0064	0.0137
12.24	0.0077	0.0191	0.0033	0.0097
16.33	0.0029	0.0073	0.0005	0.0018
20.00	-0.0004	-0.0010	-0.0018	-0.0081

4.2.2 CONFIGURATION 202 (CENTER CRACKED PANEL)

Table 4.2.2-1 lists comparative results for 202 variable thickness *K vs a* calculations. These results were computed using a stress field on the crack plane induced by a 1 lb_f point load along the panel centerline. The stresses along the crack plane were determined using FRANC and input into NASCRAC™ as a stress table. Table 4.2.2-2 shows the two variants of input stresses for each case listed in Table 4.2.2-1. The results in Table 4.2.2-1 were computed using a panel width of 10".

Table 4.2.2-1. Representative Variable Thickness *K vs a* Results for 202

CASE	a	FRANC	NASCRAC™ STRESS INPUT	NASCRAC™ LOAD/UNIT WIDTH INPUT
1. UNIFORM THICKNESS (t = 1.0)	0.5	0.134	0.134	0.134
	1.0	0.191	0.192	0.192
	1.5	0.240	0.241	0.241
	2.0	0.287	0.290	0.290
	2.5	0.342	0.344	0.344
4. UNIFORM THICKNESS (t = 2.5)	0.5	0.054	0.021	0.053
	1.0		0.032	0.076
	1.5		0.039	0.097
	2.0		0.047	0.116
	2.5		0.055	0.138
3. LINEARLY VARYING THICKNESS (t = 0.5 + 0.2x)	0.5	0.099	0.062	0.096
	1.0	0.136	0.081	0.130
	1.5	0.164	0.092	0.154
	2.0	0.189	0.101	0.173
	2.5	0.218	0.109	0.192
4. LINEARLY VARYING THICKNESS (t = 2.5 - 0.2x)	0.5	0.109	0.076	0.109
	1.0	0.164	0.122	0.167
	1.5	0.220	0.173	0.226
	2.0	0.283	0.235	0.293
	2.5	0.366	0.316	0.376
5. QUADRATICALLY VARYING THICKNESS ($t = 1.0 + 0.2x + 0.02x^2$)	0.5	0.139	0.127	0.135
	1.0	0.186	0.159	0.179
	1.5	0.221	0.172	0.205
	2.0	0.248	0.179	0.225
	2.5	0.277	0.184	0.241

As with configuration 201, the K values listed in Table 4.2.2-1 for the two different stress inputs validate the variable thickness *K vs a* solution for configuration 202

when the stress inputs in NASCRAC™ are load/unit width values on the crack plane, i.e., stress values on the crack plane multiplied by the corresponding plate thickness at that stress location. This NASCRAC™ solution uses weight function theory in which the weight function was adapted from [3] and is defined in terms of load/unit width. This type input is inconsistent with other NASCRAC™ variable thickness solutions and traditional weight function theory, where the formulation is in terms of stresses on the crack plane. This inconsistency needs to be clearly identified in the documentation. A more consistent approach is to recode the solution to accept stress input.

Table 4.2.2-2 Load Inputs for 202 Variable Thickness *K vs a* Calculations

LOADS ON CRACK PLANE										
	CASE 1		CASE 2		CASE 3		CASE 4		CASE 5	
x	σ	σ* t	σ	σ* t	σ	σ* t	σ	σ* t	σ	σ* t
0	0.097	0.097	0.039	0.097	0.127	0.064	0.025	0.062	0.182	0.091
1.02	0.095	0.095	0.038	0.095	0.115	0.081	0.035	0.079	0.168	0.088
2.04	0.097	0.097	0.039	0.097	0.106	0.097	0.046	0.097	0.154	0.090
3.06	0.101	0.101	0.041	0.101	0.099	0.110	0.059	0.111	0.143	0.098
4.08	0.105	0.105	0.042	0.105	0.091	0.119	0.071	0.120	0.131	0.109
5	0.106	0.106	0.043	0.106	0.082	0.123	0.081	0.122	0.117	0.117
6.02	0.105	0.105	0.042	0.105	0.071	0.121	0.091	0.118	0.100	0.122
7.04	0.101	0.101	0.041	0.101	0.059	0.113	0.099	0.108	0.079	0.118
8.06	0.097	0.097	0.039	0.097	0.046	0.098	0.106	0.094	0.059	0.106
9.08	0.095	0.095	0.038	0.095	0.035	0.080	0.115	0.079	0.039	0.084
10	0.097	0.097	0.039	0.097	0.026	0.064	0.126	0.063	0.024	0.060

Load = 1 lb_f along centerline for all cases.

4.2.3 CONFIGURATION 203 (SINGLE EDGE CRACK IN A PLATE)

Table 4.2.3-1 lists comparative results for 203 variable thickness *K vs a* calculations. These results were computed using a stress field on the crack plane induced by a 1 lb_f point load along the plate centerline. The stresses along the crack plane were determined using FRANC and input into NASCRAC™ as a stress table. Table 4.2.3-2 shows the two variants of input stresses for each case listed in Table 4.2.3-1. The results in Table 4.2.3-1 were computed using a panel width of 10".

NASCRAC™'s *K vs a* capability for a single edge crack in a variably thick plate compares well with FRANC results **when the input load case for NASCRAC™ consists of stress values on the crack plane**. This capability in NASCRAC™ was coded by using a generic influence function approach in which the influence function coefficients were determined numerically from an offline analysis and hardwired into NASCRAC™. This approach required that the input load values be crack plane stresses, not load per unit width. This input is consistent with weight function theory formulations. Table 4.2.3-1 does show less agreement between NASCRAC™ and FRANC for larger cracks; therefore, results for a/W > 0.4 should be used cautiously.

Table 4.2.3-1. Representative Variable Thickness *K vs a* Results for 203

CASE	a	FRANC	NASCRAC STRESS INPUT	NASCRAC LOAD/UNIT WIDTH INPUT
1. UNIFORM THICKNESS ($t = 1.0$)	1.0	.2009	.2061	.2061
	2.0	.3276	.3319	.3319
	3.0	.4946	.4951	.4951
	4.0	.7340	.7391	.7391
	5.0	1.110	1.117	1.117
2. LINEARLY VARYING THICKNESS ($t = 0.5 + 0.2x$)	1.0	.2097	.2266	.1411
	2.0	.2865	.3167	.2353
	3.0	.3709	.4137	.3539
	4.0	.4838	.5438	.5156
	5.0	.6519	.7298	.7482
3. LINEARLY VARYING THICKNESS ($t = 2.5 - 0.2x$)	1.0	.0688	.0677	.1598
	2.0	.1452	.1346	.3015
	3.0	.2708	.2392	.5104
	4.0	.4838	.4165	.8481
	5.0	.8629	.7294	1.4305
4. QUADRATICALLY VARYING THICKNESS ($t = 0.5 + 0.02x^2$)	1.0	.3412	.3682	.1890
	2.0	.4638	.5313	.2857
	3.0	.5770	.6836	.3920
	4.0	.7107	.8628	.5359
	5.0	.8971	1.090	.7333

Table 4.2.3-2. Stress Inputs for 203 Variable Thickness *K vs a* Calculations

LOADS ON CRACK PLANE								
POSITION	CASE 1		CASE 2		CASE 3		CASE 4	
x	σ	$\sigma^* t$	σ	$\sigma^* t$	σ	$\sigma^* t$	σ	$\sigma^* t$
0	0.097	0.097	0.127	0.064	0.025	0.062	0.182	0.091
1.02	0.095	0.095	0.115	0.081	0.035	0.079	0.168	0.088
2.04	0.097	0.097	0.106	0.097	0.046	0.097	0.154	0.090
3.06	0.101	0.101	0.099	0.110	0.059	0.111	0.143	0.098
4.08	0.105	0.105	0.091	0.119	0.071	0.120	0.131	0.109
5	0.106	0.106	0.082	0.123	0.081	0.122	0.117	0.117
6.02	0.105	0.105	0.071	0.121	0.091	0.118	0.100	0.122
7.04	0.101	0.101	0.059	0.113	0.099	0.108	0.079	0.118
8.06	0.097	0.097	0.046	0.098	0.106	0.094	0.059	0.106
9.08	0.095	0.095	0.035	0.080	0.115	0.079	0.039	0.084
10	0.097	0.097	0.026	0.064	0.126	0.063	0.024	0.060

Load = 1 lb_f along centerline for all cases.

4.2.4 CONFIGURATION 204 (DOUBLE EDGE CRACKS IN A PLATE)

Table 4.2.4-1 lists comparative results for 204 variable thickness *K vs a* calculations. These results were computed using a stress field on the crack plane induced by a 1 lb_f point load along the panel centerline. The stresses along the crack plane were determined using FRANC and input into NASCRAC™ as a stress table. Table 4.2.4-2 shows the two variants of input stresses

for each case listed in Table 4.2.4-1. The results in Table 4.2.4-1 were computed using a panel width of 10".

Table 4.2.4-1. Representative Variable Thickness *K vs a* Results for 204

CASE	a	FRANC	NASCRAC™ STRESS INPUT	NASCRAC™ LOAD/UNIT WIDTH INPUT
1. UNIFORM THICKNESS (t = 1.0)	0.5	0.135	0.137	0.137
	1.0	0.187	0.194	0.194
	1.5	0.230	0.240	0.240
	2.0	0.271	0.283	0.283
	2.5	0.317	0.327	0.327
2. UNIFORM THICKNESS (t = 2.5)	0.5	0.054	0.022	0.055
	1.0	0.075	0.031	0.078
	1.5	0.092	0.038	0.096
	2.0	0.108	0.045	0.113
	2.5	0.127	0.053	0.131
3. LINEARLY VARYING THICKNESS (t = 0.5 + 0.2x)	0.5	0.157	0.293	0.164
	1.0	0.203	0.346	0.214
	1.5	0.234	0.365	0.247
	2.0	0.259	0.373	0.273
	2.5	0.286	0.378	0.298
4. LINEARLY VARYING THICKNESS (t = 2.5 - 0.2x)	0.5	0.039	0.016	0.040
	1.0	0.062	0.027	0.063
	1.5	0.087	0.038	0.088
	2.0	0.110	0.052	0.115
	2.5	0.142	0.069	0.148
5. QUADRATICALLY VARYING THICKNESS ($t = 0.5 - 0.02x^2$)	0.5	0.251	0.496	0.251
	1.0	0.332	0.676	0.347
	1.5	0.388	0.772	0.405
	2.0	0.431	0.840	0.453
	2.5	0.474	0.871	0.485

Table 4.2.4-2. Stress Inputs for 204 Variable Thickness *K vs a* Calculations

LOADS ON CRACK PLANE										
	CASE 1		CASE 2		CASE 3		CASE 4		CASE 5	
x	σ	σ*thk	σ	σ*thk	σ	σ*thk	σ	σ*thk	σ	σ*thk
0	0.097	0.097	0.039	0.097	0.127	0.064	0.025	0.062	0.182	0.091
1.02	0.095	0.095	0.038	0.095	0.115	0.081	0.035	0.079	0.168	0.088
2.04	0.097	0.097	0.039	0.097	0.106	0.097	0.046	0.097	0.154	0.090
3.06	0.101	0.101	0.041	0.101	0.099	0.110	0.059	0.111	0.143	0.098
4.08	0.105	0.105	0.042	0.105	0.091	0.119	0.071	0.120	0.131	0.109
5	0.106	0.106	0.043	0.106	0.082	0.123	0.081	0.122	0.117	0.117
6.02	0.105	0.105	0.042	0.105	0.071	0.121	0.091	0.118	0.100	0.122
7.04	0.101	0.101	0.041	0.101	0.059	0.113	0.099	0.108	0.079	0.118
8.06	0.097	0.097	0.039	0.097	0.046	0.098	0.106	0.094	0.059	0.106
9.08	0.095	0.095	0.038	0.095	0.035	0.080	0.115	0.079	0.039	0.084
10	0.097	0.097	0.039	0.097	0.026	0.064	0.126	0.063	0.024	0.060

Load = 1 lb_f along centerline for all cases.

As with configurations 201 and 202, the K values listed in Table 4.2.4-1 for the two different stress inputs validate the variable thickness *K vs a* solution for configuration 204 **when the stress inputs in NASCRAC™ are load/unit width values on the crack plane**, i.e., stress values on the crack plane multiplied by the corresponding plate thickness at that stress location. This NASCRAC™ solution uses weight function theory in which the weight function was adapted from [3] and is defined in terms of load/unit width. This type input is inconsistent with other NASCRAC™ variable thickness solutions and traditional weight function theory, where the formulation is in terms of stresses on the crack plane. This inconsistency needs to be clearly identified in the documentation. A more consistent approach is to recode the NASCRAC™ solution to accept stress input.

4.2.5 CONFIGURATION 205 (AXIAL (ID) CRACK IN A HOLLOW CYLINDER)

Comparative results for the 205 variable thickness *K vs a* solution are shown in Table 4.2.5-1. These results were computed using a uniform internal radial pressure of 1 psi. The crack plane stress were calculated from thick walled cylinder solutions for pressurized cylinders. These stresses were adjusted for thickness variation and checked versus FRANC calculations. Table 4.2.5-2 lists these crack plane stresses for the cases in Table 4.2.5-1.

Table 4.2.5-1. Representative Variable Thickness *K vs a* Results for 205

CASE	a	FRANC	NASCRACTM
1. UNIFORM THICKNESS (t = 1.0)	0.5	2.11	2.14
	1.0	2.88	2.89
	1.5	3.51	3.45
	2.0	4.10	4.19
	2.5	4.74	4.81
2. UNIFORM THICKNESS (t = 2.5)	0.5	0.84	0.85
	1.0	1.15	1.15
	1.5	1.40	1.42
	2.0	1.64	1.67
	2.5	1.89	1.93
3. LINEARLY VARYING THICKNESS (t = 3.5 + 0.2x)	0.5	0.62	0.60
	1.0	0.83	0.78
	1.5	1.01	0.94
	2.0	1.17	1.08
	2.5	1.34	1.21
	3.0	1.51	1.33
	4.0	1.93	1.70

inner diameter (D) = 10", outer diameter (D) = 20", wall thickness = 5"
Load = 1 psi uniform internal radial pressure

Table 4.2.5-2. Crack Plane Stresses for 205 Variable Thickness *K vs a* Calculations

CRACK PLANE STRESSES FOR UNIFORM INTERNAL RADIAL PRESSURE			
POSITION x	σ: CASE 1	σ: CASE 2	σ: CASE 3
0	0.003	0.001	0.020
1.0	0.032	0.013	0.044
2.0	0.075	0.030	0.074
3.0	0.127	0.051	0.106
4.0	0.173	0.069	0.130
5.0	0.198	0.079	0.137

Note: Position x is measured with x = 0 at the internal surface of the cylinder.

Results from NASCRAC™'s *K vs a* capability for an inner diameter axial crack in a variably thick hollow cylinder (205) agreed with FRANC results for uniform thicknesses not equal to unity and compared reasonably well with FRANC for linearly varying thicknesses. This capability in NASCRAC™ was coded by using a generic influence function approach such that influence function coefficients were determined numerically from an offline analysis and hardwired into NASCRAC™. This approach was formulated based on crack plane stress inputs. Only one r/W ratio (r/W = 1) was analyzed since the methodology was identical in all cases and previous uniformly thick analyses of all r/W ratios

showed all the r/W configurations to be valid. Based on the general agreement between NASCRAC™ and FRANC, **this solution is valid for cracks whose length does not exceed 0.5 t, where t is the cylinder wall thickness**. For longer cracks, the results in the table above suggest that some divergence occurs. However, the NASCRAC™ solution still appears to be within reasonable engineering bounds (12%).

The physical implication of this solution is not clear. The thickness variation occurs in the plane of the crack. This implies that the cylinder length (which is equivalent to thickness in this solution) varies across the wall thickness.

4.2.6 CONFIGURATION 206 (EDGE CRACK IN A DISK)

Variable thickness K vs a comparative results for configuration 206 are presented in Tables 4.2.6-1 and 4.2.6-2. The results in Table 4.2.6-1 were computed using stresses on the crack plane induced by a single point load of 1 lb_f along the centerline of the disk. The results in Table 4.2.6-2 were computed using stresses on the crack plane induced by a distributed load whose resultant was 1 lb_f. The distributed load was applied at the quarterlines and the centerline of the disk. The stresses on the crack plane were calculated using FRANC and then input into NASCRAC™ as a one-dimensional stress table. Tables 4.2.6-3 and 4.2.6-4 list the crack plane stresses corresponding to the two load distribution cases. In all the analyses, the diameter of the disk was 10".

Table 4.2.6-1 Representative Variable Thickness *K vs a* Results for 206 with a Centerline Load

CASE	a	FRANC	NASCRAC™ STRESS INPUTS	NASCRAC™ LOAD/UNIT WIDTH INPUTS
1. UNIFORM THICKNESS (t = 1.0)	1.0	0.039	0.046	0.046
	2.0	0.143	0.151	0.151
	3.0	0.338	0.337	0.337
	4.0	0.643	0.651	0.651
	5.0	1.13	1.14	1.14
2. UNIFORM THICKNESS (t = 2.5)	1.0	0.016	0.018	0.046
	2.0	0.057	0.060	0.151
	3.0	0.135	0.135	0.337
	4.0	0.257	0.260	0.651
	5.0	0.452	0.456	1.14
3. LINEARLY VARYING THICKNESS (t = 0.5 + 0.2x)	1.0	0.064	0.071	0.047
	2.0	0.144	0.158	0.127
	3.0	0.267	0.285	0.267
	4.0	0.434	0.471	0.505
	5.0	0.674	0.732	0.865
4. LINEARLY VARYING THICKNESS (t = 2.5 - 0.2x)	1.0	-6E-4	0.002	0.003
	2.0	0.055	0.056	0.117
	3.0	0.181	0.169	0.336
	4.0	0.419	0.384	0.720
	5.0	0.863	0.767	1.37
5. QUADRATICALLY VARYING THICKNESS ($t = 0.5 - 0.02x^2$)	1.0	0.104	0.116	0.060
	2.0	0.235	0.262	0.144
	3.0	0.419	0.463	0.280
	4.0	0.644	0.736	0.500
	5.0	0.938	1.08	0.824

diameter (D) = 10"

Table 4.2.6-2. Representative Variable Thickness *K vs a* Results for 206 with a Distributed Load

CASE	a	FRANC	NASCRAC™ STRESS INPUTS	NASCRAC™ LOAD/UNIT WIDTH INPUTS
1	1.0	0.155	0.162	0.162
2	1.0	0.062	0.065	0.162
3	1.0	0.184	0.196	0.125
4	1.0	0.060	0.058	0.137
5	1.0	0.286	0.337	0.170

diameter (D) = 10"

Table 4.2.6-3. Stresses Induced by Centerline Load for 206 Variable Thickness *K vs a* Calculations

POSITION	CASE 1		CASE 2		CASE 3		CASE 4		CASE 5	
x	σ	σ*thk	σ	σ*thk	σ	σ*thk	σ	σ*thk	σ	σ*thk
0	0.003	0.003	0.001	0.003	0.020	0.010	-0.010	-0.026	0.029	0.014
1.02	0.032	0.032	0.013	0.032	0.044	0.031	0.010	0.023	0.065	0.034
2.04	0.075	0.075	0.030	0.075	0.074	0.067	0.039	0.081	0.112	0.065
3.06	0.127	0.127	0.051	0.127	0.106	0.118	0.075	0.141	0.162	0.111
4.08	0.173	0.173	0.069	0.174	0.130	0.171	0.111	0.187	0.196	0.163
5	0.198	0.198	0.079	0.198	0.137	0.205	0.135	0.202	0.203	0.203
6.02	0.173	0.173	0.069	0.174	0.111	0.189	0.130	0.168	0.160	0.196
7.04	0.127	0.127	0.051	0.127	0.075	0.143	0.106	0.116	0.104	0.155
8.06	0.075	0.075	0.030	0.075	0.039	0.081	0.074	0.066	0.050	0.091
9.08	0.032	0.032	0.013	0.032	0.010	0.023	0.044	0.030	0.009	0.020
10	0.003	0.003	0.001	0.003	-0.009	-0.021	0.022	0.011	-0.017	-0.042

Load = 1 lb_f along centerline of disk perpendicular to crack plane.

Table 4.2.6-4. Stresses Induced by Distributed Load for 206 Variable Thickness *K vs a* Calculations

POSITION	CASE 1		CASE 2		CASE 3		CASE 4		CASE 5	
x	σ	σ*thk	σ	σ*thk	σ	σ*thk	σ	σ*thk	σ	σ*thk
0	0.049	0.049	0.019	0.049	0.074	0.037	0.012	0.029	0.132	0.066
1.02	0.082	0.082	0.033	0.082	0.106	0.075	0.033	0.076	0.152	0.079
2.04	0.105	0.105	0.042	0.105	0.115	0.104	0.050	0.105	0.172	0.100
3.06	0.112	0.112	0.045	0.112	0.104	0.116	0.061	0.115	0.158	0.109
4.08	0.116	0.116	0.046	0.116	0.093	0.122	0.072	0.122	0.140	0.116
5	0.119	0.119	0.048	0.119	0.084	0.126	0.083	0.125	0.125	0.125
6.02	0.116	0.116	0.046	0.116	0.072	0.123	0.093	0.120	0.103	0.126
7.04	0.112	0.112	0.045	0.112	0.061	0.117	0.104	0.114	0.082	0.122
8.06	0.105	0.105	0.042	0.105	0.050	0.106	0.115	0.102	0.062	0.111
9.08	0.082	0.082	0.033	0.082	0.033	0.077	0.106	0.073	0.037	0.079
10	0.049	0.049	0.019	0.049	0.014	0.035	0.078	0.039	0.011	0.027

Load = 0.5 lb_f along centerline of disk, 0.25 lb_f along quarterlines

NASCRAC™'s *K vs a* capability for a single edge crack in a variably thick solid disk (206) compares reasonably well with FRANC results (within 15%) **when the input load case for NASCRAC™ consists of stress values on the crack plane.** This capability in NASCRAC was coded with a generic influence function in which the influence function coefficients were

determined numerically from an offline analysis and hardwired into NASCRAC™. This input is consistent with weight function theory formulations. The load application (centerline load versus distributed load) did not significantly affect the relative differences between NASCRAC™ and FRANC results. The agreement between NASCRAC™ and FRANC does validate this solution.

4.2.7 CONFIGURATION 207 (AXIAL (OD) CRACK IN A HOLLOW CYLINDER)

Comparative results for the 207 variable thickness *K vs a* solution are shown in Table 4.2.7-1. These results were computed using a uniform internal radial pressure of 1 psi. The crack plane stress were calculated from thick walled cylinder solutions for pressurized cylinders. These stresses were adjusted for thickness variation and checked versus FRANC calculations. Table 4.2.7-2 lists these crack plane stresses for the cases in Table 4.2.7-1.

Table 4.2.7-1. Representative Variable Thickness *K vs a* Results for 207

CASE	a	FRANC	NASCRAC™
1. UNIFORM THICKNESS (t = 1.0)	0.5	1.01	1.03
	1.0	1.59	1.62
	1.5	2.24	2.26
	2.0	2.98	3.03
	2.5	3.91	3.95
2. UNIFORM THICKNESS (t = 2.5)	0.5	0.40	0.41
	1.0	0.64	0.65
	1.5	0.90	0.91
	2.0	1.20	1.21
	2.5	1.56	1.58
3. LINEARLY VARYING THICKNESS (t = 0.5 + 0.2x)	0.5	1.14	1.20
	1.0	1.62	1.75
	1.5	2.06	2.27
	2.0	2.53	2.83
	2.5	3.07	3.46

inner diameter (D) = 10",
outer diameter (D) = 20"

Table 4.2.7-2 . Crack Plane Stresses for 207 Variable Thickness *K vs a* Calculations

CRACK PLANE STRESSES FOR UNIFORM INTERNAL RADIAL PRESSURE = 1 psi			
POSITION	σ: CASE 1	σ: CASE 2	σ: CASE 3
0	0.68	0.27	0.86
1.02	0.75	0.30	0.89
2.04	0.86	0.34	0.92
3.06	1.02	0.41	0.98
4.08	1.28	0.51	1.08
4.90	1.59	0.64	1.21

Results from NASCRAC™'s *K vs a* capability for an outer diameter axial crack in a variably thick hollow cylinder (207) agreed with FRANC results for uniform thicknesses not equal to unity and compared reasonably well with FRANC for linearly varying thicknesses.. This capability in NASCRAC™ was coded by using a generic influence function approach where influence function coefficients were determined numerically from an offline analysis and hardwired into NASCRAC™. This approach was formulated based on crack plane stress inputs. Based on the general agreement between NASCRAC™ and FRANC, this capability is valid for cracks whose length does not exceed 0.5 t, where t is the cylinder wall thickness. Based on the general agreement between NASCRAC™ and FRANC, this capability is valid for cracks with a/t < 0.5 (t is the cylinder wall thickness.). For cracks where a/t ≥ 0.5, the results for case 3 in Table 4.2.7-1 above hint of some divergence between NASCRAC™ and FRANC and hence such results should be used with less confidence.

The physical implication of this solution is not clear. The thickness variation occurs in the plane of the crack. This implies that the cylinder length (which is equivalent to thickness in this solution) varies across the wall thickness.

4.2.8 REFERENCES FOR SECTION 4.2

1. *Wawrzynek, P. FRacture ANalysis Code (FRANC) Primer for Version 2.5, Cornell University, Ithaca, NY, 1991.*
2. *Wawrzynek, P. FRacture ANalysis Code (FRANC) Version 2.3+ Release Notes, Cornell University, Ithaca, NY, 1990.*
3. *Tada, H., Paris, P.C., and Irwin, G.R., The Stress Analysis of Cracks Handbook, Del Research Corporation, 1985.*

4.3 *J vs a* CALCULATION

NASCRAC™ contains *J vs a* solutions for eight configurations. These solutions were adapted from [1] and [2]. The solutions assume that J can be calculated as the sum of an elastic J (J_e) and a plastic J (J_e). The verification and validation approach to these solutions was a four step approach: 1) verification of coded Jp equation, 2) verification of coded limit load (P_0) equation, 3) line-by-line comparison of NASCRAC™'s h_1 tables with [1] and [2], and 4) comparison of NASCRAC™ results with spreadsheet results obtained using the formulas in [1] and [2]. In step 4), J_e was calculated using $J_e = K^2/E'$ where K was obtained from the NASCRAC™ K solution and an effective crack length. In general, the *J vs a* capabilities in NASCRAC™ were found to be valid; however, several exceptions were discovered. Configuration 303, a circumferential through crack in a cylinder, was the most notable exception because it contained a runtime error. The remaining invalidities were due to the h_1 table and the method of calculating J_e, the elastic J integral. h_1 is a dimensionless function included in the J_P (plastic J) formulation. It is dependent on a/b, the crack length to specimen width ratio, and n, a hardening exponent for the Ramberg-Osgood constitutive relationship. These relationships are expressed in the following equations:

$$J_p = a\,\sigma_y\,\varepsilon_y\,c\,\frac{a}{b}\,h_1\left(\frac{P}{P_0}\right)^{n+1} \qquad \text{(eq. 4.3-1)}$$

$$h_1 = f\left(\frac{a}{b}, n\right) \qquad \text{(eq. 4.3-2)}$$

$$\frac{\varepsilon}{\varepsilon_0} = a\left(\frac{\sigma}{\sigma_0}\right)^n \qquad \text{(eq. 4.3-3)}$$

The most significant h_1 differences between NASCRAC™ and the references occurred in the plane strain case of configuration 203. Several less significant h_1 errors were also discovered for configurations 101, 202, and 204. These h_1 tables should be updated prior to releasing future NASCRAC™ versions.

For J_e, the discrepancies between the NASCRAC™ computed value (computed using the elastic version of the coded J_p formulation and an effective crack length) and a J_e computed from K, E, and an effective crack length were observed to be more severe as the analysis transitioned into the elastic-plastic and plastic regime. Although some of these discrepancies were significant (differences of 50-60%), the contribution of J_e towards the total J for these cases was insignificant.

4.3.1 CONFIGURATION 101 (COMPACT TENSION SPECIMEN)

Comparative *J vs a* results for configuration 101 are shown in Table 4.3.1-1. Plane stress and plane strain were considered as indicated. The results in Table 4.3.1-1 were calculated with three different point loads: 1, 50, and 250 kips. This range of loads provided elastic (cases 1-4,

10-13), elastic-plastic (cases 5-7, 14-16), and fully plastic (cases 8-9, 17-18) results. Material properties for the calculations are listed in Table 4.3.1-2.

Table 4.3.1-1. Representative Results for 101 *J vs a* Computations

Case	a	W	B	P	J_e NASCRAC™	J_e Reference	J_p NASCRAC™	J_p Reference	J_{TOTAL} NASCRAC™	J_{TOTAL} Reference
PLANE STRESS										
1	2.5	10	2.5	1	$3.9(10^{-5})$	$3.8(10^{-5})$	$3.6(10^{-25})$	$3.6(10^{-25})$	$3.9(10^{-5})$	$3.8(10^{-5})$
2	7.5	10	2.5	1	$1.4(10^{-3})$	$1.3(10^{-3})$	$4.6(10^{-14})$	$4.6(10^{-14})$	$1.4(10^{-3})$	$1.3(10^{-3})$
3	2.5	10	5.0	1	$9.8(10^{-6})$	$9.4(10^{-6})$	$1.7(10^{-28})$	$1.7(10^{-28})$	$9.8(10^{-6})$	$9.4(10^{-6})$
4	7.5	10	5.0	1	$3.4(10^{-4})$	$3.2(10^{-4})$	$2.2(10^{-17})$	$2.2(10^{-17})$	$3.4(10^{-4})$	$3.2(10^{-4})$
5	2.5	10	2.5	50	0.102	0.0987	$1.73(10^{-6})$	$1.73(10^{-6})$	0.102	0.0987
6	5.0	10	2.5	50	0.436	0.424	0.0214	0.0214	0.457	0.446
7	6.25	10	2.5	50	1.36*	0.641	23.7*	21.2	23.7*	21.8
8	2.5	10	2.5	250	4.4	2.4	84.7	84.7	89.1	87.0
9	3.75	10	2.5	250	17.8*	16.8	5175*	5250	5193*	5267
PLANE STRAIN										
10	2.5	10	2.5	1	$3.1(10^{-5})$	$3.4(10^{-5})$	$2.1(10^{-26})$	$2.1(10^{-26})$	$3.1(10^{-5})$	$3.4(10^{-5})$
11	7.5	10	2.5	1	$1.1(10^{-3})$	$1.1(10^{-3})$	$2.2(10^{-15})$	$2.2(10^{-15})$	$1.1(10^{-3})$	$1.1(10^{-3})$
12	2.5	10	5.0	1	$7.7(10^{-6})$	$8.4(10^{-6})$	$1.0(10^{-29})$	$1.0(10^{-29})$	$7.7(10^{-6})$	$8.4(10^{-6})$
13	7.5	10	5.0	1	$2.7(10^{-4})$	$2.9(10^{-4})$	$1.1(10^{-18})$	$1.1(10^{-18})$	$2.7(10^{-4})$	$2.9(10^{-4})$
14	2.5	10	2.5	50	0.078	0.085	$1.03(10^{-7})$	$1.03(10^{-7})$	0.078	0.085
15	5.0	10	2.5	50	0.309	0.322	$7.79(10^{-4})$	$7.79(10^{-4})$	0.310	0.323
16	6.25	10	2.5	50	0.819*	0.904	0.908*	0.886	1.757*	1.791
17	2.5	10	2.5	250	2.3	2.1	5.0	5.0	7.4	7.1
18	5.0	10	2.5	250	18.9	23.2	38020	38020	38030	38040

* Interpolated value

Table 4.3.1-2. Material Properties for *J vs a* Computations

MATERIAL PROPERTY	SYMBOL	VALUE
YOUNG'S MODULUS	E	10000 ksi
YIELD STRESS	σ_y	37 ksi
FLOW STRESS	D	50 ksi
POISSON'S RATIO	ν	0.33

NASCRAC™'s *J vs a* solution for configuration 101, compact tension specimen, agrees with [1] for the ranges specified in the documentation ($0.25 \le a/W < 1.0$, $1 \le n \le 20$); therefore, this solution is valid to the extent that reference [1] is valid. The original work from [1] used a table look-up based on a/W and n whereas NASCRAC™ uses a look-up based on a/W and 1/n; however, the J_p from NASCRAC™ and [1] are identical or nearly identical in all comparison cases (Some comparisons, i.e., 7, 9, 16, used interpolated NASCRAC™ output which led to insignificant differences between NASCRAC™ and [1].). Additionally, two discrepancies

occurred in the NASCRAC™ h_1 table for plane strain, namely, at a/W = 0.375 for n =16 and 20. Minor differences in J_e exist between NASCRAC™ and the reference values in Table 4.3.1-1 due to different computational techniques. NASCRAC™ uses the linear version of the J_p expression whereas the reference value was determined using $J_e = K_I^2/E'$. The J_e comparison is reasonable in the elastic regime and diverges as the analysis transitions into elastic-plastic and plastic conditions; therefore, the divergence is not significant until J_p dominates the total J solution. A comparison of the NASCRAC™ coded P_0 equation with [1] showed identical agreement. A final comparison between NASCRAC™ and [1] proved that the coded J_p equation reduces to the J_p equation. Future NASCRAC™ releases should include an updated h_1 table for this solution which corrects the discrepancies described above.

4.3.2 CONFIGURATION 104 (STANDARD THREE-POINT BEND SPECIMEN)

Comparative *J vs a* results for configuration 104 are shown in Table 4.3.2-1. Plane stress and plane strain were considered as indicated. The results in Table 4.3.2-1 were calculated with three different point loads: 1, 30, and 60 kips. This range of loads provided elastic (cases 1-3, 10-12), elastic-plastic (cases 4-6, 13-15), and fully plastic (cases 7-8, 16-18) results. Material properties for the calculations are listed in Table 4.3.1-2.

NASCRAC™'s *J vs a* solution for configuration 104, standard three-point bend specimen, agrees with [1] for the ranges specified in the documentation ($0.125 \le a/W \le 0.875$, $1 \le n \le 20$); hence, this solution is valid to the extent that [1] is valid. The original work from [1] used a table look-up based on a/W and n whereas NASCRAC™ uses a look-up based on a/W and 1/n; however, the J_p from NASCRAC™ and [1] are identical or nearly identical in all cases. Minor differences in J_e exist between NASCRAC™ and the reference values in Table 4.3.1-1 due to different computational techniques. NASCRAC™ uses the linear version of the J_p expression whereas the reference value was determined using $J_e = K_I^2/E'$. The J_e comparison is reasonable in the elastic regime and diverges as the analysis transitions into elastic-plastic and plastic conditions; therefore, the divergence is not significant until J_p dominates the total J solution. A comparison of the NASCRAC™ h_1 tables, coded J_p equation, and coded P_0 equation to the quantities in [1] showed identical agreement.

Table 4.3.2-1 Representative Results for 104 *J vs a* Computations

Case	a	W	B	P	J_e NASCRAC™	J_e Reference	J_p NASCRAC™	J_p Reference	J_{TOTAL} NASCRAC™	J_{TOTAL} Reference
PLANE STRESS										
1	1	4	1	1	$7.2(10^{-4})$	$7.2(10^{-4})$	$2.0(10^{-15})$	$2.0(10^{-15})$	$7.2(10^{-4})$	$7.2(10^{-4})$
2	2	4	1	1	$2.9(10^{-3})$	$2.8(10^{-3})$	$8.1(10^{-12})$	$8.1(10^{-12})$	$2.9(10^{-3})$	$2.8(10^{-3})$
3	3	4	1	1	$2.5(10^{-2})$	$2.7(10^{-2})$	$1.9(10^{-5})$	$1.9(10^{-5})$	$2.5(10^{-2})$	$2.7(10^{-2})$
4	0.5	4	1	30	0.40	0.40	1.7	1.7	2.06	2.06
5	1	4	1	30	0.96	0.98	34.9	34.9	35.9	35.9
6	1.5	4	1	30	2.9	3.1	2030	2010	2033	2010
7	0.5	4	1	60	2.96	2.99	3388	3392	3391	3395
8	1	4	1	60	14.9	16.1	$7.15(10^{4})$	$7.15(10^{4})$	$7.16(10^{4})$	$7.16(10^{4})$
PLANE STRAIN										
10	1	4	1	1	$5.7(10^{-4})$	$6.4(10^{-4})$	$1.4(10^{-16})$	$1.4(10^{-16})$	$5.7(10^{-4})$	$6.4(10^{-4})$
11	2	4	1	1	$2.2(10^{-3})$	$2.5(10^{-3})$	$4.6(10^{-13})$	$4.6(10^{-13})$	$2.2(10^{-3})$	$2.5(10^{-3})$
12	3	4	1	1	$1.7(10^{-2})$	$2.2(10^{-2})$	$1.0(10^{-6})$	$1.0(10^{-6})$	$2.0(10^{-2})$	$2.2(10^{-2})$
13	0.5	4	1	30	0.27	0.31	0.082	0.084	0.35	0.40
14	1	4	1	30	0.58	0.67	2.6	2.56	3.14	3.23
15	1.5	4	1	30	1.24	1.50	126.3	125	127.5	126.7
16	0.5	4	1	60	1.29	1.54	169	172	170	174
17	1	4	1	60	3.25	3.95	5242	5242	5245	5246
18	1.5	4	1	60	11.1	15.8	$2.59(10^{5})$	$2.56(10^{5})$	$2.59(10^{5})$	$2.56(10^{5})$

4.3.3 CONFIGURATION 202 (CENTER CRACKED PANEL)

Comparative *J vs a* results for configuration 202 are shown in Table 4.3.3-1. Plane stress and plane strain were considered as indicated. The results in Table 4.3.3-1 were calculated with two different point loads: 1 and 25 ksi. This range of loads provided elastic (cases 1-3, 7-9), elastic-plastic (cases 4, 10), and fully plastic (cases 5-6, 11-12) results. Material properties for the calculations are listed in Table 4.3.1-2.

NASCRAC™'s *J vs a* solution for configuration 202, center cracked panel, is valid for the ranges specified in the documentation ($0.0 \le a/W < 0.875$, $1 \le n \le 20$); hence, this solution is valid top the extent [1] is valid. The original work from [1] used a table look-up based on a/W and n whereas NASCRAC™ uses a look-up based on a/W and 1/n; however, the J_p from NASCRAC™ and [1] are in general agreement for all cases. Small differences (< 3% for plane stress, < 16% for plane strain) do exist between the NASCRAC™ h_1 table and the h_1 table in [1] for a/W = 0.125 and n = 10, 13, 16, and 20 but probably are not significant to the final result. Differences in J_e also exist between NASCRAC™ and the reference values in Table 4.3-3-1 due to different computational methods. NASCRAC™ uses the linear version of the J_p expression whereas the reference value was determined using $J_e = K_I^2/E'$. The J_e comparison, however, is reasonable in

the elastic regime and diverges as the analysis transitions into elastic-plastic and plastic conditions; therefore, the divergence is not significant until J_p dominates the total J solution. A comparison of the coded P_0 equation with [1] showed identical agreement. Also a reduction of the coded J_p equation compared identically to the J_p equation in [1].

Table 4.3.3-1. Representative Results for 202 *J vs a* Computations

Case	a	W	σ	J_e NASCRAC™	J_e Reference	J_p NASCRAC™	J_p Reference	J_{TOTAL} NASCRAC™	J_{TOTAL} Reference
PLANE STRESS									
1	2	8	1	$6.8(10^{-4})$	$6.8(10^{-4})$	$1.0(10^{-15})$	$1.0(10^{-15})$	$6.8(10^{-4})$	$6.8(10^{-4})$
2	4	8	1	$1.8(10^{-3})$	$1.8(10^{-3})$	$6.0(10^{-14})$	$6.0(10^{-14})$	$1.8(10^{-3})$	$1.8(10^{-3})$
3	6	8	1	$5.0(10^{-3})$	$5.1(10^{-3})$	$5.6(10^{-11})$	$5.6(10^{-11})$	$5.0(10^{-3})$	$5.1(10^{-3})$
4	2	8	25	0.478	0.482	2.48	2.48	2.96	2.96
5	4	8	25	1.41	1.43	143	143	144	144
6	6	8	25	14.9	11.3	$1.33(10^5)$	$1.33(10^5)$	$1.33(10^5)$	$1.33(10^5)$
PLANE STRAIN									
7	2	8	1	$5.3(10^{-4})$	$6.0(10^{-4})$	$2.2(10^{-16})$	$2.2(10^{-16})$	$5.3(10^{-4})$	$6.0(10^{-4})$
8	4	8	1	$1.4(10^{-3})$	$1.6(10^{-3})$	$1.3(10^{-14})$	$1.3(10^{-14})$	$1.4(10^{-3})$	$1.6(10^{-3})$
9	6	8	1	$3.9(10^{-3})$	$4.5(10^{-3})$	$8.5(10^{-12})$	$8.5(10^{-12})$	$3.9(10^{-3})$	$4.5(10^{-3})$
10	2	8	25	0.348	0.396	0.520	0.520	0.869	0.917
11	4	8	25	0.935	1.08	31.2	31.2	32.2	32.3
12	6	8	25	3.37	4.12	$2.03(10^4)$	$2.03(10^4)$	$2.03(10^4)$	$2.03(10^4)$

4.3.4 CONFIGURATION 203 (SINGLE EDGE CRACK IN A PLATE)

Comparative *J vs a* results for configuration 203 are shown in Table 4.3.4-1. Plane stress and plane strain were considered as indicated. The results in Table 4.3.4-1 were calculated with two different point loads: 1 and 25 ksi. This range of loads provided elastic (cases 1-3, 6-8), elastic-plastic (cases 4, 9), and fully plastic (cases 5, 10) results. Material properties for the calculations are listed in Table 4.3.1-2.

Table 4.3.4-1. Representative Results for 203 *J vs a* Computations

Case	a	W	σ	J_e NASCRAC™	J_e Reference	J_p NASCRAC™	J_p Reference	J_{TOTAL} NASCRAC™	J_{TOTAL} Reference
PLANE STRESS									
1	2	8	1	$1.4(10^{-3})$	$1.4(10^{-3})$	$6.0(10^{-15})$	$6.0(10^{-15})$	$1.4(10^{-3})$	$1.4(10^{-3})$
2	4	8	1	$1.0(10^{-2})$	$1.0(10^{-2})$	$9.1(10^{-11})$	$9.1(10^{-11})$	$1.0(10^{-2})$	$1.0(10^{-2})$
3	6	8	1	$1.6(10^{-1})$	$1.7(10^{-1})$	$4.1(10^{-3})$	$4.1(10^{-3})$	$1.6(10^{-1})$	$1.7(10^{-1})$
4	2	8	25	1.31	1.32	14.2	14.2	15.5	15.5
5	4	8	25	772	813	$2.16(10^5)$	$2.16(10^5)$	$2.17(10^5)$	$2.17(10^5)$
PLANE STRAIN									
6	2	8	1	0.0011	0.0012	$5.9(10^{-16})$	$4.7(10^{-16})$	$1.1(10^{-3})$	$1.1(10^{-3})$
7	4	8	1	0.008	0.0090	$4.1(10^{-12})$	$2.3(10^{-12})$	$8.0(10^{-3})$	$8.0(10^{-3})$
8	6	8	1	0.11	0.13	$3.0(10^{-4})$	$1.2(10^{-4})$	$1.1(10^{-1})$	$1.1(10^{-1})$
9	2	8	25	0.81	0.92	1.41	1.12	2.22	2.04
10	4	8	25	13.6	17.4	$9.88(10^3)$	$5.59(10^3)$	$9.89(10^3)$	$5.61(10^3)$

The *J vs a* solution for configuration 203, single-edge crack in a plate, **is not valid for plane-strain elastic-plastic and plastic fracture.** Cases 9 and 10 and the J_p results in cases 6-8 in Table 4.3.4-1.provide evidence of this invalidity. The reason for this invalidity is differences between the NASCRAC™ h_1 values and [1] h_1 values as shown in Table 4.3.4-2. These differences ranged as high as 63%.

Table 4.3.4-2. NASCRAC™ and Reference h_1 Values for Configuration 203 in Plane Strain

a/b	n = 1		n = 3		n = 5		n = 10		n = 13		n = 16	
	NAS	[1]	NAS	[1]	NAS	[1]	NAS	[1]	NAS	[1]	NAS	[1]
1/8	4.95	5.01	8.57	9.09	11.5	12.7	16.1	21.7	18.1	27.3	19.9	34.4
1/4	4.34	4.42	4.64	5.16	3.82	4.50	2.17	2.74	1.55	1.93	1.11	1.82
3/8	3.88	3.97	2.63	2.88	1.68	1.92	0.54	0.70	0.28	0.40	0.14	0.22
1/2	3.40	3.45	1.69	2.02	0.93	1.22	0.21	0.38	0.09	0.19	0.04	0.10
5/8	2.86	2.89	1.30	1.70	0.70	1.11	0.15	0.42	0.06	0.24	0.03	0.14
3/4	2.34	2.38	1.25	1.56	0.77	1.13	0.23	0.59	0.12	0.41	0.06	0.29
7/8	1.91	1.93	1.37	1.43	1.10	1.18	0.70	0.81	na	na	na	na

This *J vs a* solution was found to be valid in the specified ranges ($0.0 \le a/W < 0.875$, $1 \le n \le 20$) for **plane strain elastic fracture and for plane stress elastic, elastic-plastic, and plastic fracture.** The minor differences observed in the J_e values in Table 4.3.4-1 for these cases were due to different computational techniques. NASCRAC™ uses the linear version of the J_p expression given in [1] whereas the reference value was calculated using $J_e = K_I^2/E'$ with K_I being calculated using an effective crack length. Although the J_e comparison is less agreeable in the elastic-plastic and plastic regimes, this is inconsequential because J_p dominates the total J solution in these regimes. A comparison of the NASCRAC™ coded P_0 equation and J_p equation with [1] showed identical agreement.

4.3.5 CONFIGURATION 204 (DOUBLE EDGE CRACKS IN A PLATE)

Comparative *J vs a* results for configuration 204 are shown in Table 4.3.5-1. Plane stress and plane strain were considered as indicated. The results in Table 4.3.5-1 were calculated with two different point loads: 1 and 25 ksi. This range of loads provided elastic (cases 1-3, 7-9), elastic-plastic (cases 4, 10-11), and fully plastic (cases 5-6, 12) results. Material properties for the calculations are listed in Table 4.3.1-2.

Table 4.3.5-1. Representative Results for 204 *J vs a* Computations

Case	a	W	σ	J_e NASCRAC™	J_e Reference	J_p NASCRAC™	J_p Reference	J_{TOTAL} NASCRAC™	J_{TOTAL} Reference
PLANE STRESS									
1	2	8	1	$8.1(10^{-4})$	$8.0(10^{-4})$	$4.7(10^{-16})$	$4.7(10^{-16})$	$8.1(10^{-4})$	$8.0(10^{-4})$
2	4	8	1	$1.8(10^{-3})$	$1.8(10^{-3})$	$1.5(10^{-14})$	$1.5(10^{-14})$	$1.8(10^{-3})$	$1.8(10^{-3})$
3	6	8	1	$4.0(10^{-3})$	$4.0(10^{-3})$	$1.2(10^{-11})$	$1.2(10^{-11})$	$4.0(10^{-3})$	$4.0(10^{-3})$
4	2	8	25	0.585	0.574	1.13	1.13	1.71	1.70
5	4	8	25	1.33	1.32	34.7	34.7	36.1	36.1
6	6	8	25	6.19	5.75	$2.95(10^4)$	$2.95(10^4)$	$2.95(10^4)$	$2.95(10^4)$
PLANE STRAIN									
7	2	8	1	$6.4(10^{-4})$	$7.1(10^{-4})$	$7.1(10^{-17})$	$7.1(10^{-17})$	$6.4(10^{-4})$	$7.1(10^{-4})$
8	4	8	1	$1.4(10^{-3})$	$1.6(10^{-3})$	$8.2(10^{-16})$	$8.2(10^{-16})$	$1.4(10^{-3})$	$1.6(10^{-3})$
9	6	8	1	$3.2(10^{-3})$	$3.5(10^{-3})$	$7.8(10^{-14})$	$7.7(10^{-14})$	$3.2(10^{-3})$	$3.5(10^{-3})$
10	2	8	25	0.420	0.468	0.169	0.169	0.589	0.636
11	4	8	25	0.937	1.05	1.97	1.97	2.90	3.02
12	6	8	25	2.24	2.79	185	183	187	186

The NASCRAC™ *J vs a* solution for 204 is generally valid in plane stress and plane strain for the ranges specified in the documentation ($0.125 \le a/W < 0.875$, $1 \le n \le 20$). However, several isolated differences between the h_1 tables in NASCRAC™ and [1] were discovered. For plane stress, four discrepancies were found: n = 16, a/W = 0.5 and n = 20, a/W = 0.5, 0.625, and 0.75. For plane strain discrepancies in the NASCRAC™ h_1 table occurred for all n values at a/W = 0.875 and for n=13 and 20 at a/W = 0.625.

Table 4.3.5-1 contains minor differences in J_e between NASCRAC™ and the reference value. These differences are due to different computational methods. NASCRAC™ uses the linear version of the J_p expression whereas the reference value was determined using $J_e = K_I^2/E'$. The J_e comparison, however, is reasonable in the elastic regime and diverges as the analysis transitions into elastic-plastic and plastic conditions; therefore, the divergence is not significant until J_p dominates the total J solution.

A comparison of the coded P_0 equation with [1] showed identical agreement. In addition, the coded J_p equation was shown to reduce to the J_p equation in [1]. Thus, as noted above, this solution is valid except for the h_1 differences described.

4.3.6 CONFIGURATION 205 (AXIAL (ID) CRACK IN A HOLLOW CYLINDER)

Comparative *J vs a* results for configuration 205 are shown in Table 4.3.6-1. The results in Table 4.3.6-1 were calculated with two different point loads: 1 and 30 ksi. This range of loads provided elastic (cases 1-6), elastic-plastic (cases 7, 9, 11), and fully plastic (cases 8, 10, 12) results. Material properties for the calculations are listed in Table 4.3.1-2.

Table 4.3.6-1. Representative Results for 205 *J vs a* Computations

Case	a	B	R	σ	J_e NASCRAC™	J_e Reference	J_p NASCRAC™	J_p Reference	J_{TOTAL} NASCRAC™	J_{TOTAL} Reference
1	2	8	40	1	$1.6(10^{-3})$	$1.0(10^{-3})$	$1.2(10^{-15})$	$1.2(10^{-15})$	$1.6(10^{-3})$	$1.0(10^{-3})$
2	6	8	40	1	0.028	0.020	$3.0(10^{-11})$	$3.1(10^{-11})$	0.028	0.020
3	2	8	80	1	$1.4(10^{-3})$	$1.2(10^{-3})$	$6.8(10^{-16})$	$6.8(10^{-16})$	$1.4(10^{-3})$	$1.2(10^{-3})$
4	6	8	80	1	0.036	0.032	$2.3(10^{-11})$	$2.3(10^{-11})$	0.036	0.032
5	2	8	160	1	$1.2(10^{-3})$	$1.3(10^{-3})$	$5.6(10^{-16})$	$5.6(10^{-16})$	$1.2(10^{-3})$	$1.3(10^{-3})$
6	6	8	160	1	0.048	0.048	$1.8(10^{-11})$	$1.8(10^{-11})$	0.048	0.048
7	2	8	40	30	1.8	1.3	21.4	21.4	23.2	22.7
8	4	8	40	30	14.4	7.6	919	919	934	927
9	2	8	80	30	1.5	1.3	12.1	12.1	13.6	13.4
10	4	8	80	30	17.8	14.0	593	593	611	607
11	2	8	160	30	1.3	1.6	9.9	9.9	11.2	11.5
12	4	8	160	30	19.1	26.4	525	525	544	551

The NASCRAC™ *J vs a* solution for configuration 205, axial inside crack in a hollow cylinder, is valid for the ranges specified in the documentation (R/b = 5, 10, 20; $0.125 \le a/b \le 0.75$; $1 \le n \le 10$). The original work from [1] used a table look-up based on a/W and n whereas NASCRAC™ uses a look-up based on a/W and 1/n; however, the J_p from NASCRAC™ and [1] are in general agreement and vary only due to differences in the h_1 for a few isolated cases. More significant differences exist between the NASCRAC™ J_e value and the reference J_e value. These differences are due to different computational methods. NASCRAC™ uses the linear version of the J_p expression whereas the reference value was computed using $J_e = K_I^2/E'$. However, the J_e comparison is reasonable in the elastic regime. The J_e comparison diverges more as the analysis transitions into elastic-plastic and plastic conditions but by this stage the J solution is dominated by J_p and hence the disagreement is not significant. Comparison of the NASCRAC™ coded P_0 equation and J_p equation with [1] showed identical agreement.

4.3.7 CONFIGURATION 303 (CIRCUMFERENTIAL THROUGH CRACK IN A CYLINDER)

Configuration 303 *J vs a* results from NASCRAC™ version 2.0 could not be generated due to a runtime error. The runtime error, a *divide by zero* error, occurred because the variable *PI* (Figure 4.3.7-1) was not defined in subroutine *GETJS* and therefore was automatically set to zero by the computer. A second error, the definition of the mean radius of the cylinder (*RIOB* in Figure 4.3.7-1), was also discovered. The mean radius was incorrectly defined in *GETJS* as the inner radius plus one-half of the arc length (*WIDTHS(1)*), not the inner radius plus one-half the cylinder wall thickness (*WIDTHS(2)*). Both errors were corrected offline. Results from the corrections, which are given in Table 4.3.7-1, are in good agreement with [2]. In Table 4.3.7-1, the *Reference* columns represent results calculated from [2] and using $J_e = K_I^2/E'$, the *PI* column contains results from a offline code in which only the first error, the assignment of *PI*, was corrected, and, finally, the *PI and Rm* column contains results from the offline code in which both errors were corrected. The results in Table 4.3.7-1 clearly indicate that merely defining *PI* will not make this *J vs a* solution valid.

```
      SUBROUTINE GETJS(XFCTR)
        .
        .
      XNC=SHARDN
        .
C
C     THRU WALL CRACK IN A CYLINDER
C
      CAL=0.0625
      CAH=0.5
      XNL=1.
      XNH=7.
      AB=ANOW(1)/(PI*(WIDTHS(3)+0.5*WIDTHS(1)))
      CALL WARNJ(AB,CAL,CAH,XNC,XNL,XNH)
      B=WIDTHS(1)
      T=WIDTHS(2)
      RIOB=(WIDTHS(3)+0.5*WIDTHS(1))/WIDTHS(2)
      IF (RIOB.LE.7.5) THEN
        CNAME='TCT5'
      ELSE IF (RIOB.GT.7.5 .AND. RIOB.LE.15.) THEN
        CNAME='TCT1'
      ELSE
        CNAME='TCT2'
      END IF
      CALL JINT
      RETURN
      END
```

Figure 4.3.7-1. Subroutine *GETJS* Showing Errors in *PI* and *RIOB* (Mean Radius) Assignments

Table 4.3.7-1. Results from an Offline Version of Configuration 303 *J vs a*

Case	J_e Reference	J_e Pi	J_e Pi & RIOB	J_p Reference	J_p Pi	J_p Pi & RIOB	J_{total} Reference	J_{total} Pi	J_{total} Pi & RIOB
1	2.20E+0	2.14E+0	2.29E+0	1.87E+2	1.61E+2	1.88E+2	1.90E+2	1.63E+2	1.90E+2
2	5.48E+0	5.15E+0	5.88E+0	7.07E+2	4.91E+2	7.08E+2	7.13E+2	4.96E+2	7.14E+2
3	2.43E+1	1.59E+1	2.54E+1	6.63E+3	2.41E+3	6.62E+3	6.65E+3	2.42E+3	6.65E+3
4	3.64E+2	9.95E+1	6.17E+3	2.91E+6	3.60E+4	2.53E+6	2.91E+6	3.61E+4	2.54E+6
5	2.34E-3	2.26E-3	2.41E-3	2.57E-7	2.20E-7	2.57E-7	2.34E-3	2.26E-3	2.41E-3
6	5.62E-3	5.38E-3	6.06E-3	9.70E-7	6.74E-7	9.71E-7	5.62E-3	5.38E-3	6.06E-3
7	1.99E-2	1.57E-2	2.26E-2	9.09E-6	3.30E-6	9.08E-6	1.99E-2	1.57E-2	2.26E-2
8	1.80E-1	7.34E-2	2.34E-1	3.99E-3	4.94E-5	3.47E-3	1.84E-1	7.34E-2	2.38E-1
9	2.34E-3	2.26E-3	2.41E-3	5.43E-1	5.08E-1	5.43E-1	5.46E-1	5.11E-1	5.45E-1
10	5.62E-3	5.38E-3	6.06E-3	1.37E+0	1.21E+0	1.36E+0	1.37E+0	1.22E+0	1.37E+0
11	1.98E-2	1.57E-2	2.26E-2	5.10E+0	3.54E+0	5.09E+0	5.11E+0	3.56E+0	5.11E+0
12	1.80E-1	7.33E-2	2.33E-1	5.54E+1	1.65E+1	5.24E+1	5.56E+1	1.66E+1	5.26E+1

4.3.8 CONFIGURATION 401 (CIRCUMFERENTIAL CRACK (ID) IN A HOLLOW CYLINDER)

Comparative *J vs a* results for configuration 401 are shown in Table 4.3.8-1. The results in Table 4.3.8-1 were calculated with two different point loads: 1 and 30 ksi. This range of loads provided elastic (cases 1-6), elastic-plastic (cases 7, 9, 11), and fully plastic (cases 8, 10, 12) results. Material properties for the calculations are listed in Table 4.3.1-2.

Table 4.3.8-1. Representative Results for 401 *J vs a* Computations

Case	a	b	R	σ	J_e NASCRAC™	J_e Reference	J_p NASCRAC™	J_p Reference	J_{TOTAL} NASCRAC™	J_{TOTAL} Reference
1	2	8	40	1	$7.9(10^{-4})$	$8.9(10^{-4})$	$4.2(10^{-16})$	$4.2(10^{-16})$	$7.9(10^{-4})$	$8.9(10^{-4})$
2	6	8	40	1	$6.9(10^{-3})$	$7.3(10^{-3})$	$7.1(10^{-12})$	$7.1(10^{-12})$	$6.9(10^{-3})$	$7.3(10^{-3})$
3	2	8	80	1	$8.6(10^{-4})$	$1.0(10^{-3})$	$4.9(10^{-16})$	$4.9(10^{-16})$	$8.6(10^{-4})$	$1.0(10^{-3})$
4	6	8	80	1	$9.2(10^{-3})$	$1.1(10^{-2})$	$9.9(10^{-12})$	$9.9(10^{-12})$	$9.2(10^{-3})$	$1.1(10^{-2})$
5	2	8	160	1	$9.2(10^{-4})$	$1.2(10^{-3})$	$5.3(10^{-16})$	$5.3(10^{-16})$	$9.2(10^{-4})$	$1.2(10^{-3})$
6	6	8	160	1	$1.2(10^{-2})$	$1.6(10^{-2})$	$1.2(10^{-11})$	$1.2(10^{-11})$	$1.2(10^{-2})$	$1.6(10^{-2})$
7	2	8	40	30	0.78	0.89	7.5	7.5	8.2	8.4
8	4	8	40	30	2.8	3.0	219	219	222	222
9	2	8	80	30	0.86	1.1	8.6	8.6	9.5	9.7
10	4	8	80	30	3.9	4.6	291	291	295	296
11	2	8	160	30	0.93	1.3	9.5	9.5	10.4	10.8
12	4	8	160	30	5.2	7.7	370	370	375	378

The NASCRAC™ *J vs a* solution for configuration 401, inner diameter circumferential crack in a hollow cylinder, is valid for the ranges specified in the documentation ($0.0 \le a/b \le 0.75$, $1 \le n \le 20$). The original work from [1] used a table look-up based on a/b and n whereas NASCRAC™ uses a look-up based on a/b and 1/n; however, the J_p from NASCRAC™ and [1]

are in agreement for all cases. Similarly, the NASCRAC™ h_1 tables and the h_1 tables in [1] are in agreement. Differences in J_e do exist between NASCRAC™ and the reference value in Table 4.3.8-1 due to different computational methods. NASCRAC™ uses the linear version of the J_p expression whereas the reference value was determined using $J_e = K_I^2/E'$. The J_e comparison, however, is reasonable in the elastic regime and only diverges as the analysis transitions into elastic-plastic and plastic conditions where J_e is insignificant to the total J solution. A comparison of the coded P_0 equation with [1] showed identical agreement and a reduction of the coded J_p equation matched the J_p equation in [1].

4.3.9 REFERENCES FOR SECTION 4.3

1. *Kumar, V., German, M.D., and Shih, C.F., An Engineering Approach for Elastic-Plastic Fracture Analysis, NP-1931, Research Project 1237-1, prepared by General Electric Company for Electric Power Research Institute, July, 1981.*
2. *Kumar, V., et al, Advances in Elastic-Plastic Fracture Analysis, NP-3607, Research Project 1237-1, Final Report, prepared by General Electric Company for Electric Power Research Institute, July, 1984.*

4.4 CALCULATION OF CRACK OPENING AREAS

Five NASCRAC™ configurations have crack opening area (COA) solutions available. These configurations include 201, 202, 301, 302, and 303. The COA solutions in NASCRAC™ were adapted from [1]. Verification and validation of NASCRAC™'s COA capabilities consisted of code checks of closed form equations and comparative results using analytical and numerically integrated solutions. No significant errors were discovered in the COA solutions; however, several minor discrepancies were found. Table 4.4-1 lists these discrepancies and suggested corrections. Each error is described in detail in sections following the table. NASCRAC™'s COA solutions are valid once these errors have been corrected.

Table 4.4-1. Discrepancies in NASCRAC's COA Solutions

CONFIGURATION	ERROR	CORRECTION
201	PLANE STRAIN ASSUMPTION*	DOCUMENT THE ASSUMPTION
202	PLANE STRAIN ASSUMPTION* H/W ≥ 2 ASSUMPTION*	DOCUMENT THE ASSUMPTIONS
302	TYPOGRAPHICAL ERROR IN SOURCE CODE	CORRECT SPELLING IN SOURCE
303	TYPOGRAPHICAL ERROR IN SOURCE CODE	CORRECT SPELLING IN SOURCE

* Not an error per se but an undocumented assumption that could lead to a misinterpretation

4.4.1 CONFIGURATION 201 (CRACK IN AN INFINITE PLATE)

Comparative results for 201 COA calculations are listed in Table 4.4.1-1. The reference values in Table 4.4.1-1 were computed by integrating the crack opening displacement function from [2] over the crack length per the following equation:

$$COA_{201} = 2\int_0^a \frac{4\sigma}{E'}\sqrt{a^2 - x^2}\,dx$$

In this equation E' = E for plane stress and $E/(1-\nu^2)$ for plane strain and the origin for the x axis is located at the center of the crack. The integral was mulitplied by 2 because crack symmetry was assumed.

Table 4.4.1-1. Representative Results for 201 COA Calculations

a	E	ν	σ	COA NASCRAC™	COA [2]
0.1	$30(10^6)$	0.25	1.0	$1.96(10^{-9})$	$1.96(10^{-9})$
0.5	$30(10^6)$	0.25	1.0	$4.91(10^{-8})$	$4.91(10^{-8})$
1.0	$30(10^6)$	0.25	1.0	$1.96(10^{-7})$	$1.96(10^{-7})$
1.5	$30(10^6)$	0.25	1.0	$4.42(10^{-7})$	$4.42(10^{-7})$
2.0	$30(10^6)$	0.25	1.0	$7.85(10^{-7})$	$7.85(10^{-7})$
2.5	$30(10^6)$	0.25	1.0	$1.23(10^{-6})$	$1.23(10^{-6})$
3.0	$30(10^6)$	0.25	1.0	$1.77(10^{-6})$	$1.77(10^{-6})$
3.5	$30(10^6)$	0.25	1.0	$2.41(10^{-6})$	$2.41(10^{-6})$
4.0	$30(10^6)$	0.25	1.0	$3.14(10^{-6})$	$3.14(10^{-6})$

The coded solution in NASCRAC™ matches the integrated closed form solution exactly for plane strain. Additionally, the NASCRAC™ and reference results in Table 4.4.1-1, which are both plane strain results, agree. Thus, this solution is valid for plane strain. NASCRAC™ documentation, however, does not identify this plane strain assumption to the user. If this solution is used to calculate COA for plane stress, the computed results would underestimate the COA by approximately 11% for aluminum because Poisson's ratio is relatively high (0.33) and hence the $(1-\nu^2)$ term in the denominator of E' is not negligible. Therefore, the documentation for this solution should be amended to clarify that the solution is for plane strain only. Additionally, the documentation should clearly identify the expected units for material properties. For example, with English units, yield stress, Young's modulus, and crack plane stress are input in ksi.

4.4.2 CONFIGURATION 202 (CENTER CRACKED PANEL)

Comparative crack opening area results for configuration 202 are shown in Table 4.4.2.-1. [1] contains the closed form equation coded in NASCRAC™ and [3] contains a weight function solution; hence, results from [1] verified the NASCRAC™ solution and results from [3] validated the solution.

Table 4.4.2-1. Representative Results for 202 COA Calculations

a	W	E	ν	σ	COA NASCRAC™	COA [3]	COA [1]
0.1	10	$30(10^6)$	0.25	1000	$1.96(10^{-6})$	n/a	$1.96(10^{-6})$
0.5	10	$30(10^6)$	0.25	1000	$4.92(10^{-5})$	n/a	$4.92(10^{-5})$
2	10	$30(10^6)$	0.25	1.0	$8.03(10^{-7})$	$8.33(10^{-7})$	
4	10	$30(10^6)$	0.25	1.0	$3.46(10^{-6})$	$3.46(10^{-6})$	
6	10	$30(10^6)$	0.25	1.0	$9.10(10^{-6})$	$9.33(10^{-6})$	
8	10	$30(10^6)$	0.25	1.0	$2.20(10^{-5})$	$2.17(10^{-5})$	
0.6	5	$30(10^6)$	0.25	1000	$7.12(10^{-5})$	n/a	$7.12(10^{-5})$
1.2	5	$30(10^6)$	0.25	1000	$2.92(10^{-4})$	n/a	$2.92(10^{-4})$
1.8	5	$30(10^6)$	0.25	1000	$6.87(10^{-4})$	n/a	$6.87(10^{-4})$
2.4	5	$30(10^6)$	0.25	1000	$1.31(10^{-3})$	n/a	$1.31(10^{-3})$

The results listed in Table 4.4.2-1 are for plane strain. As with configuration 201, the 202 COA solution as coded is a plane strain solution. If this solution is used to calculate COA for plane stress, the computed results would underestimate the COA by approximately 11% for an aluminum panel because Poisson's ratio is relatively high (0.33) and hence the $(1-\nu^2)$ term in the denominator of E' would not be negligible.

A comparison of NASCRAC™'s coded solution and a first order closed form solution derived by integrating the near field displacement function from [1] agrees within 25%. The discrepancy in this comparison was expected since the near field displacement function cannot

adequately describe displacement from crack tip to crack center. The solution as coded exactly matches the COA equation in [1] and the algorithm logic is functional as indicated by the identical agreement between NASCRAC™ and [1] in Table 4.4.2-1. Table 4.4.2-1 also shows the comparison of NASCRAC™ to [3]. The results from [3] are only valid for panel height to width ratio (H/W) ≥ 2.

Based on the results in Table 4.4.2-1, the NASCRAC™ 202 COA solution is valid for plane strain and H/W ≥ 2. For plane stress, the solution will underestimate the COA by a factor of $(1-\nu^2)$. Therefore, the documentation for this solution should be amended to clarify that the solution is for plane strain only. Additionally, the documentation should clearly identify the expected units for material properties. For example, with English units, yield stress, Young's modulus, and crack plane stress are input in ksi.

4.4.3 CONFIGURATION 301 (THROUGH CRACK IN A SPHERE)

Table 4.4.3-1 lists 301 COA results for NASCRAC™ and [1]. In this table R represents the midsurface radius of the sphere, t is the wall thickness of the sphere, λ is $a/(t\ R)^{1/2}$, E is Young's modulus, ν is Poisson's ratio, and σ is the membrane stress. The solution in [1] is limited to $0 < \lambda \leq 3$.

Table 4.4.3-1. Representative Results for 301 COA Calculations

a	R	t	$\lambda = a/(t\ R)^{1/2}$	E	ν	σ	COA NASCRAC™	COA [1]
0.1	2.0	0.2	0.158	$30(10^6)$	0.25	1.0	$1.998(10^{-9})$	$1.998(10^{-9})$
0.5	2.0	0.2	0.791	$30(10^6)$	0.25	1.0	$7.110(10^{-8})$	$7.110(10^{-8})$
1.0	2.0	0.2	1.581	$30(10^6)$	0.25	1.0	$5.548(10^{-7})$	$5.548(10^{-7})$
1.5	2.0	0.2	2.372	$30(10^6)$	0.25	1.0	$2.288(10^{-6})$	$2.288(10^{-6})$
1.0	10.0	0.2	1.000	$30(10^6)$	0.25	1.0	$3.379(10^{-7})$	$3.379(10^{-7})$
2.0	10.0	0.2	2.000	$30(10^6)$	0.25	1.0	$3.101(10^{-6})$	$3.101(10^{-6})$
3.0	10.0	0.2	3.000	$30(10^6)$	0.25	1.0	$1.374(10^{-5})$	$1.374(10^{-5})$

The 301 COA solution coded in NASCRAC™ compared exactly with the 301 COA equation in [1]. Identical results in Table 4.4.3-1 between NASCRAC™ and [1] verify the functionality of the coded algorithm. This COA solution is valid for the documented range of λ based on these two comparisons.

The documentation for this solution needs two clarifications: 1) clearly identify the input radius as the inside radius of the sphere, and 2) document that the formulation is for thin walled pressure vessels where $\sigma = pR/2t$ is the membrane stress and p is pressure.

4.4.4 CONFIGURATION 302 (AXIAL THROUGH CRACK IN A CYLINDER)

Table 4.4.4-1 lists 302 COA results for NASCRAC™ and [1]. In this table R represents the midsurface radius of the sphere, t is the wall thickness of the sphere, λ is $a/(t\ R)^{1/2}$, E is Young's modulus, ν is Poisson's ratio, and σ is the circumferential membrane stress. The solution in [1] is limited to $0 < \lambda \leq 5$.

Several λ values (6.325, 9.487, 10.0) are highlighted in Table 4.4.4-1 as a means of identifying the effects of a typographical error in this COA solution. This typographical error, which is highlighted in the Figure 4.4.4-1, allows NASCRAC™ to execute the 302 COA solution for an invalid λ, i.e, $\lambda > 5$. As shown in Figure 4.4.4-1, NASCRAC™ assigns a value to the variable *ALP* and attempts to use this variable as a logic check in an IF-THEN statement. *ALP*, however, is misspelled as *APL* in the second logic check of the IF-THEN statement. Since *APL* has not been explicitly assigned a value, the computer implicitly sets it to zero. Thus, in the second logic check *APL* is always less than 5 and hence NASCRAC™'s built-in error check will never reach the third logic check where λ (*ALP*) > 5 and an error statement is written. This error can easily be fixed in future NASCRAC™ releases by implementing the correctly spelled variable.

Table 4.4.4-1. Representative Results for 302 COA Calculations

a	R_{mid}	t	$\lambda = a/(t\ R)^{1/2}$	E	ν	σ	COA NASCRAC™	COA [1]
0.1	2.0	0.2	0.158	$30(10^6)$	0.25	1.0	$1.99(10^{-9})$	$1.99(10^{-9})$
0.5	2.0	0.2	0.791	$30(10^6)$	0.25	1.0	$6.83(10^{-8})$	$6.83(10^{-8})$
1.0	2.0	0.2	1.581	$30(10^6)$	0.25	1.0	$5.04(10^{-7})$	$5.04(10^{-7})$
4.0	2.0	0.2	***6.325***	$30(10^6)$	0.25	1.0	***$6.63(10^{-5})$***	***n/a***
6.0	2.0	0.2	***9.487***	$30(10^6)$	0.25	1.0	***$3.08(10^{-4})$***	***n/a***
1.0	10.0	0.1	1.000	$30(10^6)$	0.25	1.0	$3.19(10^{-7})$	$3.19(10^{-7})$
5.0	10.0	0.1	5.000	$30(10^6)$	0.25	1.0	$6.92(10^{-5})$	$6.92(10^{-5})$
10.0	10.0	0.1	***10.000***	$30(10^6)$	0.25	1.0	***$9.44(10^{-4})$***	***n/a***

The coded solution compares exactly to [1] in a line-by-line comparison and in the results listed in Table 4.4.4-1 when $0 < \lambda \leq 5$; therefore, this solution is valid when λ does not exceed these limits. A future NASCRAC™ release should correct the described typographical error. In addition, the documentation for this solution needs two clarifications: 1) clearly identify the input radius as the inside radius of the sphere, and 2) document that the formulation is for thin walled pressure vessels where $\sigma = pR/t$ is the circumferential membrane stress and p is pressure.

```
      SUBROUTINE GETCOA
       .
 302  CONTINUE
       .
           R=WIDTHS(3)+WIDTHS(2)/2.
      ALP=ANOW(1)/SQRT(WIDTHS(2)*R)
           IF (ALP.GT.0.0 .AND. ALP.LE.1.0) THEN
        GOALP=ALP*ALP+0.625*ALP**4
           ELSE IF (ALP.GT.1. .AND. APL.LE.5.) THEN
        GOALP=.14+0.36*ALP*ALP+0.72*ALP**3+0.405*ALP**4
           ELSE
        WRITE(NFLLPT,2001)
 2001   FORMAT(1X,'ALPHA MUST BE BETWEEN 0 AND 5')
             RETURN
           END IF
      XK(IDEF,1)=SIGINF*2.*3.14159*WIDTHS(2)*R*GOALP/YOUNGS
     &           *(1.-POISSN*POISSN)
      GOTO 998
C
 303  CONTINUE
       .
           R=WIDTHS(3)+WIDTHS(2)/2.
           ALPH=ANOW(1)/(SQRT(R*WIDTHS(2)))
           IF (0.0 .LT. ALPH .AND. ALPH.LE.1) THEN
        GOALPH=ALPH**2+0.16*ALPH**4
           ELSE IF (1. .LE. ALPH .AND. ALPH.LE. 5.0) THEN
        GOALPH=0.02+0.81*ALPH**2+0.30*APLH**3+0.03*ALPH**4
           ELSE
             WRITE(NFLLPT,2001)
             GOTO 998
           END IF
      XK(IDEF,1)=SIGINT*2.*3.14159*R*WIDTHS(2)*GOALPH/YOUNGS
                *(1.-POISSN*POISSN)
      GOTO 998
       .
      RETURN
      END
```

Figure 4.4.4-1. Typographical Errors in *GETCOA* for Configurations 302 and 303

4.4.5 CONFIGURATION 303 (CIRCUMFERENTIAL THROUGH CRACK IN A CYLINDER)

Table 4.4.5-1 lists 303 COA results for NASCRAC™ and [1]. In this table R represents the midsurface radius of the sphere, t is the wall thickness of the sphere, λ is $a/(t\,R)^{1/2}$, E is Young's modulus, ν is Poisson's ratio, and σ is the circumferential membrane stress. The solution in [1] is limited to $0 < \lambda \leq 5$.

Table 4.4.5-1. Representative Results for 303 COA Calculations

a	R_{mid}	t	$\lambda = a/(t\,R)^{1/2}$	E	v	σ	COA NASCRAC™	COA [1]
0.1	2.0	0.2	0.158	$30(10^6)$	0.25	1.0	$1.97(10^{-9})$	$1.97(10^{-9})$
0.5	2.0	0.2	0.791	$30(10^6)$	0.25	1.0	$5.40(10^{-8})$	$5.40(10^{-8})$
1.0	10.0	0.5	0.447	$30(10^6)$	0.25	1.0	$2.03(10^{-7})$	$2.03(10^{-7})$
1.5	10.0	0.5	0.671	$30(10^6)$	0.25	1.0		$4.74(10^{-7})$
2.0	10.0	0.5	0.894	$30(10^6)$	0.25	1.0	$8.86(10^{-7})$	$8.86(10^{-7})$
1.0	2.0	0.2	1.581	$30(10^6)$	0.25	1.0	***$1.75(10^{-7})$***	***$2.68(10^{-7})$***
2.5	10.0	0.5	1.118	$30(10^6)$	0.25	1.0		***$1.47(10^{-6})$***
3.0	10.0	0.5	1.342	$30(10^6)$	0.25	1.0	***$1.54(10^{-6})$***	***$2.26(10^{-6})$***
4.0	10.0	0.5	1.789	$30(10^6)$	0.25	1.0	***$2.87(10^{-6})$***	***$4.55(10^{-6})$***
5.0	10.0	0.5	2.236	$30(10^6)$	0.25	1.0	***$4.73(10^{-6})$***	***$8.02(10^{-6})$***

The COA results highlighted in Table 4.4.5-1 depict the effects of a typographical error the 303 solution. This error, which occurs in the variable *ALPH* in Figure 4.4.4-1 above, causes NASCRAC™ to overestimate COA by 30-40% in some cases. In Figure 4.4.4-1, the final two highlighted lines show that during calculation of *GOALPH*, the third order term of ALPH is misspelled as APLH. This misspelling causes the aforementioned 30-40% overestimates results when $1 < \text{ALPH} \leq 5$. This error can easily be fixed in a future NASCRAC™ release by implementing the correctly spelled variable.

The 303 COA coded solution compares exactly to [1] in a line-by-line comparison and in the results listed in Table 4.4.5-1 when $0 < \lambda \leq 1$; therefore, this solution is valid for $\lambda \leq 1$. A future NASCRAC™ release should correct the described typographical error. In addition, the documentation for this solution needs two clarifications: 1) clearly identify the input radius as the inside radius of the sphere, and 2) document that the formulation is for thin walled pressure vessels where $\sigma = pR/2t$ is the longitudinal membrane stress and p is pressure.

4.4.6 REFERENCES FOR SECTION 4.4

1. *Tada, H., Paris, P.C., and Irwin, G.R., The Stress Analysis of Cracks Handbook, Del Research Corporation, 1985.*
2. *Broek, D., Elementary Engineering Fracture Mechanics , 4th ed, Martinus Nijhoff, Boston, 1986, pp 80.*
3. *Wu, X.R. and Carlsson, A.J., Weight Functions and Stress Intensity Factor Solutions, Pergamon Press, New York, p.505-506.*

4.5 LIFE CALCULATION BY FATIGUE CRACK GROWTH

The *life calculation by fatigue crack growth capability* in NASCRAC™ verification and validity evaluation was completed in two independent studies. The first study verified the NASCRAC™ code using code checks and spread sheet analyses. This study included verification of the NASCRAC™ crack growth logic in the relevant subroutines and verification of the five coded fatigue crack growth equations in NASCRAC™. The five crack growth equations are listed in Table 4.5-1.

Table 4.5-1. Fatigue Crack Growth Equations Coded into NASCRAC

PARIS
WALKER
MODIFIED FORMAN
COLLIPRIEST
HOPKINS-RAU

The second fatigue crack growth study focused on the validity of the NASCRAC™ fatigue crack growth results based on four distinct test sets. Descriptions of the four test sets are listed in Table 4.5-2.

Table 4.5-2. Crack Growth Equations Coded into NASCRAC™

TEST ID	TEST DESCRIPTION	PARAMETERS
I-1-A	LIFE DUE TO FATIGUE	CONSTANT AMPLITUDE LOAD; NO TRANSITIONING
I-2-A	LIFE DUE TO FATIGUE	CONSTANT AMPLITUDE LOAD; WITH TRANSITIONING
I-3-A	LIFE DUE TO FATIGUE	CONSTANT AMPLITUDE LOAD; RESIDUAL STRESS FIELD
III-1	PROOF TEST	CONSTANT AMPLITUDE LOAD

4.5.1 VERIFICATION OF CODED CRACK GROWTH SUBROUTINES AND EQUATIONS

Verification of the fatigue crack growth capability in NASCRAC™ included a check of the crack growth equations for coding errors and a check of the algorithm for logic errors. The coding check was accomplished by comparing NASCRAC™'s five coded crack growth equations with the NASCRAC™ theory manual and with the references listed in the manual. No coding errors were discovered in the equations.

Spread sheets and a FORTRAN crack growth routine were constructed to verify the logic of the crack growth algorithm. Results from these tools were compared to results from a stand alone version of the subroutine *DADNDT* and its related subroutines. *DADNDT* is NASCRAC™'s driver subroutine for fatigue crack growth.

Tables 4.5.1-1 through 4.5.1-5 lists comparative results used to verify the crack growth logic in NASCRAC™. Tables 4.5.1-1 through 4.5.1-3 show results from the Paris, Walker, and Collipriest fatigue crack growth equations. These results were computed for a compact tension specimen (configuration 101) subjected to 100 constant amplitude load cycles with P_{max} = 20 kips, P_{min} = 4 kips, and R = 0.2. The geometry for the simulations was a_i = 0.25", plate width (W) = 3.0", and plate thickness (B) = 1.0". The typographical error in the K solution for configuration 101 (see Section 4.1.1.1) was negated in the verification spreadsheets by using the NASCRAC™

version of the 101 K equation. The agreement between NASCRAC™ and the spreadsheet results in Tables 4.5.1-1 through 4.5.1-3 verify that these three NASCRAC™ crack growth equations (Paris, Walker, and Collipriest) are coded correctly and that the crack growth logic is **correct for constant amplitude loads when material properties are held constant, i.e., independent of R.**

Table 4.5.1-1 . Representative Paris Results for Constant Amplitude Loads R = 0.2, C = 3.8 (10^{-9}) and n = 2.925.

CYCLE	FORTRAN da/dN (10^{-5})	NASCRAC™ da/dN (10^{-5})
10	5.022	5.022
20	5.033	5.033
30	5.044	5.044
40	5.055	5.055
50	5.066	5.066
60	5.077	5.077
70	5.088	5.088
80	5.099	5.099
90	5.110	5.110
100	5.122	5.122

Table 4.5.1-2. Representative Walker Results for Constant Amplitude Loads R = 0.2, C = 3.8 (10^{-9}), m = 2.925, n = 2.925.

CYCLE	FORTRAN da/dN (10^{-5})	NASCRAC™ da/dN (10^{-5})
10	1.427	1.427
20	1.428	1.428
30	1.429	1.429
40	1.430	1.430
50	1.431	1.431
60	1.432	1.432
70	1.433	1.433
80	1.434	1.434
90	1.434	1.434
100	1.435	1.435

Table 4.5.1-3 Representative Collipriest Results for Constant Amplitude Loads R = 0.2, C = 3.8 (10^{-9}), n = 2.925, K_c=50.0, ΔK_{th} = 2.5

CYCLE	FORTRAN da/dN (10^{-4})	NASCRAC™ da/dN (10^{-4})
10	1.681	1.681
20	1.706	1.706
30	1.732	1.732
40	1.759	1.759
50	1.786	1.786
60	1.815	1.815
70	1.844	1.844
80	1.874	1.874
90	1.906	1.906
100	1.939	1.939

Results from the verification of NASCRAC™'s Hopkins-Rau fatigue crack growth algorithm are presented in Table 4.5.1-4. These results were computed for a 203 specimen (single edge crack in a plate) subjected to 2000 constant amplitude load cycles with s_{max} = 25 ksi, s_{min} = 20 ksi kips, and R = 0.8. The geometry for the simulation was a_i = 0.1" and plate width (W) = 10.0". The plate thickness was uniform with a value of unity.

Table 4.5.1-4 Representative Hopkins-Rau Results for Constant Amplitude Loads

$R = 0.8$, $C = 1.07\ (10^{-8})$, $m = 2.925$, $K_c = 30.0$, $\Delta K_{th} = 2.5$, $R_{th} = 1.73$, $A_{th} = 1.41$, $B_{th} = 1.73$

CYCLE	HOPKINS-RAU NASCRAC™ ALGORITHM	HOPKINS-RAU BIGIF ALGORITHM	NASCRAC™
200	.1006	.1002	.1006
400	.1012	.1005	.1012
600	.1019	.1007	.1019
800	.1025	.1009	.1025
1000	.1032	.1011	.1032
1200	.1038	.1014	.1038
1400	.1045	.1016	.1045
1600	.1051	.1018	.1051
1800	.1058	.1021	.1058
2000	.1065	.1023	.1065

Analyzing the Hopkins-Rau equation was difficult because independent references were not readily available. Reference [1], the NASCRAC™ reference for the Hopkins-Rau equation, describes experimental work and hints at a form of the crack growth equation but does not explicitly list the equation or an algorithm for the equation. Reference [2], another NASCRAC™ reference for Hopkins-Rau, contains an explanation of equations and describes and lists the algorithm coded in the BIGIF code. Apparently, the NASCRAC™ solution was adapted from BIGIF; however, the two solutions are coded differently and compute slightly different results as shown in Table 4.5.1-4. Based on this comparison with the BIGIF algorithm, **the Hopkins-Rau crack growth equation algorithm in NASCRAC is not valid**. Use of this NASCRAC™ capability should be avoided.

The modified Forman equation is shown in equation 4.5.1-1. Constant amplitude spreadsheet calculations for this equation compared identically to NASCRAC™ results as shown in Table 4.5.1-5. These results were computed identically to the Paris, Walker, and Collipriest results in Tables 4.5.1-1 through 4.5.1-3, i.e., for a compact tension specimen subjected to 100 constant amplitude load cycles with P_{max} = 20 kips, P_{min} = 4 kips, and R = 0.2. In these spreadsheet calculations, the material constants for the equation did not depend on R ratio. However, [3] discussed two errors in the NASCRAC™ modified Forman algorithm which are evident when results are compared to NASA/FLAGRO results. First, the material constant m in this equation is a function of R in the original formulation [4]. Second, K_c, the fracture toughness, depends on thickness in [4] as shown in equation 4.5.1-2. As coded in NASCRAC™ these two parameters are constant with m = 0 and K_c set in the material library or by the user. To demonstrate the effects of these coding errors, a parametric study was conducted which compared modified Forman results from NASCRAC™, NASA/FLAGRO, and a FORTRAN routine specifically coded for the study.

$$\frac{da}{dN} = C(1-R)^m \Delta K^n \frac{[\Delta K - (1-C_O R)^d \Delta K_{th}]^p}{[(1-R)K_c - \Delta K]^q} \qquad \text{eq. 4.5.1-1}$$

$$K_c = (1 + B_k e^{-\omega})\, K_{Ic} \qquad \text{eq. 4.5.1-2}$$

Table 4.5.1-5 Representative Modified Forman Results for Constant Amplitude Loads
$R = 0.2, C = 3.8\ (10^{-9}), m = 0.0, n = 2.897,$
$C_0 = d = 1, p = q = 0.5, K_c = 43.6, \Delta K_{th} = 2.5$

CYCLE	FORTRAN da/dN (10^{-4})	NASCRAC™ da/dN (10^{-4})
10	2.089	2.089
20	2.120	2.120
30	2.153	2.153
40	2.186	2.186
50	2.221	2.221
60	2.257	2.257
70	2.294	2.294
80	2.332	2.332
90	2.372	2.372
100	2.413	2.413

The parametric study computed the fatigue life for an edge crack in a plate (Configuration 203 in NASCRAC™) using the three previously mentioned programs: NASCRAC™, FLAGRO, and a FORTRAN routine. The FORTRAN routine used the K solution from the NASCRAC™ manual plus the material properties for AL 2219-T851 found in the NASCRAC library. These properties were identical to those in the FLAGRO library. In the FORTRAN code, all material properties were held constant and da/dN was computed cycle by cycle. Four different load cases were calculated: R = 0.0, 0.2, 0.5, and 0.8. The results of the study are presented in Table 4.5.1-6

The agreement between the NASCRAC™ and FORTRAN results in Table 4.5.1-6 and the disagreement with FLAGRO indicates that NASCRAC™ maintains a constant m throughout its modified Forman fatigue crack growth calculations. By maintaining m= 0, The $(1-R)^M$ term in the modified Forman equation becomes unity in all cases. In the four cases in Table 4.5.1-6, FLAGRO calculated the m value as 0.0, -1.645,- 0.803, and -0.0658 for R = 0.0, 0.2, 0.5, and 0.8 respectively. Since m is frequently less than zero, setting m= 0 causes NASCRAC™ to compute a reduced crack growth rate when R > 0.0.

Table 4.5.1-6. NASCRAC™, FLAGRO and FORTRAN code Values of a Parametric Study for Configuration 203 ($W = 10", t = 1", \sigma_{max} = 25$ ksi)

R = 0									
Cycles	a			K_{max}			da/dN		
	NASCRAC™	FORTRAN	FLAGRO	NASCRAC™	FORTRAN	FLAGRO	NASCRAC™	FORTRAN	FLAGRO
0	.1000	---	---	15.77	---	---	2.18e-5	---	---
500	.1123	.1121	.1122	16.72	16.70	16.69	2.73e-5	2.71e-5	2.71e-5
1000	.1279	.1275	.1275	17.85	17.83	17.83	3.50e-5	3.47e-5	3.48e-5
1500	.1479	.1474	.1475	19.20	19.17	19.20	4.63e-5	4.60e-5	4.62e-5
2000	.1754	.1745	.1747	20.92	20.89	20.91	6.48e-5	6.41e-5	6.45e-5
2500	.2152	.2138	.2142	23.22	23.15	23.15	9.82e-5	9.66e-5	9.66e-5
3000	.2800	.2770	.2777	26.57	26.43	26.45	1.71e-4	1.66e-4	1.67e-4

Table 4.5.1-6. NASCRAC™, FLAGRO and FORTRAN code Values of a Parametric Study for Configuration 203 (W = 10", t =1", σ_{max} = 25 ksi) (Continued)

R = 0.2									
Cycles	a			K_{max}			da/dN		
	NASCRAC™	FORTRAN	FLAGRO	NASCRAC™	FORTRAN	FLAGRO	NASCRAC™	FORTRAN	FLAGRO
0	.1000	---	---	15.77	---	---	1.14e-2	---	---
1000	.1131	.1128	.1196	16.77	16.75	17.24	1.45e-5	1.43e-5	2.31e-5
2000	.1296	.1291	.1481	17.96	17.94	19.21	1.88e-5	1.86e-5	3.51e-5
3000	.1515	.1508	.1940	19.43	19.40	22.06	2.55e-5	2.52e-5	6.02e-5
4000	.1820	.1809	.2821	21.32	21.27	26.70	3.66e-5	3.61e-4	1.32e-4
5000	.2280	.2261	.6032	23.91	23.82	39.73	5.79e-5	5.68e-5	1.08e-3
6000	.3073	.3035	n/a	27.87	27.70	n/a	1.10e-4	1.07e-4	n/a
R = 0.5									
Cycles	a			K_{max}			da/dN		
	NASCRAC™	FORTRAN	FLAGRO	NASCRAC™	FORTRAN	FLAGRO	NASCRAC™	FORTRAN	FLAGRO
1000	.1032	.1033	.1054	16.02	16.00	16.21	3.11e-6	3.11e-6	5.64e-6
5000	.1173	.1170	.1338	17.08	17.06	18.26	3.98e-6	3.95e-6	8.88e-6
10000	.1411	.1405	.2000	18.75	18.72	22.35	5.68e-6	5.63e-6	1.97e-5
15000	.1763	.1755	.4118	20.98	20.94	32.43	8.78e-6	8.79e-6	9.73e-5
20000	.2351	.2335	n/a	24.30	24.22	n/a	1.58e-5	1.56e-5	n/a
25000	.3612	.3515	n/a	30.30	29.88	n/a	4.09e-5	3.82e-5	n/a
R = 0.8									
Cycles	a			K_{max}			da/dN		
	NASCRAC™	FORTRAN	FLAGRO	NASCRAC™	FORTRAN	FLAGRO	NASCRAC™	FORTRAN	FLAGRO
1000	.1002	.1002	.1002	15.78	15.78	15.79	2.07e-7	2.07e-7	2.30e-7
50000	.1114	.1114	.1128	16.66	16.65	16.77	2.54e-7	2.53e-7	2.89e-7
100000	.1260	.1256	.1293	17.71	17.68	17.96	3.21e-7	3.18e-7	3.75e-7
200000	.1687	.1677	.1813	20.52	20.47	21.32	5.67e-7	5.60e-7	7.30e-7
300000	.2543	.2521	.3054	25.29	25.18	27.79	1.31e-6	1.28e-6	2.17e-6

Since the disagreement between NASCRAC™ and FLAGRO was caused by setting m = 0 in NASCRAC™, it was necessary to verify NASCRAC™ if an appropriate m was used. To verify the code, NASCRAC™ was executed with a constant amplitude load spectrum using an m equivalent to one output from FLAGRO. Table 4.5.1-7 shows the results of these computations. In this table, the NASCRAC™ results using the FLAGRO m agree well with the FLAGRO results. These results verify that **the observed problem in NASCRAC™ can be corrected for constant amplitude loading by inputting the correct value of m.** However, it should be noted that **a simple fix is not possible for variable amplitude loading because m has to be computed for each given R ratio.**

Table 4.5.1-7. Parametric Study for Configuration 203 using NASCRAC™, FLAGRO and NASCRAC with FLAGRO m values (W =10.0", t =1.0", σ_{max} = 25 ksi)

R = 0				R = 0.2			
Cycles	da/dN			Cycles	da/dN		
	NASCRAC™	Input m	FLAGRO		NASCRAC™	Input m	FLAGRO
0	2.18e-5	2.18e-5	n/a	0	1.14e-2	1.65e-5	n/a
500	2.73e-5	2.73e-5	2.71e-5	1000	1.45e-5	2.33e-5	2.31e-5
1000	3.50e-5	3.50e-5	3.48e-5	2000	1.88e-5	3.53e-5	3.51e-5
1500	4.63e-5	4.63e-5	4.62e-5	3000	2.55e-5	6.03e-5	6.02e-5
2000	6.48e-5	6.48e-5	6.45e-5	4000	3.66e-5	1.33e-4	1.32e-4
2500	9.82e-5	9.82e-5	9.66e-5	5000	5.79e-5	n/a	1.08e-3
3000	1.71e-4	1.71e-4	1.67e-4	6000	1.10e-4	n/a	n/a
R = 0.5				R = 0.8			
Cycles	da/dN			Cycles	da/dN		
	NASCRAC™	Input m	FLAGRO		NASCRAC™	Input m	FLAGRO
1000	3.11e-6	5.79e-6	5.64e-6	1000	2.07e-7	2.30e-7	2.30e-7
5000	3.98e-6	9.24e-6	8.88e-6	50000	2.54e-7	2.90e-7	2.89e-7
10000	5.68e-6	2.12e-5	1.97e-5	100000	3.21e-7	3.77e-7	3.75e-7

K_c in FLAGRO is computed according to equation 4.5.1-2; therefore, K_c in NASCRAC™ does not match K_c in FLAGRO except for a plate thickness of unity. FLAGRO requires a thickness input for this computation whereas NASCRAC™ assumes the thickness to be unity for the case of constant thickness. Using the K_c equation listed above, the FLAGRO calculated K_c for Al 2219-T851 and a plate thickness of 1" is 43.6 ksi. This calculated value is the same as the NASCRAC™ database K_c value. But for a case with thickness of 2", the FLAGRO calculated K_c for Al 2219-T851 is 30.64 ksi whereas the NASCRAC™ database K_c is 43.6 ksi. If the NASCRAC™ K_c value is larger than the FLAGRO value, the computed NASCRAC™ da/dN will again be reduced compared to the FLAGRO computation.

Table 4.5.1-8. Loading Spectrum for Verification of Spectrum Loading Capability

BLOCK	MAXIMUM LOAD	CYCLES
1	19.5	10
2	0.5	4
3	1.0	4
4	0.5	4
5	6.0	100
6	8.0	50
7	30.0	4
8	28.0	10

The Paris and Walker equations were used to verify NASCRAC™'s spectrum loading capability and implementation of the R ratio dependency. For each of these equations and the compact tension configuration, a spread sheet of 186 cycles with eight different loading blocks was created to calculate da/dN and crack length. A description of the load spectrum is given in Table 4.5.1-8. Three different R values were considered: 0.1, 0.0, and -1.0. The values of da/dN and crack length from the spread sheet of each equation were compared cycle by cycle to results from the NASCRAC™ code. For both the Paris and Walker equations, exact agreement with the FORTRAN calculated reference solution was observed for each R value when the input material constants (m, C) were assumed independent of R .

4.5.2 VALIDATION OF FATIGUE CRACK GROWTH RESULTS USING TESTS WITH CONSTANT AMPLITUDE LOADS

Fatigue crack propagation tests were performed under constant amplitude loading on 2219-T851 aluminum in four series of tests; I-1-a, I-2-a, I-3-a and III-a. The loading parameters for these tests are defined in Figure 4.5.2-1. These tests are described in Sections 4.5.2.1 through 4.5.2.5.

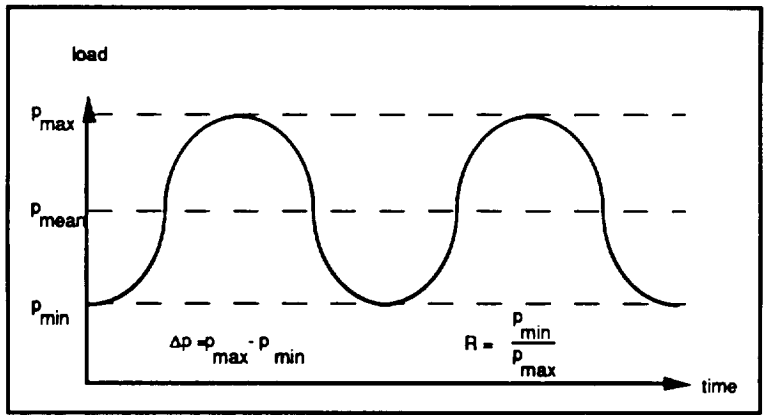

Figure 4.5.2-1. Load Parameters for Constant Amplitude Fatigue

4.5.2.1 Test Series I-1-a: Fatigue Crack Propagation Without Transitioning

The geometry for test series I-1-a is defined in Figure 4.5.2.1-1. Two distinct sets of tests were performed in this series. The two sets had similar geometry but different dimensions. These sets were denoted I-1i-a and I-1ii-a. The average dimensions for the two sets in this series are given in Tables 4.5.2.1-1 and 4.5.2.1-2. Constant amplitude loads were applied to the test specimens until a transition occured. For this series, a transition was defined as either crack tip 1 reaching corner a or crack tip 2 reaching corner β, as defined in Figure 4.5.2.1-1. The number of cycles before transition, denoted l_1, was calculated by fitting a quadratic polynomial to crack lengths measured for the two 5000 cycle intervals just before transition and the crack length measured for the first 5000 cycle interval following the transition. The number of cycles for which the crack tip would be at the corner was interpolated from this polynomial. In all tests performed in both sets of this series, crack tip 2 determined the transition.

Experimentally-observed and NASCRAC™-predicted crack lengths for test set I-1i-a are shown in Figures 4.5.2.1-2 and 4.5.2.1-3. The number of cycles before transition, l_1, is not available for test I-1i-a/1. Therefore, this test is not considered in the averages of Table 4.5.2.1-1. The input for the NASCRAC™ analysis is summarized in Table 4.5.2.1-3. A photograph of a typical post-transition crack surface is shown in Figure 4.5.2.1-4.

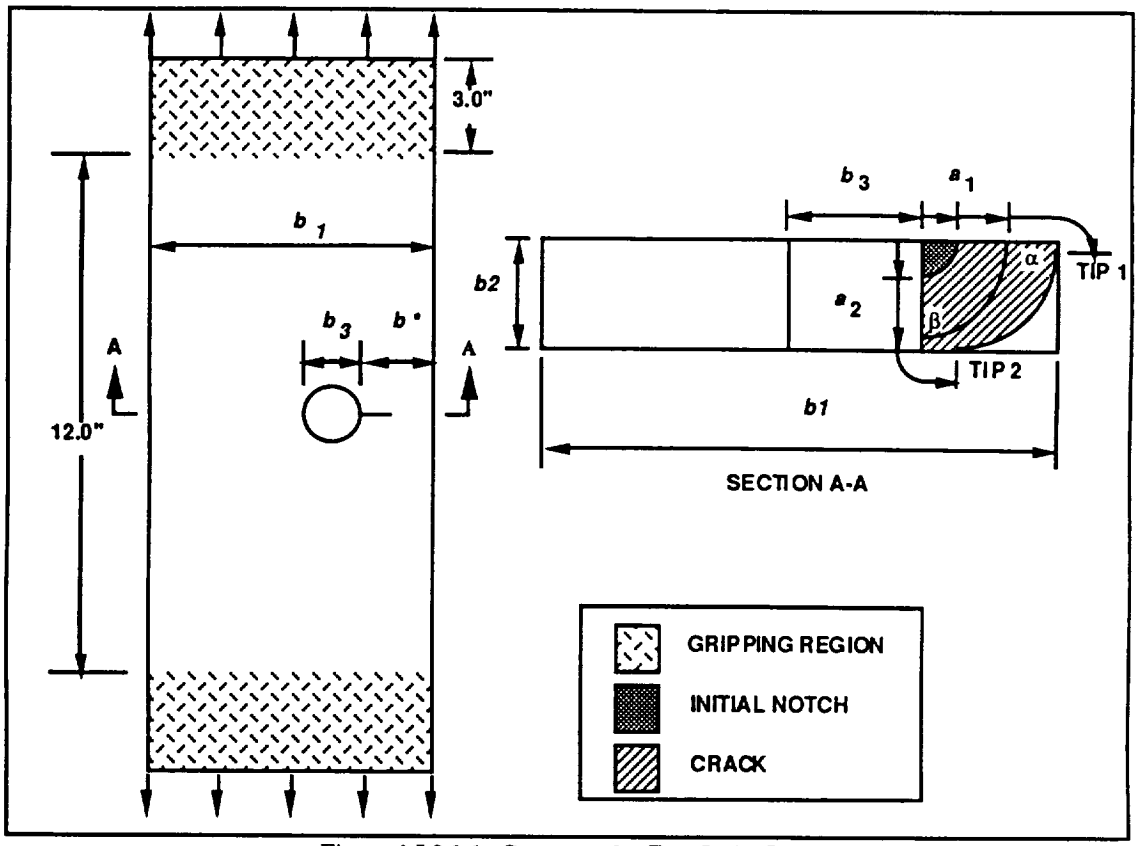

Figure 4.5.2.1-1. Geometry for Test Series I-1-a

Table 4.5.2.1-1. Average Dimensions for Test Set I-1i-a

NUMBER OF TESTS		3
DIMENSION	AVERAGE VALUE	UNITS
$a1(0)$	0.263	INCHES
$a2(0)$	0.253	INCHES
$b1$	3.000	INCHES
$b2$	0.503	INCHES
$b3$	0.497	INCHES
b^*	0.521	INCHES
Δp	11.65	KIPS
R-ratio	0.200	-
$l1$	29,170	CYCLES

Table 4.5.2.1-2. Average Dimensions for Test Set I-1ii-a

NUMBER OF TESTS		4
DIMENSION	AVERAGE VALUE	UNITS
$a1(0)$	0.252	INCHES
$a2(0)$	0.258	INCHES
$b1$	3.000	INCHES
$b2$	0.502	INCHES
$b3$	0.498	INCHES
b^*	1.958	INCHES
Δp	11.66	KIPS
R-ratio	0.201	-
$l1$	42,120	CYCLES

Table 4.5.2.1-3. NASCRAC-Input for Analysis of Test Set I-1i-a

	NASCRAC™ INPUT	VALUE	CORESPONDING TEST DIMENSION
MODEL	601		I-1-a
GEOMETRY	a1	0.263	$a1(0)$
	a2	0.253	$a2(0)$
	B	0.521	b^*
	t	0.503	$b2$
	r	0.249	$b3/2$
	W	3.000	$b1$
LOADING	TRANSIENT 1 RANGE: EQ. A R-RATIO	500 CYCLES 7.72 0.200	FATIGUE LOADS: FIGURE 5.5.2-1 TABLE 4.5.2.1-1
	BLOCK	1X TRANSIENT 1	
MATERIAL PROPERTIES	2219-T851 AL, T-L & L-T 75F	ALUM3 # 104	2219-T851 LAB AIR

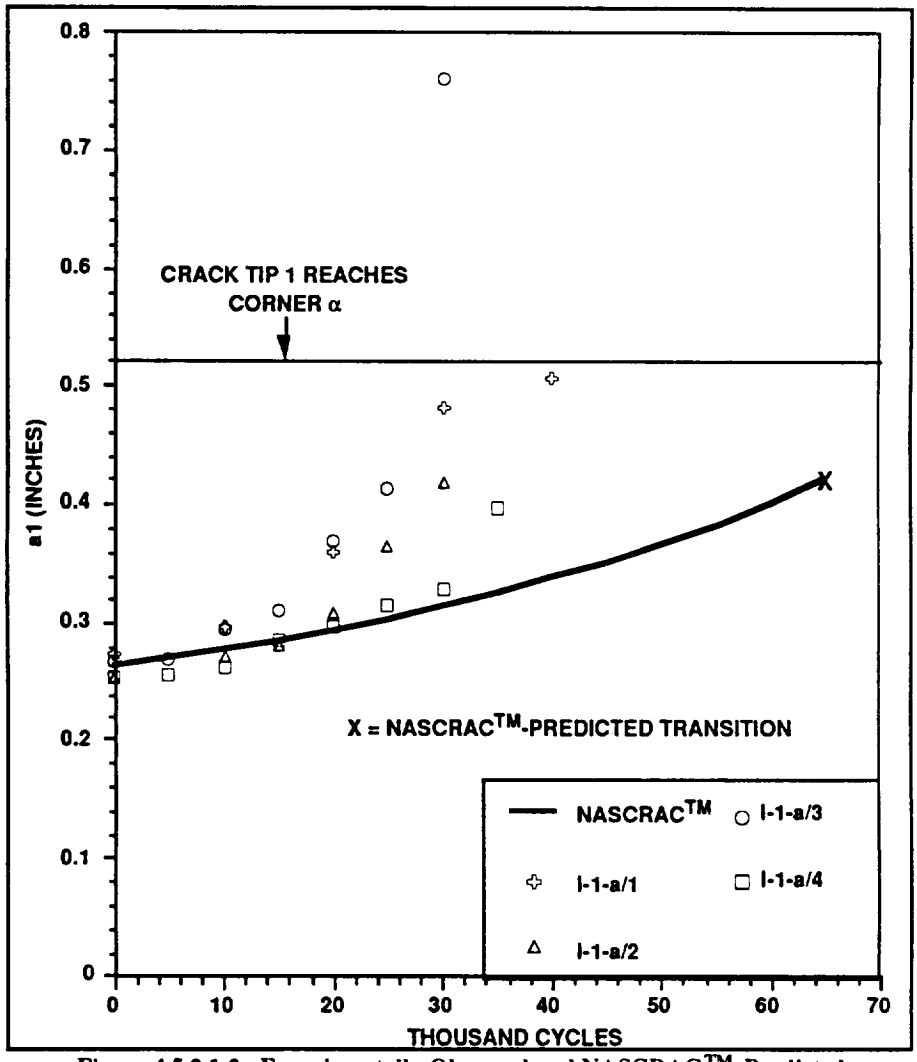

Figure 4.5.2.1-2. Experimentally-Observed and NASCRAC™-Predicted Crack Length $a1$ Versus Cycles for Test Set I-1i-a

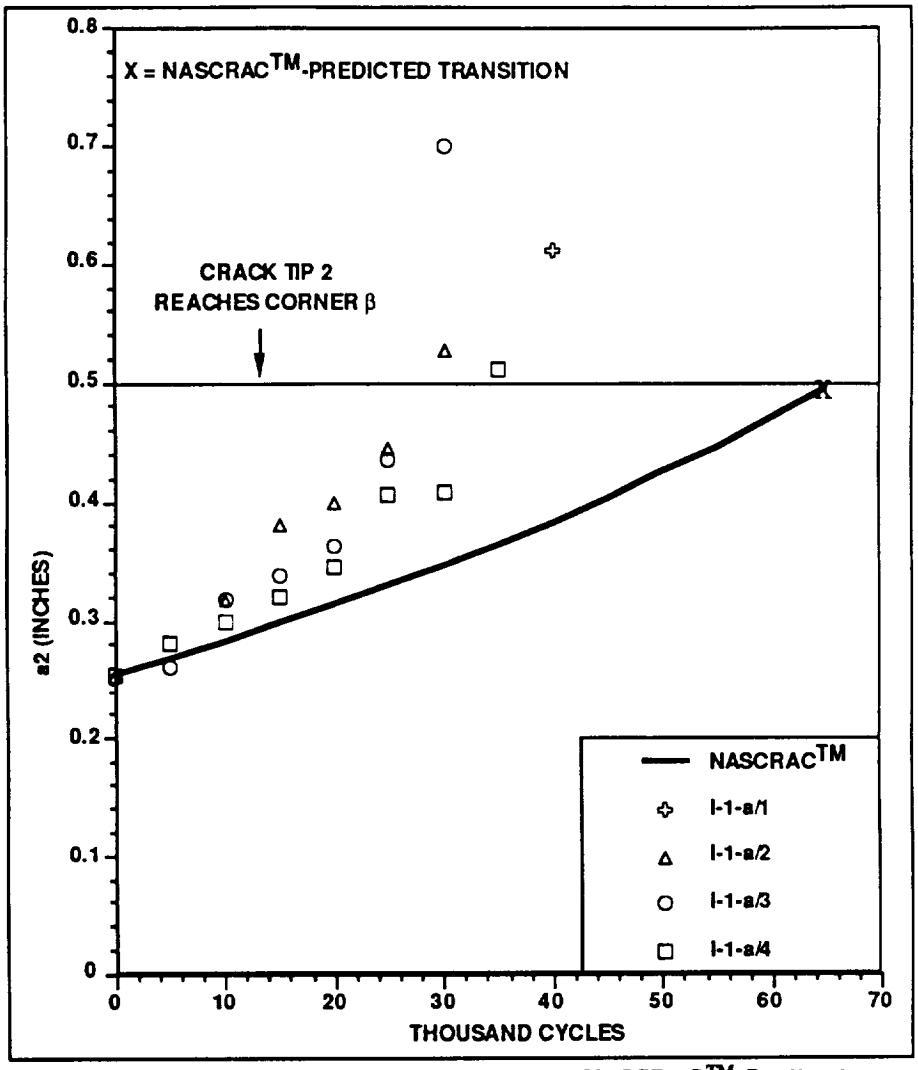

Figure 4.5.2.1-3. Experimentally-Observed and NASCRAC™-Predicted Crack Length *a*2 versus Cycles for Test Set I-1ii-a

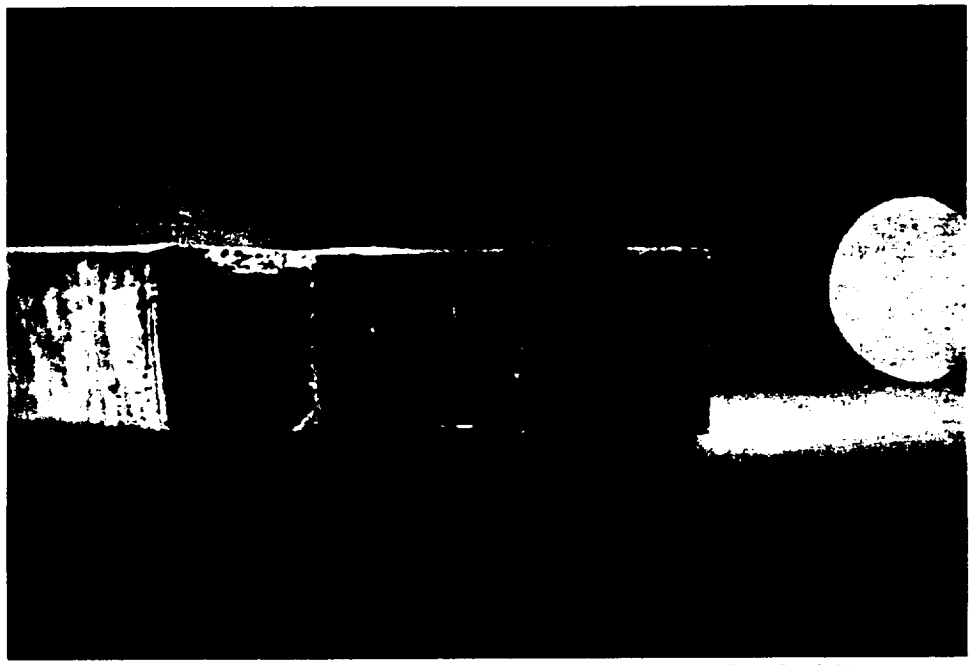

Figure 4.5.2.1-4. Typical Post-Transition Crack Shape for Test Set I-1i-a

NASCRAC™-predicted l_1 is 65,000 cycles, approximately 120% greater than the average experimentally-observed l_1 for this test set. For nearly the entire NASCRAC™-predicted fatigue life, NASCRAC™-predicted crack lengths a_1 and a_2 do not match experimentally-observed crack lengths.

To investigate the source of these discrepancies, three boundary element analyses were performed. Elliptical crack fronts, connecting crack tip locations observed in test I-1i-a/4 at 10,000 and 20,000 cycles, and the initial notch were analyzed with FRANC3D. These fronts are shown in Figure 4.5.2.1-5. The loading for these analyses was the far field stress corresponding to the amplitude of fatigue loads applied to this test. NASCRAC™ stress intensity factor calculations were performed using the same geometry and applied loads as in the FRANC3D analyses.

The FRANC3D- and NASCRAC™-calculated stress intensity factors are shown in Figures 4.5.2.1-6 through 4.5.2.1-8. FRANC3D caclulates stress intensity factors along the entire crack front. NASCRAC™ calculates RMS-average stress intensity factors for each crack tip. As anticipated, FRANC3D calculated K_{II} and K_{III} are less than 1% of K_I values.

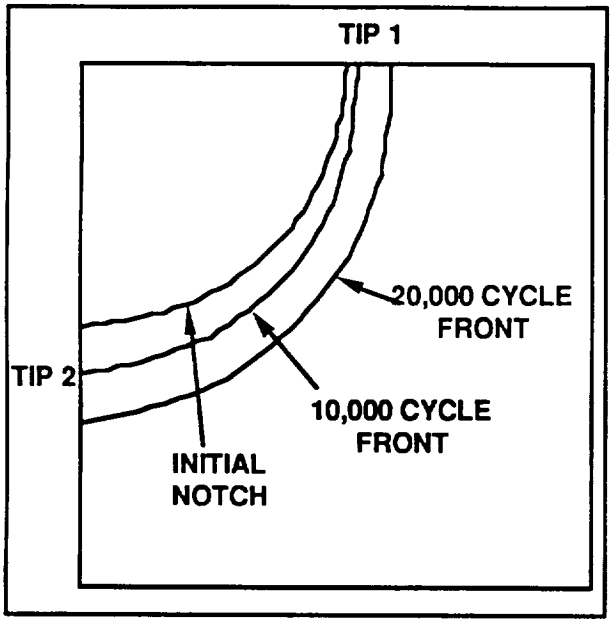

Figure 4.5.2.1-5. Crack Fronts for Analyses of Test I-1i-a/4

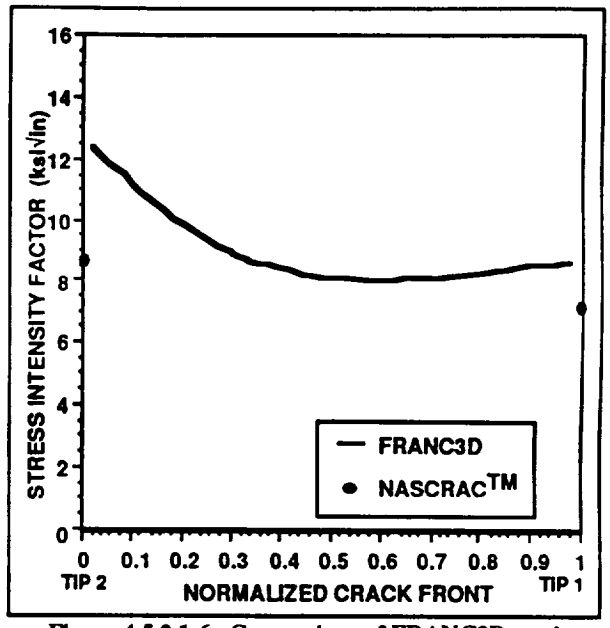

Figure 4.5.2.1-6. Comparison of FRANC3D- and NASCRAC™-Calculated K for Initial Notch

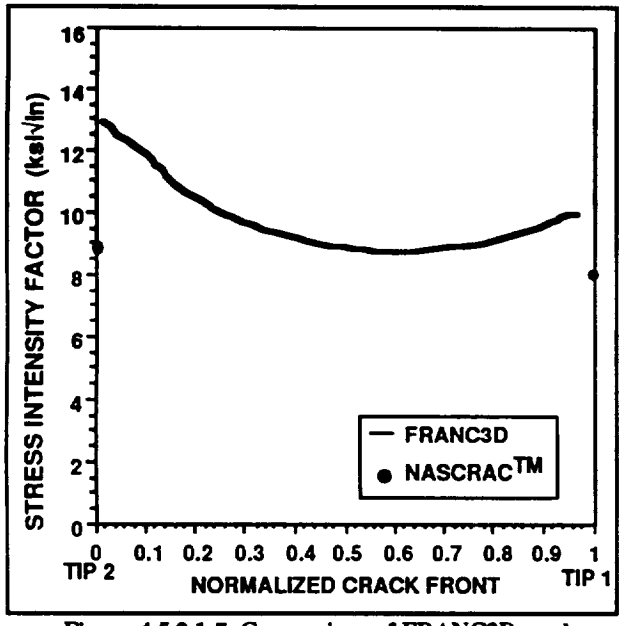

Figure 4.5.2.1-7. Comparison of FRANC3D- and NASCRAC™-Calculated K for 10,000 Cycle Elliptical Crack Front

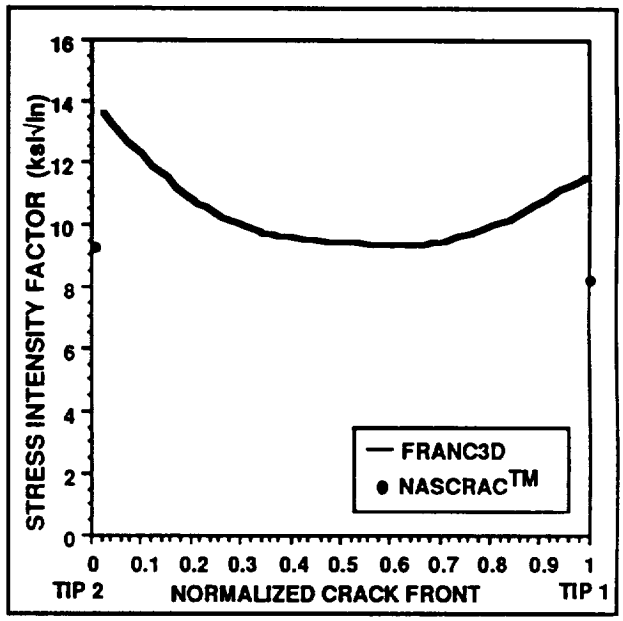

Figure 4.5.2.1-8 Comparison of FRANC3D- and NASCRC™ C-Calculated K for 20,000 Cycle Elliptical Crack Front

The FRANC3D-calculated stress intensity factors vary as much as 4.5 ksi√inch along each crack front, and are highest near tip 2 and lowest near the middle of the crack front. NASCRAC™-calculated stress intensity factors do not match the FRANC3D-calculated stress intensity factors near the two crack tips. This difference could explain the difference between predicted and observed crack growth rates. An RMS average of the FRANC3D-calculated stress intensity factors would be closer to the NASCRAC™-calculated values. The RMS averaging is investigated in the discussion of set ii of this test series.

A check on the applicability of linear elastic fracture mechanics (LEFM) should be considered. The FRANC3D analyses indicate that gross section yielding would not occur in these tests. The process zone surrounding the crack front must also be evaluated. A first order estimate of the plane stress process zone size is,

$$r_y = \frac{1}{2\pi}\frac{K^2}{\sigma_y^2} \qquad 4.5.2.1\text{-}1$$

All relevent dimensions should be much larger than this length. Often, it is assumed that ten times the process zone size is required for LEFM. The following analysis is based on the maximum FRANC3D-calculated stress intensity factors along the crack front at the maximum load applied during a fatigue cycle. These values are 12.2 ksi$\sqrt{in}$ for the initial notch and 17.5 ksi$\sqrt{in}$ for the 20,000 cycle elliptical crack front. Assuming a yield stress of 53 ksi, the process zone size estimated by equation 4.5.2-1 is 0.0084 inches for the intial notch and 0.017 inches for the 20,000 cycle elliptical front. With a curved crack front in three dimensions, it is not clear what "length" should be compared to the process zone size. However, there is greater than 0.17 inches of uncracked ligament near the middle of the crack front for the entire fatigue life that is considered in this test series. Therefore, it is reasonable to assume that LEFM is applicable for this configuration for most of the fatigue life before the transition. This check does not need to be performed on set ii; the ligament in set ii is larger than that of set i, and the slower crack growth in set ii indicates lower stress intensity factors.

In summary, NASCRAC™-predicted fatigue life is significantly longer than the experimentally-observed life in Test Set I-1i-a. Based on the discussion in this section, the following conclusions may be made regarding this observation:

- FRANC3D-calculated stress intensity factors near the crack tips of the three cracks analyzed are up to 50% greater than NASCRAC™-calculated stress intensity factors. This difference is enough to explain the difference between NASCRAC™-predicted and experimentally-observed number of cycles before transition, l_1.

- Some, but not all of the difference in calculated stress intensity factors might be explained by RMS averaging along the crack front. The RMS averaging will be investigated later in this section.

The geometry for Test Set I-1ii-a is similar to that of Test Set I-1i-a, and is shown in Figure 4.5.2-1. Average dimensions for Test Set I-1ii-a are given in Table 4.5.2.1-2. Experimentally-observed and NASCRAC™-predicted crack lengths for Test Set I-1ii-a are shown in Figures 4.5.2.1-9 and 4.5.2.1-10. The input for the NASCRAC™ analysis are summarized in Table 4.5.2.1-4. In addition to the four tests described in Table 4.5.2.1-2, a fifth test was performed. This test was similar to the other four tests, but was stopped prior to transition to

allow the pre-transition crack front to be seen. This crack front is shown in Figure 4.5.2.1-11. A photograph of a post-transition crack front from Test Set I-1ii-a is shown in Figure 4.5.2.1-12.

Table 4.5.2.1-4. NASCRAC™ Input for Analysis of Test Set I-1ii-a

	NASCRAC™ INPUT	VALUE	CORESPONDING TEST DIMENSION
MODEL	601		I-1-a
GEOMETRY	a1	0.252	$a1(0)$
	a2	0.258	$a2(0)$
	B	1.958	b^*
	t	0.502	$b2$
	r	0.249	$b3/2$
	W	4.415	$b1$
LOADING	TRANSIENT 1	1000 CYCLES	FAR FIELD STRESS FROM FATIGUE LOADS: FIGURE 4.5.2-1 TABLE 4.5.2.1-3
	RANGE: EQ. A	7.74	
	R-RATIO	0.201	
	BLOCK	1X TRANSIENT 1	
MATERIAL PROPERTIES	2219-T851 AL, T-L & L-T 75F	ALUM3 # 104	2219-T851 LAB AIR

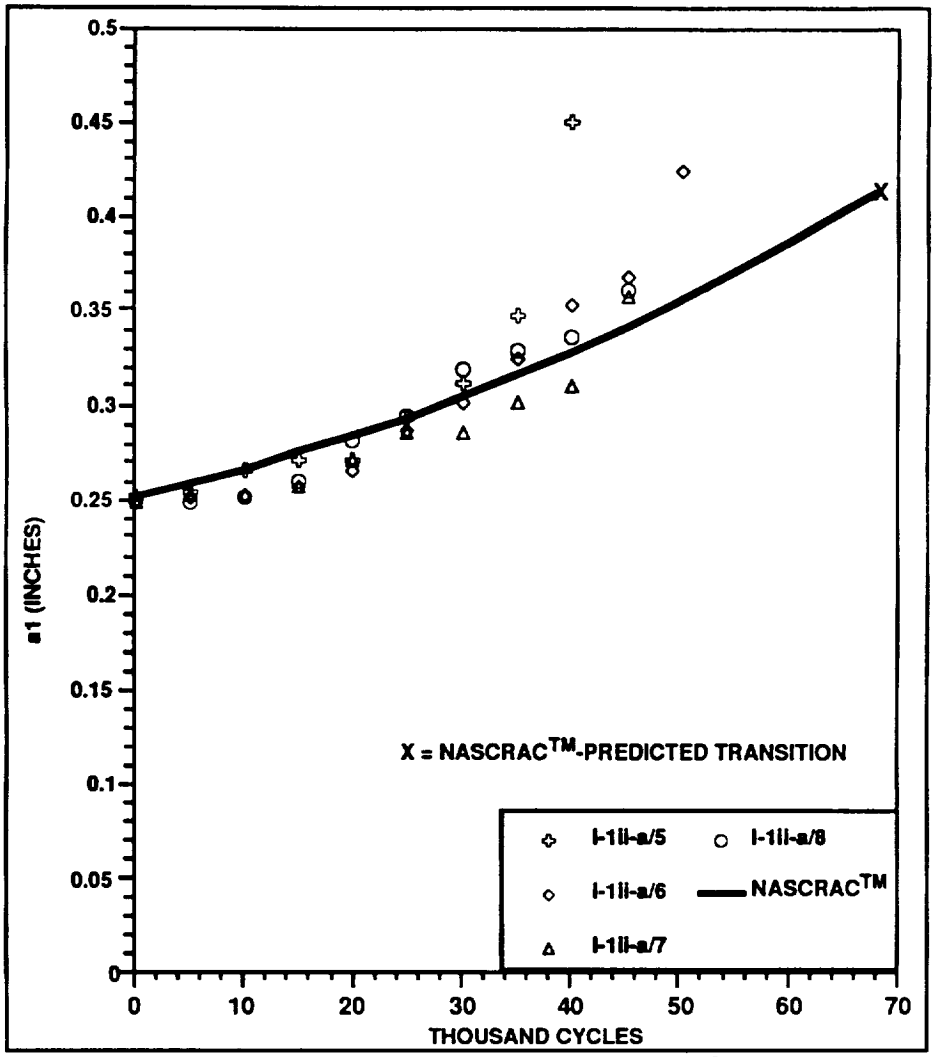

Figure 4.5.2.1-9. Experimentally-Observed and NASCRAC™-Predicted Crack Length *a*1 Versus Cycles for Test Set I-1II-a

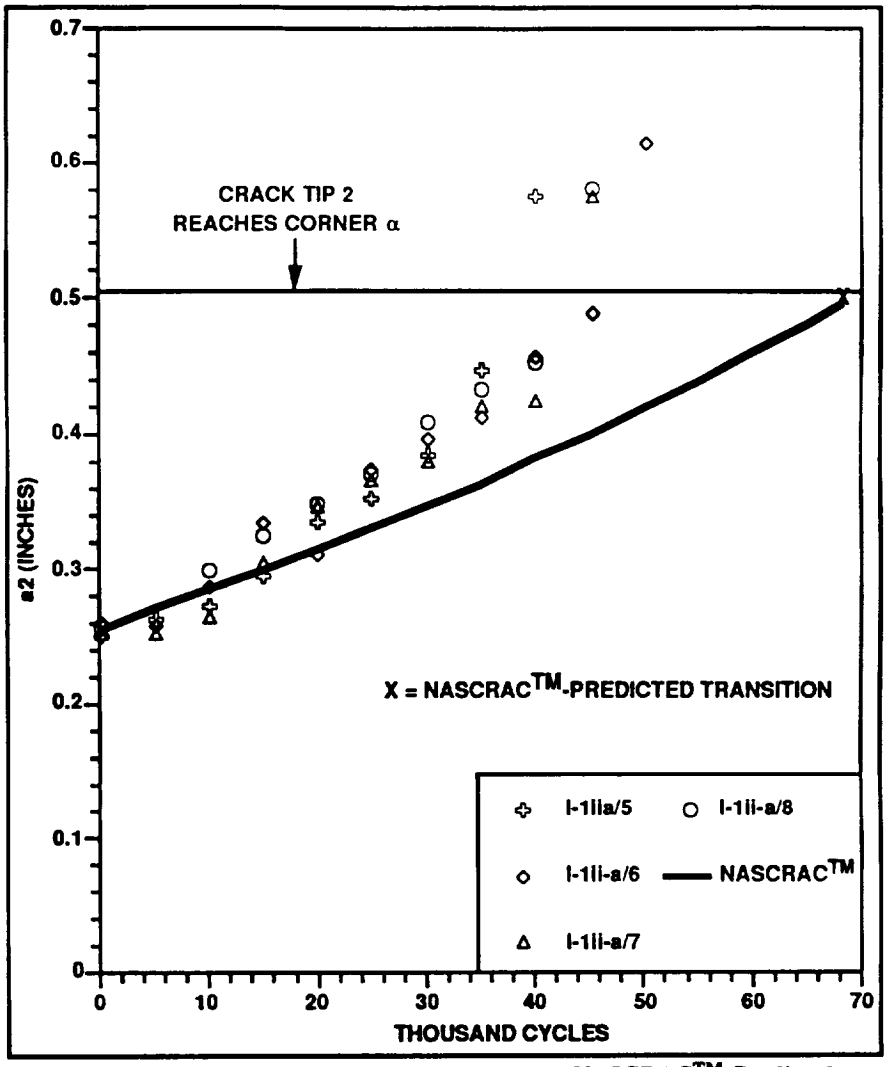

Figure 4.5.2.1-10. Experimentally-Observed and NASCRAC™-Predicted Crack Length *a*2 Versus Cycles for Test Set I-1Ii-a

Figure 4.5.2.1-11. Pre-Transition Crack Shape for Test Series I-1ii-a

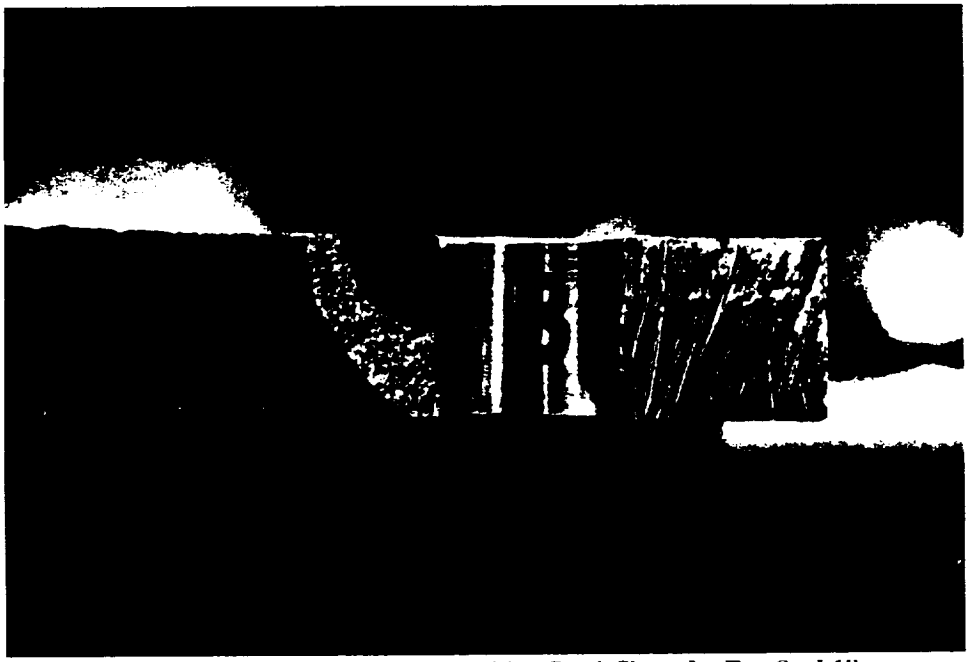

Figure 4.5.2.1-12. Typical Post-Transition Crack Shape for Test Set I-1ii-a

The NASCRAC™-predicted cycles before transition, l_1, is approximately 60% greater than the experimentally-observed number of cycles before transition. NASCRAC™-predicted crack length a_1 is within the range of experimentally-observed crack length a_1 for the first 40,000 cycles of fatigue crack growth. NASCRAC™-predicted crack length a_2 is outside the range of experimentally observed crack length a_2 after 20,000 cycles of fatigue crack growth.

The geometry for this set of tests cannot be modeled directly by NASCRAC™. The code requires the crack to grow into the smaller of the two ligaments. While not an error, this is a shortcoming in the program. A substitute geometry, denoted I-1ii-w, was used for the NASCRAC™ analysis of this test set. The geometry for test set I-1ii-a is denoted I-1ii. The two geometries are shown in Figure 4.5.2.1-13. The only difference between geometry I-1ii-w and geometry I-1ii is that the width of the specimen is increased so the uncracked ligament is slightly larger than the cracked ligament. The far field stress for the NASCRAC™ analysis was chosen to match that calculated for the tests.

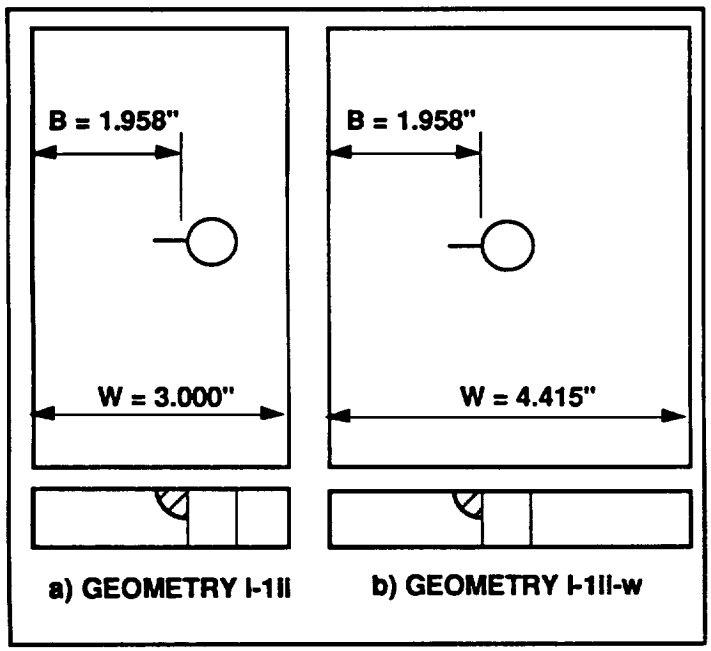

Figure 4.5.2.1-13. Experimental Geometry I-1ii and Substitute Geometry I-1ii-w

To determine whether the substitute geometry was appropriate to model the actual set of tests, two-dimensional stress intensity factor calculations were performed using FRANC2D. The geometries used for these analyses were similar to those shown in Figure 4.5.2.1-13. However, a through crack was assumed so that two-dimensional analyses could be used. Plots of K versus crack length a_1, for a_1= 0.05 to 0.55 inches are shown in Figure 4.5.2.1-14. For all crack lengths analyzed, the stress intensity factor for the substitute geometry, I-1ii-w, is is less then the stress intensity factor for the experimental geometry, I-1ii. The difference is 6% for a = 0.05 inches and increases to 9% for a = 0.55 inches. Given these stress intensity factors, the modified Forman parameters in the NASCRAC™ material library for 2219-T851 aluminum predict crack growth rates for geometry I-1ii-w 15% to 30% less than for geometry I-1ii. This analysis indicates that the two geoemtries might have significantly different fatigue lives. However, there are limits to how well a two-dimensional analysis can model a three-dimensional quarter-elliptical crack shape. Therefore, further conclusions can not be drawn from the two-dimensional analyses.

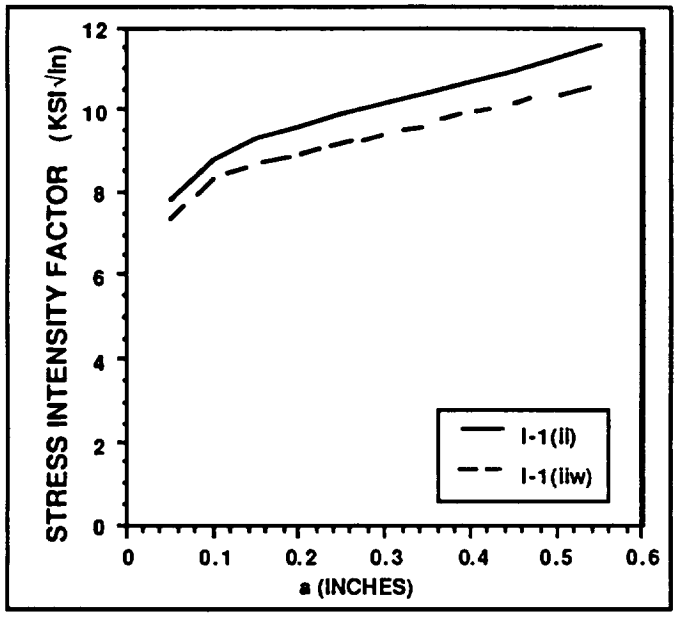

Figure 4.5.2.1-14. FRANC2D-Calculated K_I Versus *a* for two Dimensional Models of Test Geometry and Substitute Geometry

Two three-dimensional boundary element analyses were performed for a quarter-elliptical crack with $a_1 = 0.248$ inches and $a_2 = 0.256$ inches. This crack is comparable to the size and shape of an initial notch in this test series. The first analysis used geometry I-1ii. The second analysis used the substitute geometry I-1ii-w. The loading for both analyses was the far-field stress corresponding to the load amplitudes in this set of tests. A NASCRAC™ analysis was performed using the same geometry and loads as the second boundary element analysis. FRANC3D-calculated stress intensity factors from both both boundary element analyses, and the NASCRAC™-calculated stress intensity factors are shown in Figure 4.5.2.1-15. FRANC3D calculates stress intensity factors along the entire crack front. NASCRAC™ calculates RMS-averaged stress intensity factors for each crack tip.

Due to the averaging involved in NASCRAC™-calculation of stress intensity factors, FRANC3D and NASCRAC™ calculate two different types of stress intensity factors. To provide a better means of comparison, FRANC3D K's were averaged in the manner described in Section 2.3 of the NASCRAC™ Theory Manual. These values are denoted FRANC3D $\overline{K}(i)$, where i is a crack tip. To ease calculations, it was assumed that values of stress intensity factors were distributed along equal increments of the angle ϕ. Actually, these values were distributed along equal length increments along the crack front s, Figure 4.5.2.1-16. As the crack front analyzed was nearly a circle ($a1 = 0.248$, $a2 = 0.256$ inches) the maximum error in the Δs associated with any spanned $\Delta\phi$ is 2.5%. The results of these calculations are shown in Table 4.5.2.1-5.

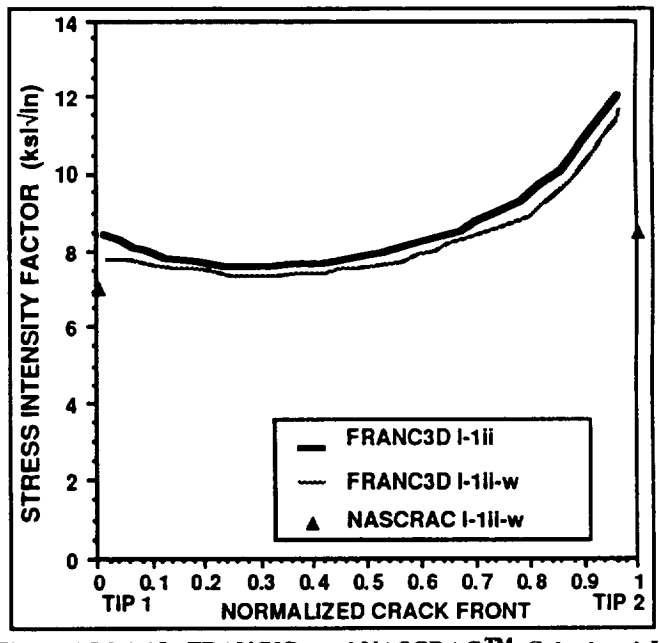

Figure 4.5.2.1-15. FRANC3D- and NASCRAC™-Calculated K for Initial Notch

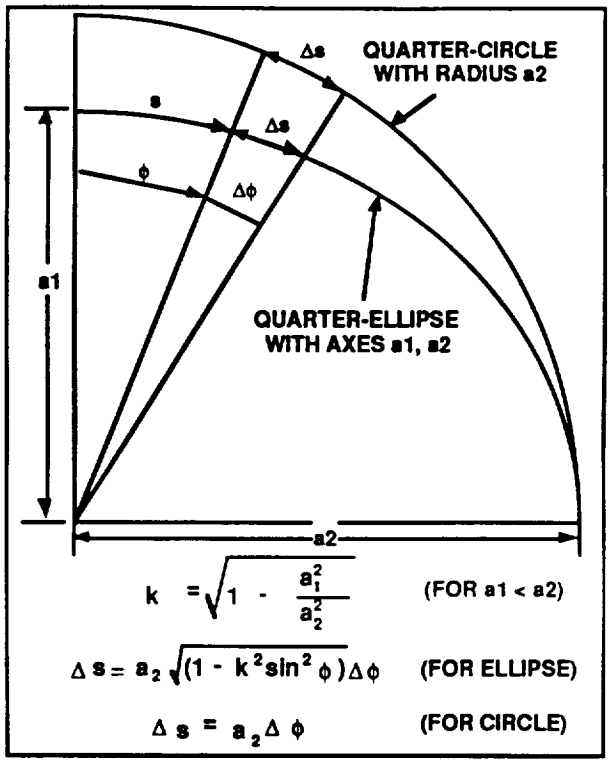

Figure 4.5.2.1-16. Definition of Angle ϕ and Length s for $\overline{K}$ Calculations

Table 4.5.2.1-5 Comparison of Calculated SIF's for Initial Notch

SOLUTION	$\overline{K}(1)$ ksi√in	% DIFFERENCE FROM FRANC3D I-1ii $\overline{K}(1)$	$\overline{K}(2)$ ksi√in	% DIFFERENCE FROM FRANC3D I-1ii $\overline{K}(2)$	Kmax ksi√in	% DIFFERENCE FROM FRANC3D I-1ii Kmax
FRANC3D I-1ii	7.9	---	9.3	---	12.2	---
FRANC3D I-1ii-w	7.7	-2.5%	9.0	-3.2%	11.8	-3.3%
NASCRAC I-1ii-w	7.3	-7.6%	8.6	-7.5%	8.6	-29.5%

The difference between FRANC3D calculated stress intensity factors for the two geometries, no more than 3.3%, is less than the difference calculated by the two-dimensional analyses shown in Figure 4.5.2.1-14. The trend of Figure 4.5.2.1-14 indicates that this difference would increase as the crack size increases.

The difference between NASCRAC™- and FRANC3D-calculated $\overline{K}$ is less than the accuracy given for some of the other NASCRAC™ geometries (10% for models 605 and 702, for example). This difference would cause differences in predicted fatigue life. However, the difference between the maximum FRANC3D K (at tip 2) and the NASCRAC™ $\overline{K}(2)$ is much larger. According to the modified Forman parameters given for 2219-T851 aluminum in the NASCRAC™ materials library, the 30% difference results in crack growth rates that vary by more than a factor of two.

In general, as the crack propagates, the variation of stress intensity factors along the crack front should reduce. The difference between the RMS average stress intensity factors and the maximum stress intensity factors along the crack front will reduce as the varaition along the crack fronts reduce. However, the difference does not appear to reduce for the elliptical crack shapes analyzed for Test Set I-1i-a. The crack front from Test I-1ii-a/9, shown in Figure 4.5.2.1-7, does not intersect the free surface at 90° at crack tip 2. This shows that the observed crack front is not elliptical. It is possible that the difference between the actual and NASCRAC™ crack shapes accounts for some of the difference in observed and predicted crack growth rates. This issue requires further investigation.

From the observations of Figures 4.5.2.1-9 and 4.5.2.1-10, it is apparent that the NASCRAC™-predicted number of cycles before transition, l_1, is significantly greater than l_1 experimentally-observed in Test Set I-1ii-a. The following conclusions may be made regarding this observation:

- The effect of the substitute geometry on stress intensity factor calculation is small compared to other errors in stress intensity factor calculation.

- The difference between FRANC3D RMS K's and NASCRAC™ K's for configuration 601 is within the accuracy bounds published for other NASCRAC™ configurations. However, this difference does account for some of the observed fatigue life discrepancies.

- The difference between the maximum FRANC3D-calculated stress intensity factors and the NASCRAC™-calculated stress intensiy factors for model 601 is likely to explain most of the difference between NASCRAC™-predicted and experimentally-observed l_1 for test series I-1-a.

4.5.2.2 Test Series I-2-a: Fatigue Crack Propagation with Transitioning

The geometry for this test series is described in Figure 4.5.2.2-1. Average dimensions are given in Table 4.5.2.2-1. The loading parameters, Δp and R-ratio, are defined in Figure 4.5.2-1. Two transitions are defined for this test series. The first transition occurs when crack tip 1 reaches corner α. The second transition occurs when crack tip 2 reaches corner β. For every test of this series discussed in this section, cyclic loads were applied until the second transition occured.

The numbers of cycles before the first and second transitions are defined as l_1 and l_2, respectively. Both of these numbers are calculated by fitting a quadratic polynomial to crack lengths measured at the two 5000 cycle intervals just before transition and the crack length measured at the first 5000 cycle interval following the transition. The number of cycles for which the crack tip would be at the appropriate corner was interpolated from this polynomial.

Experimentally-observed and NASCRAC-predicted crack lengths a_1, a_2 and a_3 are plotted versus cycles in Figures 4.5.2.2-2, 4.5.2.2-3 and 4.5.2.2-4. The definitions of crack lengths used

in these comparisons are those given in Figure 4.5.2.2-1. These definitions do not correspond with NASCRAC™ definitions of crack length, which change throughout the test. Furthermore, NASCRAC™ definitions of crack lengths are not applicable to some of the observed crack shapes. This issue is addressed in greater detail in the section 4.10.1: Crack Transitioning. A photograph of a post-second-transition crack front is shown in Figure 4.5.2.2-5.

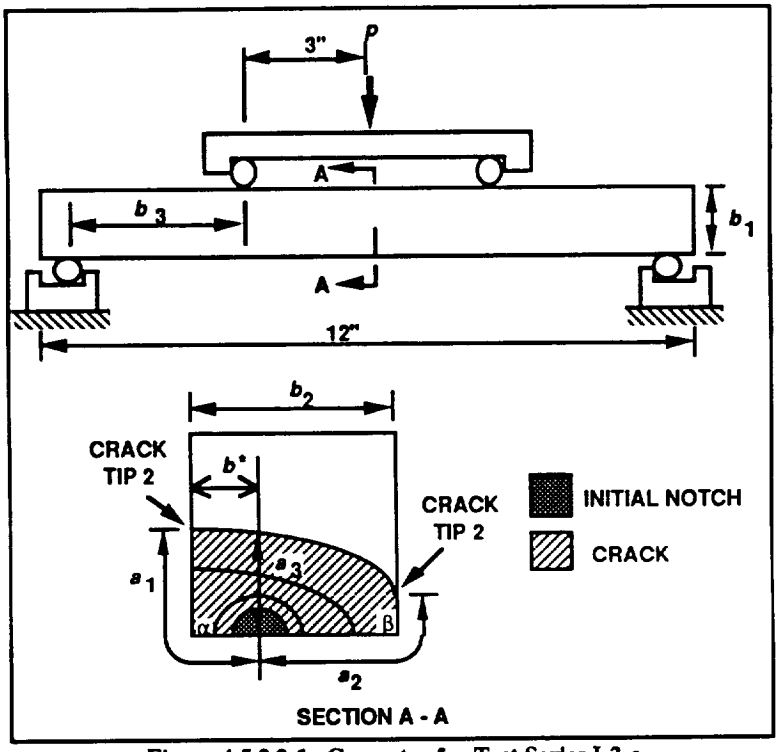

Figure 4.5.2.2-1. Geometry for Test Series I-2-a

Table 4.5.2.2-1. Average Dimensions for Test Series I-2-a

NUMBER OF TESTS		14
DIMENSION	AVERAGE VALUE	UNITS
$A1(0)$	0.254	INCHES
$a2(0)$	0.254	INCHES
$a3(0)$	0.256	INCHES
$b1$	2.000	INCHES
$b2$	1.500	INCHES
$b3$	2.408	INCHES
b^*	0.497	INCHES
Δp	11.48	KIPS
R-ratio	0.217	-
$l1$	55,605	CYCLES
$l2$	107,398	CYCLES

Table 4.5.2.2-2. NASCRAC™ Input For Analysis Of Test Series I-2-a

	NASCRAC™ INPUT	VALUE	CORRESPONDING TEST DIMENSION
MODEL	702		I-2-a
GEOMETRY	a1	0.256	$a3(0)$
	a2	0.254	$a1(0)$
	a3	0.254	$a2(0)$
	W1	2.000	$b1$
	W2	0.497	b^*
	W3	1.003	$b2 - b^*$
LOADING	TRANSIENT 1 RANGE:EQUATIONB R-RATIO:	1000 CYCLES 13.82, -13.82 0.217	FATIGUE LOADS: FIGURE 4.5.2-1 TABLE 4.5.2.2-1
	BLOCK	1 X TRANSIENT 1	
MATERIAL PROPERTIES	2219-T851 Al L-T, T-L 75F	ALUM3 #104	2219-T851 Al LAB AIR

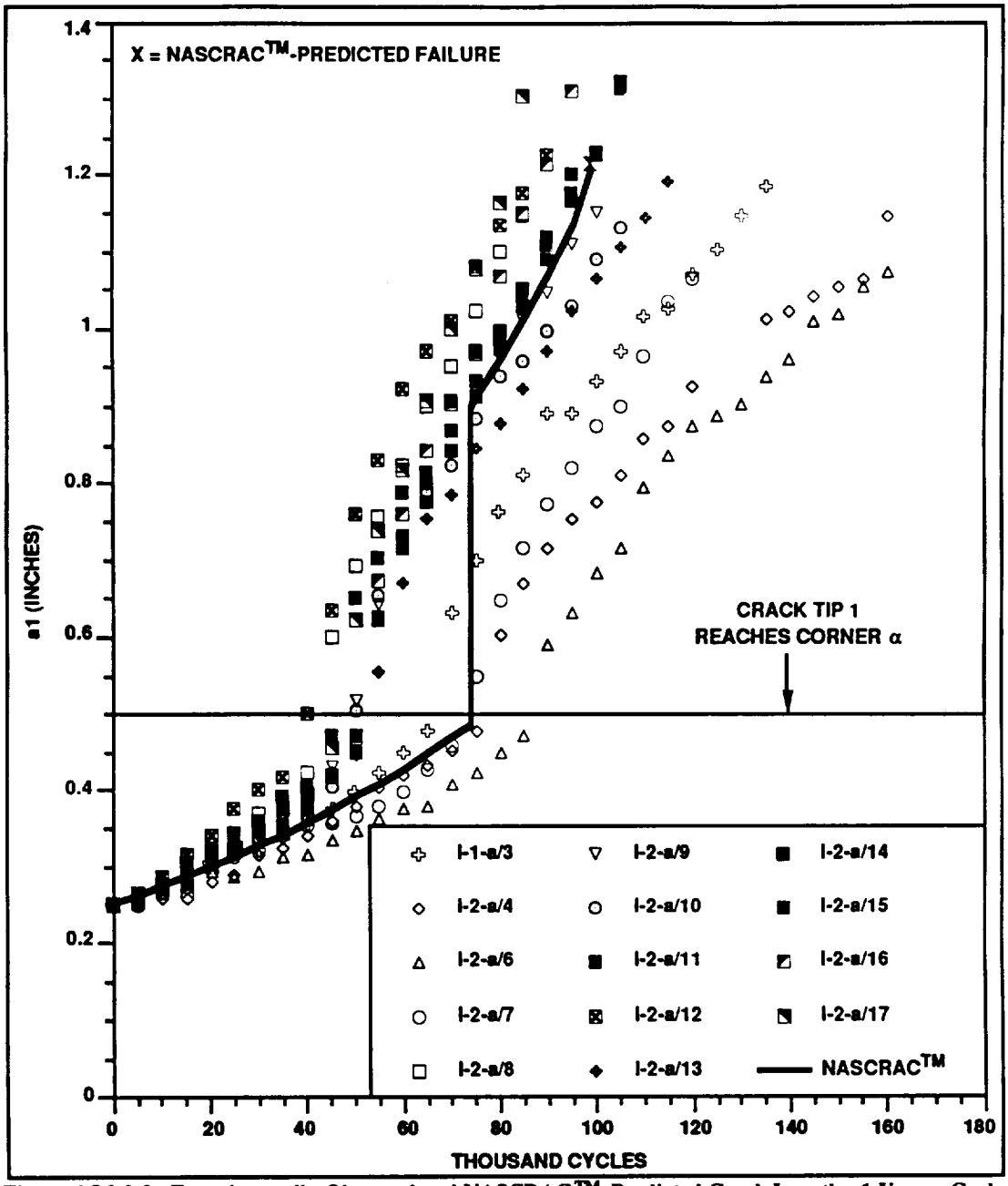

Figure 4.5.2.2-2. Experimentally-Observed and NASCRAC™-Predicted Crack Length *a*1 Versus Cycles for Test Series I-2-a

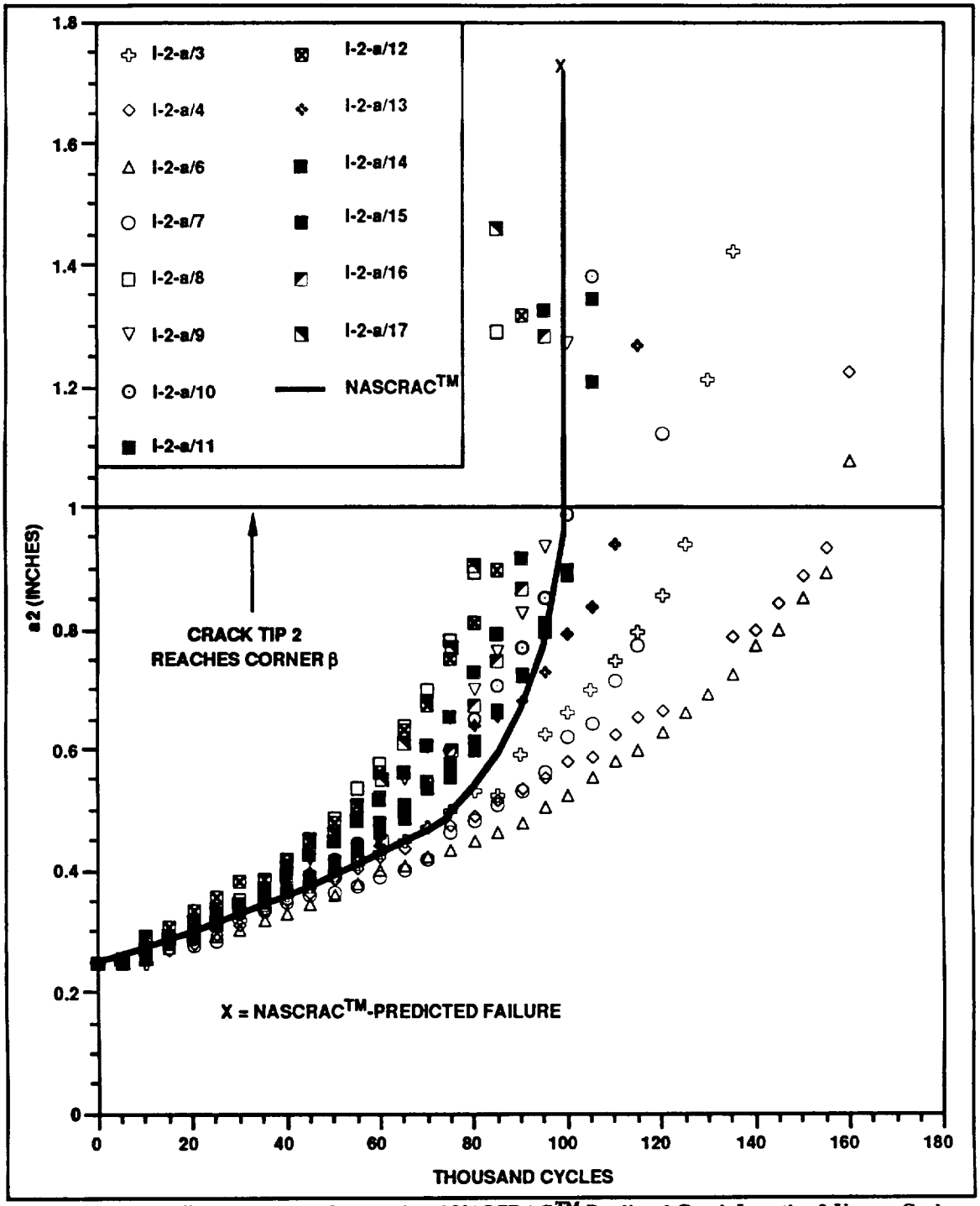

Figure 4.5.2.2-3. Experimentally-Observed and NASCRAC™-Predicted Crack Length *a*2 Versus Cycles for Test Series I-2-a

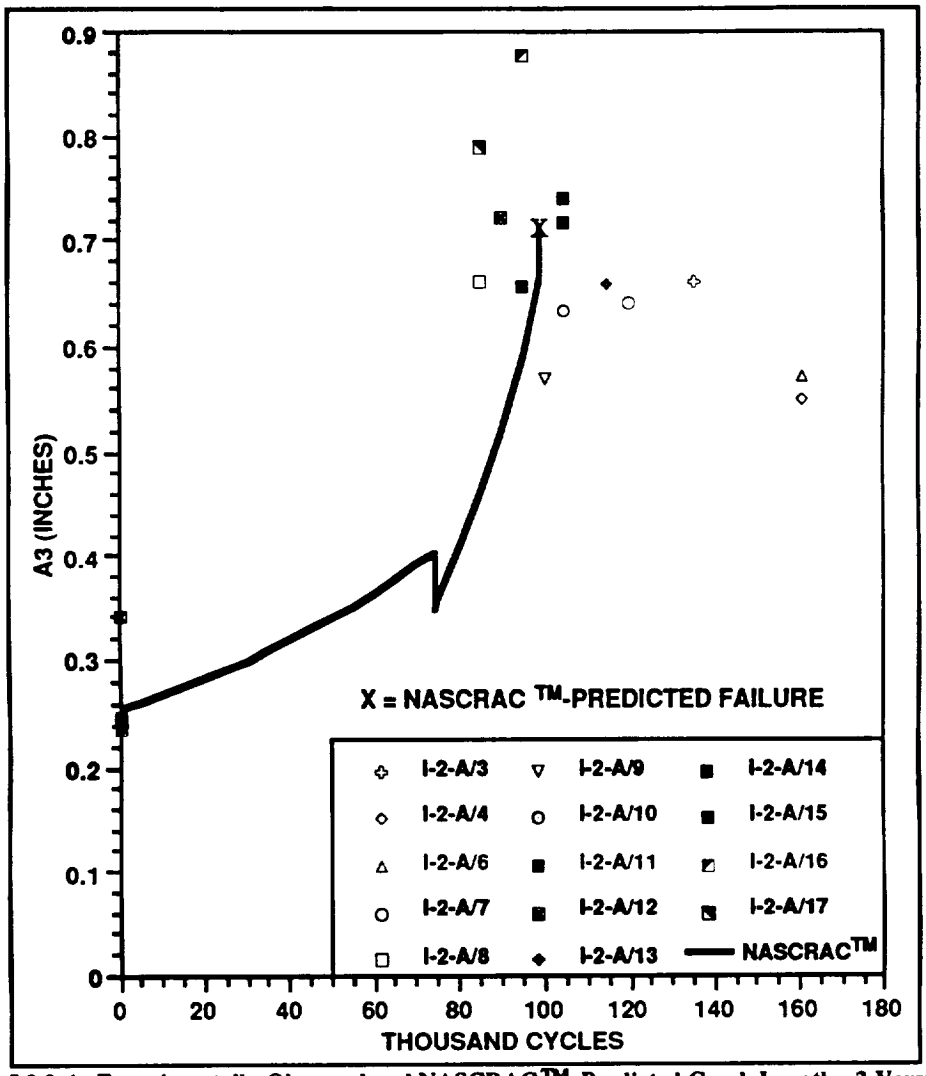

Figure 4.5.2.2-4. Experimentally-Observed and NASCRAC™-Predicted Crack Length *a*3 Versus Cycles for Test Series I-2-a

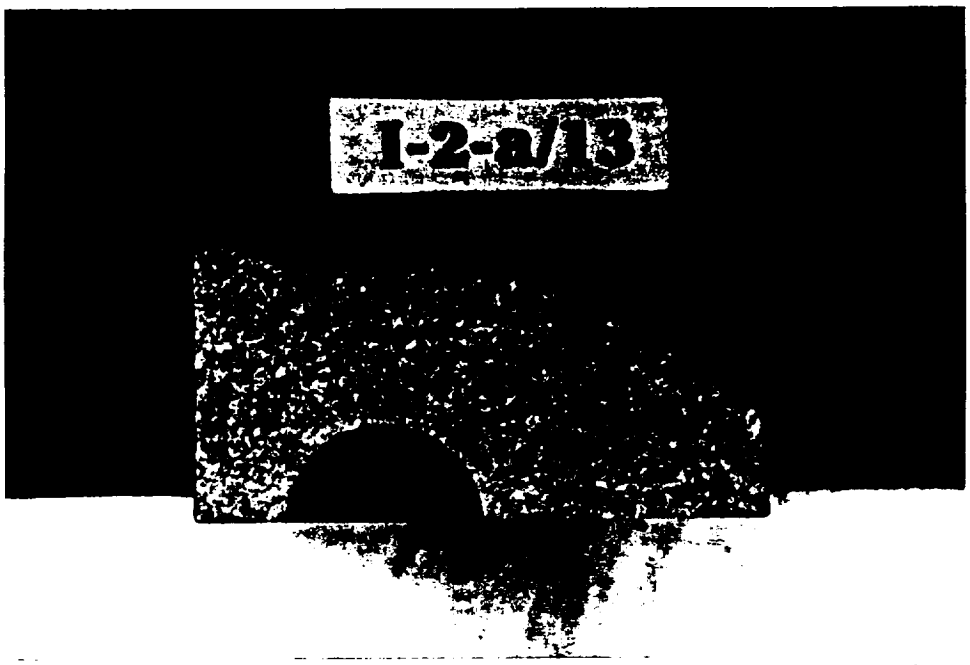

Figure 4.5.2.2-5. Typical Crack Front Following Second Transition in Test Series I-2-a

NASCRAC™-predicted crack lengths remain in the range of observed crack lengths throughout the entire predicted life. The range of experimentally-observed l_1 for this test series is from 39,485 cycles to 86,391 cycles. NASCRAC™-predicted l_1 is 33% greater than the average experimentally-obsevered l_1.

The range of experimentally-observed l_2 for this test series is from 81,193 cycles to 158,254 cycles. NASCRAC™-predicted l_2 is 8% less than the average observed l_2. The difference between NASCRAC™-predicted l_1 must be considered when evaluating the accuracy of NASCRAC™-predicted l_2. NASCRAC™-crack transitioning capability will be discussed more thoroughly in Section 4.10.

To summarize, NASCRAC™-predicted crack lengths, as defined in Figure 4.5.2.2-1, are not continuous throughout the course of the test. The following conclusions regarding this observation can be made:

- It is likely that NASCRAC™-crack-growth predictions near either of the crack transitions will be inaccurate.

- NASCRAC™-predictions will not indicate the fatigue life that occurs while the crack is transitioning. While, in general, this assumption is conservative, in some instances it might be advantagous to consider this additional fatigue life.

Despite these conclusions, NASCRAC™-predicted crack lengths are in the range of experimental observations for the duration of the fatigue life in Test Series I-2-a. Therefore, it is concluded that:

- NASCRAC™-model 702 predicts constant amplitude fatigue crack growth well for the pre-transition crack growth in Test Series I-2-a.

- In light of the experimentally observed scatter, in some instances, the NASCRAC™ transition capability does predict overall fatigue life satisfactorily.

Crack growth behavior near the first transition, and the available fatigue life that is not predicted by NASCRAC™ as a result of the NASCRAC™-transition algorithm are considered in Section 4.10.1: Crack transitioning.

4.5.2.3 Test Series I-3-a: Fatigue Crack Propagation through a Residual Stress Field

The objective of test series I-3-a was to validate NASCRAC™'s crack propagation through a residual stress field capability. The tests in this series are described in greater detail in the section on elastic plastic stress redistribution. However, two of the tests in this series were constant amplitude fatigue crack tests and hence are discussed in this section. The two tests had significantly different initial notch sizes, and will be discussed individually.

The geometry for this test series is shown in Figure 4.5.2.3-1. Tests in this series were not conducted to failure and no obvious transition occurred. The dimensions of test I-3-a/2 are given in Table 4.5.2.3-1. Input for a NASCRAC™ analysis of this test is given in Table 4.5.2.3-2. Experimentally-observed and NASCRAC™-predicted crack length versus cycles are shown in Figure 4.5.2.3-2. A photograph of the surface is shown in Figure 4.5.2.3-3.

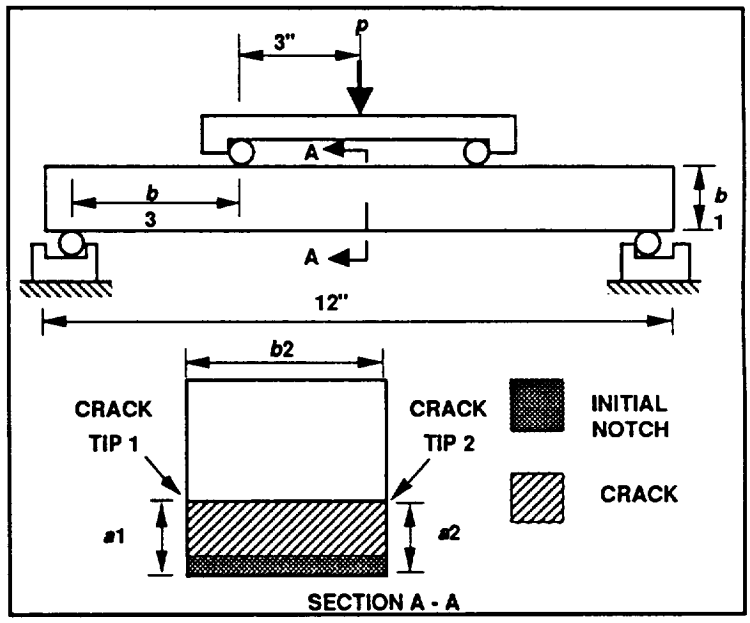

Figure 4.5.2.3-1. Geometry for Test Series I-3-a

Table 4.5.2.3-1. Dimensions for Test I-3-a/2

NUMBER OF TESTS		1
DIMENSION	AVERAGE VALUE	UNITS
$a1(0)$	0.018	INCHES
$a2(0)$	0.019	INCHES
$b1$	1.991	INCHES
$b2$	0.653	INCHES
$b3$	2.409	INCHES
Δp	6.258	KIPS
R-ratio	0.2237	-

Table 4.5.2.3-2. Input for NASCRAC™ Analysis of Test I-3-a/2

	NASCRAC™ INPUT	VALUE	CORRESPONDING TEST DIMENSION
MODEL	203		I-3-a/2
GEOMETRY	a	0.0185	$(a1(0) + a2(0))/2$
	W	1.991	$b1$
LOADING	TRANSIENT 1 RANGE: EQ. B R-RATIO	1000 CYCLES 17.47, -17.55 0.2237	FATIGUE LOADS FIGURE 4.5.2-1 TABLE 4.5.2.3-1
	BLOCK	1 X TRANSIENT 1	
MATERIAL PROPERTIES	2219-T851 Al L-T, T-L 75F	ALUM3 #104	2219-T851 Al LAB AIR

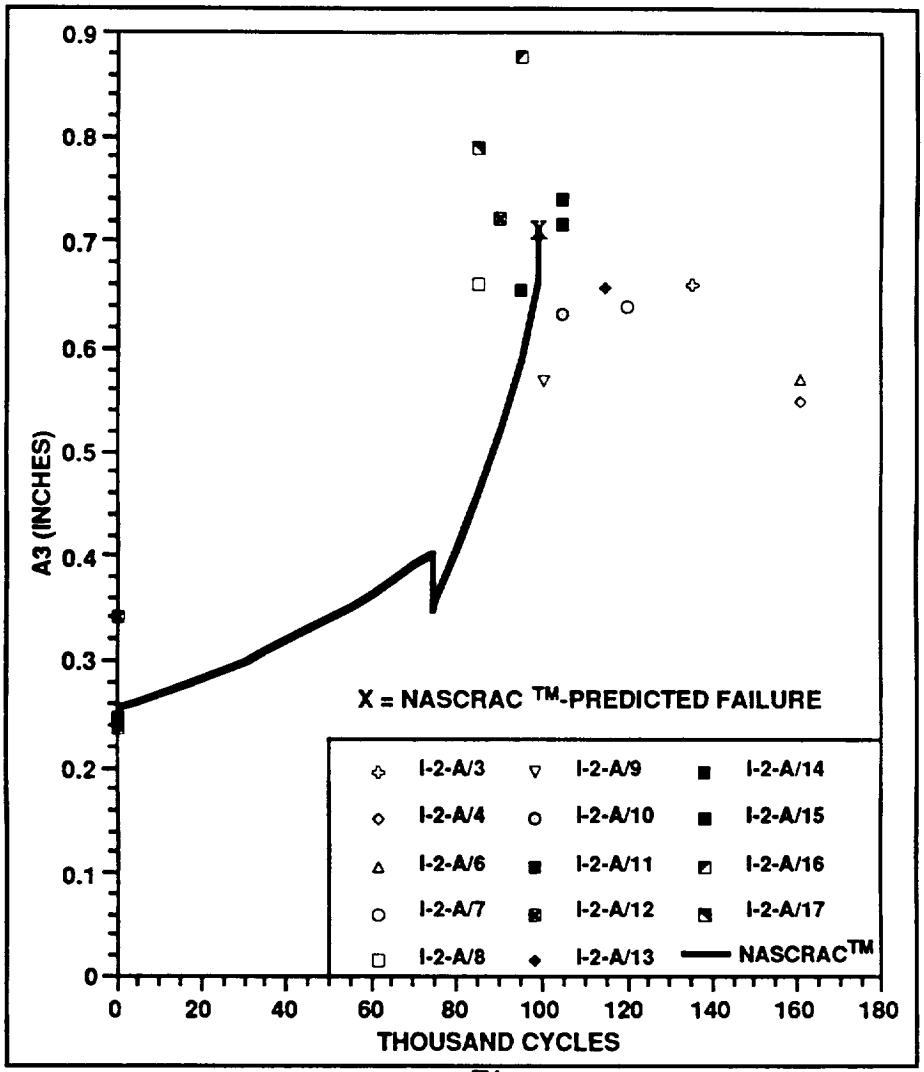

Figure 4.5.2.3-2. Experimentally-Observed and NASCRAC™-Predicted Crack Length Versus Cycles for Test I-3-a/2

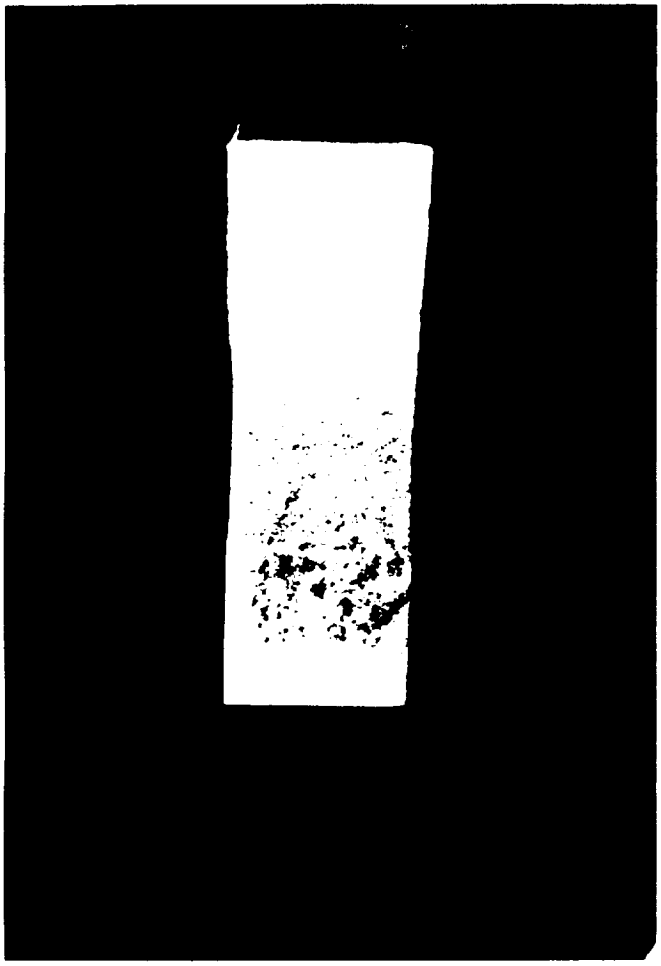

Figure 4.5.2.3-3. Photograph of Crack Surface for Test Series I-3-a

NASCRAC™-predicted crack lengths match the experimentally-observed crack lengths well. However, some of the fatigue life of test I-3-a/2 was spent in the crack initiation phase. It is unknown how much of the fatigue life of this test is spent in the crack intiation phase. It is possible that a significant number of cycles are spent intiating the crack from the notch. These cycles is not modeled by NASCRAC™, as the NASCRAC™ analysis assumes a sharp, intial crack. Also, for much of the fatigue life of this test the crack length falls into what is known as the small crack regime. Small cracks, less than about 0.020 inches beyond the initial notch, have been observed to grow faster than larger cracks under the same applied stress intensity factors [5]. Furthermore, the verification work described in subsection 4.5.1 indicates differences in the crack growth models used in NASCRAC™ and FLAGRO. The implementation of m in the NASCRAC™ crack growth model negates some of the effect of R-ratio on fatigue crack growth. The R-ratio can be particularly important at low values of ΔK. With these possible sources of error, it is impossible to conclude whether these factors are insignificant, or cancelling each other out.

Test I-3-a/6 was also a constant amplitude fatigue crack growth test. The dimensions of test I-3-a/6 are given in Table 4.5.2.3-3. Fatigue loading of this test continued for 2,600,000 cycles without fatigue crack intiation occurring. Two NASCRAC™ analyses of this test were performed. The inputs for these analyses are given in Tables 4.5.2.3-4 and 4.5.2.3-5. The only difference between these two analyses was the initial crack size varied by 0.0005 inches, less than the accuracy of the intial notch measurements. NASCRAC™ analysis 1 of test I-3-a/6 calculates stress intensity factor below the threshold stress intensity factor, and thus an infinite fatigue life. NASCRAC™ analysis 2 of test I-3-a/6 predicts a fatigue life of 375,000 cycles.

Table 4.5.2.3-3. Dimesions for Test I-3-a/6

NUMBER OF TESTS		1
DIMENSION	AVERAGE VALUE	UNITS
$a1(0)$	0.003	INCHES
$a2(0)$	0.003	INCHES
$b1$	2.000	INCHES
$b2$	0.652	INCHES
$b3$	2.407	INCHES
Δp	6.394	KIPS
R-RATIO	0.2048	-

Table 4.5.2.3-4. Input for NASCRAC™ Analysis 1 of Test I-3-a/6

	NASCRAC™ INPUT	VALUE	CORRESPONDING TEST DIMENSION
MODEL	208		I-3-a/6
GEOMETRY	a	0.003	$(a1(0) + a2(0))/2$
	W	2.000	$b1$
LOADING	TRANSIENT 1 RANGE: EQUATION B R-RATIO	1000 cycles 17.70, -17.70 0.2048	FATIGUE LOADS FIGURE 4.5.2-1 TABLE 4.5.2.3-2
	Block	1X TRANSIENT 1	
MATERIAL PROPERTIES	2219-T851 Al L-T, T-L 75F	ALUM3 #104	2219-T851 Al LAB AIR

Table 4.5.2.3-5 Input for NASCRAC™ Analysis 2 of Test I-3-a/6

	NASCRAC™ Input	Value	Corresponding Test Dimension
MODEL	208		I-3-a/6
GEOMETRY	a	0.0035	$(a1(0) + a2(0))/2$
	W	2.000	b1
LOADING	TRANSIENT 1 RANGE: EQUATION B R-Ratio	1000 CYCLES 17.70, -17.70 0.2048	FATIGUE LOADS FIGURE 4.5.2-1 TABLE 4.5.2.3-2
	Block	1X TRANSIENT 1	
MATERIAL PROPERTIES	2219-T851 Al L-T, T-L 75F	ALUM3 #104	2219-T851 Al LAB AIR

From the discussion of Section 4.5.1 and the observations regarding test I-3-a/2 the following conclusions may be made:

- There is good agreement between NASCRAC™-predicted and experimentally-observed crack lengths in the two tests. However, three possible sources of error are present in these tests. The NASCRAC™ crack growth model does not calculate m properly. This is likely to cause problems in predicted crack growth rates for low ΔK. Small crack effects are likely to be present during most of the fatigue life. Crack intiation is likely to be a significant portion of the fatigue life. It is possible that these effects are all significant, but compensate for each other.

Based on a comparison of NASCRAC™ analyses 1 and 2 of test I-3-a/6 it is concluded that:

- NASCRAC™-predicted fatigue life can be extremely sensitive to small changes in initial crack sizes when the intial crack length is small.

4.5.2.4 Test Series III-a: Constant Amplitude Fatigue Related to Proof Tests

Test series III-a was designed to validate NASCRAC™'s proof test logic. However, stage 1 of each test in this series consisted of constant amplitude fatigue crack growth. Results from this stage will be discussed in this section. The geometry for test series III-a is shown in Figure 4.5.2.4-1. The average dimensions for this test series are given in Table 4.5.2.4-1. Input for a NASCRAC™-analysis of stage 1 of this test series is given in Table 4.5.2.4-2. The first stage of this test series consisted 120,000 fatigue cycles in all but two of the tests. The remaining two tests had 90,000 cycles and 100,000 cycles applied in the first stage.

Experimentally-observed and NASCRAC™-predicted crack lengths versus cycles are shown in Figure 4.5.2.4-2 and 4.5.2.4-3. A typical crack front is shown in Figure 4.5.2.4-4. The crack front that existed after 20,000 cycles is indicated by the darker, semi-elliptical shape on the crack face.

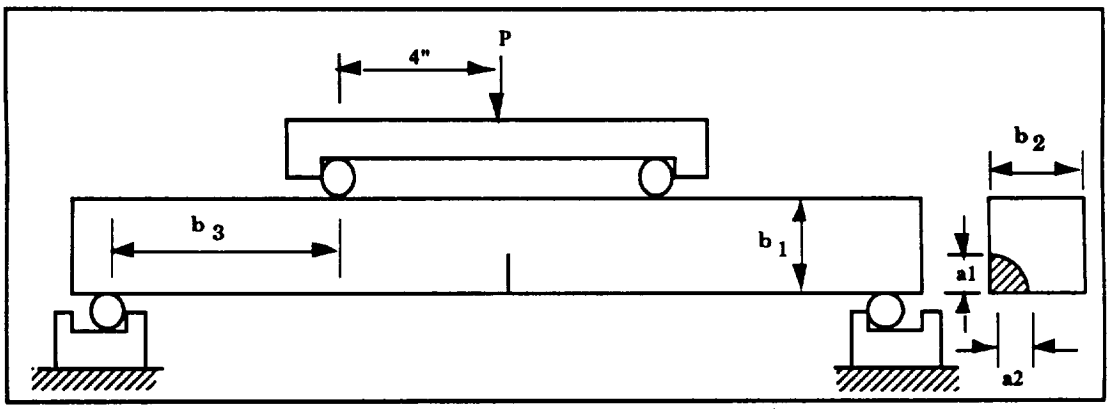

Figure 4.5.2.4-1. Geometry for Test Series III-a

Table 4.5.2.4-2. Average Dimensions for Test Series III-a

NUMBER OF TESTS		9
DIMENSION	AVERAGE VALUE	UNITS
$a1(0)$	0.25	INCHES
$a2(0)$	0.25	INCHES
$b1$	3.001	INCHES
$b2$	3.001	INCHES
$b3$	6.034	INCHES
Δp	20.97	KIPS
R-RATIO	0.2319	-

Table 4.5.2.4-2 Input for NASCRAC™ Analysis of Stage 1 for Test Series III

	NASCRAC™ INPUT	VALUE	CORRESPONDING TEST DIMENSION
MODEL	605		I-2-a
GEOMETRY	a1	0.250	$a1(0)$
	a2	0.250	$a2(0)$
	W1	3.001	$b1$
	W2	3.001	$b2$
LOADING	TRANSIENT 1 RANGE: EQ. B R-RATIO:	1000 CYCLES 14.045, -9.360 0.2319	FATIGUE LOADS: FIGURE 4.5.2-1 TABLE 4.5.2.4-1
	BLOCK	1X TRANSIENT 1	
MATERIAL PROPERTIES	2219-T851 Al L-T, T-L 75F	ALUM3 #104	2219-T851 Al LAB AIR

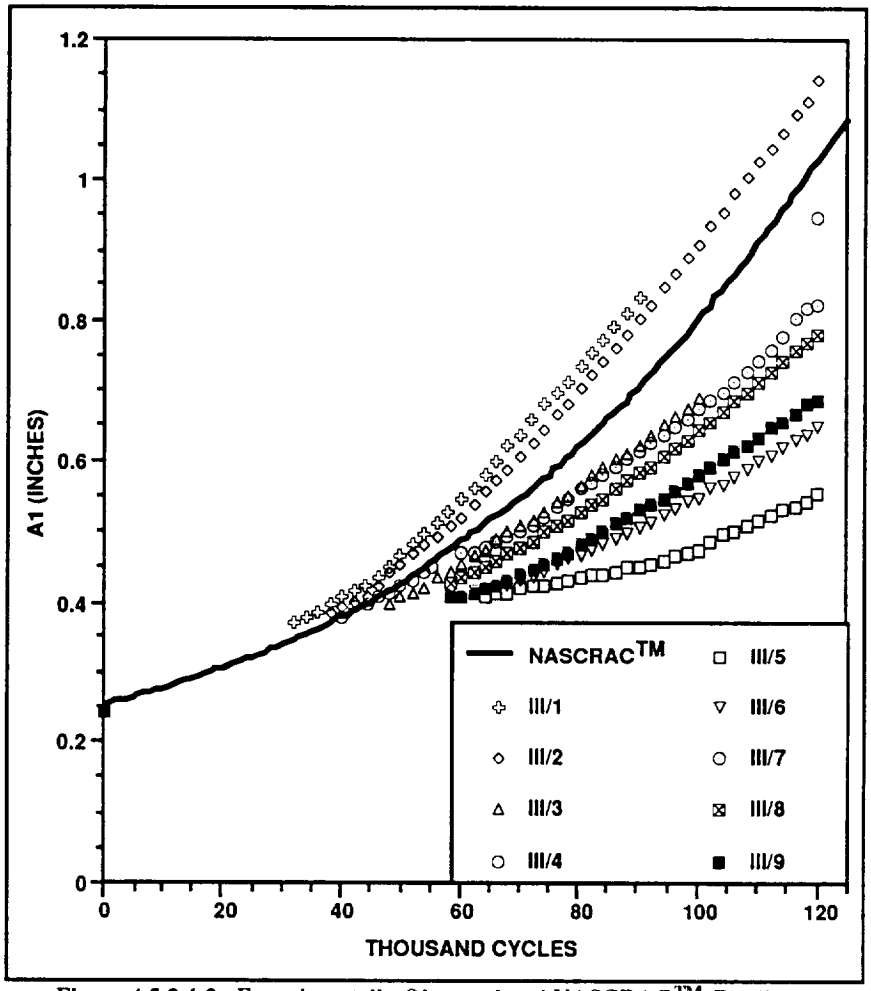

Figure 4.5.2.4-2. Experimentally-Observed and NASCRAC™-Predicted Crack Length a_1 Versus Cycles for Stage 1 of Test Series III-a

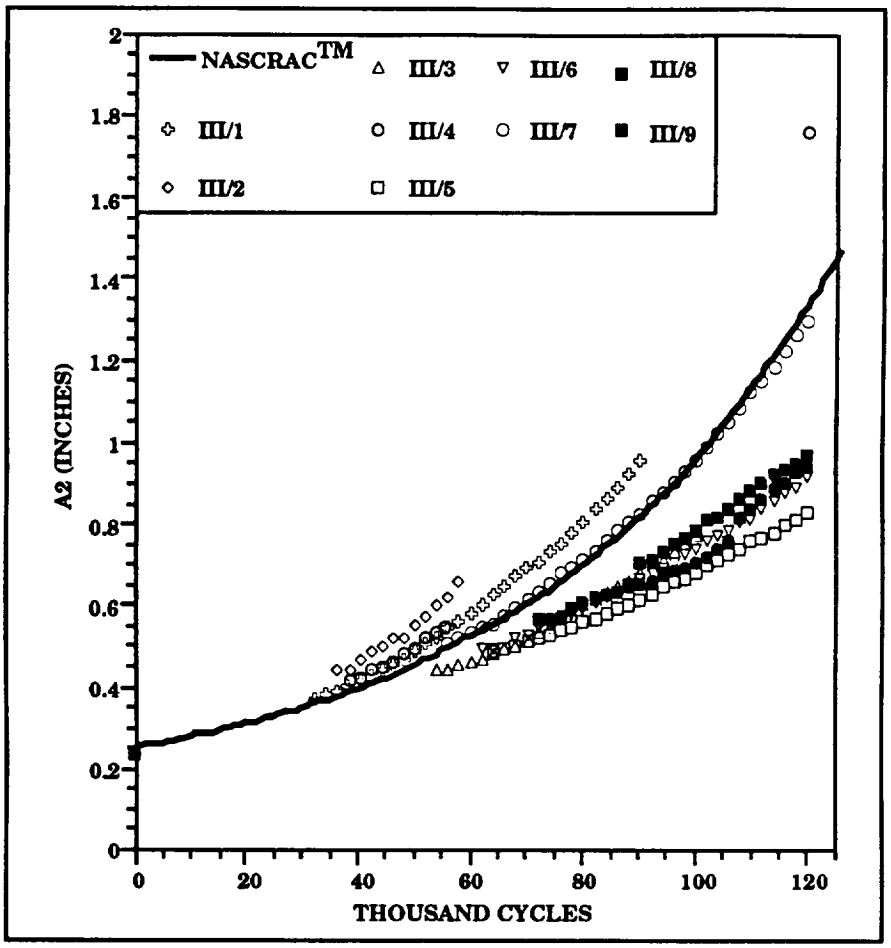

Figure 4.5.2.4-3. Experimentally-Observed and NASCRAC™-Predicted Crack Length a_2 Versus Cycles for Stage 1 of Test Series III-a

Figure 4.5.2.4-4. Crack Front from Test Series III-a

The NASCRAC™-predicted crack lengths remain in the range of experimentally-observed crack lengths for the duration of Stage 1 of this test series. From this observation, the following conclusion can be made:

- NASCRAC™ model 605 predicts fatigue crack growth well for Stage 1 of test series III-a.

4.5.2.5 Test I-2-a/5: Non Planar Fatigue Crack Growth

A fundamental assumption in any NASCRAC™ analysis is that cracks remain planar. The specimen geometry and loading in all of the previously described tests was chosen so that this assumption was true throughout the entire test. One test was performed in which this assumption was relaxed. The geometry for this test, I-2-a/5, is shown in Figure 4.5.2.4-5. This test was designed to test the limits of the NASCRAC™-planar crack assumption. Inputs for the NASCRAC™ analysis of this test are given in Table 4.5.2.5-2. Experimentally-observed and NASCRAC™-predicted crack lengths a_1, a_2 and a_3, as defined by Figure 4.5.2.5-1, are shown in Figures 4.5.2.5-2 through 4.5.2.5-4. Two views of the fatigue crack surface are noted in Figure 4.5.2.5-1 Photographs from these two views are shown in Figures 4.5.2.5-5 and 4.5.2.5-6.

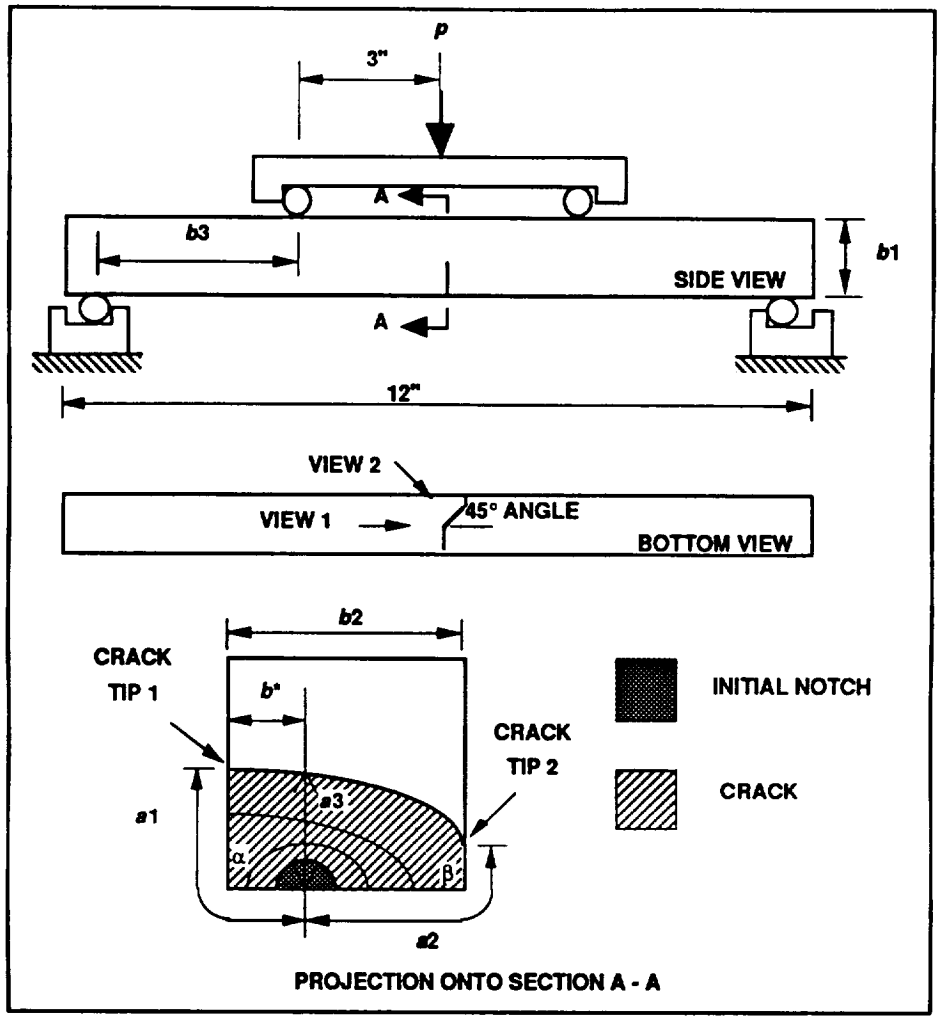

Figure 4.5.2.5-1. Geometry for Test I-2-a/5

Table 4.5.2.5-1 Average dimensions for test I-2-a/5

NUMBER OF TESTS		1
DIMENSION	VALUE	UNITS
$a1(0)$	0.184	INCHES
$a2(0)$	0.184	INCHES
$a3(0)$	0.251	INCHES
$b1$	2.000	INCHES
$b2$	1.500	INCHES
$b3$	2.412	INCHES
b^*	0.508	INCHES
Δp	11.54	KIPS
R-ratio	0.214	-
$l1$	106,812	CYCLES
$l2$	171,006	CYCLES

Table 4.5.2.5-2. NASCRAC™ Input For Analysis Of Test I-2-a/5

	NASCRAC™ INPUT	VALUE	CORRESPONDING TEST DIMENSION
MODEL	702		I-2-a
GEOMETRY	a1	0.251	$a3(0)$
	a2	0.184	$a1(0)$
	a3	0.184	$a2(0)$
	W1	2.000	$b1$
	W2	0.508	b^*
	W3	0.992	$b2-b^*$
LOADING	TRANSIENT 1 RANGE:EQ. B R-RATIO:	1000 CYCLES 13.92, -13.92 0.214	FATIGUE LOADS: FIGURE 4.5.2-1 TABLE 4.5.2.5-1
	BLOCK	1 X TRANSIENT 1	
MATERIAL PROPERTIES	2219-T851 Al L-T, T-L 75F	ALUM3 #104	2219-T851 Al LAB AIR

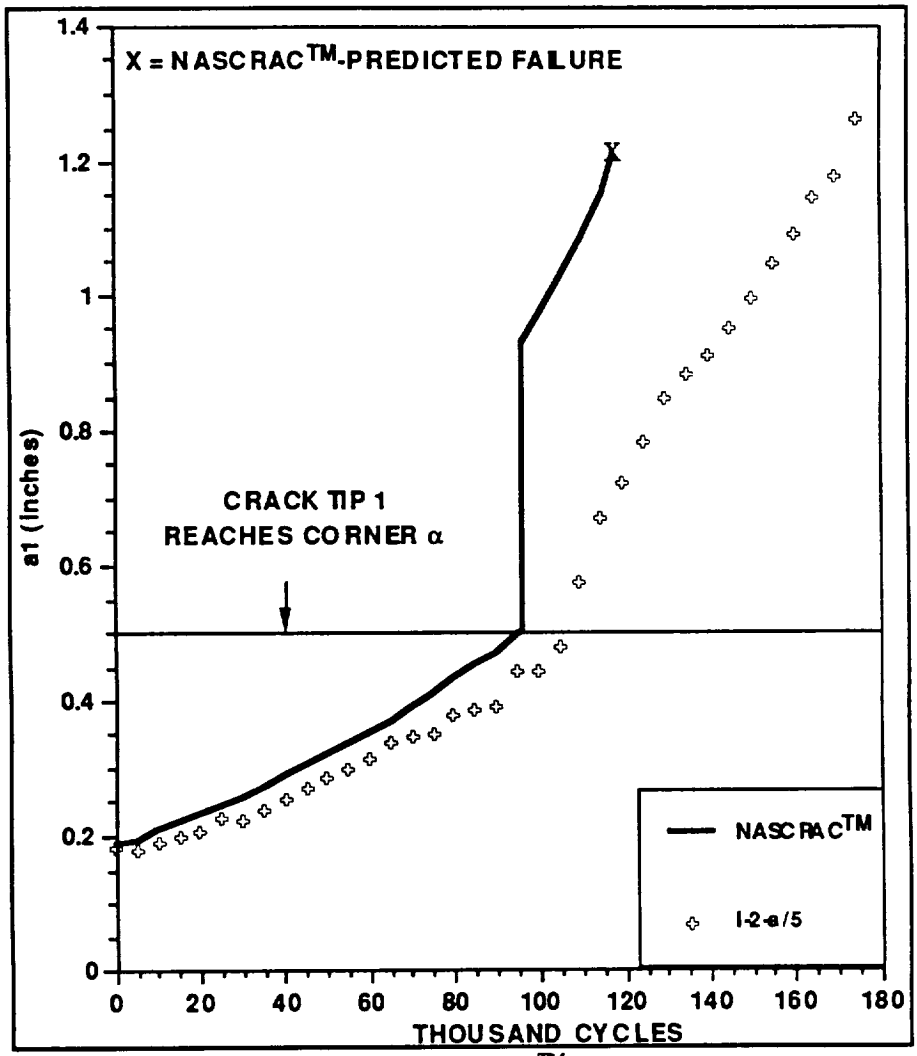

Figure 4.5.2.5-2. Experimentally-Observed and NASCRAC™-Predicted Crack Length $a1$ Versus Cycles

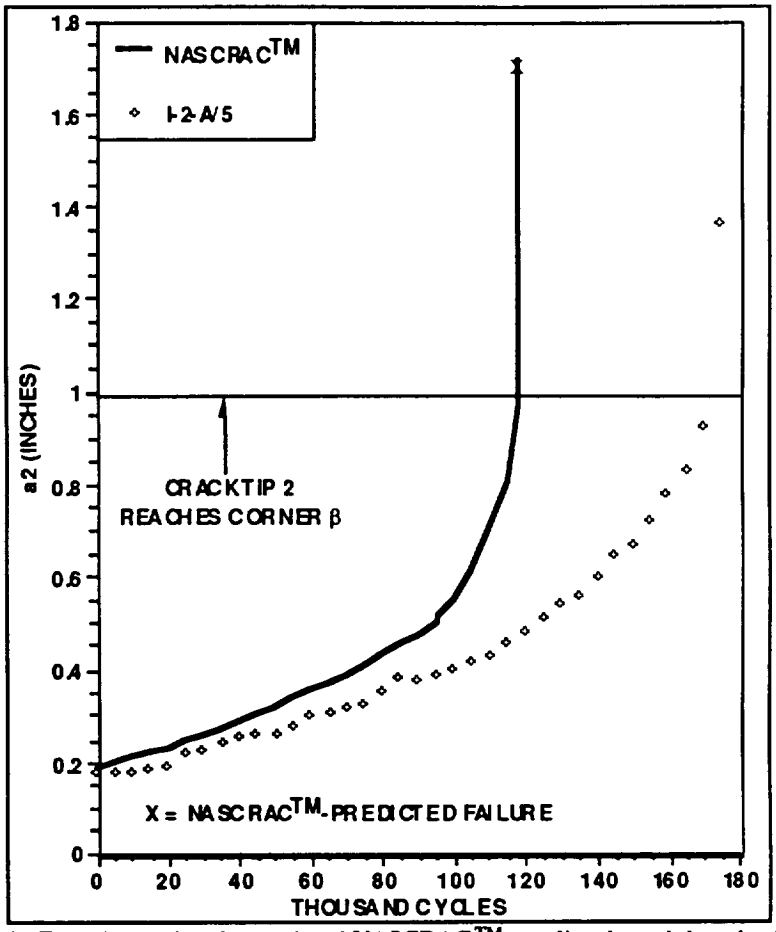

Figure 4.5.2.5-3. Experimentally-observed and NASCRAC™-predicted crack length *a*2 versus cycles

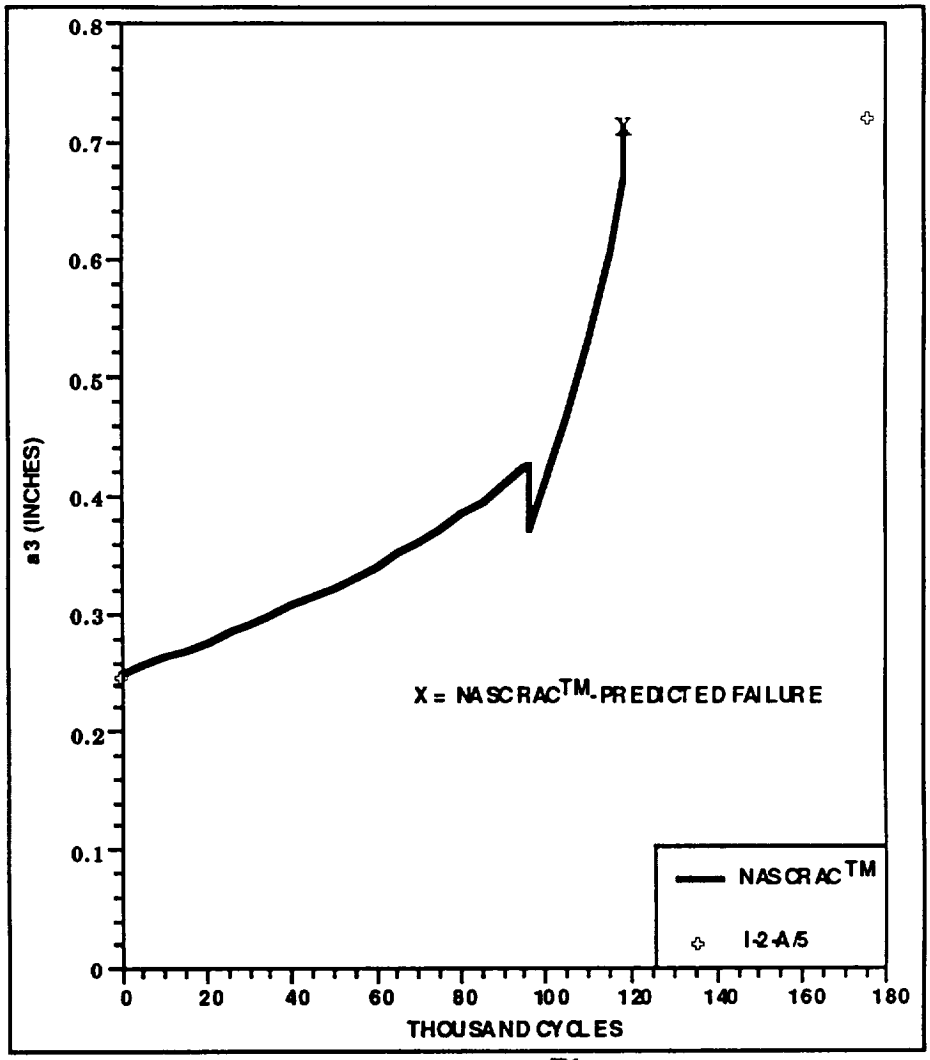

Figure 4.5.2.5-4 Experimentally-observed and NASCRAC™-predicted crack length $a3$ versus cycles

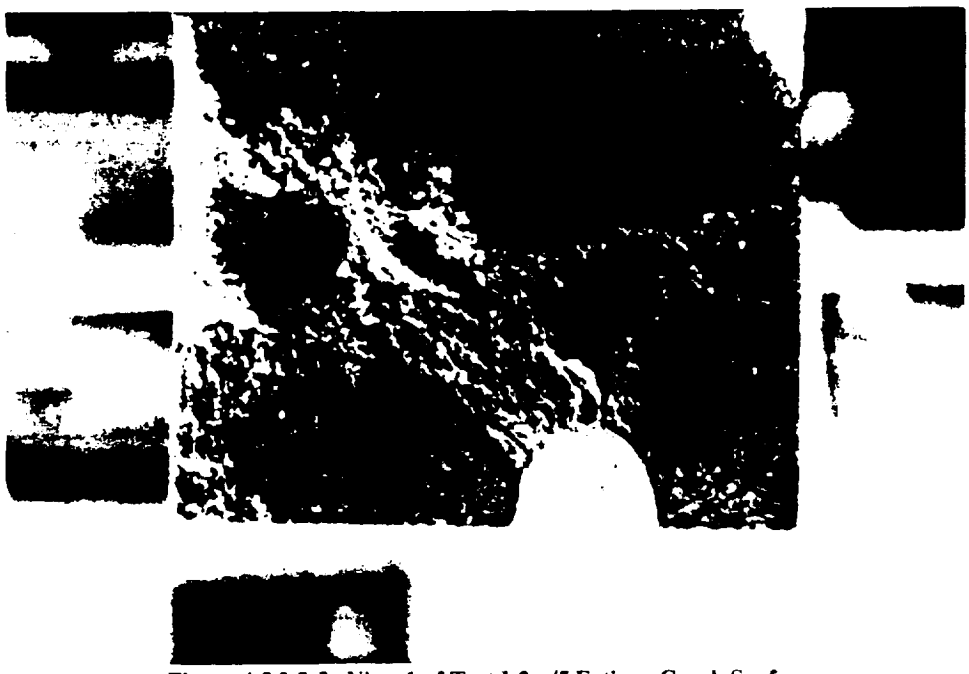

Figure 4.5.2.5-5. View 1 of Test I-2-a/5 Fatigue Crack Surface

Figure 4.5.2.5-6. View 2 of test I-2-a/5 Fatigue Crack Surface

NASCRAC™ requires the observed non-planar crack to be modeled as as a planar crack. The initial crack input to NASCRAC™ was the projection of the actual crack onto the plane section A-A shown in Figure 4.5.2.5-1. The projected crack is not a semi-circle. Rather, it is a semi-ellipse with the horizontal axis smaller than the vertical axis. Using a planar crack the same size as the initial notch for NASCRAC™ as an input results in even more conservative predictions.

Two boundary element analyses have been performed for test I-2-a/5. The first analysis was of the initial notch. In the second analysis, the crack was propagated a small increment, as predicted by FRANC3D calculations, from the initial analysis. Two views of the crack modeled in this analysis are shown in Figure 4.5.2.5-7.

By design, NASCRAC™ calculates only Mode I SIF. Figure 4.5.2.5-8 shows NASCRAC™ calculated SIF's compared to FRANC3D calculated SIF's for the initial notch. The initial NASCRAC™ calculated K_I values are roughly twice as large as the FRANC3D calculated K_I values. The magnitude of the largest FRANC3D calculated K_{II} values is the same as the FRANC3D calculated K_I. The largest K_{III} value occurs at the top of the crack and is approximately half of the FRANC3D calculated K_I.

After a small crack-propagation increment, the FRANC3D calculated SIF's change much more than does the NASCRAC™-calculated SIF's. These values are shown in Figure 4.5.2.5-9. FRANC3D calculated K_{II} values reduce to nearly 0. FRANC3D calculated K_{III} increases at the top of the crack by roughly 25%. FRANC3D calculated K_I increases by roughly 30% at the top and 75% at the corners of the crack. NASCRAC™ calculated K_I increases by only 2%.

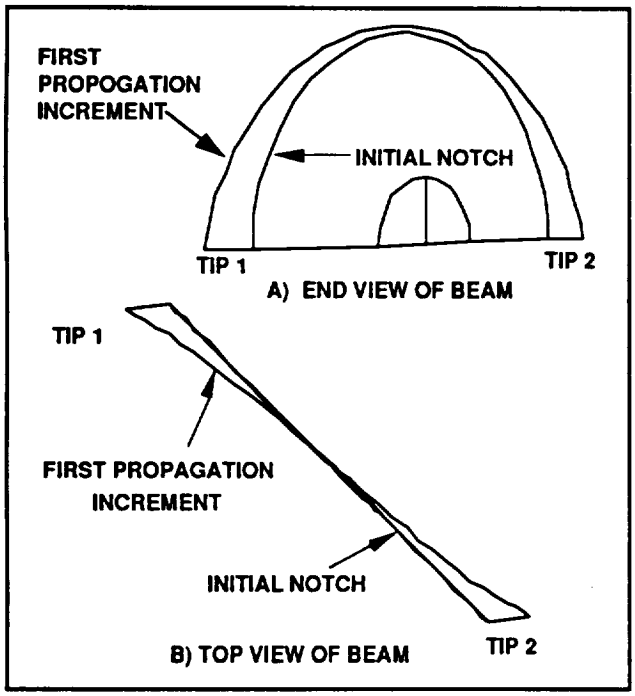

Figure 4.5.2.4-7. Initial Notch and First Propagation Increment for FRANC Analysis

Although K_{II} reduces to zero as the crack propagates, Mode II is influential in the direction of crack propagation. It is clear from the photographs of the crack front in Figures 4.5.2.5-5 and 4.5.2.5-6 that Mode III is influential in fatigue crack propagation, particularly near the top of the initial notch. As the test progresses, the 45° twist in the initial notch becomes less prominent in the crack front. Therefore, as the crack propagates, the importance of K_{III} compared to K_I will diminish.

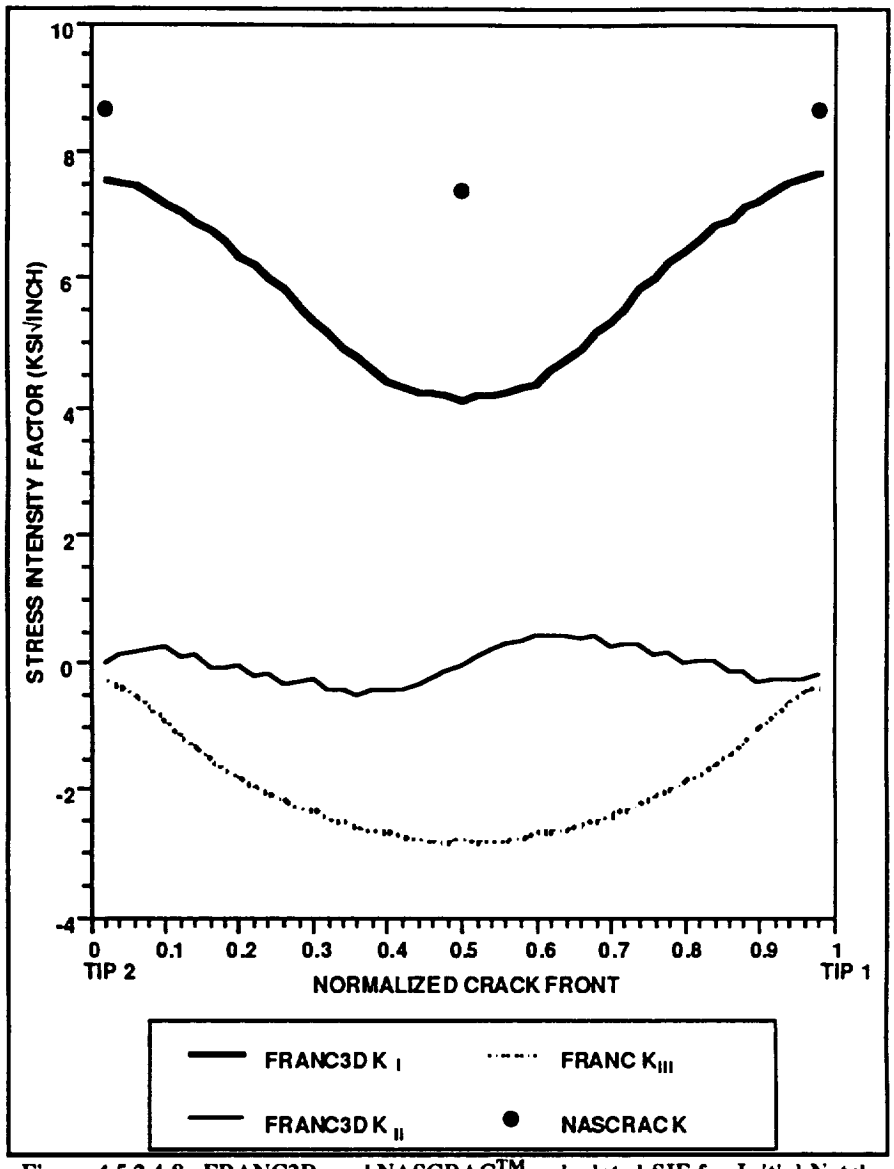

Figure 4.5.2.4-8. FRANC3D- and NASCRAC™-calculated SIF for Initial Notch

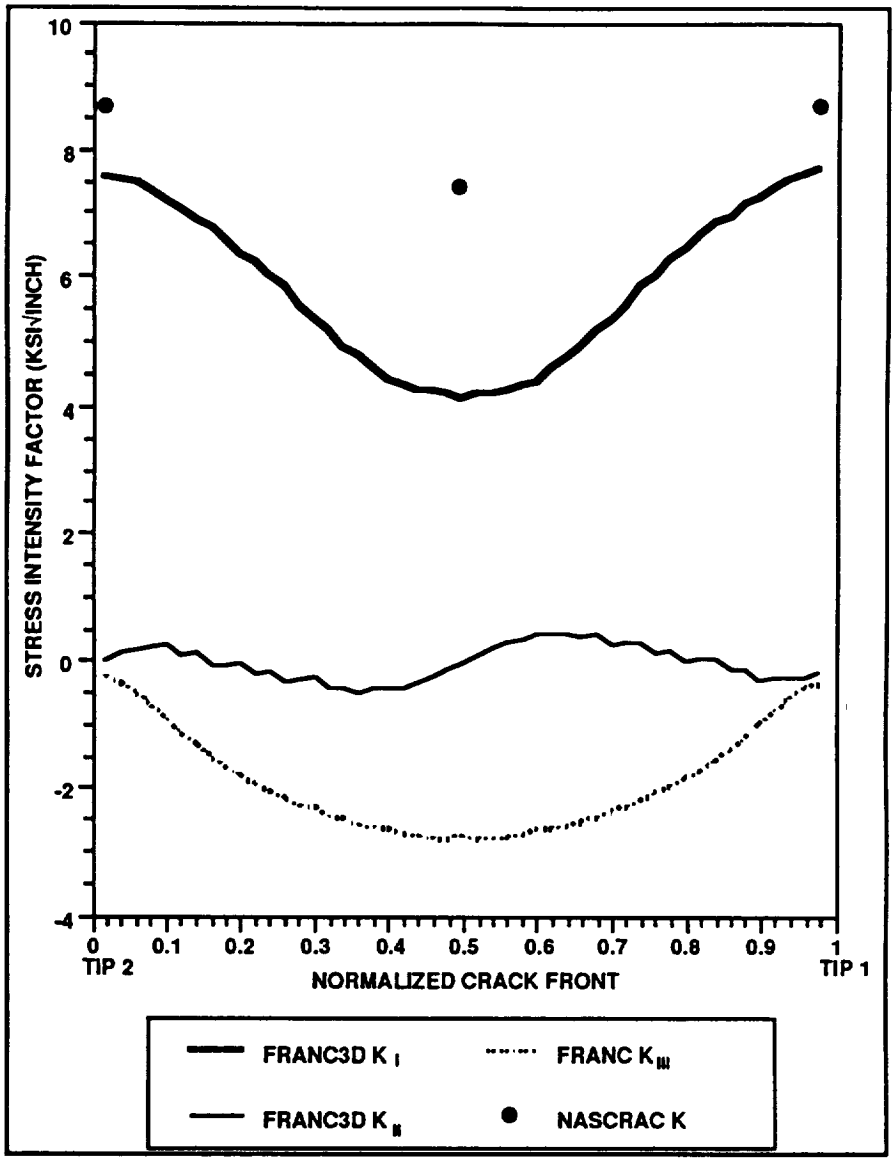

Figure 4.5.2.5-9. FRANC3D- and NASCRAC™-Calculated SIF for Small Increment from Initial Notch

In this test, the crack grows so that the crack approaches being perpendicular to the principle direction of stresses. When the true crack is modeled as a planar projection of the true crack, NASCRAC™ predicts pre-transition crack growth within anticipated scatter of experimental observations. The following conclusions are drawn regarding this observation:

- In this case, NASCRAC™'s planar crack assumption leads to conservative life prediction. This observation, however, cannot be generalized without more investigation. In some circumstances, particularly in a case where the principle stresses in a body do not remain in the same orientation, the NASCRAC™ planar crack assumption may become unconservative.

4.5.3 REFERENCES FOR SECTION 4.5

1. *Yuen, A., Hopkins, S.W., Leverant, G.R., and Rau, C.A., "Correlations between Fracture Surface Appearance and Fracture Mechanics Parameters for Stage II Fatigue Propagation in Ti-6Al-4V", Metallurgical Transactions, 1973, vol 5, pp 1833-1842.*
2. *Besuner, P.M.m et al, D., BIGIF - Fracture Mechanics Code for Structures, Electric Power Research Institute Report NP-1830-CCM, Palo Alto, CA, 1981.*
3. *Favenesi, J., et al, "NASCRAC Fracture Mechanics Computer Code Verification", Proc 1992 Conf Advanced Earth-to-Orbit Propulsion Technology, NASA/MSFC, Huntsville, 1992.*
4. *Forman, R.G., Derivation of Crack Growth Properties of Materials for NASA/FLAGRO, NASA/JSC Materials Branch Report 86-ES5-1, Houston, 1986.*
5. *Newman, J.C. Jr., Swain, M.H., Phillips, E.P. An Assessment of the Small-Crack Effect for 2024-T3 Aluminum Alloy, Small Fatigue Cracks Proceedings of the Second Engineering Foundation International Conference/Workshop, Santa Barbara, CA, Jan. 5-10, 1986 Ritchie, R.O., Lankford, J., ed.*

4.6 CALCULATION OF TOLERABLE CRACK SIZE

The tolerable crack size capability in NASCRAC^{TM} determines the initial crack length for a specified configuration given a required number of load cycles. The tolerable crack size verification and validation process was divided into two phases as shown in Figure 4.6-1. Phase I of the effort was an algorithm verification phase. NASCRAC^{TM} predictions of tolerable crack size were compared to fatigue life capability to fatigue crack growth calculations from an in-house FORTRAN code using the compact tension configuration. The NASCRAC^{TM} predicted tolerable crack length was used as the initial crack length and propagated forward to failure in the FORTRAN code. NASA/FLAGRO was also used as a tool for the algorithm verification by comparing its predicted life calculations to NASCRAC^{TM}'s predicted tolerable crack size.

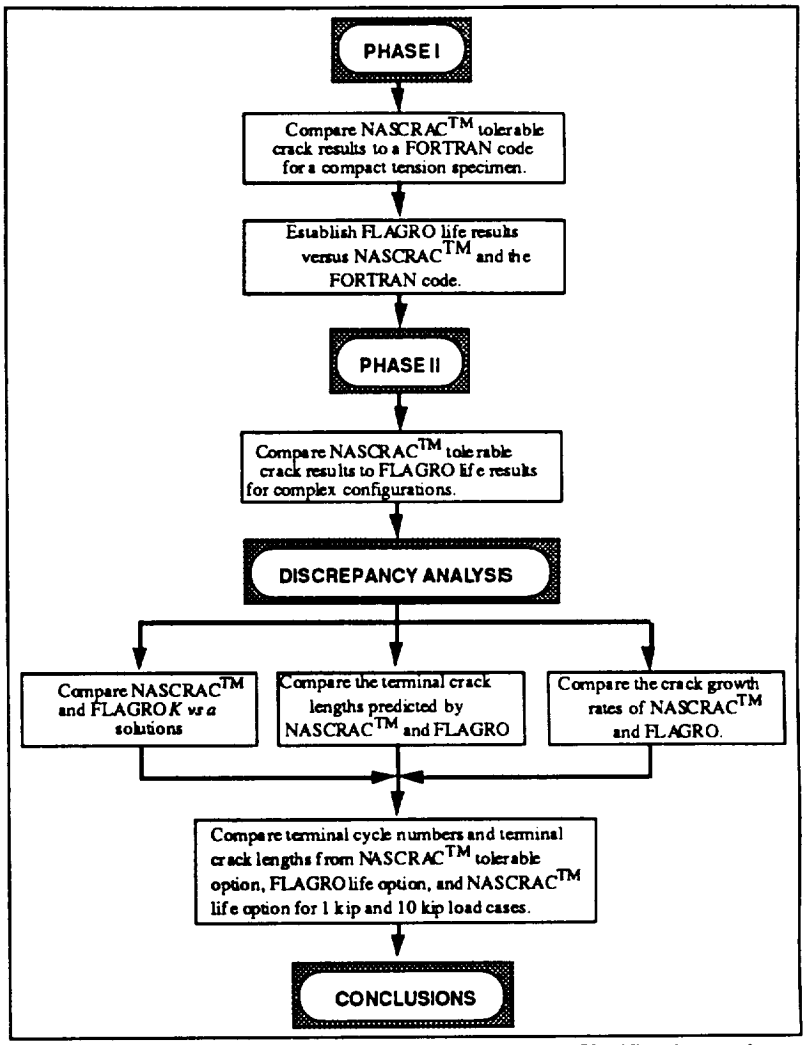

Figure 4.6-1. ***Calculation of Tolerable Crack Size*** **Verification and Validation Process**

Phase II of the tolerable crack V/V verification process evaluated more complex configurations: configuration 208, a through crack from a hole in a finite plate, and configuration 404, an edge-crack in a solid circular bar. In this phase, NASCRAC^{TM}'s tolerable crack predictions were compared to FLAGRO's crack growth calculations. The NASCRAC^{TM} predicted tolerable crack length was used as the initial crack length and propagated forward to failure in FLAGRO.

Observed differences in the results from Phase II led to four additional comparisons of the 208 and 404 configurations. These comparisons provided data which accounted for the differences.

4.6.1 VERIFICATION OF THE NASCRAC™ TOLERABLE CRACK ALGORITHM

Preliminary verification of the tolerable crack size capability in NASCRAC™ was accomplished using comparisons to an in-house FORTRAN code. These comparisons were based on a compact tension specimen (Figure 4.6.1-1) and the Paris crack growth equation. The NASCRAC™ predicted tolerable crack size was used as an initial crack length in the FOTRAN code and propagated to failure. Two NASCRAC™ integration methods, cycle-by-cycle and piecewise linear, were compared to cycle-by-cycle integration in the FORTRAN code. The compartive study consisted of three different values of the *cycles per block* parameter and the three different values of the *cycles to failure* parameter. The comparative results are tabulated in Table 4.6.1-1.

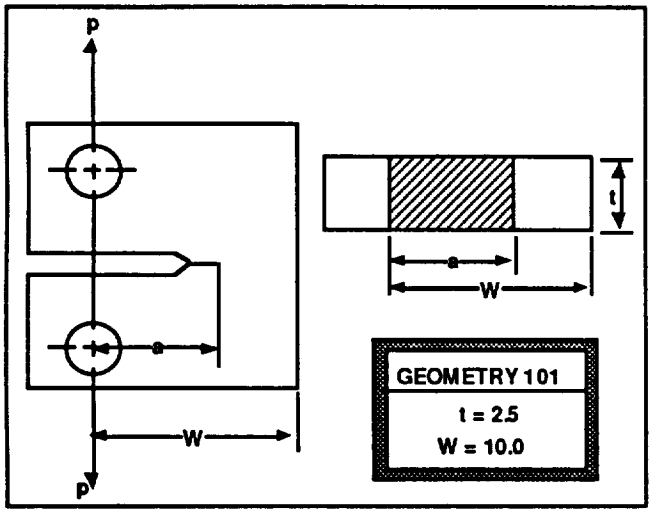

Figure 4.6.1-1. Configuration 101 Geometry Specifications for Tolerable Crack Studies

The results in Table 4.6.1-1 show that NASCRAC™ and the FORTRAN code were in good agreement on the predicted fatigue life (cycles to failure) and the final crack length a_f. This table does not include piecewise linear results from the FOTRAN code since this option was not available. The *calculated tolerable a* column lists the predicted tolerable crack size from NASCRAC™. This crack size was the initial crack length in the FORTRAN fatigue life calculation. Cases 2 and 4 are NASCRAC™ runs identical to cases 1 and 3, respectively, except that integration was done by the piecewise linear method, which is the default method in NASCRAC™. A comparison of cases 3 and 4 shows that minor variations in the predicted cycles to failure are possible for the different integration procedures in NASCRAC™ but that the calculated tolerable crack size is identical for the two integration procedures. In case 7, the observed difference between NASCRAC™ and the FORTRAN code is due to the discretization of the results controlled by the cycles per block parameter. For cases 1 and 2, where just a few cycles to failure are required (< 1000), the standard procedure seems to overshoot the tolerable initial crack length but the cycle-by-cycle technique easily predicts the tolerable crack length. The over estimated length in case 2 did indicate an initial K greater than K_{Ic}

Table 4.6.1-1. Comparison of Tolerable Crack Results for Configuration 101

Case	Integration method	Cycles/ block	Requested cycles to failure	Calculated tolerable a (NASCRA™)	Cycles to failure (NASCRAC™)	Cycles to failure (FORTRAN)	a_f (NASCRAC™)	a_f (FORTRAN)
1	cycle-by-cycle	1	1000	7.103	1000	1000	7.201	7.201
2	piecewise	1	1000	7.529	0	n/a	7.529	n/a
3	cycle-by-cycle	100	100000	5.084	104500	104500	7.198	7.200
4	piecewise	100	100000	5.084	98700	n/a	7.443	n/a
5	piecewise	1	100000	5.085	98526	n/a	7.446	n/a
6	piecewise	25000	$2.5\,(10^9)$	n/a	n/a	n/a	n/a	n/a
7	cycle-by-cycle	25000	100000	4.978	100000	125,000	6.292	7.201

Case 6 in Table 4.6.11 revealed a flaw in the NASCRAC™ algorithm. In this case a large number of cycles to failure was requested. Figure 4.6.1-2 lists an abridged output file from this case. NASCRAC™ attempts to reduce the initial crack size and iterate as expected. However, after four iterations the program began to oscillate between the crack length estimtaes of the third and fourth iteration. This oscillation was caused by the threshold value of ΔK. Due to the number of cycles to failure requested, NASCRAC™ had to search for a relatively small tolerable crack size. At a certain point the initial estimate of crack size became too small to cause crack growth, i.e., $\Delta K < \Delta K_{th}$. Thus, NASCRAC™ doubled the estimate of initial crack size, which was the same estimate as the previous iteration. This doubling and halving of the crack length estimate led to the observed oscillatory behavior.

```
 PROBLEM TITLE : Case 6 -- Standard procedure

     TYPE OF ANALYSIS
->        Initial (Tolerable) Crack Size Calculation

     Crack Growth Analysis Performed by
->        Standard Procedure

     Load Interactions Model Used -
->        No Load Interactions

         Crack Driving force  - K or Delta K
   Max. Fractional Increment of Crack Size between two Steps =     0.1000
         Accuracy of (IF) Area Integration (1, 2, OR 3)    = 2
         Accuracy of Singularity Integration (1 to 5)      = 2
         Number of Life Cycles (BLOCKS) for which Initial
                     Crack Size is to be Calculated =    1.00000E+05

->   Compact Tension Specimen                    101
     Initial Crack Dimension(1) =    3.00000
              BODY WIDTHS(1) =   10.00000
              BODY WIDTHS(2) =    2.50000


      MATERIAL PROPERTIES DATA
          MATERIAL - 2219-T851 AL, L-T & T-L, 75F

          Paris Equation :                    C=  1.0700E-08
                                              m=     2.897
                                 DELTAK THRESHOLD=     2.500


     TOTAL NUMBER OF TRANSIENTS ENTERED :  1
          TRANSIENT NUMBER =         1
           TRANSIENT TITLE = Constant amplitude load
           TRANSIENT TYPE =       CYCL
          NUMBER OF CYCLES = 2.5000E+04
          CRACK GROWTH LAW = PARIS EQUATION


MAXIMUM STRESS DEFINED BY EQUATION TYPE :  6 WHICH IS ...
STRESS DEFINED BY PIN LOAD, PIN LOAD (FORCE) =  1.0000E+01
MULTIPLICATION FACTOR =     1.00000E+00
R-RATIO =  0.2000
Loading Block consists of the following transients -
Transient Number     1   Repeated        1   Time(s).
```

Figure 4.6.1-2. Typical Tolerable Crack Size Output File

```
DETAILS OF ITERATIONS PERFORMED

 Iteration Number =  1 - -
*** For Transient #  1 & for Crack DOF 1 Kmax is exceeding Kic **
 Crack Degrees of Freedom 1  : A1  =   3.00000
 Number of Cycles = 3.014709E+01
** WARNING: Specified initial crack size(s) are too big.
        All the crack sizes are reduced by 50 %

 Iteration Number =  1 - -
*** For Transient #  1 & for Crack DOF 1 Kmax is exceeding Kic **
 Crack Degrees of Freedom 1  : A1  =   1.50000
 Number of Cycles = 1.035336E+02
** WARNING: Specified initial crack size(s) are too big.
        All the crack sizes are reduced by 50 %

 Iteration Number =  1 - -
*** For Transient #  1 & for Crack DOF 1 Kmax is exceeding Kic **
 Crack Degrees of Freedom 1  : A1  =   0.75000
 Number of Cycles = 2.066827E+02
** WARNING: Specified initial crack size(s) are too big.
        All the crack sizes are reduced by 50 %

 Iteration Number =  1 - -
*** For Transient #  1 & for Crack DOF 1 Kmax is exceeding Kic **
 Crack Degrees of Freedom 1  : A1  =   0.37500
 Number of Cycles = 6.961500E+24
** WARNING: Specified initial crack size(s) are too small.
        All the crack sizes are increased by 100 %

 Iteration Number =  1 - -
*** For Transient #  1 & for Crack DOF 1 Kmax is exceeding Kic **
 Crack Degrees of Freedom 1  : A1  =   0.75000
 Number of Cycles = 2.066827E+02
** WARNING: Specified initial crack size(s) are too big.
        All the crack sizes are reduced by 50 %

 Iteration Number =  1 - -
*** For Transient #  1 & for Crack DOF 1 Kmax is exceeding Kic **
 Crack Degrees of Freedom 1  : A1  =   0.37500
 Number of Cycles = 6.961500E+24
** WARNING: Specified initial crack size(s) are too small.
        All the crack sizes are increased by 100 %

 Iteration Number =  1 - -
*** For Transient #  1 & for Crack DOF 1 Kmax is exceeding Kic **
 Crack Degrees of Freedom 1  : A1  =   0.75000
 Number of Cycles = 2.066827E+02
** WARNING: Specified initial crack size(s) are too big.
        All the crack sizes are reduced by 50 %
```

Figure 4.6.1-2. (Continued)

The cases shown in Table 4.6.1-2 provided checks of the fatigue life capabilities of the FORTRAN code and FLAGRO. All three codes were in good agreement. The differences between NASCRAC™ and FLAGRO in cases 4 and 5 can be traced to the modified Forman discrepancies discussed in Section 4.5.1.

Table 4.6.1-2. Life Calculation Comparison for Tolerable Crack V/V Tools

CASE	CODE	CRACK GROWTH LAW	REQUESTED CYCLES TO FAILURE	INITIAL a	CYCLES TO FAILURE	FINAL a
1	FORTRAN	PARIS	100000	7.103	373,000	7.174
2	NASCRAC™	PARIS	100000	7.103	362,000	7.200
3	FLAGRO	PARIS	100000	7.103	371,000	7.174
4	NASCRAC™	MOD. FORMAN	100000	7.103	68,000	7.203
5	FLAGRO	MOD. FORMAN	100000	7.103	56,000	7.170

Note: The NASCRAC ™ results were adjusted to compensate for the error in configuration 101.

4.6.2 EXAMPLE V/V CASES FOR NASCRAC™'S TOLERABLE CRACK CAPABILITY

The second stage of the tolerable crack V/V process was to investigate configuration 208, a through crack from a hole in a finite plate, and configuration 404, an edge-crack in a solid circular bar. This was completed by executing NASCRAC™ tolerable crack size analysis for 100,000 cycles to failure. The NASCRAC™ predicted tolerable crack length was used as the initial crack length in FLAGRO and propagated forward to failure. Two geometric cases with four different load spectrums were evaluated for each of the two configurations. The modified Forman equation with appropriate K_c values was used to model the crack growth. The geometric cases for configuration 208 and 404 are shown in Figures 4.6.2-1 and 4.6.2-2, respectively. The results of the evaluations are shown in Figures 4.6.2-3 through 4.6.2-6.

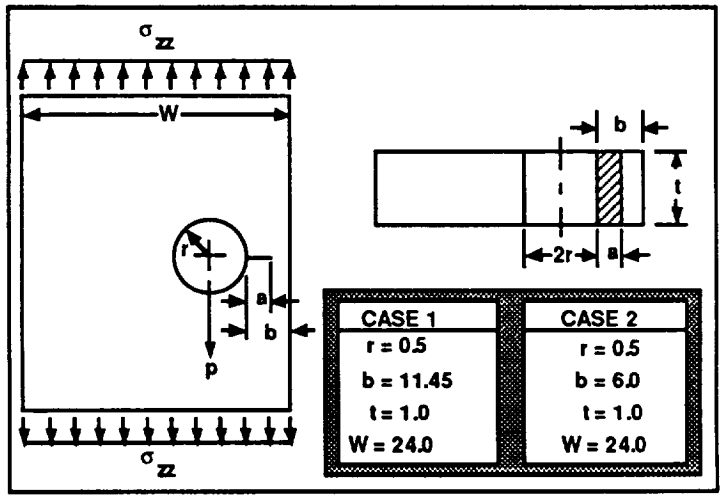

Figure 4.6.2-1. Configuration 208 Geometry Specifications for Tolerable Crack Studies

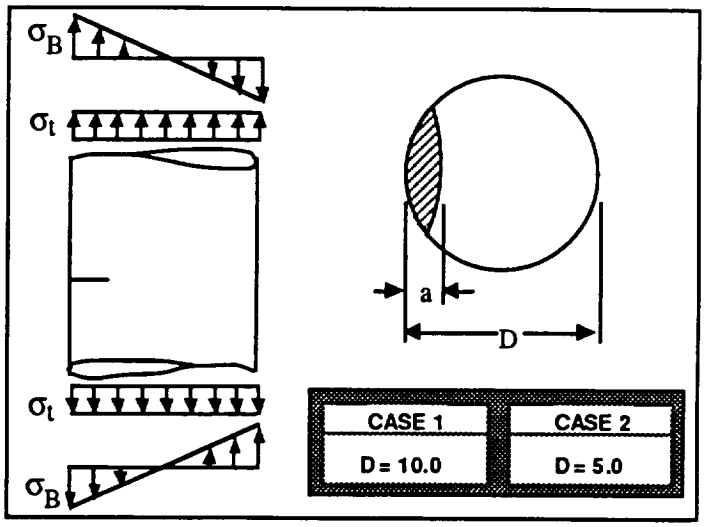

Figure 4.6.2-2. Configuration 404 Geometry Specifications for Tolerable Crack Studies

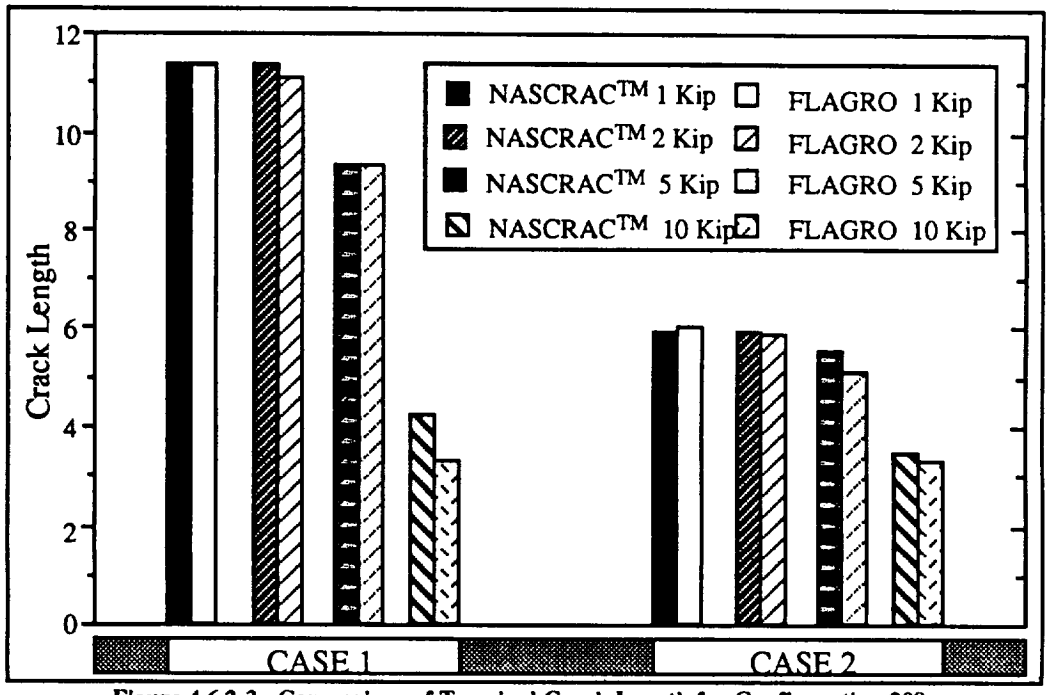

Figure 4.6.2-3. Comparison of Terminal Crack Length for Configuration 208

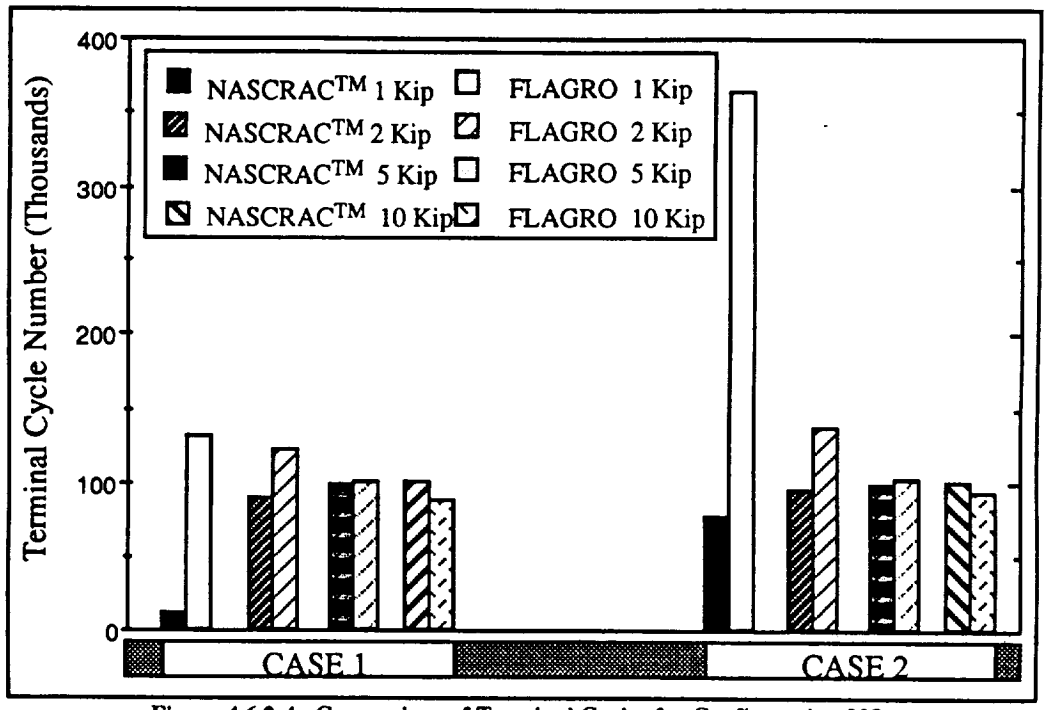

Figure 4.6.2-4. Comparison of Terminal Cycles for Configuration 208

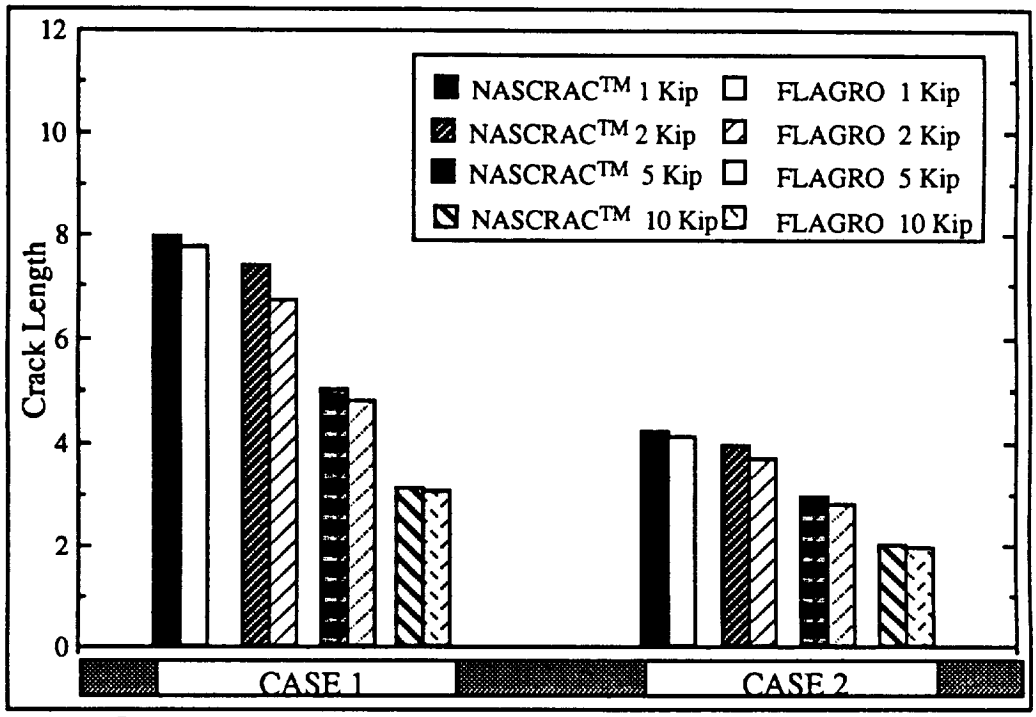

Figure 4.6.2-5. Comparison of Terminal Crack Length for Configuration 404

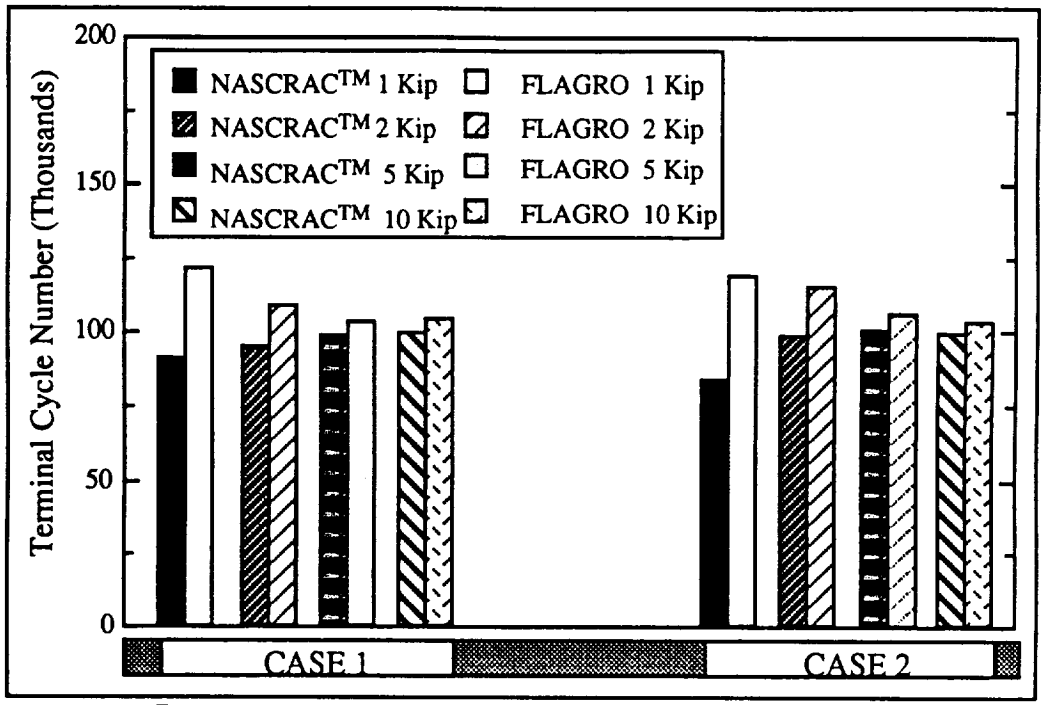

Figure 4.6.2-6. Comparison of Terminal Cycles for Configuration 404

Figures 4.6.2-3 and 4.6.2-5 show the crack lengths at failure from NASCRAC™ and FLAGRO are in good agreement for the two configurations and the four different loadings. The results shown in Figures 4.6.2-4 and 4.6.2-6 also show reasonable agreement with the exception of the 1 kip loading cases. The figures show a trend of FLAGRO predicting a higher number of terminal cycles compared to NASCRAC™. In the 1 kip loading cases, the results show that FLAGRO predicts a longer life than NASCRAC™ by a factor of 5 for configuration 208 and by a factor of 1.5 for configuration 404. These results for a 1 kip load reveal a significant discrepancy in NASCRAC™.

In order to understand why FLAGRO consistently predicted a longer life relative to NASCRAC™, a comparison of *K vs a* for each case was performed to verify that the codes calculated similar stress intensity solutions. The results of the configuration 208 cases, shown in Table 4.6.2-1, show good agreement between the K values in NASCRAC™ and FLAGRO. The configuration 404 K results, shown in Table 4.6.2-2, were identical for the two codes.

Table 4.6.2-1. Comparative Stress Intensity Factors for Configuration 208

CONFIGURATION 208 CASE 1			CONFIGURATION 208 CASE 2		
a	NASCRAC ™ K	FLAGRO K	a	NASCRAC K™	FLAGRO K
1.0	1.840	1.838	1.0	1.862	1.860
2.0	2.229	2.227	2.0	2.309	2.308
4.0	2.938	2.936	4.5	4.077	4.075
8.625	5.243	5.241	--	--	--

Table 4.6.2-2. Comparative Stress Intensity Factors for Configuration 404

CONFIGURATION 404 CASE 1			CONFIGURATION 404 CASE 2		
a	NASCRAC ™ K	FLAGRO K	a	NASCRAC ™ K	FLAGRO K
0.5	0.878	0.878	1.0	1.241	1.241
1.0	1.419	1.419	2.0	2.006	2.006
1.5	2.104	2.104	3.0	2.976	2.976
2.0	3.095	3.095	4.0	4.377	4.377
2.5	4.640	4.640	5.0	6.561	6.561
3.0	7.270	7.270	6.0	10.281	10.281

The *K vs a* analyses led to two further comparisons: crack growth rate versus number of cycles and crack length versus number of cycles. These two comparisons, shown in Figure 4.6.2-7, used configuration 208 with corrected K_C and m values in the NASCRAC™ execution as per Section 4.5.1. The fatigue life option in each code was employed to propagate a 2.5" crack to failure.

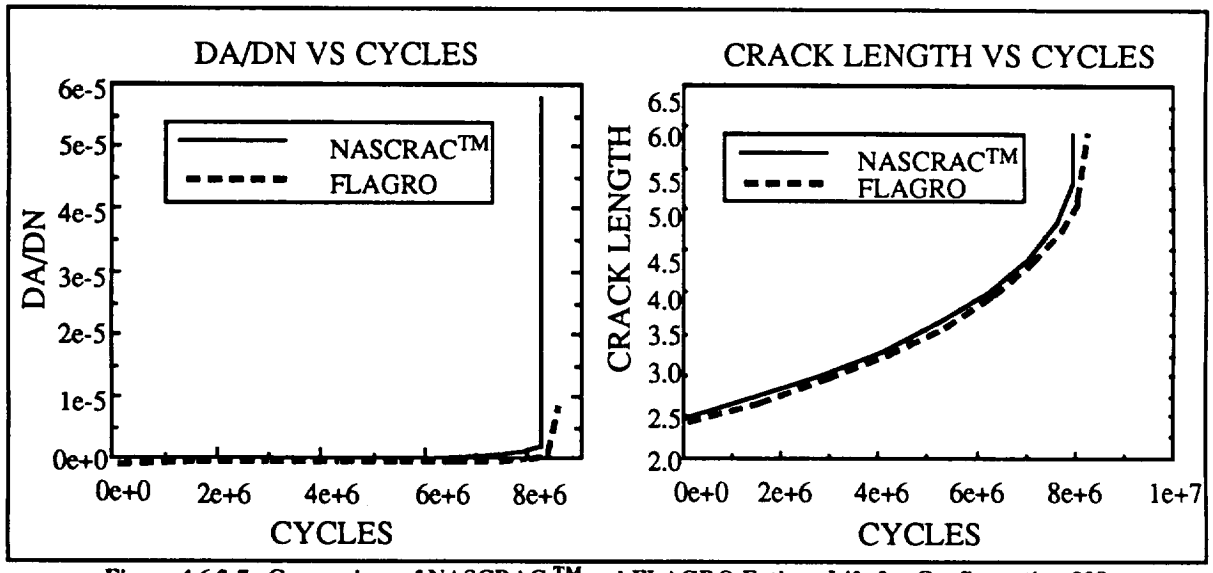

Figure 4.6.2-7. Comparison of NASCRAC ™ and FLAGRO Fatigue Life for Configuration 208

In the fatigue life calculations in Figure 4.6.2-7, FLAGRO predicts a slightly longer life and a similar final crack length compared to NASCRAC™. The observed differences can be traced to the rate of crack growth rate, da/dN. For both codes the da/dN is approximately 7.5 x 10^6 cycles. At this point, NASCRAC™ and FLAGRO experience an increase in slope, but NASCRAC™'s change in slope is much larger than FLAGRO's. This leads to the longer life in FLAGRO for an equivalent initial crack length. Thus, the *K vs a* and da/dN data lead to the conclusion that the observed differences between NASCRAC™'s tolerable crack prediction and FLAGRO's life prediction is caused by minor differences in the modified Forman crack growth model employed in each code. The configuration 208 1 kip load case shown in Figures 4.6.2-3 through 4.6.2-6 is an exception to this conclusion.

Figure 4.6.2-4 clearly shows the discrepancy in the 1 kip load case. Two additional cases were used to investigate this discrepancy. In both cases , NASCRAC™'s tolerable crack size analysis was performed using a critical K value of 30.1 ksi$\sqrt{in}$, 100,000 cycles to failure, and configuration 208 with the geometry given in Figure 4.6.2-1, case 1. The NASCRAC™ predicted tolerable crack length was used as the initial crack length and propagated forward to failure in FLAGRO and NASCRAC™ using the fatigue life options. The two cases differed only in the applied load: case A used a load of 1 kip and case B used a load of 10 kips. The results of the investigation are shown in Figure 4.6.2-8.

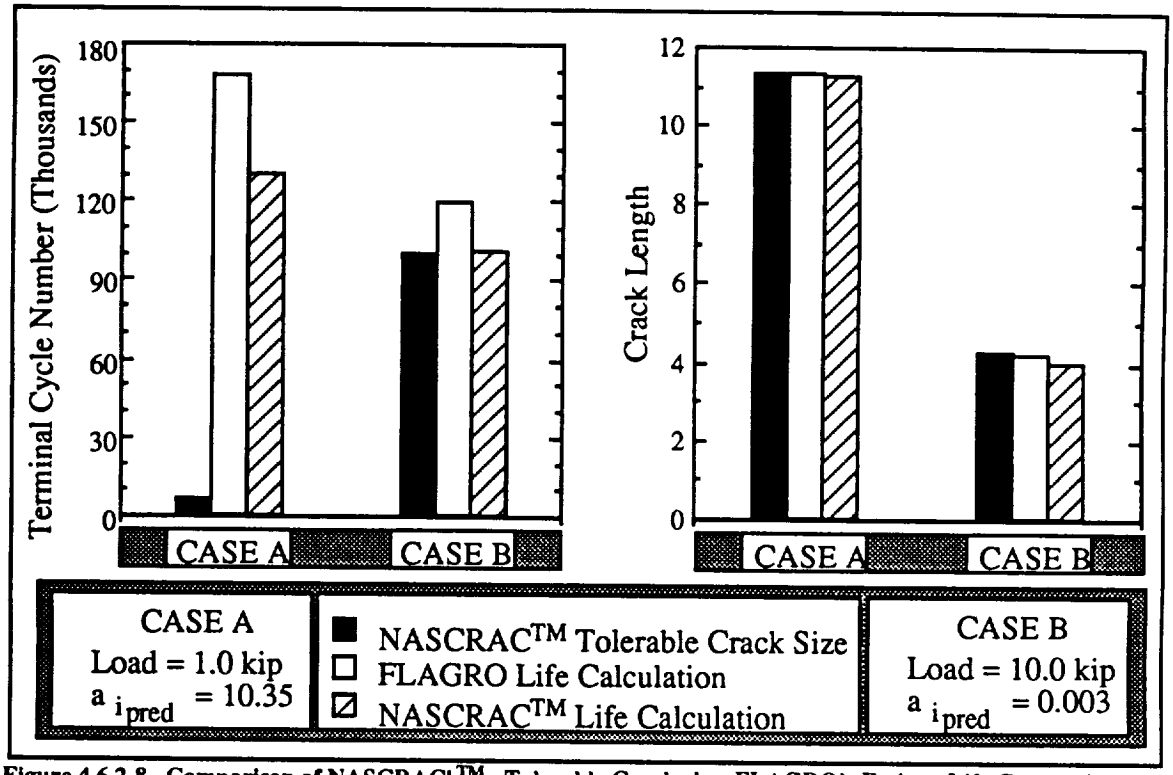

Figure 4.6.2-8. Comparison of NASCRAC™s Tolerable Crack size, FLAGRO's Fatigue Life Calculation, and NASCRAC Fatigue Life Calculation for Configuration 208 and Different Load Cases.

The results in Figure 4.6.2-8 show a discrepancy in NASCRAC™'s tolerable crack size prediction of the terminal cycle for the 1 kip load case but good agreement of the predicted crack lengths for the three different analyses in both load cases. This discrepancy is probably due to the invalidity of the tolerable crack size when the crack length exceeds 99% of the body width. Analysts should disregard tolerable crack predictions if NASCRAC™ issues a warning that the crack length exceeds 99% of the body width.

To summarize the V/V results for NASCRAC™'s tolerable crack capability, the results show that the capability is functional. Predicted crack lengths are reasonable for the crack growth equations employed. The documentation should emphasize that the most efficient way to run this capability is with the standard procedure (piecewise linear) crack growth integration technique where the number of cycles per block is set to one. This set-up is demonstrated in Examples 6-9 and 6-10 of the NASCRAC™ User's Manual. This recommendation should be caveated when a

small number of cycles to failure are requested. In this case it is more accurate to use cycle-by-cycle integration. Also the user should be aware of the oscillatory effect described in Section 4.6.1. **Finally and most importantly, NASCRAC™ tolerable crack results should not be used whenever NASCRAC™ issues a warning in the output that the crack length exceeded 99% of the body width, i.e., when geometry instead of K_{Ic} is the reason for failure.**

4.7 PROOF TEST LOGIC

Verification and validation testing of NASCRAC™'s *Proof Test Logic* capability is discussed in this section. The accurate prediction of remaining fatigue life following a proof load requires successful performance of two tasks:

1) Predict the largest crack of a given aspect ratio and location that can survive a given proof load.

2) Calculate the remaining fatigue life for the largest crack calculated in (1).

NASCRAC™ capability for these two tasks, and *Proof Test Logic* in whole, have been tested for validity primarily by laboratory tests.

4.7.1 PREDICTION OF LARGEST SURVIVING CRACK

Stage 2 of test series III-a was a near-failure proofload, designed to validate NASCRAC™'s *largest surviving crack* calculation. The geometry for these tests is shown in Figure 4.7.1-1. Parameters that describe the load history for these tests are defined in Figure 4.7.1-2. The proofload in stage 2 was applied in either a three point bend or four point bend configuration. The average dimensions for this test series are given in table 4.7.1-1. Two average values of b_3 for the proofloads are given.

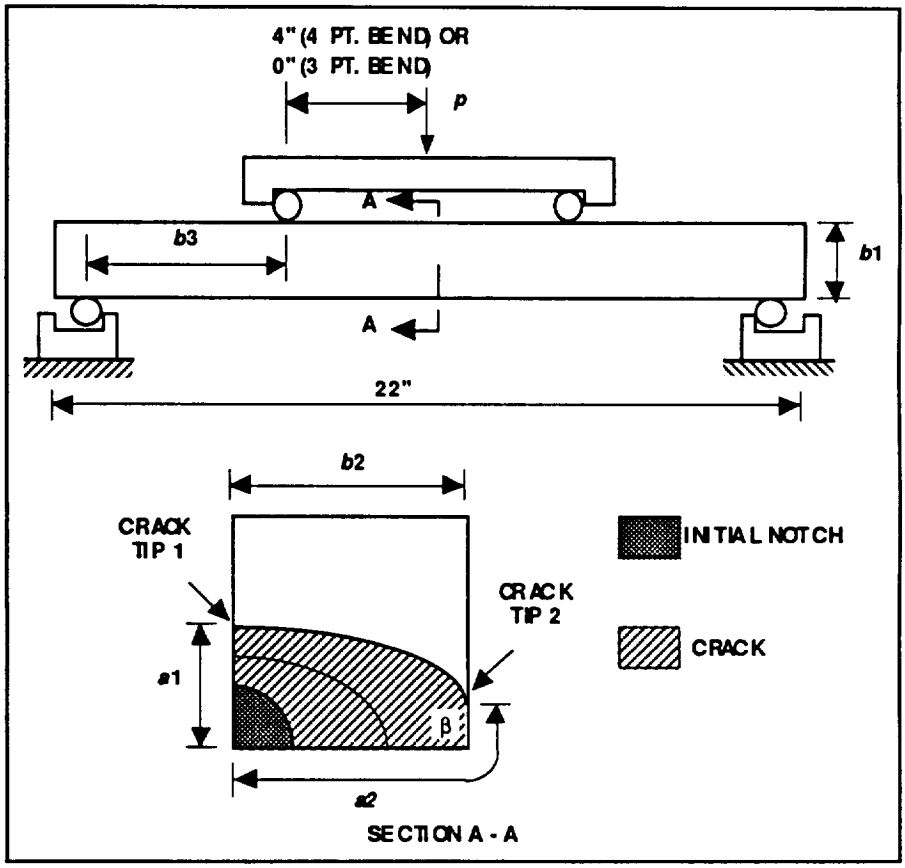

Figure 4.7.1-1. Geometry for Test Series III-a

One represents the set of specimens loaded with the three point bend configuration, one represents the set of specimens loaded with the four point bend configuration. The average value of b_3 for stage 3 is also given. The definition of b_3 from Figure 4.7.1-1 is applicable to all three cases. In this section, the magnitude of the proofload is described by the extreme fiber bending stress, as calculated by linear elastic beam theory for an uncracked beam.

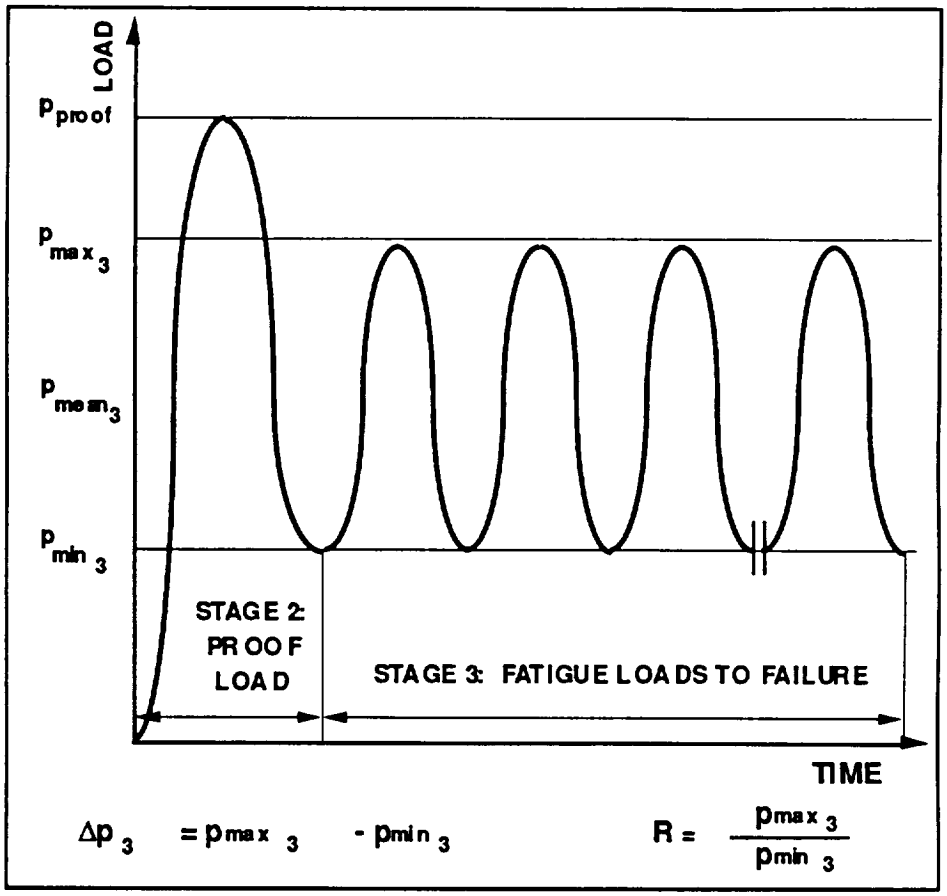

Figure 4.7.1-2. Definitions of Load History for Stages 2 and 3 in Test Series III-a

Table 4.7.1-1. Average Dimensions for Test Series III-a

NUMBER OF TESTS		9
DIMENSION	AVERAGE VALUE	UNITS
$a1$(STAGE 2)	0.795	INCHES
$a2$(STAGE 2)	1.160	INCHES
$b1$	3.001	INCHES
$b2$	3.001	INCHES
$b3_{proof}$ (3 pt. CONFIG.)	6.082	INCHES
$b3_{proof}$ (4 pt. CONFIG.)	10.026	INCHES
$b3_{stage3}$	6.034	INCHES
Δp_3	20.97	KIPS
R-RATIO$_{stage3}$	0.2294	

The size and shape of the cracks in stage 2 varied. Ellipses connecting the nine crack tips experimentally-observed at the beginning of stage 2 are shown in Figure 4.7-3. Crack length a_1 ranged from 0.558 to 1.150 inches. Crack length a_2 ranged from 0.782 to 1.906 inches. Figure 4.7.1-4 shows the observed crack length a_2 as a function of observed crack length a_1.

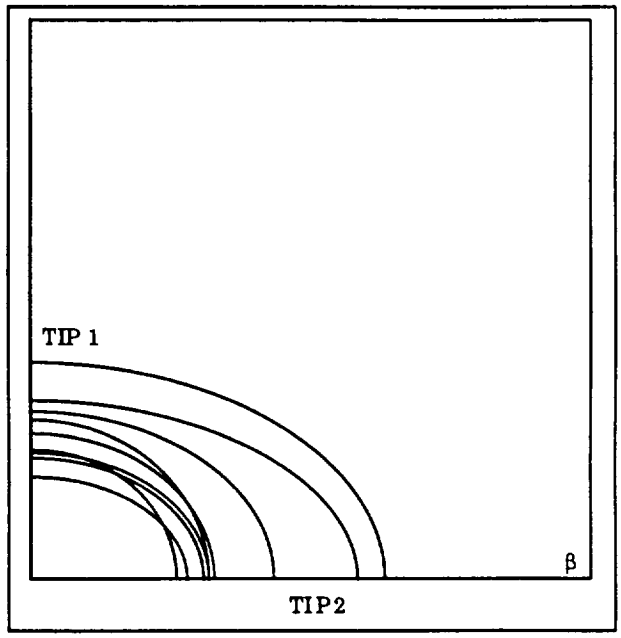

Figure 4.7.1-3. Interpolated-Observed-Crack Shapes at Beginning of Stage 2 in Test Series III-a

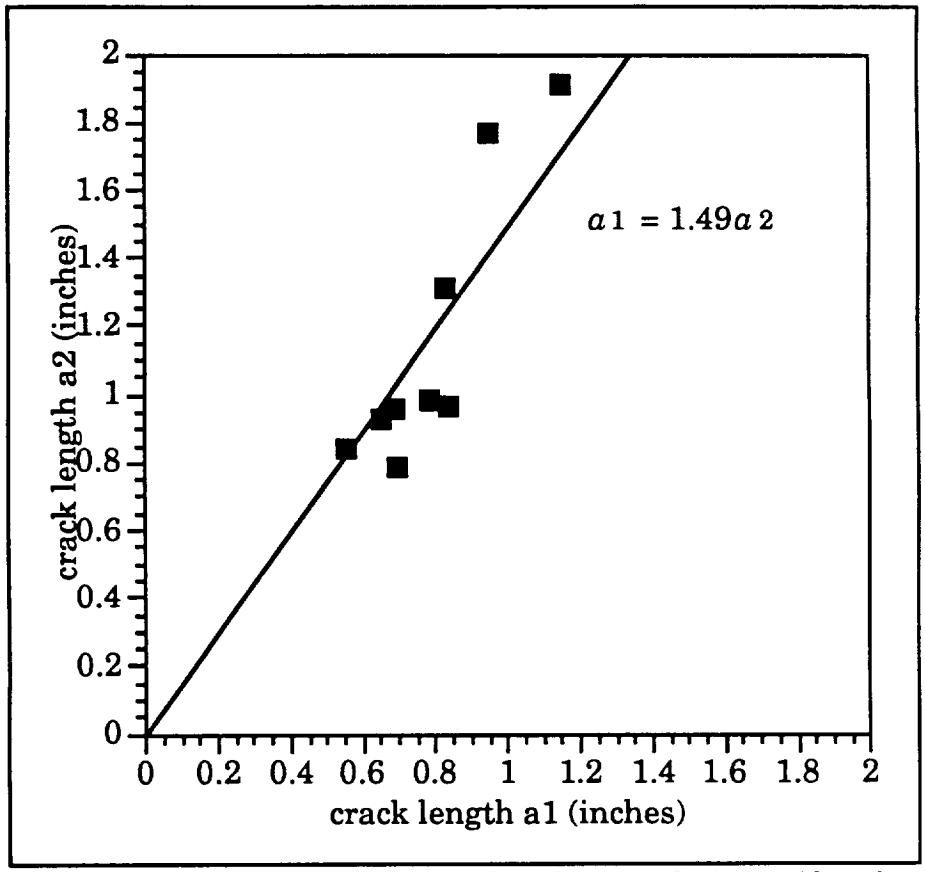

Figure 4.7.1-4. Experimentally-Observed Crack Lengths at Beginning of Stage 2

NASCRAC™ proof test analyses were performed for proof loads ranging from 22 to 55 ksi for the extreme fiber bending stress. The input for these analyses is given in Table 4.7.1-2.

The aspect ratio was chosen by the straight line through the origin that best fit the experimentally-observed crack lengths shown in Figure 4.7.1-4. As described in Section 4.8, there was reason to expect that the cracks encountered at the end of Stage 1 would be dominated by plane strain behavior. Therefore, the K-R curve used for these analyses was a horizontal line from Kc = 30ksi$\sqrt{in}$. The proofload applied in these analyses was varied. The NASCRAC™-predicted largest surviving and experimentally-observed cracks are plotted versus applied proofload in Figure 4.7.1-5. The NASCRAC™-predicted and experimentally-observed remaining life are described in Section 4.7.3.

Table 4.7.1-2. Input for NASCRAC™ Proof Test Analyses

	NASCRAC™ INPUT	VALUE	CORRESPONDING TEST DIMENSION
MODEL	605		TEST SERIES III-a
GEOMETRY	ASPECT RATIO	1.499	*a*2/ *a*1
	W1	3.001	*b*1
	W2	3.001	*b*2
LOADING	TRANSIENT 1 MAX: EQ. B R RATIO:	1 cycle VARIED 0	PROOF LOAD FIGURE 4.7.1-2
	TRANSIENT 2 RANGE: EQ. B R-RATIO:	5000 cycles 14.05, -9.37 0.2294	FATIGUE LOADS FIGURE 4.7.1-2 TABLE 4.7.1-1
	BLOCK	1 X TRANSIENT 1 TRANSIENT 2 REPEATED TO FAILURE	
MATERIAL PROPERTIES	2219-T851 Al L-T & T-L	ALUM3 #104	2219-T851 Al lab air
	K-R CURVE	Kc = 30 ksi	

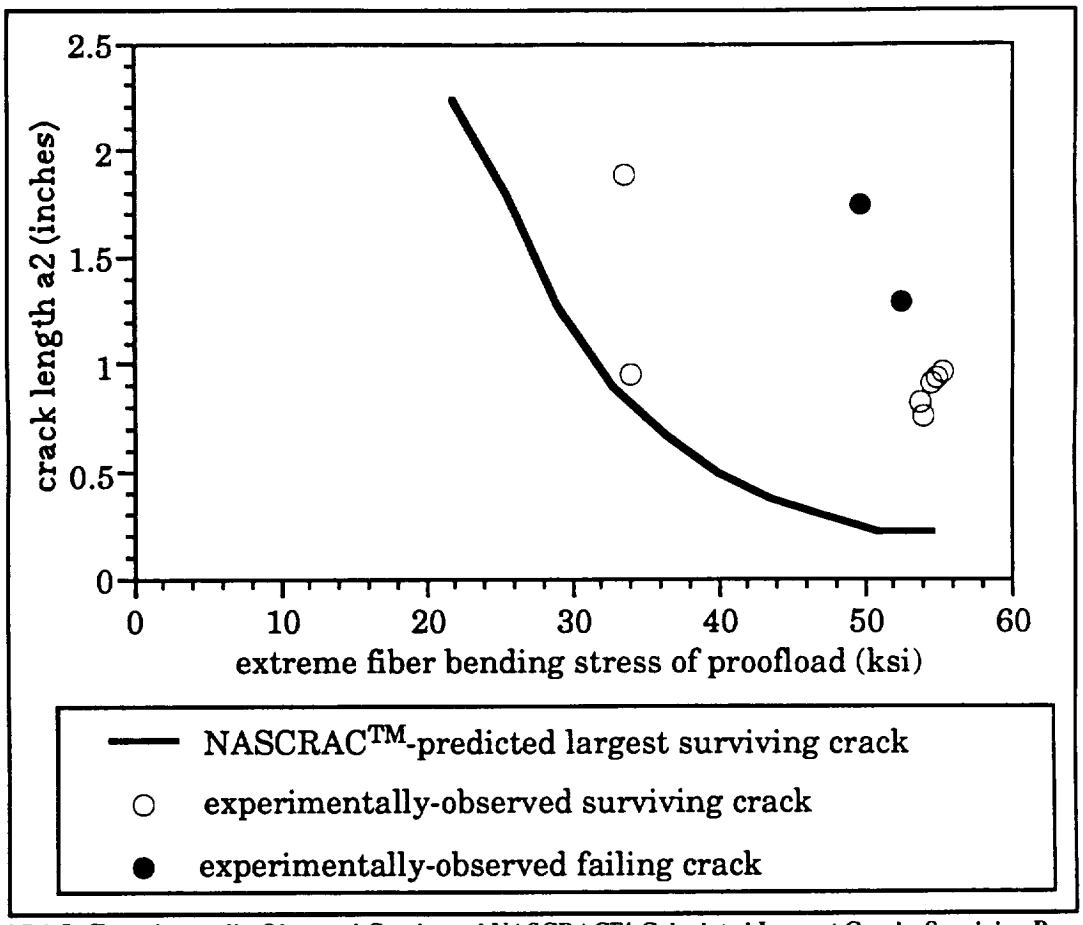

Figure 4.7.1-5. Experimentally-Observed Cracks and NASCRAC™-Calculated Largest Cracks Surviving Proof Loads

The yield stress of the material is approximately 53 ksi. Therefore, LEFM is not applicable to the proofloads with the extreme fiber bending stress in the range of 48 to 56 ksi. However, the proofloads where the extreme fiber bending stress is approximately 34 ksi are still in the LEFM range. There are two experimentally-observed cracks that survived proofloads near 34 ksi. Both of these cracks were larger than the NASCRAC™-predicted largest crack for this proofload. Therefore, it is concluded that for this configuration, **[NASCRAC™ can under-predict the size of the largest surviving crack following a proofload.]**

4.7.2 REMAINING LIFE CALCULATION

The second part of proof test logic evaluation was the testing of the remaining life prediction following the proofload. To perform an unbiased test of remaining life calculation, all NASCRAC™ analyses in this subsection used experimentally-observed crack sizes for input.

Stage 1 of this series was fatigue crack propagation from an initial notch. The purpose of stage 1 was twofold: to validate NASCRAC™ fatigue crack propagation for model 605, and to create a series of fatigue cracks of different sizes with realistic aspect ratios.

The results of stage 1 are described in Section 4.5.2.4. The main conclusion from this section is: **NASCRAC™ model 605 predicts fatigue crack growth well for stage 1 of test series III-a.**

This result gives an indication that both the NASCRAC™ stress intensity factor solution and crack growth model for 2219-T851 aluminum were appropriate for this test. Therefore, any difference (beyond the anticipated experimental scatter) between NASCRAC™-predicted and experimentally-observed fatigue crack growth is considered to be the result of retardation due to the proofload.

Table 4.7.2-1 shows the experimentally-observed retardation, $\upsilon 1$, as defined in Section 4.11, in stage 3 of this test series. Retardation was calculated, and more thoroughly investigated in Section 4.11. Tests III-a/4 and III-a/7 did not survive the proofload. Therefore, l_{rem} is zero for these tests. Due to experimental error, the retardation, $\upsilon 1$, was not available for tests III-a/1, III-a/2 and III-a/8.

Table 4.7.2-1. Experimentally-Observed Retardation and Remaining Life in Stage 3 of Test Series III-a

TEST	l_{rem}	RETARDATION	
	(CYCLES)	(CYCLES)	(% of *l*rem)
III-a/1	114,152	n. a.	- -
III-a/2	48,478	n. a.	- -
III-a/3	386,245	200,300	52
III-a/4	0	0	- -
III-a/5	385,124	155,952	40
III-a/6	348,011	145,900	42
III-a/7	0	0	- -
III-a/8	515,458	n. a.	- -
III-a/9	551,728	390,375	71

Retardation following the proofload accounts for a significant portion of the remaining fatigue life in this test series. However, it is likely that the magnitude of the proofload was large enough to invalidate LEFM for some of the test specimens.

NASCRAC™-proof test logic does not account for retardation following the proofload. However, NASCRAC™ can model fatigue crack growth retardation as part of a fatigue life prediction analysis. Therefore, two NASCRAC™ fatigue life prediction analyses were performed for each of the tests summarized in Table 4.7.2-1. The input for the NASCRAC™ analyses is summarized in Table 4.7.2-2. The first NASCRAC™ analysis used the Wheeler retardation model to account for fatigue crack growth retardation following the proofload. The value of K_c was increased from 30 to 51 ksi$\sqrt{\text{inch}}$ to model the K at which the specimens were observed to fail. The second analysis did not account for retardation. The results of these analyses are summarized in Table 4.7.2-3.

Table 4.7.2-2. Base Input for NASCRAC™ Analyses of Test Series III-a

	NASCRAC™ INPUT	VALUE	CORRESPONDING TEST DIMENSION
MODEL	605		III-a STAGES 2 and 3
GEOMETRY	a1	varied	$a1$(STAGE 2)
	a2	varied	$a2$(STAGE 2)
	W1	3.001	$b1$
	W2	3.001	$b2$
LOADING	TRANSIENT 1 MAX: EQ. B R-RATIO:	1 cycle varied 0	STAGE 2 load FIGURE 4.7.1-2
	TRANSIENT 2 RANGE: EQ B R RATIO:	5000 CYCLES 14.01, -9.34 0.2294	STAGE 3 LOADS FIGURE 4.7.1-2 TABLE 4.7.1-1
	BLOCK	1 X TRANSIENT 1 TRANSIENT 2 REPEATED TO FAILURE	
material properties	2219-T851 Al L-T, T-L 75F	ALUM3 #104	2219-T851 Al LAB AIR
	SIGYS	53	
	YOUNGS	10,000	
	POISSN	0.33	
	NWheeler	1.3	
	CWheeler	2.0	
	Kc	51.0	

Table 4.7.2-3. Experimentally-Observed and NASCRAC™-Predicted Remaining Life for Tests in Series III-a

TEST	EXPERIMENTALLY OBSERVED	NASCRAC™-PREDICTED	
		NO RETARDATION	WHEELER RETARDATION
	(CYCLES)	(CYCLES)	(CYCLES)
III-a/1	114,152	65,000	70,000
III-a/2	48,478	20,000	25,000
III-a/3	386,245	75,000	150,000
III-a/4	0	0	0
III-a/5	385,124	80,000	155,000
III-a/6	348,011	70,000	145,000
III-a/7	0	0	0
III-a/8	515,458	0	0
III-a/9	551,728	0	0

Based on Table 4.7.2-2, it is concluded that:

- Given the proper initial crack size, NASCRAC™-predicted remaining life is, in some cases, more than 300,000 cycles less than the experimentally-observed remaining life. Accounting for retardation in the NASCRAC™ analyses relieves some but not all of the discrepancy.

NASCRAC™ predicts failure upon crack transition, whereas some fatigue life was experimentally-observed beyond this transition. In three tests, the number of cycles of fatigue life remaining following transitions was measured. These observations are given in Table 4.7.2-2. For comparison, the life remaining following the proofload is also given.

Table 4.7.2-4. Fatigue Life Remaining after Proof Load and after Transition, Test Series III-a

TEST	*l*rem-PROOF	*l*rem-TRANSITION	
	(CYCLES)	(CYCLES)	(% of *l*rem-PROOF)
/6	348016	14300	4
/8	515458	49800	10
/9	551728	26400	5

The available life beyond transition is less significant than the retardation. The experimentally-observed remaining life after the transition, and the experimentally-observed retardation, as defined in Section 4.11, are not enough to account for the discrepancy between NASCRAC™-predicted and experimentally-observed life remaining after the proofload. The definition of retardation from Section 4.11 is somewhat arbitrary, and does not represent the additional fatigue life due to the overload exactly.

4.7.4 SYNTHESIS OF PROOF TEST LOGIC

The NASCRAC™-guaranteed remaining life and experimentally-observed remaining life are plotted versus applied proofload in Figure 4.7.3-1. The input for the NASCRAC™ analyses are summarized in Table 4.7.1-2. The magnitude of the proof load was varied in both the experiments and the NASCRAC™ analyses.

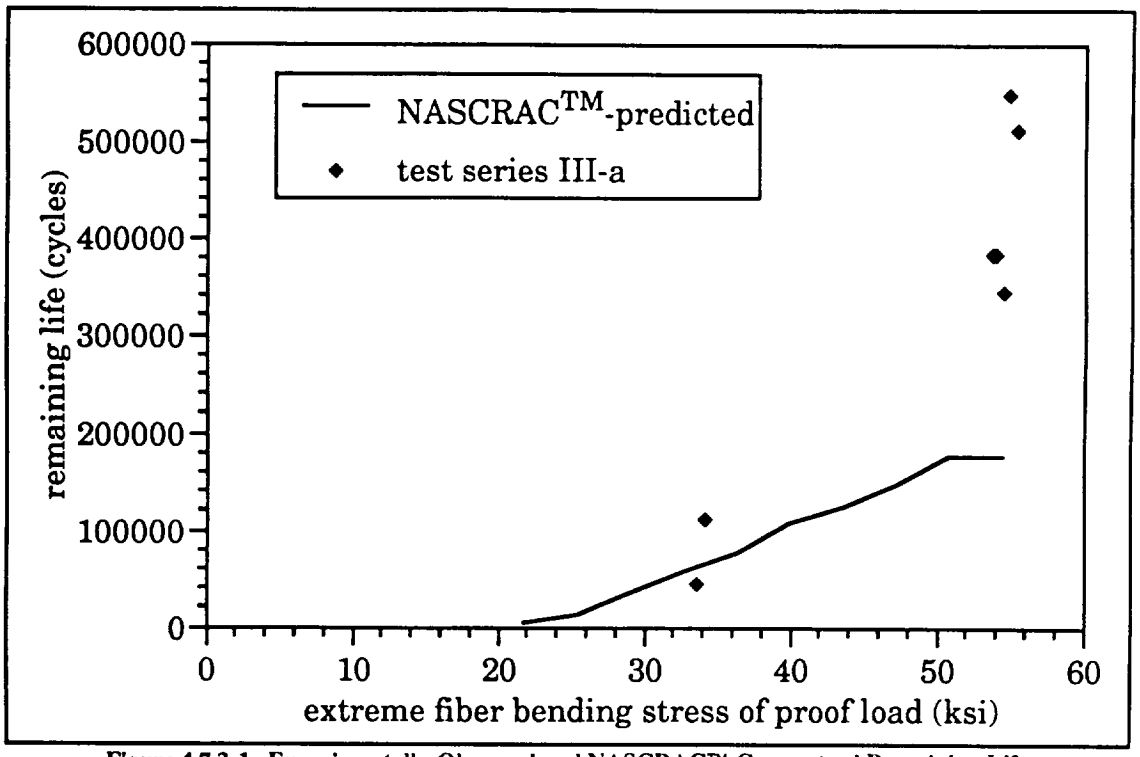

Figure 4.7.3-1. Experimentally-Observed and NASCRAC™-Guaranteed Remaining Life

It was found that cracks much larger than the NASCRAC™-predicted largest crack survived the proofloads. In one case, this resulted in a NASCRAC™-guaranteed remaining life greater than the experimentally-observed remaining life. In many cases , the NASCRAC™-guaranteed remaining life was much less than the observed remaining life. Retardation following the proofload accounted for much of the additional fatigue life. Fatigue crack propagation beyond NASCRAC™-predicted failure also accounts for additional remaining life. Based on these observations, it is concluded that **NASCRAC™ proof test logic is invalid for the tests performed. Use of this capability should be avoided.**

4.8 TEARING INSTABILITY ANALYSIS

NASCRAC™'s *"tearing instability analysis"* capability provides an analyst with an automated means of determining the stress level at which a crack in a plane stress specimen will grow catastrophically to failure. Prior to this critical stress level, tearing of the specimen will occur in a stable manner and will be arrested due to the increased tearing resistance of the material caused by plasticity at the crack tip.

In the NASCRAC™ theory manual, the criteria for tearing instability are given as:

$$K_{applied} > K_{material} \quad \textit{and} \quad dK_{applied}/da > dK_{material}/da$$

where $K_{applied}$ = the stress intensity factor due to the applied stress, $K_{material}$ = the crack growth resistance K corresponding to the initial load and crack length, $dK_{applied}/da$ = the slope of the $K_{applied}$ curve (where the $K_{applied}$ curve is linear from (0, 0) to (a, $K_{applied}$)), and $dK_{material}/da$ = the slope of the crack growth resistance curve at $K_{material}$. The tearing instability option in NASCRAC™ requires input of a crack growth resistance curve (K-R curve) in tabular format or as a power law function ($K_{material} = C_1 (\Delta a)^p$). According to the tearing instability criteria listed above, NASCRAC™ differentiates the crack growth resistance curve to determine the stress level at which an instability occurs.

Figure 4.8-1 presents a flow chart of the NASCRAC™ tearing instability algorithm. This chart maps the code contained in subroutines *TEAR* and *GROTER* and function *RKAOUT*. This chart and a review of the source code suggests that NASCRAC™ does not employ the aforementioned tearing criteria because it never computes a derivative of the K-R curve. Instead, NASCRAC™ incrementally grows a crack using multiples of the input stress; K corresponding to the multiplied stress value and the total crack length (including Δa due to tearing); and Δa from the K-R curve. This incremental growth continues for a given stress level until Δa is smaller than a hardwired tolerance (0.001) or the length of the crack exceeds 99% of the body width of the specimen. To predict failure, this algorithm requires that a K-R curve input in tabular form includes value of Δa that will allow a + Δa to exceed 99% of the body width of the specimen.

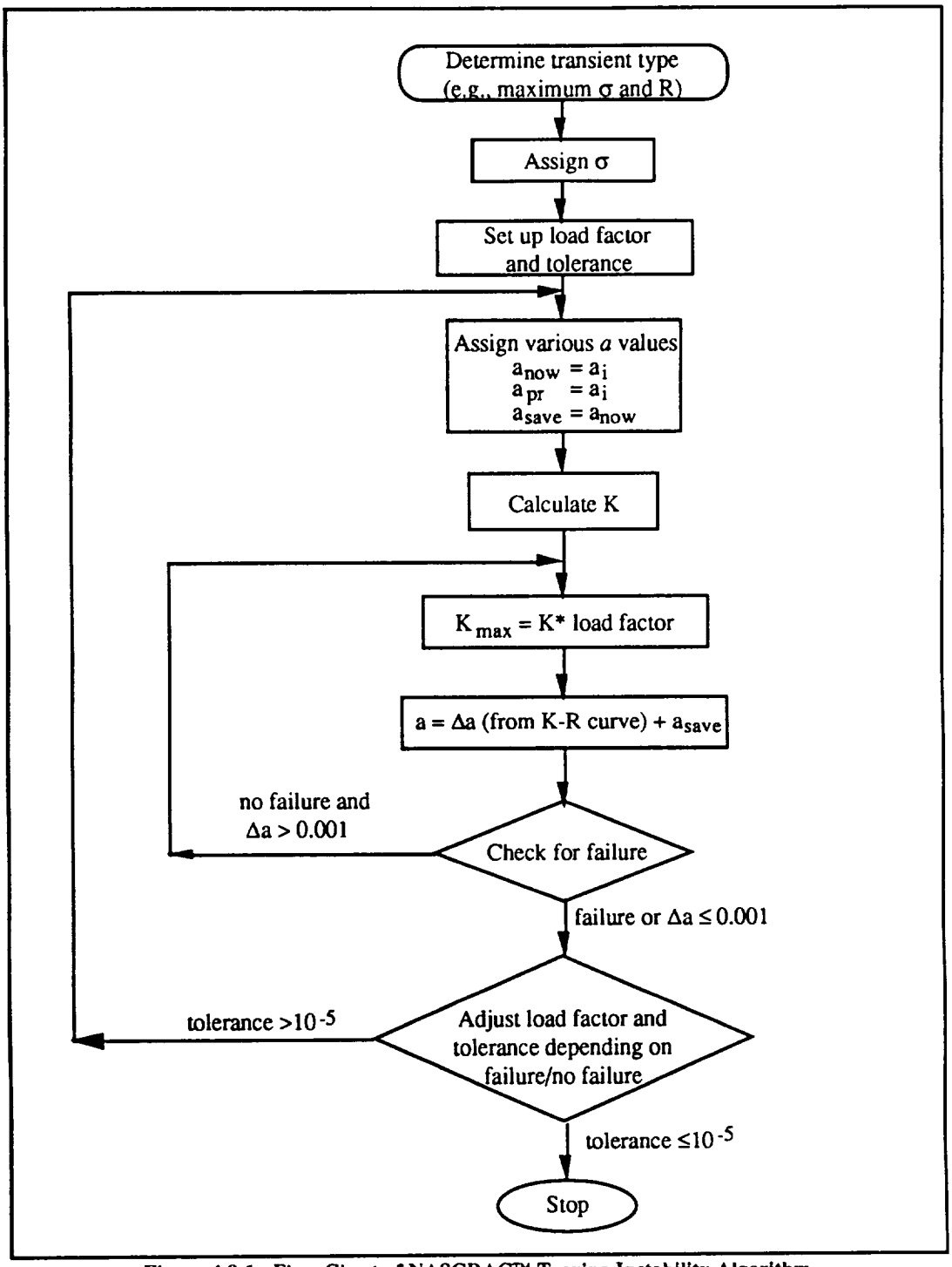

Figure 4.8-1. Flow Chart of NASCRAC™ Tearing Instability Algorithm

A review of the NASCRAC™ tearing instability capability for three dimensional configurations indicated that the capability has little applicability to three-dimensional configurations available in NASCRAC™. To verify this conclusion, an electronic literature search of the subject headings *stability*, *instability*, and *tear* was completed. The search included all articles published in journals since 1988. No articles documenting three dimensional stable tearing

under load control conditions were found. This lack of literature sources supported the conclusions of the analyses described in Section 4.8.1: the multi-degree of freedom NASCRAC™ configurations will not satisfy both the plane stress conditions required for stable tearing and LEFM requirements at the tearing load. Therefore, a check of the NASCRAC™ source code was performed to compare the coded algorithm with the theoretical description and as a tool to analyze tearing in two-dimensional cracked bodies. This effort is described in Section 4.8.2. Experimental data for three-dimensional tearing was obtained from test series III-a. This data is discussed in Section 4.8.3.

4.8.1 ANALYSIS OF NASCRAC™ ALGORITHM FOR THREE DIMENSIONAL BODIES

In NASCRAC™, tearing instability analyses may be performed with the knowledge of a tearing resistance curve, K-R, and a $K_{applied}$-a curve. Figure 4.8.1-1 illustrates a typical tearing resistance analysis. The K-R curve is superimposed on the graph such that Δa = zero coincides with the initial crack length, a_o. Four $K_{applied}$-a curves, corresponding to increasing loads P_1 through P_4, are shown. For initial crack size, a_o, the load P_1 does not result in $K > K_{Ic}$. Therefore, no crack propagation occurs. Crack propagation begins at load P_2, when $K_{applied} = K_{Ic}$. At load P_3, the crack has propagated a length Δa_3. After this propagation increment $K_{applied} = K_R$. The result is a stable crack of length, $a_o + \Delta a_3$. At load P_4, the tangents of the $K_{applied}$-a and the K_R-Δa curves are equal. Therefore, crack propagation is unstable.

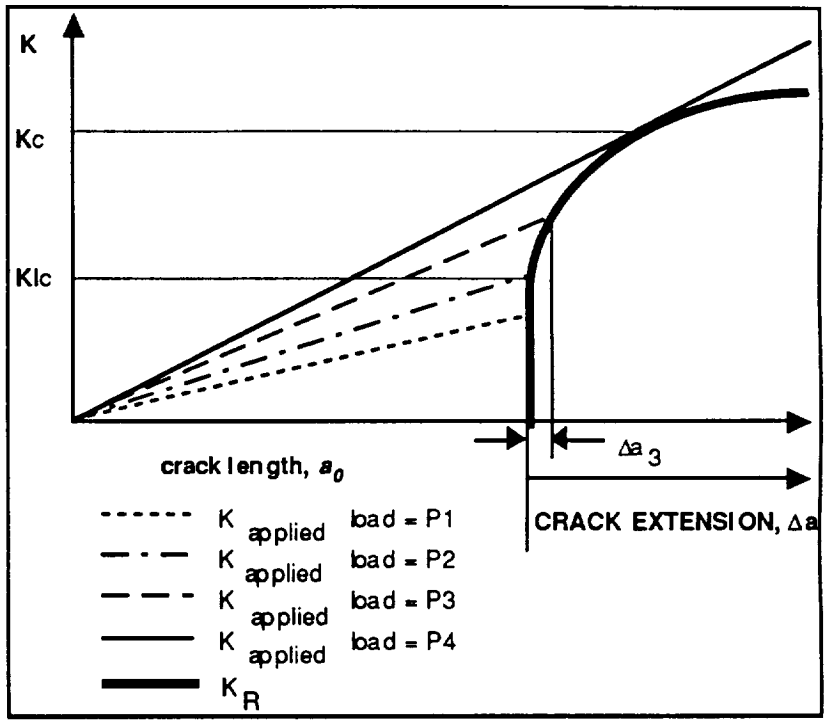

Figure 4.8.1-1. Typical Elastic Tearing Instability Analysis

K-R curves are generally considered material properties. However, these curves are affected by a characteristic length, the thickness of the experimental specimens. Typical thickness dependent behavior of these curves is illustrated in Figure 4.8.1-2. As specimen thickness increases, the slope of the K-R curve is reduced. This trend continues until the conditions of constraint are plane strain for the entire crack front. The result of these plane strain conditions is

that the slope of the K-R curve is zero. ASTM Standard E-399 defines the thickness, B, at which plane strain conditions may be assumed as:

$$B = 2.5\left(\frac{K_I}{\sigma_o}\right)^2, \qquad (4.8.1\text{-}1)$$

where K_I is the applied mode I stress intensity factor and σ_o is the material yield stress. The length, B, is an important design criterion for stable tearing tests.

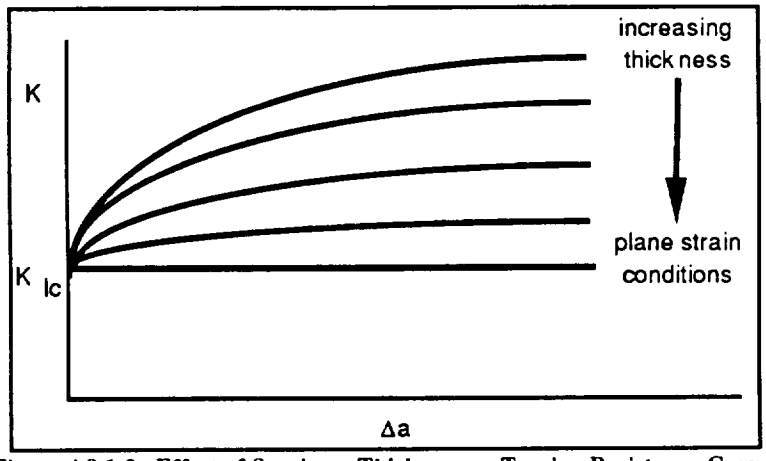

Figure 4.8.1-2. Effect of Specimen Thickness on Tearing Resistance Curves

For through cracks, the specimen thickness determines the conditions of constraint along the crack front, and therefore the nature of the K-R curve. In two-dimensional crack problems the specimen thickness is also the length of the crack front. However, for three-dimensional cracks, as shown in Figure 4.8.1-3, the thickness is not the same as the crack front length. Material far from the crack front will not affect the conditions of constraint along the crack front. Therefore, neither specimen width nor thickness is a good description of the conditions of constraint along a three-dimensional crack front. The crack lengths are not likely to be appropriate descriptions of constraint either; crack length does not affect crack constraint in three dimensional cases. The length of the crack front might be a more consistent length to characterize the conditions of constraint along the crack front, and hence was used to characterize K-R curves for three-dimensional analyses for the evaluation of NASCRAC™.

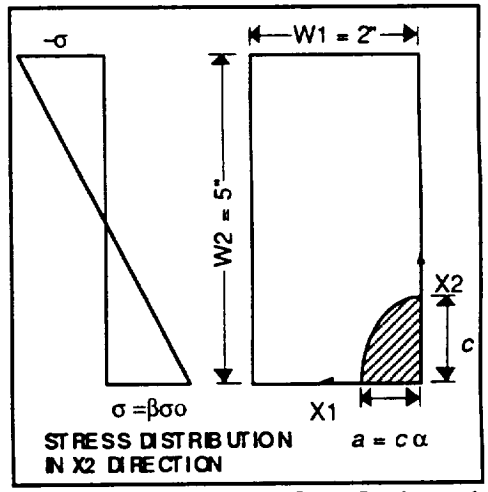

Figure 4.8.1-3. Specimen Cross Section and Load Distribution for 3D Tearing Instability Test

The following requirements are necessary to experimentally test the NASCRAC™ three dimensional elastic tearing stability capability:

I Crack must be 3D
Either a corner (2 DOF), surface (3 DOF) or imbedded (4 DOF) crack must be used. NASCRAC™ model 605, a corner crack in a plate, is a possible test configuration.

II Linear elastic fracture mechanics (LEFM) must apply
A major assumption in LEFM is small scale yielding. To have the near tip fields be described by K, the plastic zone at the crack tip must be small compared to all characteristic lengths of the specimen. One of the factors that determines the size of the plastic zone is the ratio of the far field stress, σ, to the yield stress, σ_o, of the material. In the limiting case of $\sigma = \sigma_o$, the plastic zone extends throughout the entire body.

III Tearing must be initiated
For the initiation of tearing, $K_{applied}$ must be greater than or equal to K_{Ic} .

IV Stable tearing must occur before instability occurs
For stable tearing to occur, condition III must be met and the slope of the K-R curve must be greater than the slope of the $K_{applied}$-a curve for some range of crack length $a_o + \Delta a$. Note that as the specimen thickness increases, the slope of the K-R curve decreases.

A possible test configuration is proposed in Figure 4.8.1-3 for a 2219-T851 aluminum specimen subjected to a monotonically increasing load to failure. This design satisfies condition I and can be modeled by NASCRAC™ configuration 605. The crack size and shape of this quarter-elliptical crack can be uniquely described by the crack length, a, and the aspect ratio, α, defined as

$$\alpha = \frac{a}{c}. \qquad 4.8.1\text{-}2$$

Condition II dictates that LEFM be applicable. A parameter, β, was defined as the ratio of far field extreme fiber bending stress, σ, to the material yield stress, σ_o:

$$\beta = \frac{\sigma}{\sigma_o} \qquad 4.8.1\text{-}3$$

This parameter describes the likelihood that LEFM applies. As β approaches 1.0, far field yielding is approached. Therefore, LEFM is less likely to be applicable. For the proposed design, β was set to 0.5, which satisfies condition II.

Preliminary calculations suggested that $\alpha = 0.5$ was an acceptable aspect ratio. Given $\alpha = 0.5$, $\beta = 0.5$, $K_{Ic} = 30.0$ ksi$\sqrt{\text{in}}$ and the geometry shown in Figure 4.8.1-3, NASCRAC™

calculations showed that the smallest crack for which $K = K_{Ic}$ (condition III) was $a = 0.65$ inches and $c = 1.3$ inches.

For this analysis, the path length of the crack front, s, was compared to the length, B, as calculated from equation 4.8.1-1. In terms of a and α, the path length, s, of a quarter-elliptical crack was approximated by:

$$s = \frac{\pi a}{2}\sqrt{\left(\frac{\alpha^2 + 1}{2\alpha^2}\right)} \qquad 4.8.1\text{-}4$$

For $a = 0.65$" and $\alpha = 0.5$, the path length, s, is 1.6". For 2219-T851 aluminum (when $K = K_{Ic}$) the length, B, at which plane strain conditions develop is 0.9". For plane strain conditions the K-R curve will be flat, as shown in the plane strain curve in Figure 4.8.1-2. For these conditions, any tearing that occurs will be unstable because the slope of the $K_{applied}$-a curve will be positive for this geometry and loading. Therefore, condition IV cannot be satisfied.

The analysis outlined above proved that conditions I through IV could not be satisfied simultaneously for the proposed test design. Is a design possible in which conditions I through IV are satisfied simultaneously? A more general analysis was performed to answer this question.

A surface crack in an semi-infinite body under uniform far-field load was assumed. From [1], the stress intensity factor for this configuration is,

$$K_{Imax} \approx \frac{1.12\sigma}{\frac{3\pi}{8} + \frac{\pi}{8}\frac{a^2}{c^2}}\sqrt{\pi a} \qquad 4.8.1\text{-}5$$

Figure 4.8.1-4. shows the geometry for this configuration. NASCRAC™ semi-, quarter- and elliptical crack solutions are based on the solution for an elliptical crack in an infinite body. Therefore, it is assumed that equation 4.8.1-5 is a reasonable approximation for any cracks modeled in NASCRAC™ that satisfy condition I, that is, semi- or quarter- elliptical cracks. For bending loads, the extreme fiber bending stress was substituted for the uniform far field stress in 4.8.1-5. Substituting the load and geometry of Design 1 into equation (5) predicts K_{Imax} = 34.5 ksi$\sqrt{in}$. The NASCRAC™ predicted value for this crack size and load is 30.2 ksi$\sqrt{in}$. The error of 15% was deemed acceptable for the purpose of this analysis.

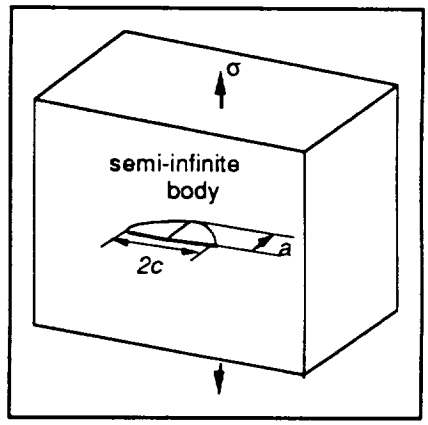

Figure 4.8.1-4. Geometry for K_{Imax} Solution of Equation 4.8.1-5

To satisfy condition III, K_{Imax} in equation 4.8.1-5 was set to K_{Ic}. Restating equation 4.8.1-5 in terms of the parameters defined in 4.8.1-2 and 4.8.1-3 leads to:

$$K_{Ic} = \frac{5.06\beta\sigma_o\sqrt{a}}{3+\alpha^2} \qquad 4.8.1\text{-}6$$

The parameter β in equation 4.8.1-6 gives an indication of the likelihood of condition II being met.

To satisfy condition IV, it was necessary, but not sufficient, for either the $K_{applied}$-a curve to have a negative slope, or the K-R curve to have a positive slope. When monotonically increasing loads are applied to cracked bodies, as in NASCRAC™ simulations, the slope of the $K_{applied}$-a curves are typically positive. Therefore, it was necessary to test in a situation where the K-R curve has a positive slope. In other words, the characteristic length must be less than the plane strain condition length, B.

A parameter, λ, is defined in equation 4.8.1-7 as the ratio of the crack front length to the length B,

$$\lambda = \frac{s}{2.5\left(\frac{K_I}{\sigma_o}\right)^2}, \qquad 4.8.1\text{-}7$$

where s is the path length of the crack front required to reach K_{Ic} for a given load and aspect ratio, and σ_o and K_{Ic} are the material properties. The slope of the K_R-Δa curves decrease as the parameter λ increases, until the slope is effectively zero at λ = 1.0. Therefore, the value of λ represents the propensity for stable tearing. Combining equations 4.8.1-4 and 4.8.1-6 with equation 4.8.1-7 leads to:

$$\lambda = \frac{0.0245}{\beta^2}\left(\frac{\alpha^2+1}{2\alpha^2}\right)^{\frac{1}{2}}\left(3+\alpha^2\right)^2 \qquad 4.8.1\text{-}8$$

A plot of λ versus α, for various values of β is given in Figure 4.8.1-5. The parameters of design 1 are indicated on this graph. The parameters of design 2, which will also be described, are indicated.

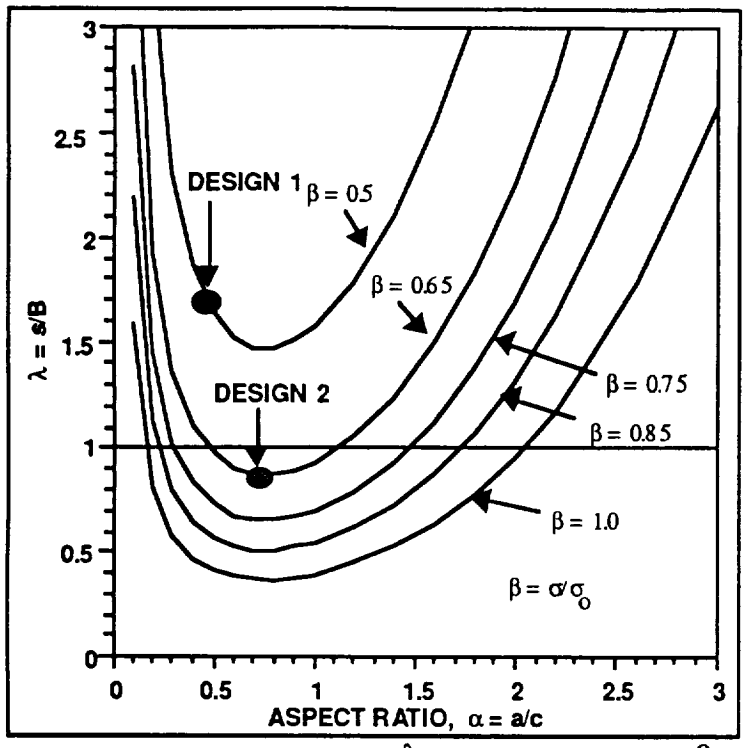

Figure 4.8.1-5 . Design Parameter λ as a Function of α and β

It is significant that λ is a function only of the two dimensionless parameters α and β. Therefore, the choice of overall size and material of the test specimen do not affect the outcome. It is apparent from the graph that for a given value of β, λ has a minimum value at α approximately equal to 0.75. Therefore, $\alpha = 0.75$ is a good value to optimize design suitability. Note that the intersection of $\beta < 1$ and $\lambda < 1$ is a minimum requirement for conditions I through IV to be met. In an ideal test design, both values would be less than 0.5. However, there are no values of α for which this is true.

Nonetheless, this analysis was sufficient to show that the set of situations in which conditions I through IV are met simultaneously is limited, if not empty. However, there is no value of β or λ which gives an absolute definition of unacceptable. Furthermore, assumptions have been made in defining λ, and approximations have been made in calculating the formula for λ. For the sake of thoroughness, a second design was analyzed.

Design 2 was formulated using insight obtained from the general analysis. A value of $\alpha = 0.75$ appears to be optimal for the design criteria. The value of β was chosen to be 0.65. Except for crack size, the geometry is the same as that shown in Figure 4.8.1-3. NASCRAC™ simulations show that the minimum crack size to obtain $K_I = K_{ic}$ at the given load (condition III) is $a = 0.4125$, $c = 0.55$. For this crack size and load, the K_I estimated by equation 4.8.1-6 is 32.6 ksi$\sqrt{in}$. For this design, equation 4.8.1-6 was an adequate approximation of the NASCRAC™ simulation.

Condition II may be checked with a first order estimation of the plane stress plastic zone size r_p, given by:

$$r_p = \frac{1}{2\pi}\left(\frac{K_I}{\sigma_o}\right)^2 \qquad 4.8.1\text{-}9$$

The estimated plastic zone size is 0.05 inches, or 12% of the crack length, a. The size of the plastic zone r_p relative to the crack length a is likely to preclude the use of K_I as a tearing

criterion. The plastic zone size at K_{Ic} is dependent only on material properties. Therefore, the crack length, *a*, must be increased to make LEFM applicable. However, the crack length, *s*, is a linear function of *a*, and there is a maximum length of *s* that is acceptable.

Condition IV may be checked with equation 4.8.1-4. For $a = 0.55$ inches and $\alpha = 0.75$, $s = 0.76$ inches, which is only slightly less than the plane strain length of $B = 0.9$ inches. Clearly, *a* can not be increased by much without violating condition IV. It appears that geometric constraints govern the design process.

The parameterized graph in Figure 4.8.1-5 also illustrates the design constraints. The approximate location of design 2 is indicated on the graph. The applicability of LEFM can be improved only by reducing β. This would result in a larger crack at the initiation of tearing, and therefore the process zone will be a smaller fraction of the crack length. However, β cannot be decreased without increasing λ, which is already close to the maximum allowable value of 1.

The general analysis shows that the difficulties in reaching an acceptable design are material independent. This analysis suggests that an aspect ratio of $\alpha = 0.75$ is optimal for the given design constraints. Design 2 suggests that stable linear elastic tearing might only occur in NASCRAC™ 3D geometries only when LEFM and the significance of any plane stress conditions along the crack front are questionable.

The assumption that the crack front length, *s*, is the characteristic length for the K-R curves of 3D cracks is untested. The only other possible choice for a characteristic length is the specimen width or thickness. Both of these lengths are approximately equal to or greater than the crack front length, *s*. Therefore, the choice of width or thickness as the characteristic length for K-R curves would not influence the outcome of these analyses. Two other assumptions that were made in these analyses are: (1) the length B defines a length at which the K-R curve is flat, and (2) LEFM is not applicable when the process zone estimated by equation 4.8.1-9 reaches 10% of the crack length.

In conclusion, [**the NASCRAC™ capability to simulate stable tearing in a 3D body does not appear to be applicable to available configurations.**]. A test design in which LEFM is questionable and the extent of stable tearing is minimal appears to be the most likely situation in which all required conditions for a 3D NASCRAC™ tearing instability analysis are satisfied. NASCRAC™'s three-dimensional tearing algorithm was not experimentally validated because a suitable test configuration could not be designed.

4.8.2 VERIFICATION OF NASCRAC™ ALGORITHM FOR LIMITED 2-D APPLICATIONS

To verify the operation of the NASCRAC™ tearing instability algorithm for one-dimensional cracks, a test case was developed and analyzed step-by-step. Figure 4.8.2-1 shows the geometry of the test specimen. Figure 4.8.3-2 and Table 4.8.2-1 show the K-R curve and data,

respectively, used in the test case. The initial crack length of the specimen was 0.3 inches and the input stress value was 20 ksi. For this configuration, NASCRAC™ predicted a tearing instability when the stress reached 27.7 ksi, a factor of 1.385 greater than the input stress.

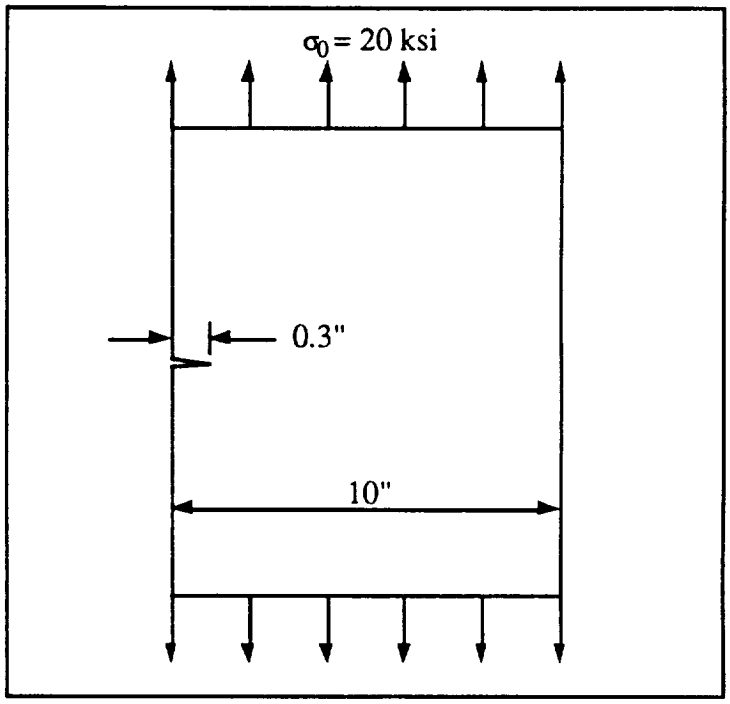

Figure 4.8.2-1, Geometry of Tearing Instability Test Case

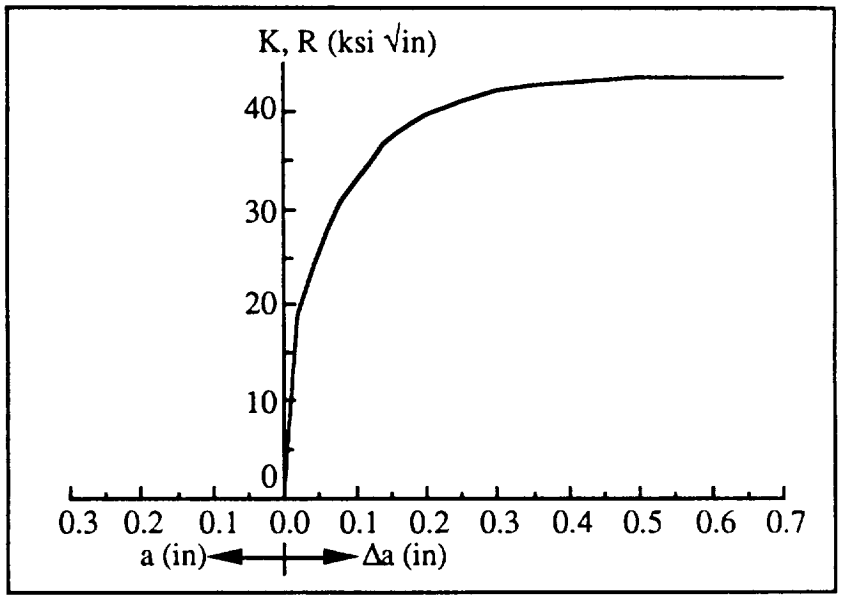

Figure 4.8.2-2. Crack Growth Resistance Curve for Tearing Instability Test Case

Table 4.8.2-1. Crack Growth Resistance Curve Data for Tearing Instability Test Case

Δa (INCHES)	CRACK RESISTANCE K (ksi √in)	dK/d(Δa) [1] (ksi √in /in)
0.00	0.0	na
0.01	11.4	475
0.02	19.0	312.5
0.04	23.9	217.5
0.06	27.7	170
0.08	30.7	132.5
0.10	33.0	97.5
0.12	34.6	87.5
0.14	36.5	80
0.16	37.8	60
0.18	38.9	50
0.20	39.8	36.5
0.25	41.2	23
0.30	42.1	15
0.35	42.7	10
0.40	43.1	6.5
0.50	43.6	2.5
0.60	43.6	0.0
99.0	43.6	na

1 based on a central difference calculation,
$dK/d(Da) = 0.5*[((K_{n+1} - K_n)/(Da_{n+1} - Da_n)) + ((K_n - K_{n-1})/(Da_n - Da_{n-1}))]$

The test case results suggest that $dK_{applied}/da > dK_{material}/da$ does not occur until the stress factor reaches 1.47 or, equivalently, when $K_{applied} = 32.38$ ksi√in. Table 4.8.2-2 lists the series of calculations which led to this conclusion. The $dK_{material}/da$ values in Table 4.8.2-2 were computed using interpolated values of the central difference values listed in Table 4.8.2-1. A more exact analysis was attempted by curve fitting a power law ($K_{material} = C_1 (\Delta a)^p$) to the crack resistance curve using the data points Δa = 0.08 and Δa = 0.16 to obtain C_1 and p. With this curve fit, the predicted critical stress factor was 1.444. This result and the NASCRAC™ predicted critical stress factor of 1.385 are also shown in Table 4.8.2-2.

Table 4.8.2-2. Calculated Values of K and dK/da for the Tearing Instability Test Case

STRESS FACTOR	$K_{applied} = K_{material}$ (ksi √in)	$dK_{applied}/da = K/a$ (ksi √in /in)	$dK_{material}/da$ (ksi √in /in)
1.0	22.03	73.4	253.8
1.3	28.63	95.4	158.4
1.385	30.51	101.7	134.9
1.4	30.84	102.8	130.4
1.5	33.04	110.1	97.3
1.46	32.16	107.2	110.3
1.47	32.38	107.9	106.9
1.444	31.81	106.0	106.0 [1]

1 based on first derivative of curve fit function, $K_{material} = 65.52 (Da)^{0.30}$

In summary, the NASCRAC™ tearing instability capability has been verified. It is a functioning capability if input data for the crack growth resistance curve follow a power law function as prescribed in the NASCRAC™ user's manual. However, **[the failure criteria of the coded algorithm do not adhere to the criteria listed in the NASCRAC™ theory manual.]** The coded algorithm is conservative compared to the listed criteria, i.e., NASCRAC™ will predict the occurrence of a tearing instability at a lower critical stress factor compared to a prediction using the listed criteria **as long as the K-R data in the input table extends beyond the dimensions of the specimen.**

4.8.3 EXPERIMENTALLY GENERATED K-RESISTANCE CURVES

Stage 2 of Test Series III-a was tearing tests. The geometry for this series is shown in Figure 4.8.3-1. The tearing loads are defined as NASCRAC-calculated K(1) and K(2) for crack lengths a_1 and a_2, proofload P_1 and moment arm b_3. Average values for this test series are given in Table 4.8.3-1. Crack sizes ranged from 0.558 and 0.840 inches for a_1 to 1.150 and 1.796 inches for a_2. Data from the manufacturer of this material indicates K_{Ic} of about 25 ksi$\sqrt{in}$. The value for K_{Ic} in the NASCRAC material library is 30 ksi$\sqrt{in}$. With a yield strength of 53 ksi, all but the smallest observed length of a_1, and all of the crack front lengths and the thickness of the test specimen meet the requirement for LEFM. Furthermore, the crack front length and specimen dimensions are large enough to anticipate plane strain behavior. Therefore, tearing stability theory would predict that these tests should fail at K_{Ic}.

It was observed, however, that K_{Ic} is not a good predictor of failure in these tests. Experimentally measured K-R curves are shown in Figure 4.8.3-1. The curves measured for a_1 in each test tend to be higher than the curves measured for a_2. This might indicate that the K-R curves are geometry dependent in these tests.

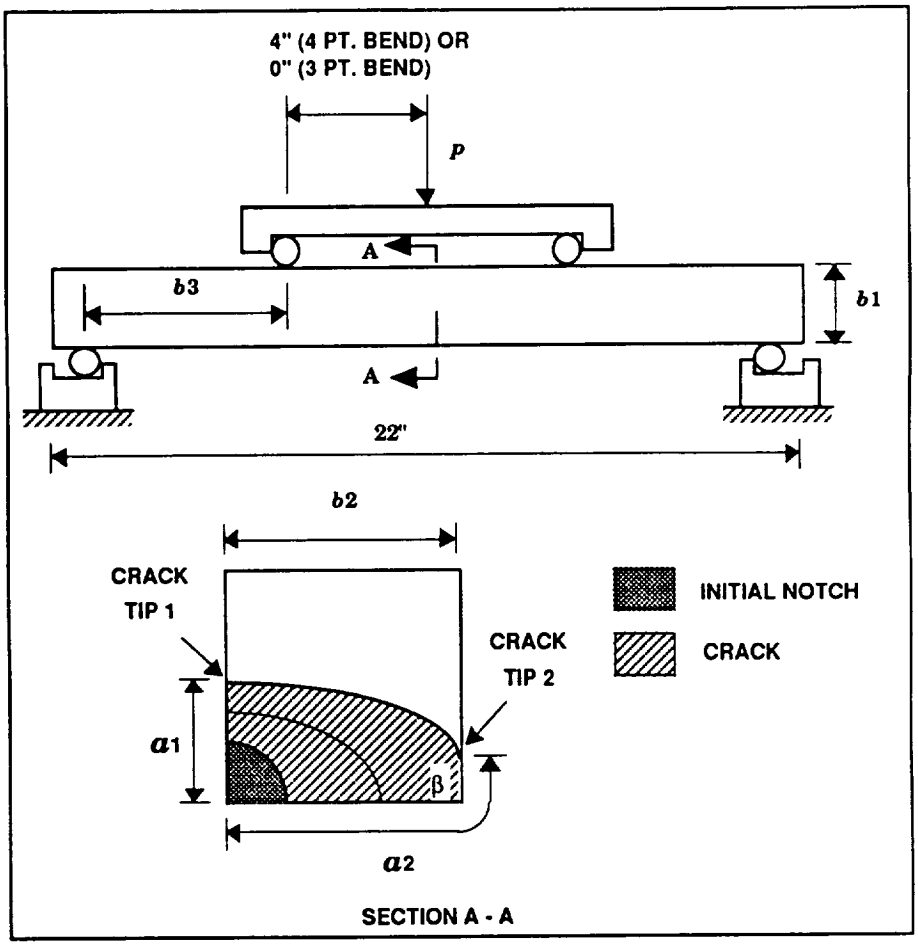

Figure 4.8.3-1. Geometry for Test Series III-a

Table 4.8.3-1. Average Values for Stage 2 and 3 of Test Series III-a

NUMBER OF TESTS		9
DIMENSION	AVERAGE VALUE	UNITS
$a1$(STAGE 2)	0.795	INCHES
$a2$(STAGE 2)	1.160	INCHES
$b1$	3.001	INCHES
$b2$	3.001	INCHES
$b3_{proof}$ (3 pt. CONFIG.)	6.082	INCHES
$b3$proof (4 pt. CONFIG.)	10.026	INCHES
$b3$stage3	6.034	INCHES
$\Delta p3$	20.97	KIPS
R $ratio_{stage\ 3}$	0.2294	
P_{proof}	VARIED	KIPD

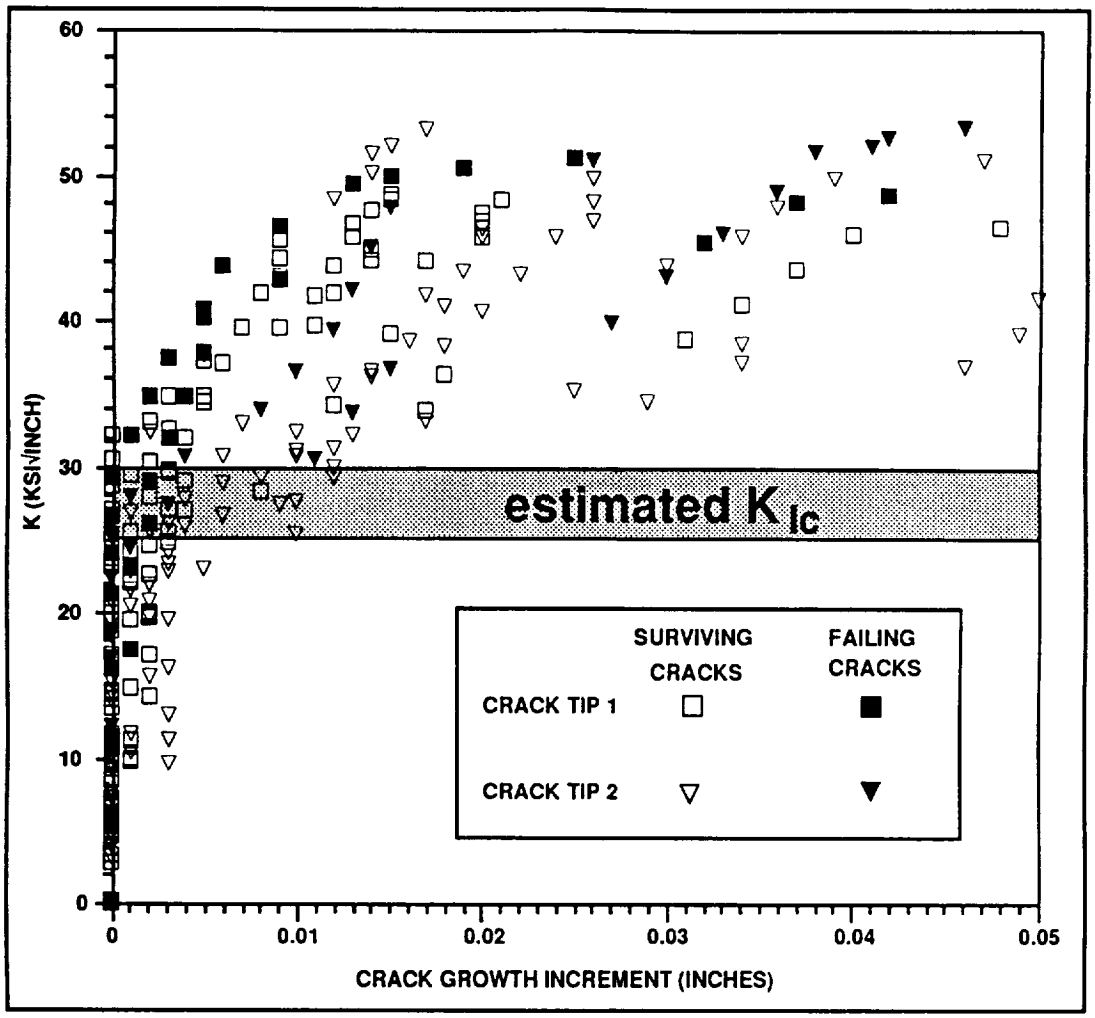

Figure 4.8.3-2. Experimentally Measured K-R Curves

Of the nine test specimens, only two failed. The NASCRAC-calculated K at failure was approximately 51 ksi√in for both tests. This is well beyond the manufacturer-reported value of approximately 25 ksi√in and the NASCRAC™ material library value of 30 Ksi√in. LEFM was probably invalid by the time the stress intensity factor reached 51 ksi√in. However, LEFM was valid between 25 and 30 ksi√in, when failure was anticipated. Based on these observations, and the analysis in Subsection 4.8.1, it is concluded that K_{IC} **is not a valid predictor of failure in this test series.**

4.8.4 REFERENCES FOR SECTION 4.8

1. *Broek, D., Elementary Engineering Fracture Mechanics, 4th ed, Martinus Nijhoff, Boston, 1986.*

4.9 CREEP CRACK GROWTH

This section describes work performed to test the validity of NASCRAC™'s *Creep Crack Growth* capability. Proper calculation of the creep crack growth parameter, C*, is essential to NASCRAC™ creep crack growth rate prediction capability. NASCRAC™ uses plastic J integral calculations to find C*. Section 4.3 describes a coding error found for the plastic J solution of configuration 303. All C*-calculations described in this section were made with a version of NASCRAC™ corrected for this error.

4.9.1 NASCRAC™ IMPLEMENTATION OF CREEP CRACK GROWTH

In a creeping material, strain rate, stress rate and stress can be related by:

$$\dot{\varepsilon} = \frac{\dot{\sigma}}{E} + B\sigma^{n_{creep}} \qquad 4.9.1\text{-}1$$

Note the similarity in the form of this equatation to the Ramberg-Osgood relationship. Neglecting elastic strains, the stress and strain rate fields take a form similar to the HRR field [1]

$$\sigma_{ij} = \left(\frac{C^*}{I_n B r}\right)^{\frac{1}{n_{creep}+1}} \tilde{\sigma}_{ij}\left(n_{creep}, \theta\right) \qquad 4.9.1\text{-}2$$

$$\dot{\varepsilon}_{ij} = \left(\frac{C^*}{I_n B r}\right)^{\frac{n_{creep}}{n_{creep}+1}} \tilde{\varepsilon}_{ij}\left(n_{creep}, \theta\right) \qquad 4.9.1\text{-}3$$

where $\tilde{\varepsilon}_{ij}\left(n_{creep}, \theta\right)$ and $\tilde{\sigma}_{ij}\left(n_{creep}, \theta\right)$ are dimensionless functions. The parameter C* is a path-independent integral defined by equation 4.9.1-4. The definitions for this equation are given in Figure 4.9.1-1.

$$C^* = \int_\Gamma \left[\dot{W}_\varepsilon dx_2 - \sigma_{ij} n_i \left(\frac{\partial \dot{u}_j}{\partial x_1}\right) ds \right] \qquad 4.9.1\text{-}4$$

where

$$\dot{W}_\varepsilon = \int \sigma_{ij} d\dot{\varepsilon}_{ij} \qquad 4.9.1\text{-}5$$

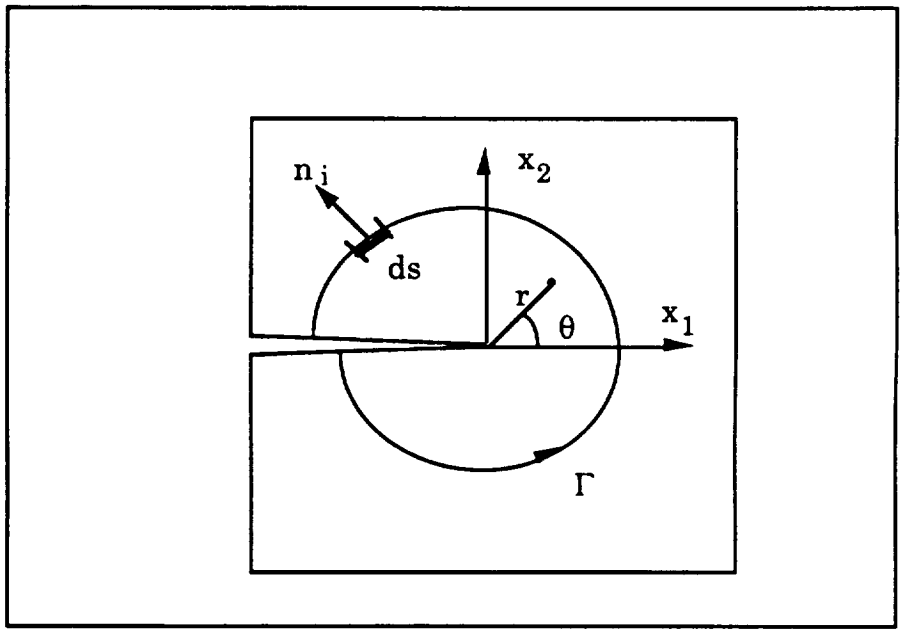

Figure 4.9.1-1. Definitions for Equation 4.9.1-4

The equation for C* is analogous to the plastic term in the J-integral, with strain rate replacing strain. Note, however, that $\dot{W}_c$ is not the same as dW_c / dt, where W_c is the term defined for the J-integral. Given C*, NASCRAC™ predicts creep crack growth rate with equation (4.9.1-6)

$$\frac{da}{dt} = C_3 \left(C^*\right)^{n_{creep}} \qquad 4.9.1\text{-}6$$

Where C_3 and n_{creep} are temperature independent material growth model parameters.

At the onset of loading, the creep strains will be zero. Therefore, the stresses near the crack tip will be better described by the K fields. In the long term, the creep strains will be much larger than the elastic strains, and the C* field will dominate. This is known as the steady state creep crack field.

For intermediate times, two methods are available in NASCRAC™ for interpolating between the initial K fields and the long term, steady state creep fields. The Riedel method calculates a parameter C(t) and the Saxena method calculates a parameter, C_t. In either method the appropriate parameter is substituted for C* in 4.9.1-6.

4.9.2 LITERATURE REVIEW OF CRACK GROWTH PARAMETERS

The C* field is not accepted as a good predictor for creep crack growth rates for all materials. For instance, Kaufman, *et al* [3] reported that creep crack growth in 2219-T851 aluminum may be described by the following relationship:

$$\log \frac{da}{dt} = 0.85K - 4.14 \qquad 4.9.2\text{-}1$$

Where K is the stress intensity factor. Benussan, *et al* [4] concluded that "there is no unique correlation between da/dt and the C* integral, the net section stress or the reference stress ..." for 2219-T851 aluminum.

Research on 6061 aluminum has been conducted by Radhakrishnan and McEvily [5, 6]. They conclude that "... within a limited range, a relation of the type

$$\frac{da}{dt} = A\left(C^*\right)^n \qquad 4.9.2\text{-}2$$

with n = 1 appears to be valid." However, they also conclude that the C* relationship "clearly showed a load dependent character" and "did not give any relationship that could be used for design." The authors recommend a parameter of the type $(\dot{\Delta} / P^{\alpha})$ to describe da/dt over a wide range, where Δ is the load-line displacement and P is the load for a compact tension test specimen.

Type 304 stainless steel was chosen for this test series since the literature indicated that the C* model is not appropriate for aluminum. Summarazing other researcher's conclusions, Ozmat, *et al* [7] summarized C* modeling efforts for 304 stainless steel: "... most investigators have found that the overall creep crack growth rates could be correlated better with a C* parameter than with K or net section stress." Ozmat, *et al* also stated that, "apparent planar [crack] growth was found only in very thin samples which most probably had plane stress deformation characteristics, and those with deep side grooves." Yokobori, *et al*[8] found that C* has some load dependence as a predictor of crack growth rates. They recommended the use of a different paramer, Q*, to predict da/dt.

Observed crack growth rates for type 304 stainless steel from several other researchers [9,10,11,12] are shown in Figure 4.9.2-1. Taira *et al* [10] reported separate test results for two different geometries. These distinct sets of data are denoted Fig 5a and Fig 5b, after the original reference. This is not intendended to be an exhaustive list, only to give an indication of the scatter found in the published data. There is more than an order of magnitude scatter in the range of observed crack growth rates for a given C*. Much of this variation was observed within each individual study.

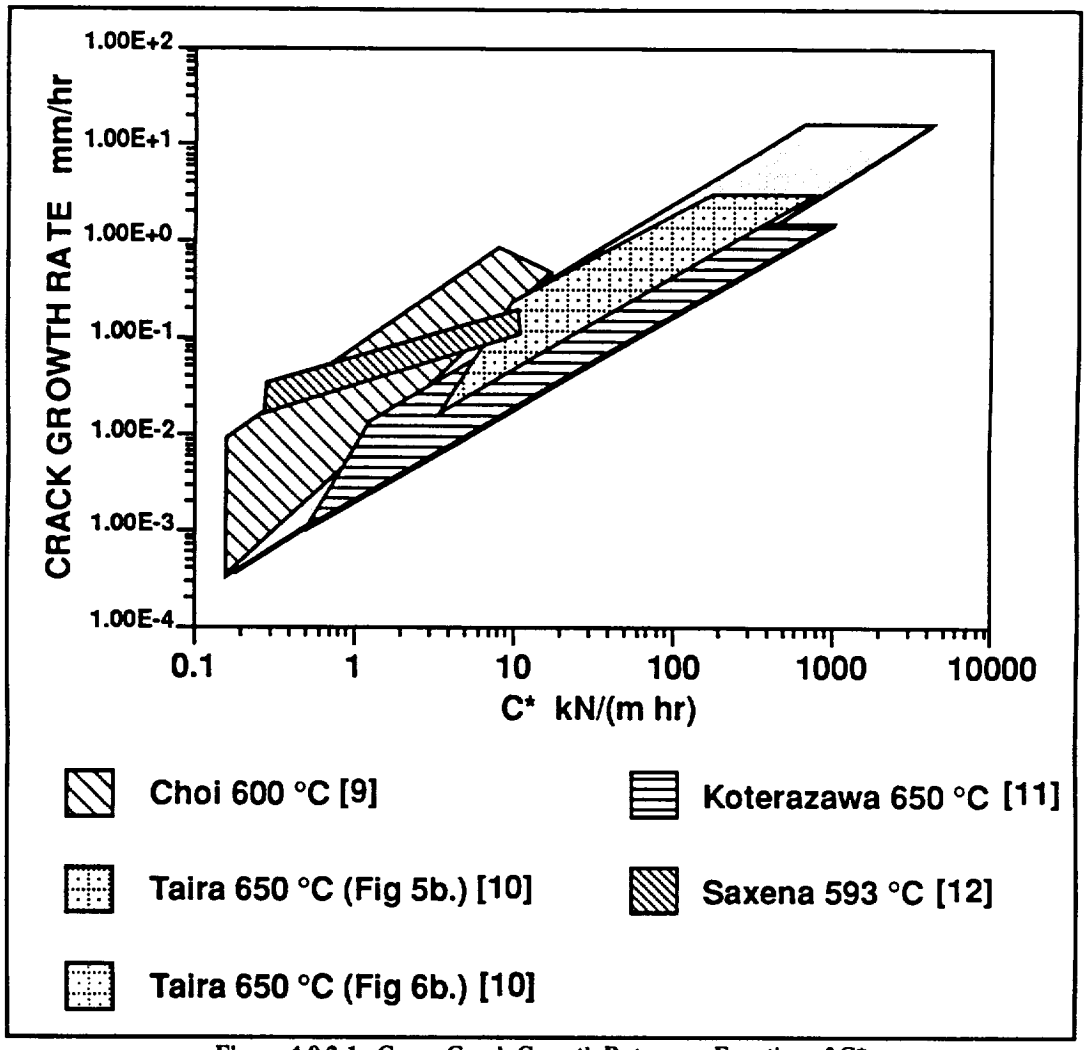

Figure 4.9.2-1. Creep Crack Growth Rates as a Function of C*

4.9.3 VALIDATION OF NASCRAC™ CREEP CRACK GROWTH PREDICTION

The geometry for test series IV-d is shown in Figure 4.9.3-1. The dimensions for the three tests in this series are given in Table 4.9.3-1. For each test, four NASCRAC™ analsyses were performed to accomodate combinations of the two different short term interpolation methods, and two sets of creep crack growth rate parameters representing the envelope of data reported in Figure 4.9.2-1 The input for these NASCRAC™ analyses is summarized in Table 4.9.3-2. Experimentally-observed and NASCRAC™-predicted crack growth are summarized in Tables 4.9.3-3 through 4.9.3-5. The crack length increment was defined as the projection of the crack onto the section A-A in Figure 4.9.3-1. Three of the six observed crack tips were diverting from the plane of section A-A. It appeared as though these cracks were in the begining stage of crack bifurcation, as described by Ozmat, *et al* [10]. The wide range of NASCRAC™-predicted crack growth rates preclude the presentation of these analyses in graphs.

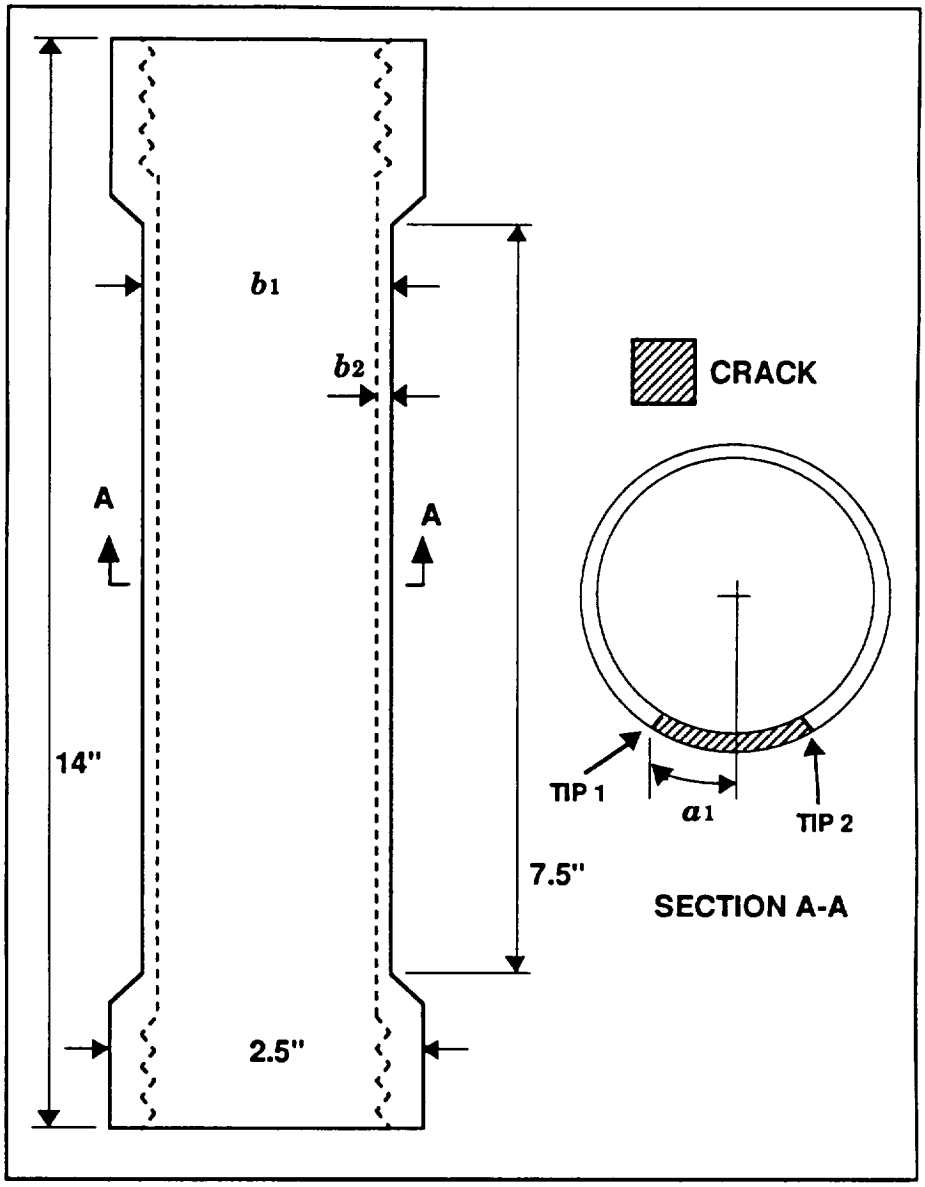

Figure 4.9.3-1. Geometry of Test Series IV-d

Table 4.9.3-1. Dimensions for Test Series IV-d

DIMENSION	IV-d/2	IV-d/3	IV-d/4	UNITS
$a1(0)$	0.399	0.546	0.395	INCHES
$b1$	0.963	0.965	0.965	INCHES
$b2$	0.10	0.10	0.10	INCHES
σ	6.6	5.8	4.9	ksi
TIME OF TEST	287	325	321	HOURS
$\Delta a1$	0.012	0.016	0.011	INCHES
$\Delta a2$	0.015	0.018	0.010	INCHES

Table 4.9.3-2. Base Input for NASCRAC™ Analysis of Test Series IV-d

	NASCRAC™ PARAMETER	VALUE			CORRESPONDING TEST DIMENSION
MODEL	303	IV-2	IV-3	IV-4	TEST SERIES IV-d
GEOMETRY	a	0.399	0.546	0.395	$a1(0)$
	W	1.513	1.516	1.516	$(b1 * \pi)/2$
	t	0.100	0.100	0.100	$b2$
	r	0.863	0.865	0.865	$b1 - b2$
LOAD	A	6.6	5.8	4.9	
MATERIAL PROPERTIES	YOUNGS	22,300			304 SS 600°C
	N	4.5			
	D	59.7			
	A'	2.29E-11			
	n_{creep}	6			
CREEP CRACKING UPPER BOUND	C3	4.8E-2			
	M	0.5			
CREEP CRACKING LOWER BOUND	C3	1.1E-2			
	M	0.962			

Figure 4.9.3-3. Experimentally-Observed and NASCRAC™-Predicted Crack Growth Increments for Test IV-d/2

TEST IV-d/2	TEST TIME = 287 HOURS	Δa (INCHES)
EXPERIMENTALLY-OBSERVED		
CRACK TIP 1		0.012
CRACK TIP 2		0.015
NASCRAC™-PREDICTED		
GROWTH PARAMETERS	INTERPOLATION METHOD	
UPPER BOUND	RIEDEL	0.064
	SAXENA	0.069
LOWER BOUND	RIEDEL	0.008
	SAXENA	0.015

Figure 4.9.3-4 Experimentally-Observed and NASCRAC™-Predicted Crack Growth Increments for Test IV-d/3

TEST IV-D/3	TEST TIME = 325 HOURS	Δa (INCHES)
EXPERIMENTALLY-OBSERVED		
CRACK TIP1		0.016
CRACK TIP2		0.018
NASCRAC™-PREDICTED		
GROWTH PARAMETERS	INTERPOLATION METHOD	
UPPER BOUND	RIEDEL	0.096
	SAXENA	0.042
LOWER BOUND	RIEDEL	0.001
	SAXENA	0.014

Figure 4.9.3-5. Experimentally-Observed and NASCRAC™-Predicted Crack Growth Increments for Test IV-d/4

TEST IV-D/4 TEST TIME = 321HOURS		Δa (INCHES)
EXPERIMENTALLY-OBSERVED		
CRACK TIP 1		0.011
CRACK TIP 2		0.010
NASCRAC™-PREDICTED		
GROWTH PARAMETERS	INTERPOLATION METHOD	
UPPER BOUND	RIEDEL	0.054
	SAXENA	0.035
LOWER BOUND	RIEDEL	0.000
	SAXENA	0.007

The experimental observations fall within the range of NASCRAC™-predictions. Based on this observation, and the observations of other researchers it is concluded that:

- Given proper material parameters, NASCRAC™ might predict creep crack growth accurately for some materials. However, the user should beware that data from any given set of tests might be valid in only a narrow range of geometry and load configurations.

4.9.5 REFERENCES FOR SECTION 4.9

1. *Riedel, H., Fracture at High Temperatures, Springer-Verlag, Berlin, 1987.*

2. *NASCRAC™ Theory Manual, Failure Analysis Associates, prepared for Marshall Space Flight Center, Palo Alto, CA, 1989.*

3. *Kaufman, J. G., Bogardus, K. O., Mauney, D. A., and Malcolm, R. C., "Creep Cracking in 2219-T851 Plate at Elevated Temperatures," Mechanics of Crack Growth, ASTM STP 590, American Society for Testing and Materials, 1976, pp. 149-168.*

4. *Bensussan, Philippe L., Jablonski, David A., and Pelloux, Regis M., "A Study of Creep Crack Growth in 2219-T851 Aluminum Alloy Using a Computerized Testing System," Metallurgical Transactions A, Vol 15A, January 1984, pp. 107-120.*

5. *Radhakrishnan, V. M., and McEvily, A. J., "A Critical Analysis of Crack Growth in Creep", Journal of Engineering Materials and Technology, Vol 102, April 1980, pp. 200-206.*

6. *Radhakrishnan, V. M., and McEvily, A. J., "Creep Crack Growth in 6061 Al-Alloy," Zeitschrift fur Mettalkunde, Vol 71, n. 3, 1980, pp. 133-135.*

7. *Ozmat, B., Argon, A. S., and Parks, D. M., "Growth Modes of Cracks in Creeping Type 304 Stainless Steel," Mechanics of Materials, Vol 11, 1991, pp. 1-17.*

8. *Yokobori, A. T., Tomizawa, H., Sakata, H., Kato, T., Kuriyama, T. "Representation of the Displacement Rate Between the Loading Points in Terms of Applied Stress and Temperature and Its Relation to Creep Crack Growth Rate, C*, P and Q* Parameters," Engineering Fracture Mechanics, Vol. 28, No. 5-6, pp. 805 - 816, 1987.*

9. *Choi, Y. H., "Creep Crack Growth Behavior in AISI 304 Stainless Steel at 873 K," Scripta Metallurgica, Vol 23, pp. 2111 - 2116, 1989.*

10. *Taira, S., Ohtani, R., Kitamura, T. "Application of J-Integral to High Temperature Crack Propagation Part I- Creep Crack Propagation," Journal of Engineering Materials and Technology, Vol 101, pp 154 - 161, April 1979.*

11. *Koterazawa, R., Takayoshi, N., "Creep-Fatigue Crack Growth and Fractography of a Type 304 Stainless Steel at Elevated Temperature," Fatigue Fract. Engng. Mater. Struct. Vol. 14, No. 1, pp. 1 - 9, 1991.*

12. *Saxena, Ashok, "Evaluation of C* for the Charaterization of Creep-Crack Growth Behavior in 304 Stainless Steel," Fracture Mechanics: Twelfth Conference, ASTM STP 700, American Society for Testing and Materials, pp. 131 - 151, 1980.*

4.10 CRACK TRANSITIONING

Verification and validation of NASCRAC™'s transitioning capability focused on three objectives:

- determination of the effect of shape limitations in NASCRAC™ (e.g., semi-elliptical, quarter-elliptical) during crack transitioning.
- analysis of f_t, the arbitrary transitioning factor in NASCRAC™.
- quantification of the effect of transition assumptions on predicted fatigue life.

4.10.1 VERIFICATION OF NASCRAC™ CRACK TRANSITION ALGORITHM

NASCRAC™ provides thirteen different paths for transition analysis. Transitioning in NASCRAC™ ranges from the simplest case, i.e., a single transition where a two degree-of-freedom crack transitions into a single degree of freedom crack, to the most complex case, i.e., three transitions in which a four degree of freedom crack eventually becomes a one degree of freedom crack. Table 4.10.1-1, which was adapted from Table 5.2 of the NASCRAC™ User's Manual [1], lists the available transition paths.

Table 4.10.1-1. Transition Paths in NASCRAC™

INITIAL CRACK CONFIGURATION	NUMBER OF DEGREES OF FREEDOM			
	4	3	2	1
BURIED ELLIPTICAL CRACK (502)	502	702	605	203
BURIED ELLIPTICAL CRACK (502)	502	702		202
SEMI-ELLIPTICAL SURFACE CRACK IN A PLATE (702)		702	605	203
SEMI-ELLIPTICAL SURFACE CRACK IN A PLATE (702)		702		202
SEMI-ELLIPTICAL (CIRCUMFERENTIAL) SURFACE CRACK IN A HOLLOW CYLINDER (703)		703		303
SEMI-ELLIPTICAL (CIRCUMFERENTIAL) SURFACE CRACK IN A HOLLOW CYLINDER (703)		703		401
SEMI-ELLIPTICAL AXIAL SURFACE CRACK IN A HOLLOW CYLINDER (704)		704		302
SEMI-ELLIPTICAL AXIAL SURFACE CRACK IN A HOLLOW CYLINDER (704)		704		205
SEMI-ELLIPTICAL SURFACE CRACK IN A HOLLOW SPHERE (705)		705		301
SEMI-ELLIPTICAL SURFACE CRACK IN A HOLLOW SPHERE (705)		705		401
QUARTER ELLIPTICAL CORNER CRACK IN A PLATE (605)			605	203
QUARTER ELLIPTICAL CRACK FROM A HOLE IN A PLATE (601)			601	208
QUARTER ELLIPTICAL CRACK FROM A HOLE IN A LUG (602)			602	209

The transition algorithm does function as described in [1] and [2]; however, analyses of NASCRAC^{TM}. results revealed problems which were caused by the basic assumption of the algorithm, the transitioning factor f_t. The errors associated with this f_t approach are discussed in the following sections. One minor implementation error was detected which needs to be documented. During execution of the crack transitioning option in NASCRAC^{TM}, a user is prompted for f_t, which is defined as *TRFCTR*. The following information is given:

TRFCTR = 1.0 Equal area basis
TRFCTR = 1.15 Transitioning performed on the basis of non-crossing cracks

The range of TRFCTR is 0.5 to 1.5. Suggested Value is 1.0

Figure 4.10.1-1. NASCRAC ^{TM} Prompt for f_t

In a transition analysis from configuration 702 to 605, any value other than 1.15 will result in f_t = 1.0 being implemented, even if the input is in the specified range.

4.10.2 VALIDATION OF NASCRAC^{TM} CRACK TRANSITIONING ALGORITHM

Test series I-2-a, fatigue crack propagation with transitioning, was designed to verify and validate NASCRAC^{TM}'s transitioning capability. Prior to performing test series I-2-a, PMMA specimens were tested to refine the test procedure. PMMA specimens were used because the crack front could be observed throughout the fatigue life tests. These tests provided data for assessing NASCRAC^{TM}'s assumption of an elliptically shaped crack front for post-transition configurations. The test geometry consisted of an off-center flaw in a nominal 1.5" by 3.0" in cross section. The beam was loaded cyclically in four point bending. Figure 4.10.2-1 shows crack fronts observed throughout the course of one PMMA test. Each front is represented by lines connecting points obtained from photographs of the crack fronts.

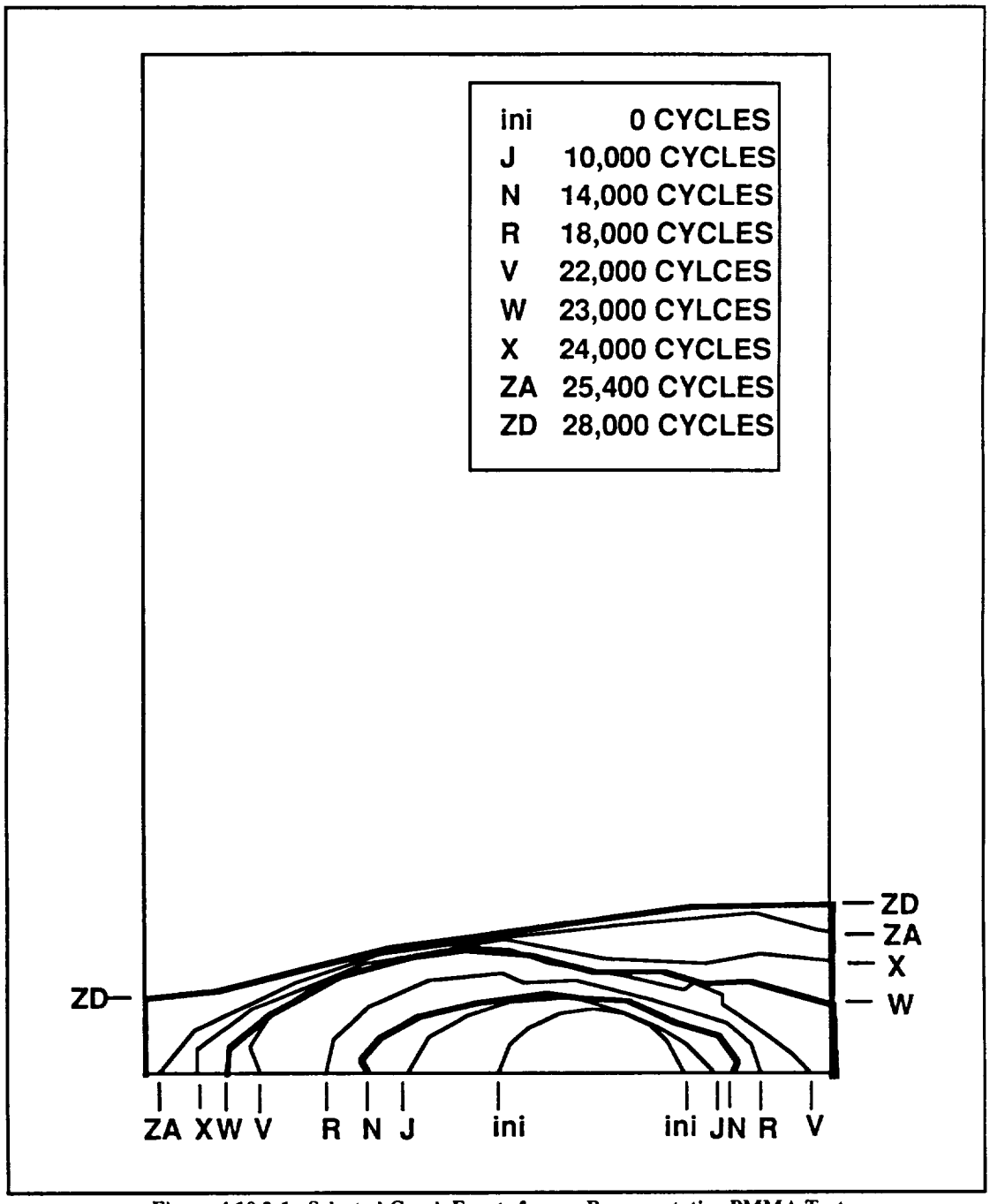

Figure 4.10.2-1. Selected Crack Fronts from a Representative PMMA Test

Some of the crack fronts shown in Figure 4.10.2-1, particularly the 23,000 cycle front "W" and the 28,000 cycle front "ZD" do not resemble ellipses. Both of these fronts occurred after a crack tip reached a corner of the beam, i.e. after the crack transitioned. These results highlight two key issues associated with the NASCRAC^{TM} transition algorithm: 1) the NASCRAC^{TM} algorithm ignores the portion of fatigue life spent when the crack is not elliptical or straight through the specimen thickness, and 2) the assumption that the crack remains nearly elliptical is not realistic.

The purpose of test I-2-a/2 was to determine crack front shapes throughout the course of crack propagation in test series I-2-a. The geometry for this test is defined in Figure 4.10.2-2. The specimen was 2219-T851 aluminum. The dimensions of this test specimen are given in Table 4.10.2-1. Parameters that describe the load history are defined in Figure 4.10.2-3. NASCRAC™ and FRANC3D stress intensity factor calculations are made for several fronts observed in this test.

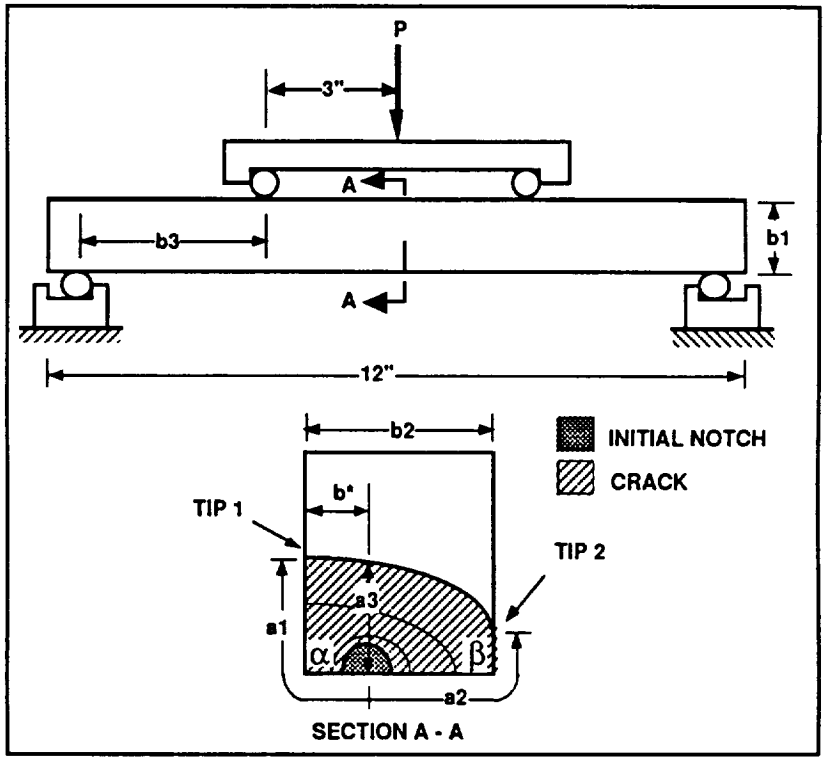

Figure 4.10.2-2, Geometry for Test Series I-2-a

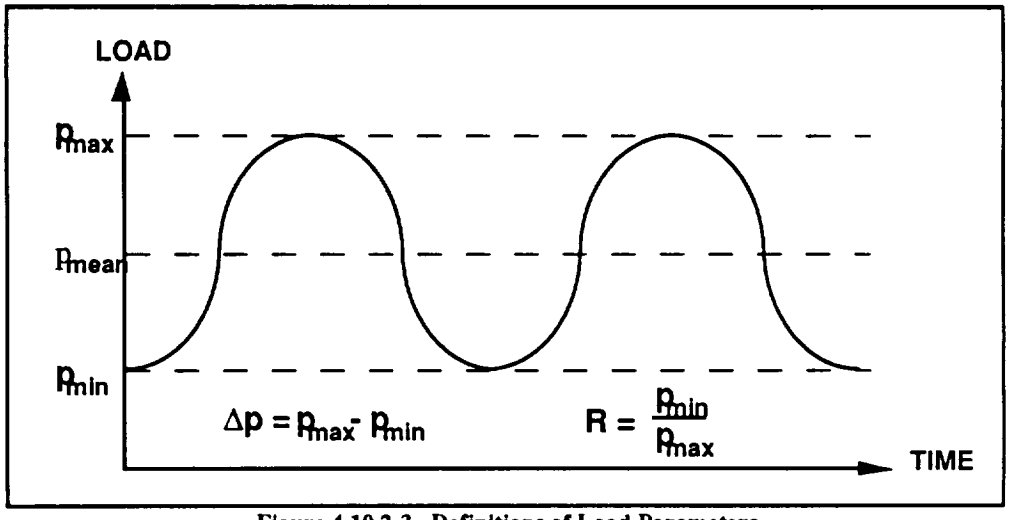

Figure 4.10.2-3. Definitions of Load Parameters

Table 4.10.2-1. Dimensions of Tests I-2-/2

DIMENSION	VALUE	UNITS
$a1(0)$	0.254	INCHES
$a2(0)$	0.254	INCHES
$a3(0)$	0.250	INCHES
$b1$	1.500	INCHES
$b2$	2.000	INCHES
$b3$	2.4	INCHES
b^*	0.500	INCHES

Two types of cyclic loads were applied to this test: fatigue crack propagation load cycles and marker load cycles. In all, 90,000 fatigue crack growth load cycles were applied to this test. For the first 30,000 fatigue cycles, Δp = 15.5 kips. For the remaining 60,000 fatigue crack growth cycles, Δp = 12.0 kips. The Rratio was 0.2 for all fatigue crack growth cycles. After every 10,000 fatigue crack growth cycles, 5000 marker cycles were applied. These additional cycles were intended to "beachmark" the fatigue surface. These marker cycles nominally had the same maximum applied load as the fatigue crack growth cycles, but only 25% of the load range. The marker cycles were not counted in the total cycle count. In all, eight 5000 cycle sets of marker loads were applied. Crack tip measurements were made on the free surface every 5000 cycles throughout the test. Because the amplitude of the fatigue crack growth cycles was varied, this test was not included in the discussion in Section 4.5.2.3. No comparisons between NASCRAC™ predicted and experimentally observed crack growth rates were made for this test.

SEM observations of the crack front from test I-2-a/2 were made. Fatigue striations were observed over some of the crack face. However, none of the observed striations were continuous over the entire crack front. Therefore, the SEM could not be used to determine the crack front history of these tests.

Parts of several beachmarked crack fronts were visible by inspection. Beachmarks could not be identified continuously along any of the eight marked fronts. However, enough front was visible to identify 10 to 12 points along each crack front. Splines were passed through these points to define the crack fronts shown in Figure 4.10.2-4. Stress intensity factor calculations were performed for the 20,000, 30,000 and 60,000 cycle crack fronts, which are shown in bold in the figure.

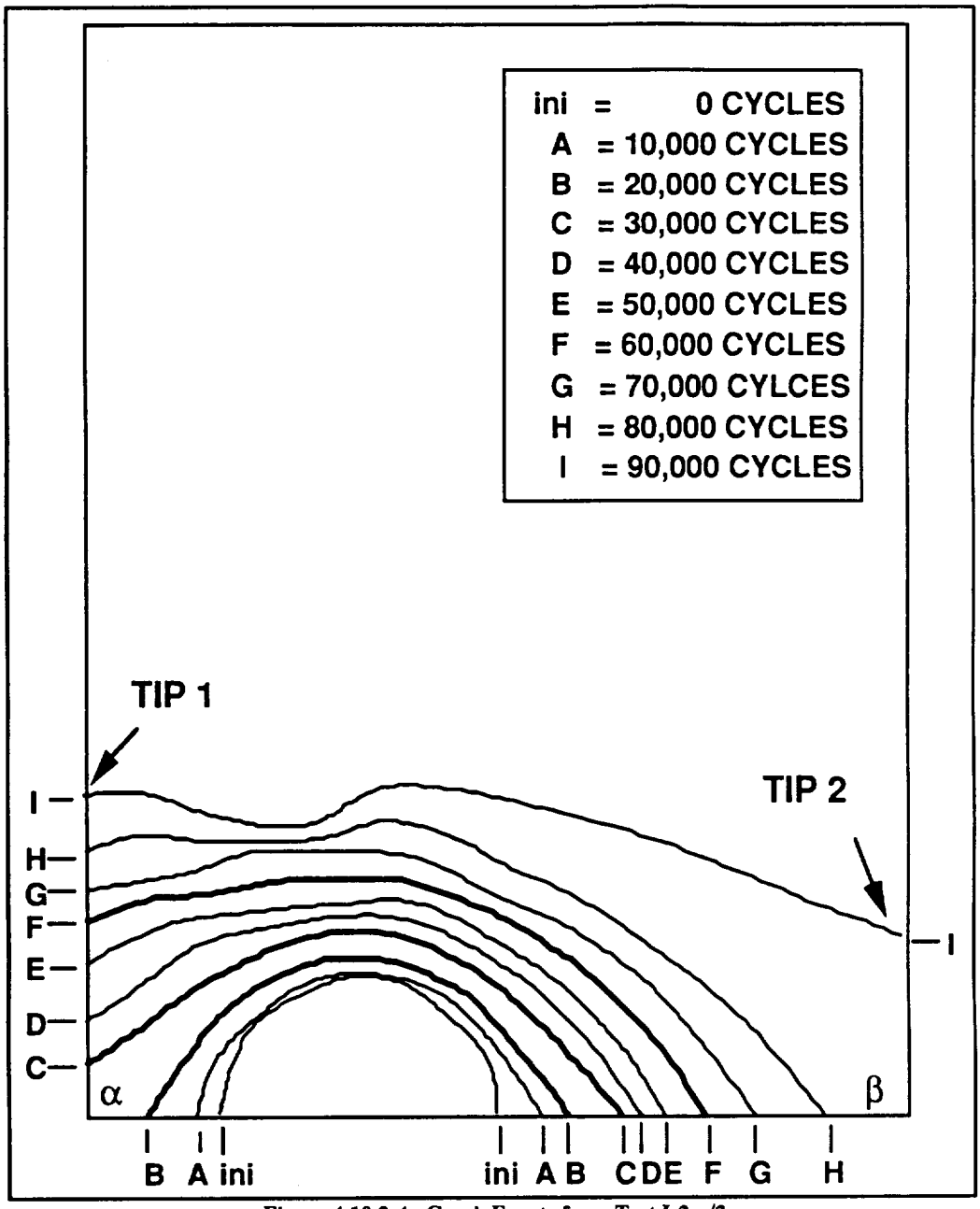

Figure 4.10.2-4. Crack Fronts from Test I-2-a/2

Figures 4.10.2-5 through 4.10.3-7 show the crack fronts observed at 20,000, 30,000 and 60,000 cycles of test I-2-a/2. FRANC3D stress intensity factor calculations were performed on these shapes. One to three NASCRAC™ "best fit" shapes are also shown in each of these figures. The best fit shapes were used as input to NASCRAC™ stress intensity factor calculations but were not the result of NASCRAC™ fatigue crack growth predictions. Figures 4.10.2-8 through 4.10.2-10 show the results of the FRANC3D and NASCRAC™ stress intensity factor calculations. FRANC3D calculates stress intensity factors along the entire crack front. The FRANC3D-calculated stress intensity factors sometimes exhibit deviations near the free surfaces. These deviations are the result of the method of stress intensity factor calculation used for these

analyses, and are spurious. Approximate values extrapolated to the surface are shown as dotted lines. NASCRAC^{TM}. calculates an RMS-averaged stress intensity factor corresponding to each crack degree of freedom.

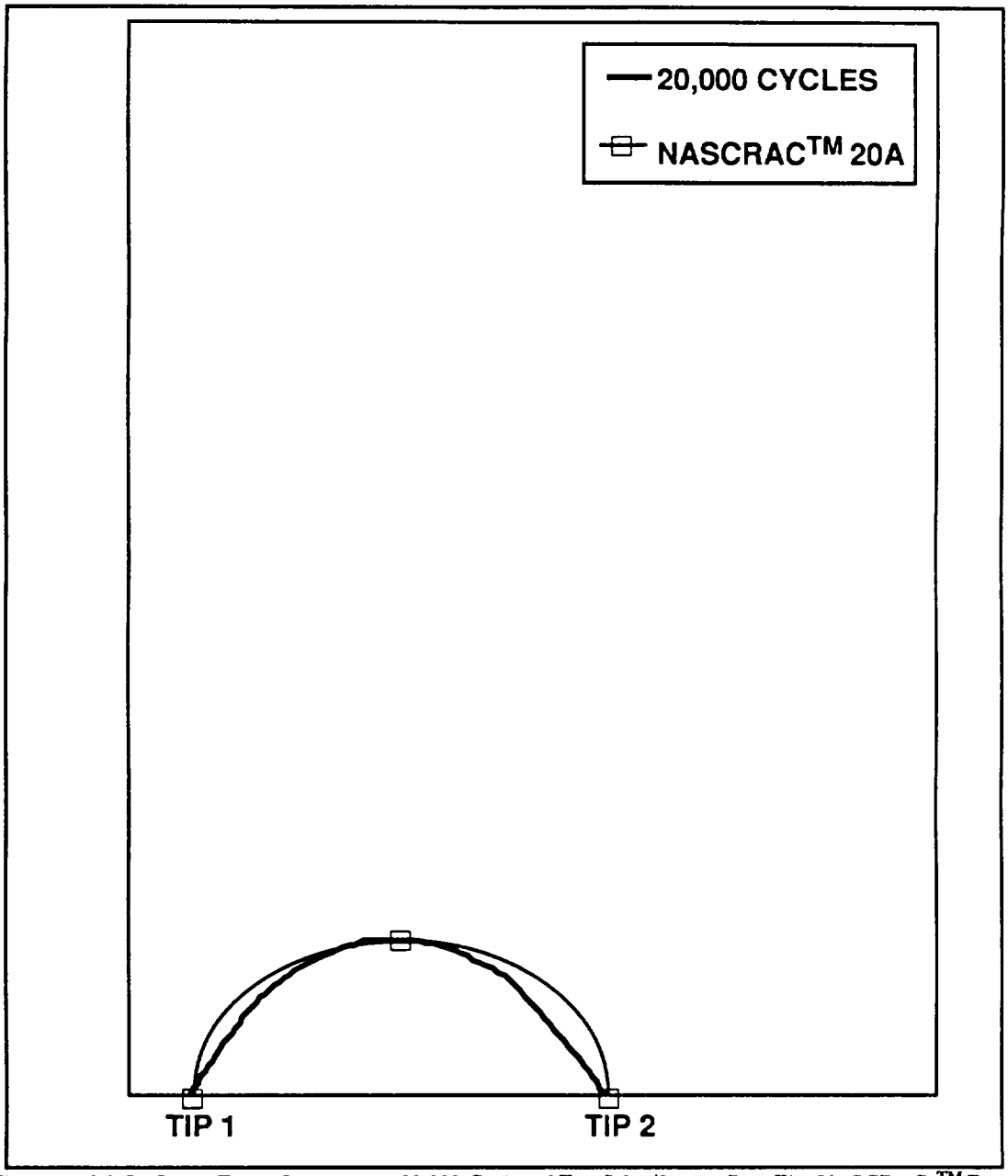

Figure 4.10.2-5. Crack Front Observed at 20,000 Cycles of Test I-2-a/2 and "Best Fit" NASCRAC ™ Front

The crack front NASCRAC^{TM} 20A is the semi ellipse that has the same locations for crack tip 1 and 2 and the same depth as observed for the 20,000 cycle crack front.

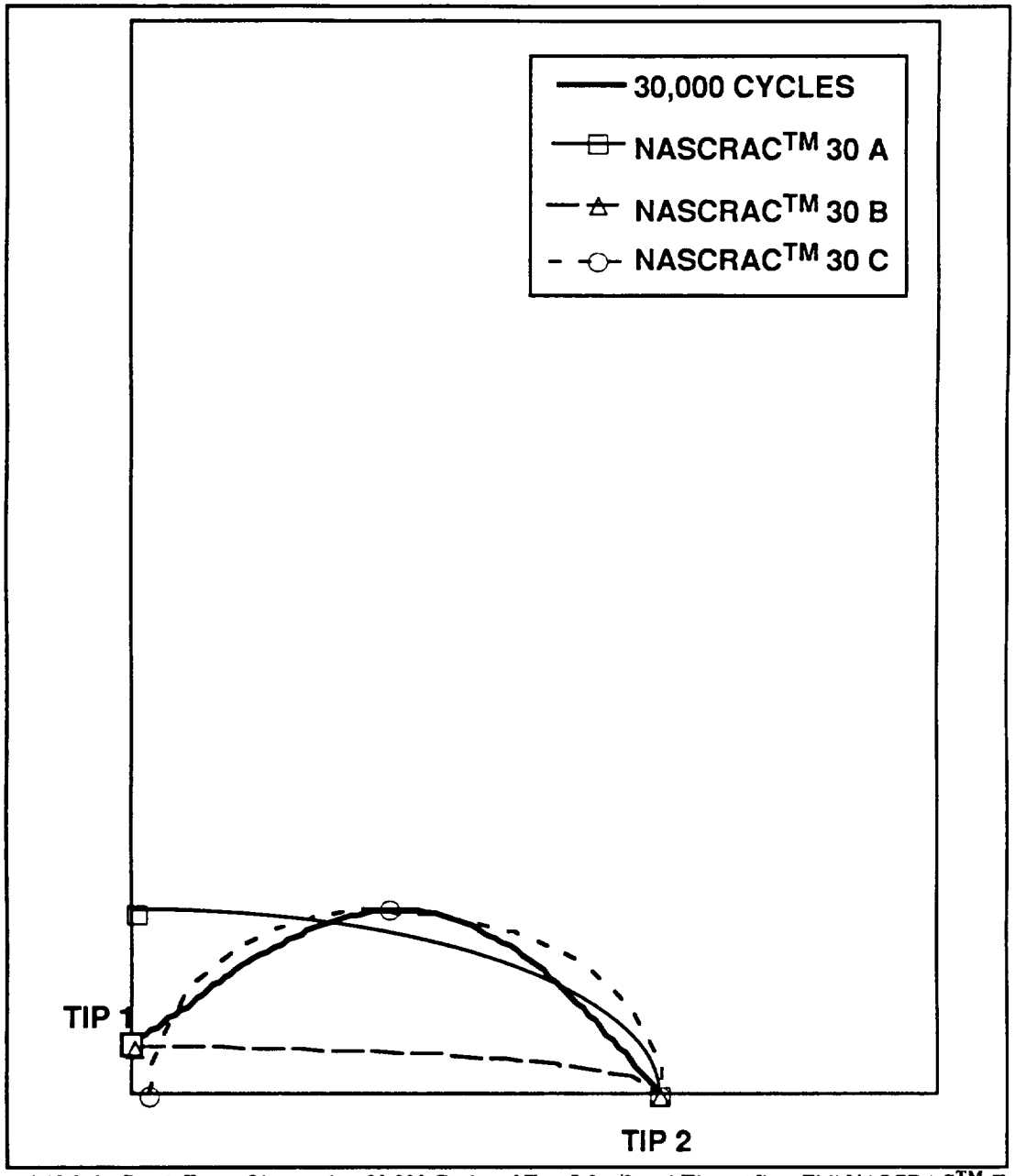

Figure 4.10.2-6. Crack Front Observed at 30,000 Cycles of Test I-2-a/2 and Three "Best Fit" NASCRAC™ Fronts

Crack front NASCRAC™ 30A is the quarter ellipse with the same crack tip 2 location and depth into the specimen as observed in the 30,000 cycle front. Crack front NASCRAC™ 30B is the quarter ellipse with the same crack tip 1 and crack tip 2 location as observed in the 30,000 cycle front. Crack front 30C is a semi ellipse with the same depth into the beam and crack tip 2 location as observed in the 30,000 cycle front. The crack tip 2 location for NASCRAC™ 30C is near the corner of the beam.

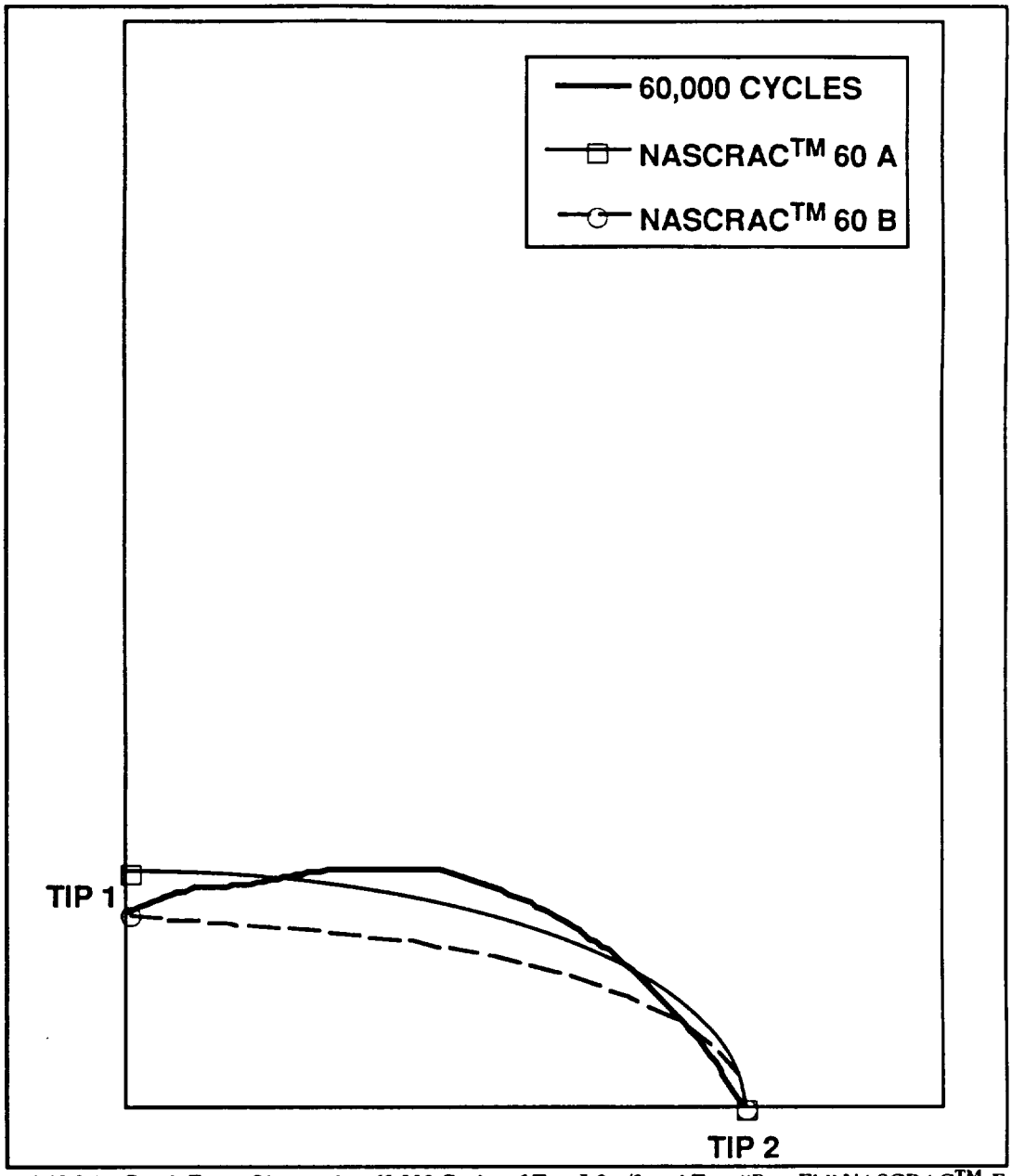

Figure 4.10.2-7. Crack Front Observed at 60,000 Cycles of Test I-2-a/2 and Two "Best Fit" NASCRAC™ Fronts

The crack front NASCRAC™ 60A is the quarter ellipse with the same crack tip 2 location and depth into the beam as observed in the 60,000 cycle front. The crack front NASCRAC™ 60B is the quarter ellipse with the same crack tip 1 and crack tip 2 locations as observed in the 60,000 cycle crack front.

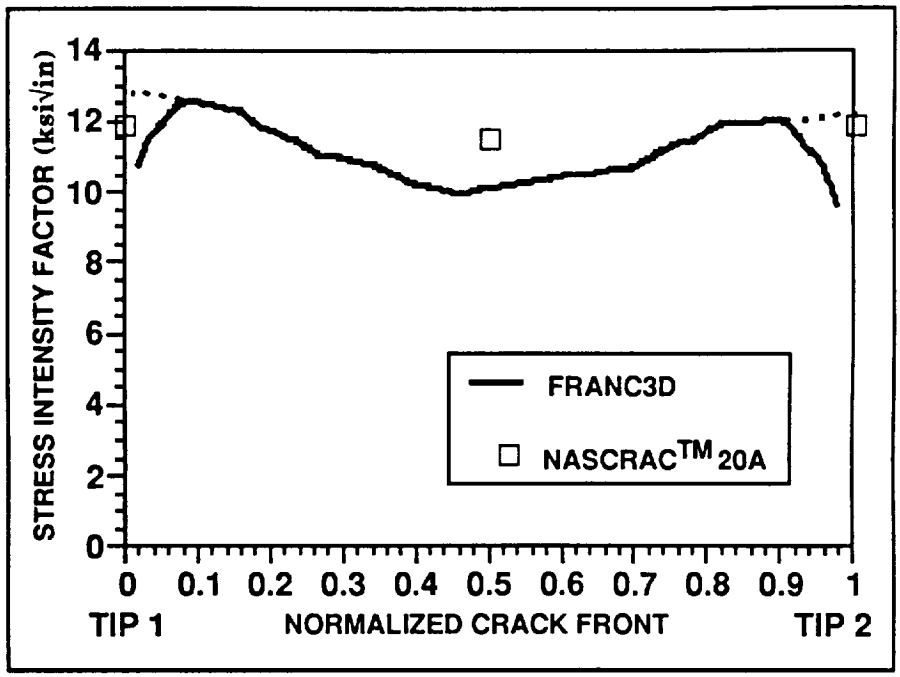

Figure 4.10.2-8. FRANC and NASCRAC Calculated SIF for 20,000-Cycle Front

The NASCRAC™ calculated stress intensity factors for front 20A were 20% greater than FRANC calculated stress intensity factors near the middle of the crack front. Some of this difference can be explained by RMS averaging. At crack tips 1 and 2, the two codes predicted similar stress intensity factors.

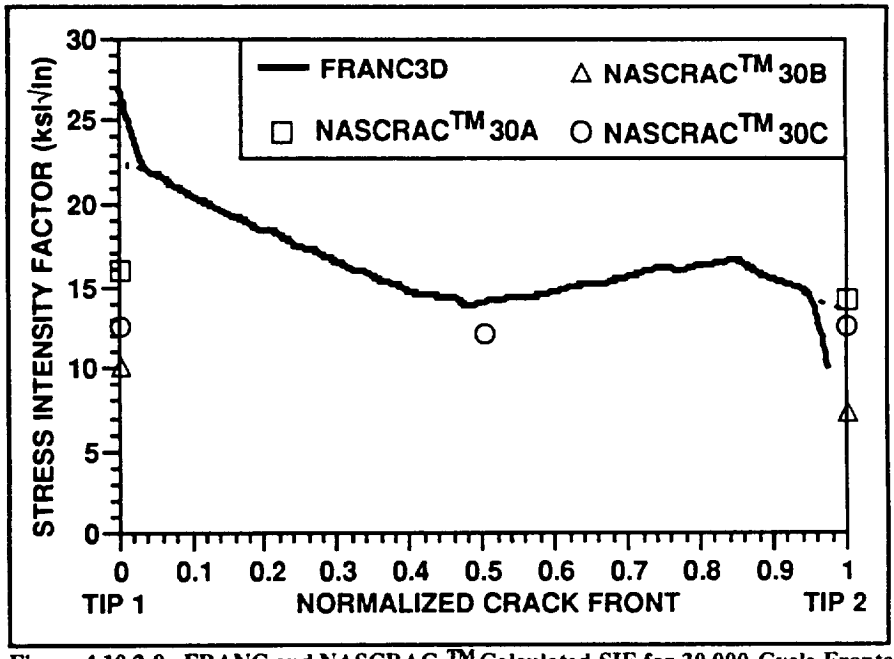

Figure 4.10.2-9. FRANC and NASCRAC ™ Calculated SIF for 30,000-Cycle Fronts

For the 30,000 cycle front, NASCRAC™ calculated stress intensity factors for all three "best fit" NASCRAC™ shapes were significantly different from the FRANC calculated stress

intensity factors near tip 1. NASCRAC™ calculated stress intensity factors for fronts 30A and 30C are close to FRANC calculated stress intensity factors near tip 2. NASCRAC™ calculations for front 30B are not close to FRANC calculated stress intensity factors at either crack tip.

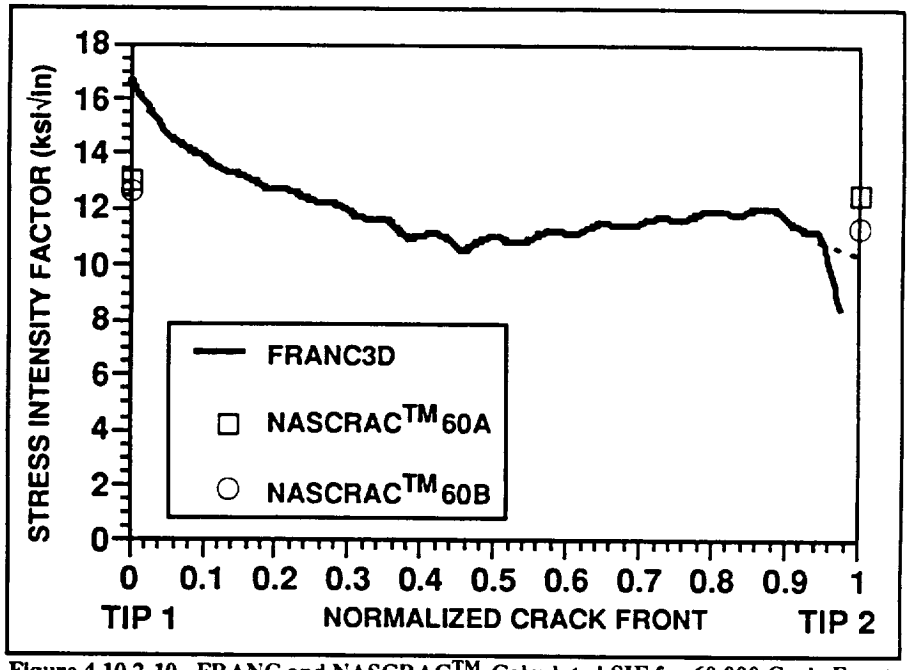

Figure 4.10.2-10. FRANC and NASCRAC™ Calculated SIF for 60,000 Cycle Fronts

NASCRAC™. calculated stress intensity factors for front 60A and 60B are within approximately 10% of FRANC calculated stress intensity factors for the 60,000-cycle crack front near tip 2. The difference between NASCRAC™. calculated stress intensity factors for front 60A and 60B and FRANC calculated stress intensity factors for the 60,000 cycle crack front near tip 2 is approximately 20% to 30%.

Based on the observations of Figures 4.10.2-5 through 4.10.2-10, in particular Figures 4.10.2-6 and 4.10.2-9, the following conclusion can be drawn: **[Some naturally occurring fatigue cracks cannot be modeled by elliptical or straight through cracks.]**

Test series I-2-a was designed to validate NASCRAC™ *fatigue crack propagation with transition* capabilities. Tests from this series have been described in Section 4.5.2.3. Aspects of these tests that specifically deal with crack transitioning will be described in this section. The geometry of these tests are defined in Figure 4.10.2-2. The load parameters, Δp and R-ratio are defined in Figure 4.10.2-3. Average values for these tests are given in Table 4.10.2-2.

Two transitions occur in each of these tests. The first transition occurs when crack tip 1 reaches corner α. The second transition occurs when crack tip 2 reaches corner β. The numbers of cycles before the transitions, denoted l_1 and l_2, are calculated by passing a quadratic polynomial through the crack lengths observed in the two 5000 cycle intervals prior to transition and the first

5000 cycle interval after transition. The number of cycles when the crack tip is at the corner is interpolated from this polynomial.

Experimentally observed and NASCRAC™ predicted crack lengths for these tests are shown in Figures 4.10.2-11 through 4.10.2-13. The crack lengths plotted in these Figures are defined in Figure 4.10.2-2. These definitions do not coincide with NASCRAC™ defined crack lengths, which change throughout the course of the test, and are not applicable to some observed shapes. The NASCRAC™ analysis was performed using the input given in Table 4.10.2-3. This is the same analysis performed for Section 4.5.2.3.

Table 4.10.2-2. Average Dimensions for Test Series I-2-a

NUMBER OF TESTS		14
DIMENSION	AVERAGE VALUE	UNITS
$a1(0)$	0.254	INCHES
$a2(0)$	0.254	INCHES
$a3(0)$	0.256	INCHES
$b1$	2.000	INCHES
$b2$	1.500	INCHES
$b3$	2.408	INCHES
b^*	0.497	INCHES
Δp	11.48	kips
R-ratio	0.217	-
$l1$	55,605	CYCLES
$l2$	107,398	CYCLES

Table 4.10.2-3. NASCRAC™ Input for Analysis of Test Series I-2-a

	NASCRAC™ INPUT	VALUE	CORRESPONDING TEST DIMENSION
MODEL	702		I-2-a
GEOMETRY	a1	0.256	$a3(0)$
	a2	0.254	$a1(0)$
	a3	0.254	$a2(0)$
	W1	2.000	$b1$
	W2	0.497	b^*
	W3	1.003	$b2$- b^*
LOADING	TRANSIENT 1 RANGE: EQ. B R-RATIO:	1000 CYCLES 13.82, -13.82 0.217	FATIGUE LOADS: FIGURE 4.5.2-1 TABLE 4.5.2.2-1
	BLOCK	1 X TRANSIENT 1	
MATERIAL PROPERTIES	2219-T851 Al L-T, T-L 75F	Alum3 #104	2219-T851 Al LAB AIR

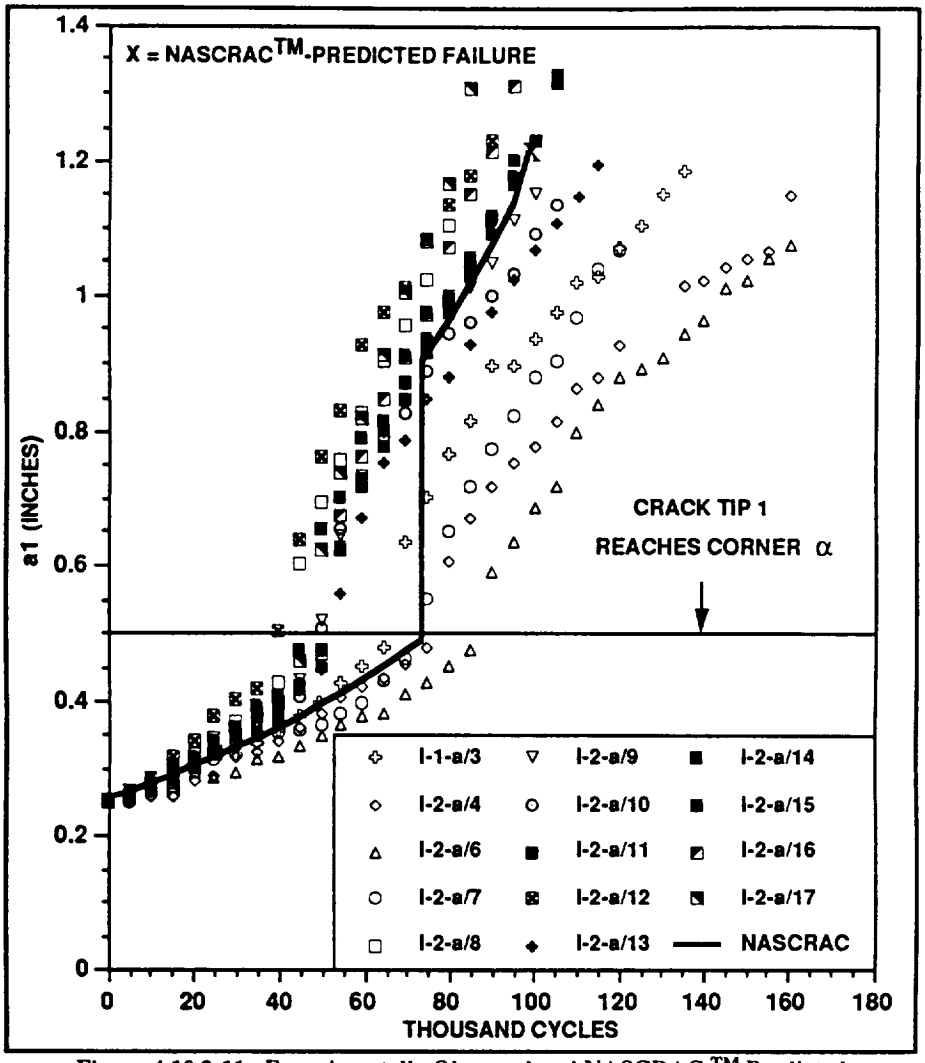

Figure 4.10.2-11. Experimentally Observed and NASCRAC ™ Predicted Crack Length *a*1 Versus Cycles for Test Series I-2-a

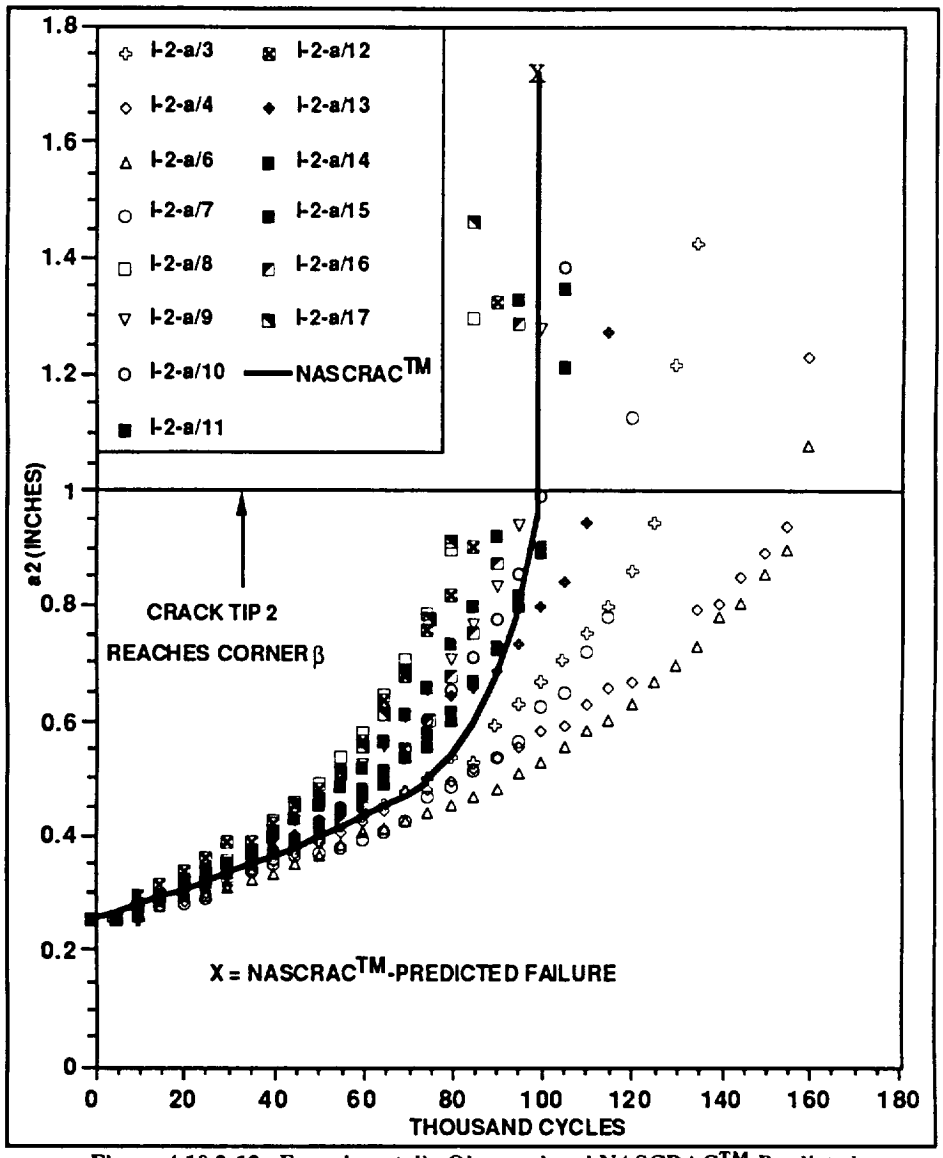

Figure 4.10.2-12. Experimentally Observed and NASCRAC™ Predicted Crack Length *a*2 Versus Cycles for Test Series I-2-a

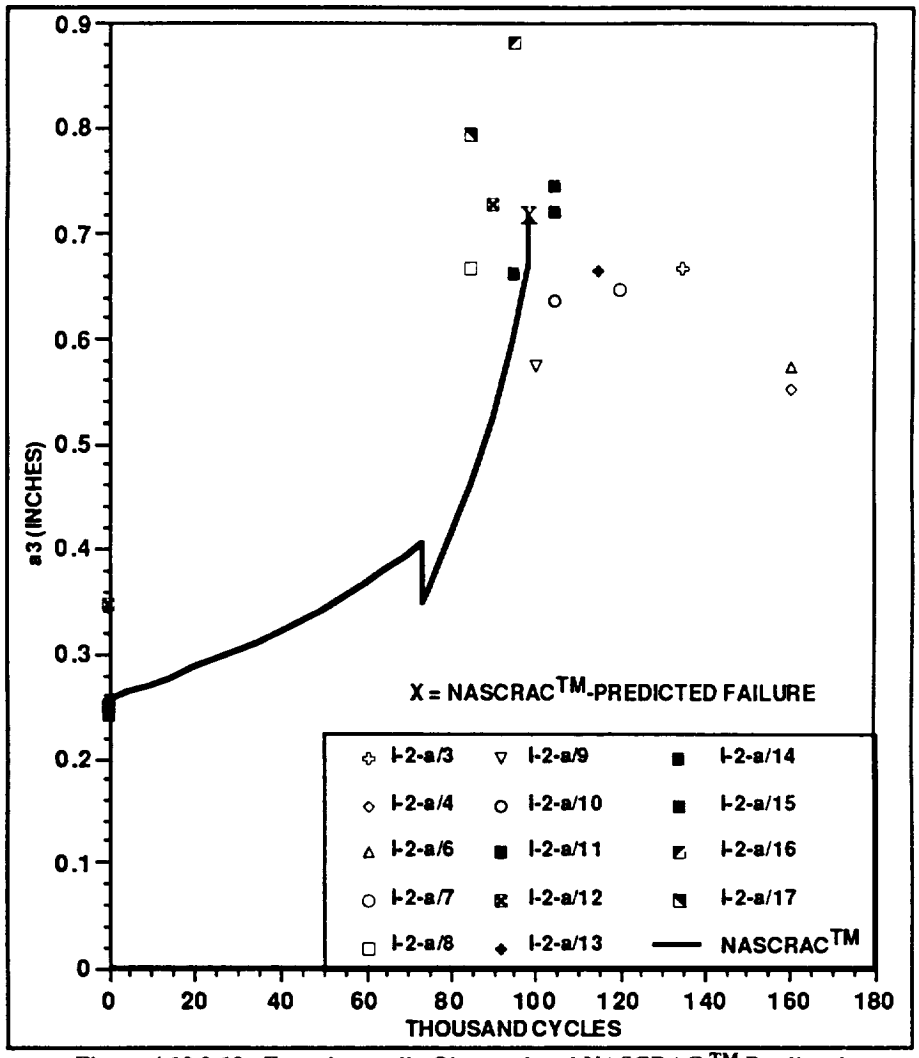

Figure 4.10.2-13. Experimentally Observed and NASCRAC™ Predicted Crack Length *a*3 Versus Cycles for Test Series I-2-a

NASCRAC™. predicts discontinuous crack lengths, as defined in Figure 4.10.2-2. At each transition, the NASCRAC™. predicted shape "jumps" to the next shape, as described in Table 4.10.1-1. This transition is assumed to occur in one cycle. At the first transition, NASCRAC™. predicted a_1 increases, while a_3 decreases. At the second transition, NASCRAC™. predicted crack lengths a_2 and a_3 increase. The transition parameter f_i is intended to be used to adjust for discontinuities at the first transition. For the simulations shown in Figures 4.10.2-10 through 4.10.2-12, f_i = 1.0 was used. Using a larger valve of f_i for the first transition will decrease the amount that a_3 decreases, but increase the amount that a_1 increases.

In practice, there will be a number of cycles in which the crack is in a "transition phase" and cannot be described well by elliptical crack fronts. The NASCRAC™. theory manual states that it is conservative to predict fatigue life by assuming a one-cycle transition [2]. Therefore, increasing f_i above 1.0, which increases the size of the post-transition crack, is unnecessary. Using $f_i < 1.0$ could compensate for cycles not predicted during the transition phase by predicting a

smaller post-transition crack. However, the number of cycles that the real crack is in the "transition phase" will usually be unknown. **[Therefore, a crack transition factor other than 1.0 should not be used unless the user has a documented basis for the choice.]**

Experimentally observed lower bound, median, mean and upper bound values of l_1 and l_2 are given in Table 4.10.2-4. To determine how much of the fatigue life was spent in the transition phase, the modified Forman parameter, C, was varied to fit NASCRAC™. predicted l_1 to the four experimentally observed values of l_1. NASCRAC™. predicted l_1 and l_2, as functions of C are shown in Figure 4.10.2-14. Except for transient 1, which was reduced to 200 cycles to allow better resolution of NASCRAC™ predicted transitions, all other NASCRAC™. input was the same as that given in Table 4.10.2-3. Table 4.10.2-5 shows the values of C that produced the four desired values of NASCRAC™. predicted l_1, and the corresponding NASCRAC™. predicted l_2. This fit compensates bias in NASCRAC™. predictions. The values of C given in Table 4.10.2-5 are not intended to be true upper bound, mean, median or lower bound values of the modified Forman parameter. Rather, these are values that produced the desired NASCRAC™. predictions for this test series.

Table 4.10.2-4. Experimentally Observed Number of Cycles before Transition, Series I-2-a

	l_1	l_2
	(THOUSAND CYCLES)	(THOUSAND CYCLES)
LOWER BOUND	41.8	81.7
MEDIAN	50.8	100.9
MEAN	55.6	107.4
UPPER BOUND	86.4	158.2

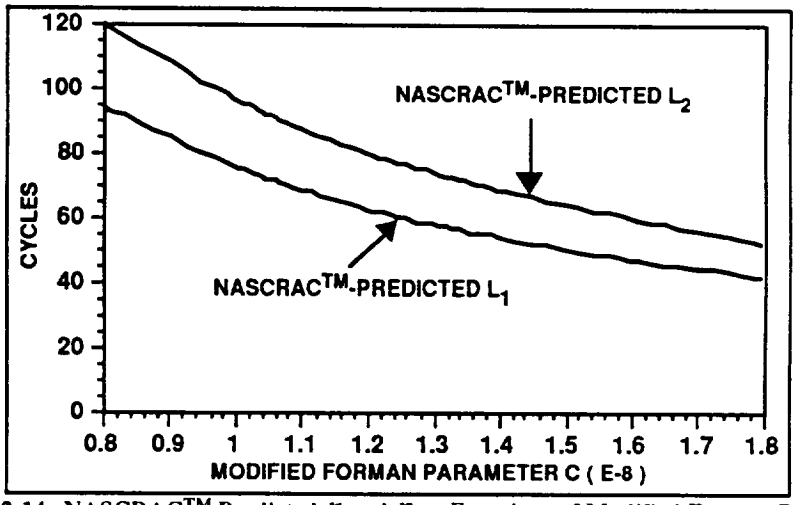

Figure 4.10.2-14. NASCRAC™ Predicted l_1 and l_2 as Functions of Modified Forman Parameter, C

Table 4.10.2-5 NASCRAC ™ Predicted l_1 and l_2 for Various Values of Modified Forman parameter, C

C	l_1	l_2	DIFFERENCE FROM OBSERVED l_2	
	(THOUSAND CYCLES)	(THOUSAND CYCLES)	(THOUSAND CYCLES)	(% of OBSERVED l_2)
1.788E-8	41.8	53.6	28.1	34
1.475E-8	50.8	65.2	35.2	35
1.350E-8	55.6	71.2	36.2	34
0.868E-8	86.4	110.8	47.4	30

If NASCRAC™ predicted l_1 matches the experimentally observed l_1, it was assumed that the major source of error in NASCRAC™ predicted l_2 was the cycles not counted during the transition phase. Therefore, comparing NASCRAC™ predicted l_2 with the corresponding experimentally observed l_2 provided an estimate of the number of cycles spent in the transition phase. For the four sets of l_1 and l_2, the absolute difference between the NASCRAC™ predicted and experimentally observed l_2 varied. However, the difference between NASCRAC™ predicted and experimentally observed l_2 was between 30 and 35% of the experimentally observed l_2 for all four cases. Based on this observation, the following conclusion can be made: **[Approximately 30 to 35% of the experimentally observed cycles before the second transition in Test Series I-2-a was spent in the "transition phase" of fatigue life that is not modeled by NASCRAC™.]**

4.10.3 REFERENCES FOR SECTION 4.10

1. *NASCRAC™ User's Manual, Failure Analysis Associates, prepared for NASA/Marshall Space Flight Center, Palo Alto, CA, 1989.*

2. *NASCRAC™ Theory Manual, Failure Analysis Associates, prepared for NASA/Marshall Space Flight Center, Palo Alto CA, 1989.*

4.11 OVERLOADS

This section describes the verification and validation testing of NASCRAC™'s [*fatigue crack growth retardation*]. Fatigue crack growth models for constant amplitude loading can be insufficient to model crack growth for spectrum loading due to the increased size of the plastic zone surrounding the crack tip following an overload. Two models, Wheeler and Willenborg, are incorporated into NASCRAC™ to model crack growth due to varying amplitude load cycles.

4.11.1 VERIFICATION OF NASCRAC™ *FATIGUE CRACK GROWTH RETARDATION* CAPABILITY

In the Wheeler model, retardation is determined using a ratio of the current plastic zone and the plastic zone due to the overload. The Wheeler model [2] is depicted in Figure 4.11.1-1 where a_0 is the crack length at the time of the overload, r_0 is the plastic zone radius (diameter) caused by the overload, a is the current crack length, and r is the plastic zone radius corresponding to the current crack length and load. The Wheeler model assumes that the calculated crack growth rate da/dN (calculated using a standard da/dN equation such as the Paris equation) will be reduced by a factor ϕ^n where ϕ is the ratio of the current plastic zone radius to the remaining overload plastic zone radius ($a_0 + r_0 - a$) and n is a material dependent parameter. When ϕ is calculated to be greater than one, i.e., when the current plastic zone radius reaches or exceeds the boundary of the overload plastic zone, ϕ is set equal to unity and retardation ceases until another overload occurs. This model can predict crack growth retardation but not acceleration.

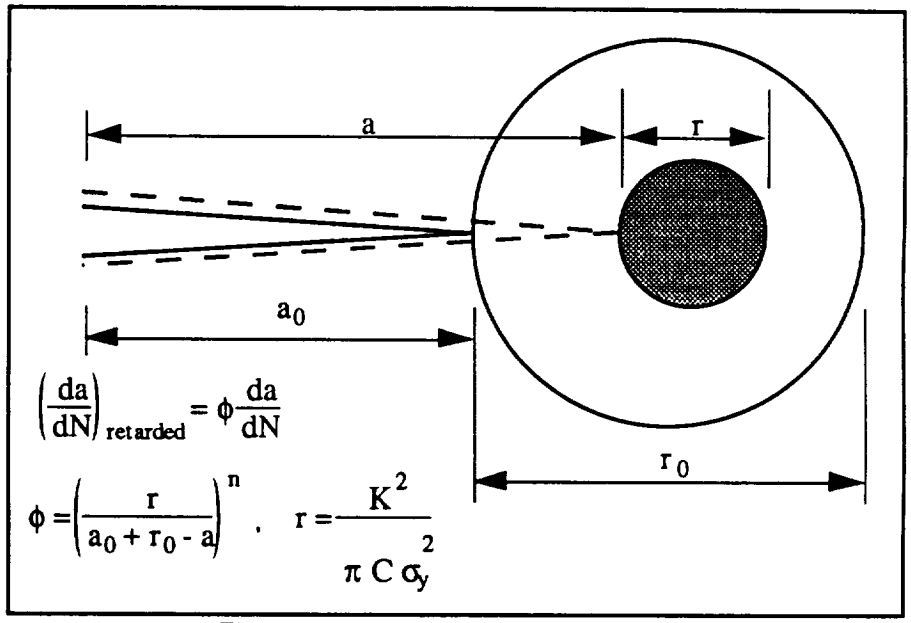

Figure 4.11.1-1. Wheeler Retardation Model

The Willenborg model uses effective stress intensity values and an effective R ratio to predict retarded crack growth [1]. Figure 4.11.1-2 displays the Willenborg concept. In Figure 4.11.1-2, r_{req} is the plastic zone radius required to reach the overload plastic zone boundary, a_0 is the crack length at the time of the overload, a is the current crack length, and r is the plastic zone radius corresponding to the current crack length and load.

The model is based on determining the stress intensity value, K_{req}, required for the current plastic zone radius to reach the overload plastic zone boundary. K_{req} is used to calculate a stress intensity reduction factor K_{red}. This reduction factor is subtracted from the current K to determine an effective K, i.e., K_{eff} for both maximum and minimum values of K in a cycle. If an effective stress intensity value is calculated to be less than zero, it is set equal to zero. With this approach, ΔK_{eff} equals ΔK unless K_{min} is set to zero. Using $K_{eff\text{-}max}$ and $K_{eff\text{-}min}$, an effective R ratio can be calculated. The effective values are used to calculate the retarded crack growth rate da/dN using a standard da/dN equation. In the Willenborg model, if the Paris equation is used to model da/dN, retardation effects are only evident when the zero assumption for K_{max_eff} and K_{min_eff} is invoked. This is because the Paris equation does not have an R dependency.

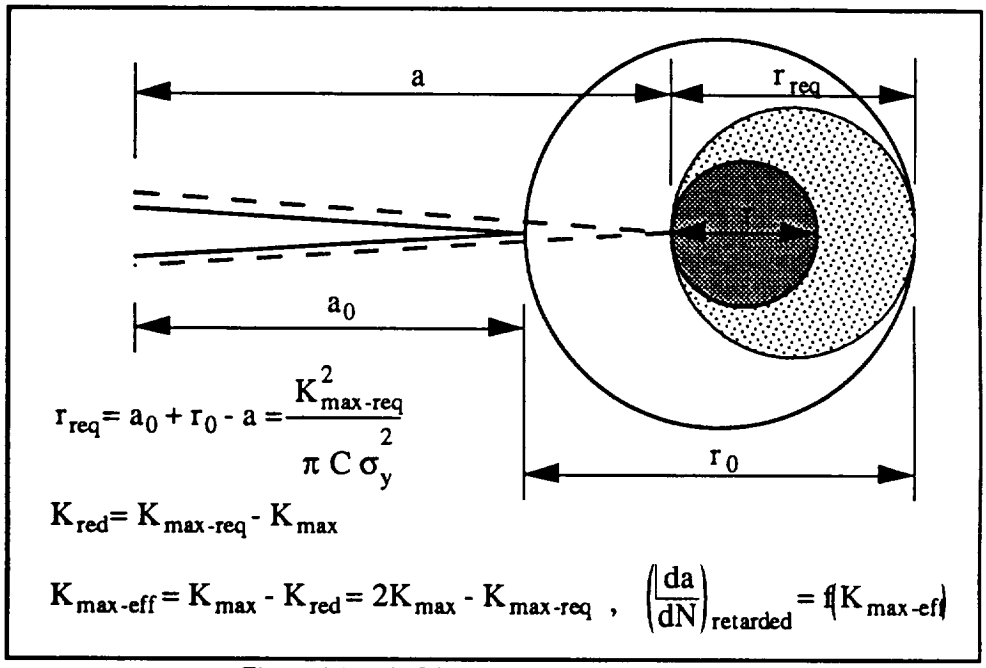

Figure 4.11.1-2. Willenborg Retardation Model

Table 4.11.1-1 presents results of a comparative study between retardation predicted by NASCRAC™ and an in-house FORTRAN code. The FORTRAN code included the Wheeler and Willenborg retardation models from [1]. In the study, the crack growth rate was calculated with the Paris equation where the Paris coefficient C_{Paris} was $1.07(10^{-8})$ and the Paris exponent m_{Paris} was 2.897. The Wheeler coefficient $C_{Wheeler}$ was set to 2.0 and the Wheeler exponent, $m_{Wheeler}$, was set to 1.3. The loading block consisted of a uniform 13.0 ksi tensile load followed by 100 cycles of a uniform 10 ksi tensile load. All loads had an R-ratio of 0. The specimen was a single edge crack in a plate (configuration 203 in NASCRAC™) with an initial crack length of 0.5", a plate width of 10.0", and a plate thickness of 1.0". The assumed material was 2219-T851 aluminum with a yield strength of 53 ksi, a Young's modulus of 10000 ksi, and a Poisson's ratio of 0.33. One difference between NASCRAC™ and the reference model was in the expression for plastic zone radius (r). The reference did not include π in its expression for r whereas NASCRAC™ included π in its expression. In all likelihood, the reference assumes π is

incorporated into $C_{Wheeler}$. In the study, identical values of $C_{Wheeler}$ and $n_{Wheeler}$ were used in NASCRAC™ and the FORTRAN code and the FORTRAN code included π in its r expression.

Table 4.11.1-1. Crack Retardation Results for NASCRAC™ and a FORTRAN Code

CYCLES	CRACK LENGTH a NO LOAD INTERACTION		CRACK LENGTH a WHEELER RETARDATION		CRACK LENGTH a WILLENBORG RETARDATION	
	NASCRAC™	FORTRAN	NASCRAC™	FORTRAN	NASCRAC™	FORTRAN
101	0.5025	0.5025	0.5013	0.5013	0.5010	0.5010
1010	0.5254	0.5254	0.5136	0.5136	0.5098	0.5099
2020	0.5528	0.5528	0.5277	0.5278	0.5200	0.5201
4040	0.6148	0.6148	0.5579	0.5582	0.5412	0.5415
10100	0.8872	0.8872	0.6673	0.6681	0.6140	0.6150
15150	1.322	1.322	0.7878	0.7895	0.6877	0.6895
17473	1.689	1.689	0.8560	0.8583	0.7265	0.7289
20200	na	na	0.9500	0.9532	0.7770	0.7801

4.11.2 VALIDATION OF NASCRAC™ ALGORITHM

In a previous effort at validating of the Wheeler and Willenborg retardation models, Schijve[3] concluded that "no systematic agreement with test results" was found. He also states that the models omit crack closure and accelerated growth effects. In general, Schijve concluded that the Wheeler and Willenborg models are simplistic and do not capture all the variables necessary to describe crack retardation. Broek[1] describes the models in detail and presents a favorable Wheeler/test comparison for a Wheeler exponent m = 1.3. Two series of tests are used to test the validity of NASCRAC™-crack growth retardation models; test series I-2-b and test series III-a. These tests are described in the following subsections.

4.11.2.1 Periodic Overloads

The geometry for test series I-2-b is given in Figure 4.11.2.1-1. The parameters that describe the load history of tests in this series are defined in Figure 4.11.2.1-2. This load series was repeated throughout the test. Average values for this test series are given in Table 4.11.2.1-1.

Two transitions occur in this test series. The first transition occurs when crack tip 1 reaches the corner α, as defined in Figure 4.11.2.1-1. The second transition occurs when crack tip 2 reaches corner β. The numbers of cycles before the two transitions are denoted l_1 and l_2. To calculate these values, a second order polynomial is passed through the crack lengths measured in the two observations prior to transition and the crack length measured in the first observation after transition. The number of cycles at which the crack tip reached the corner of the beam is interpolated from this polynomial.

Three NASCRAC™ analyses of Test Series I-2-b were performed. The input for these analyses is summarized in Table 4.11.2.1-2. In the first simulation, crack growth retardation was not accounted for. The crack growth predicted in the one overload cycle was negligible compared

to the crack growth predicted in the 999 nominal cycles. The other two analyses incorporated the Wheeler and Willenborg models, respectively, to model crack growth retardation.

Experimentally-observed and NASCRAC™-predicted crack lengths a_1, a_2 and a_3 are plotted versus cycles in Figures 4.11.2.1-3, 4.11.2.1-4 and 4.11.2.1-5. The definitions of crack lengths used in these comparisons are those given in Figure 4.11.2.1-1. These definitions do not correspond with NASCRAC™ definitions of crack length, which change throughout the test and are not applicable to some of the experimentally-observed crack shapes. This issue is addressed in greater detail in the Section 4.10.

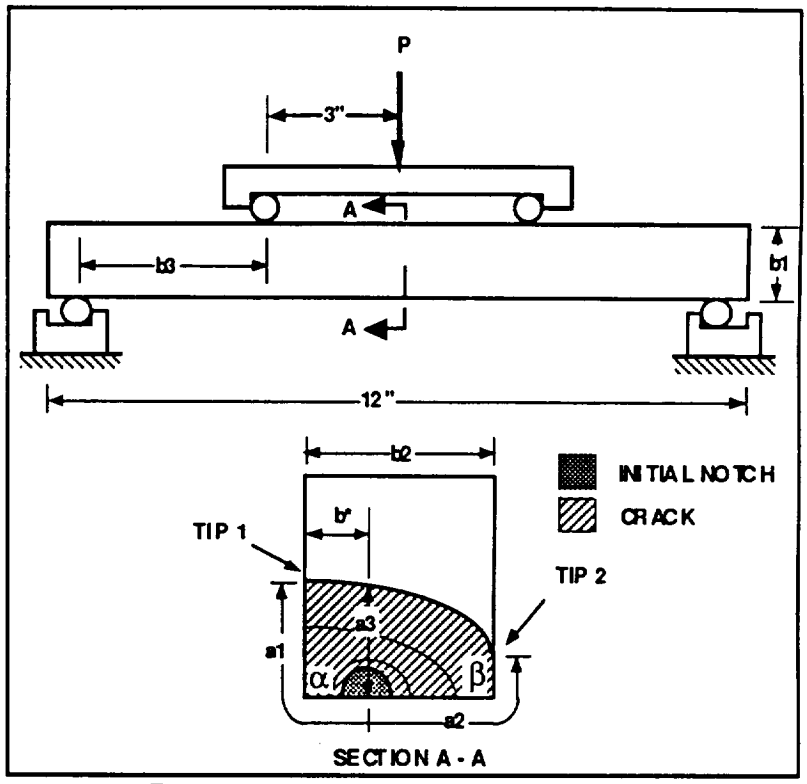

Figure 4.11.2.1-1. Geometry for Test Series I-2-b

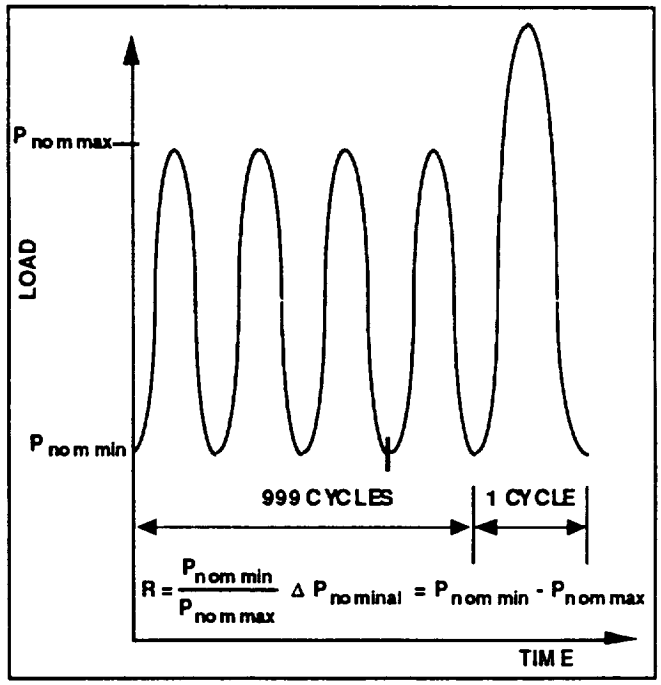

Figure 4.11.2.1-2. Definition of Load History for Test Series I-2-b

Table 4.11.2.1-1. Average Dimensions for Test Series I-2-b

NUMBER OF TESTS		2
DIMENSION	AVERAGE VALUE	UNITS
$a1(0)$	0.254	INCHES
$a2(0)$	0.254	INCHES
$a3(0)$	0.248	INCHES
$b1$	2.000	INCHES
$b2$	1.500	INCHES
$b3$	2.421	INCHES
b^*	0.508	INCHES
Δpnominal	11.51	kips
R-ratio	0.215	-
Poverload	19.45	kips
$l1$	92,281	CYCLES
$l2$	161,921	CYCLES

Table 4.11.2.1-2. NASCRAC™ Input for Analysis of Test Series I-2-b

	NASCRAC™ INPUT	VALUE	CORRESPONDING TEST DIMENSION
Model	702		I-2-b
GEOMETRY	a1	0.248	$a3(0)$
	a2	0.254	$a1(0)$
	a3	0.254	$a2(0)$
	W1	2.000	$b1$
	W2	0.508	b^*
	W3	0.992	$b2 - b^*$
LOADING	TRANSIENT 1 RANGE: EQ. B R-RATIO:	999 CYCLES 13.93, -13.93 0.215	LOAD HISTORY FIGURE 4.11.2.1-2 TABLE 4.11.2.1-1
	TRANSIENT 2 MAX: EQ. B MIN: EQ. B	1 CYCLE 23.54, -23.54 3.63, -3.63	
	BLOCK	1 X TRANSIENT 1 1 X TRANSIENT 2	
MATERIAL PROPERTIES	2219-T851 Al L-T & T-L 75F	ALUM3 #104	2219-T851 AL LAB AIR
	SIGYS	53	
	YOUNGS	10,000	
	POISSN	0.33	
	$N_{Wheeler}$	1.3	
	$C_{wheeler}$	2.0	

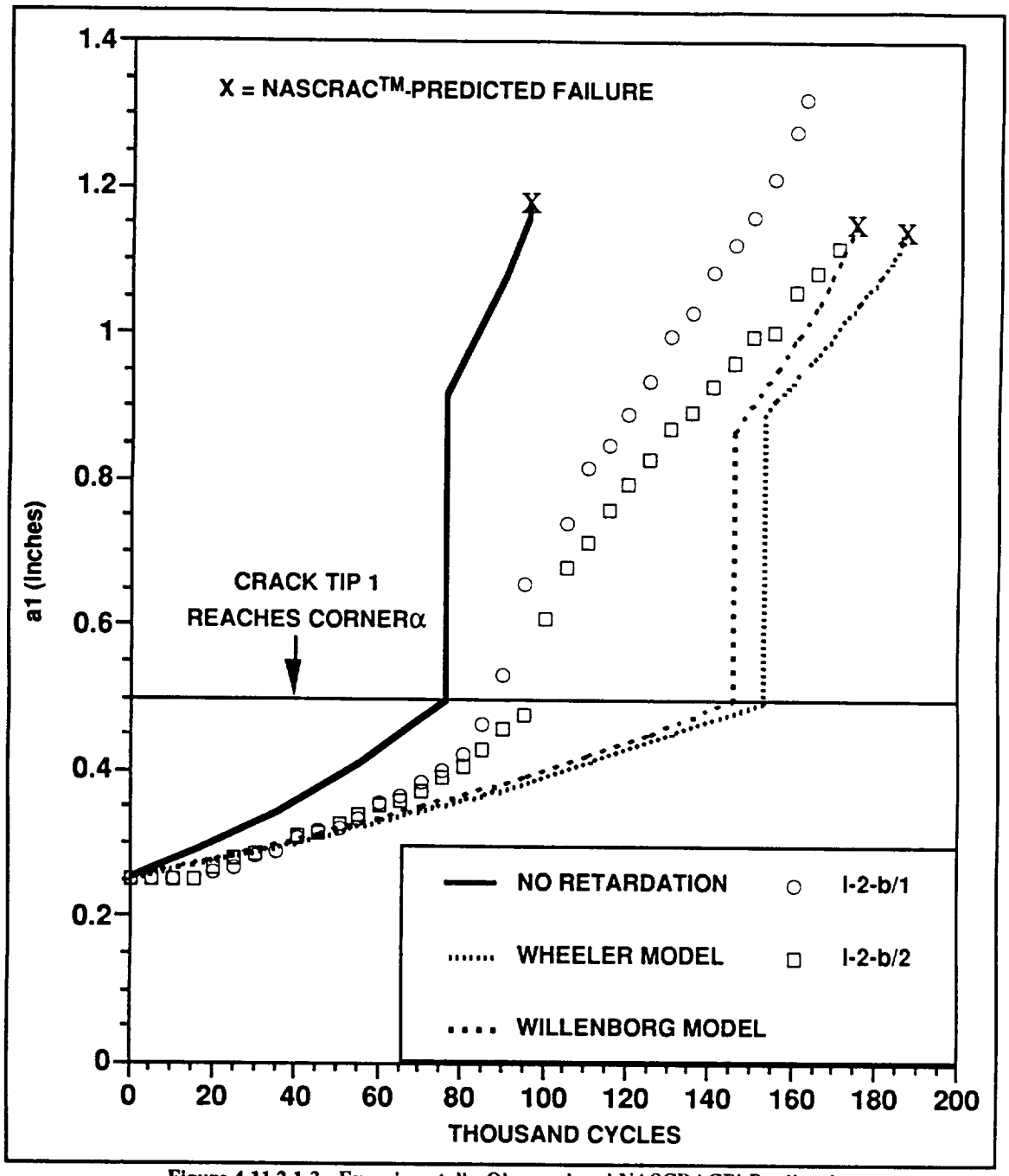

Figure 4.11.2.1-3. Experimentally-Observed and NASCRAC™-Predicted Crack Length *a*1 Versus Cycles for Test Series I-2-b

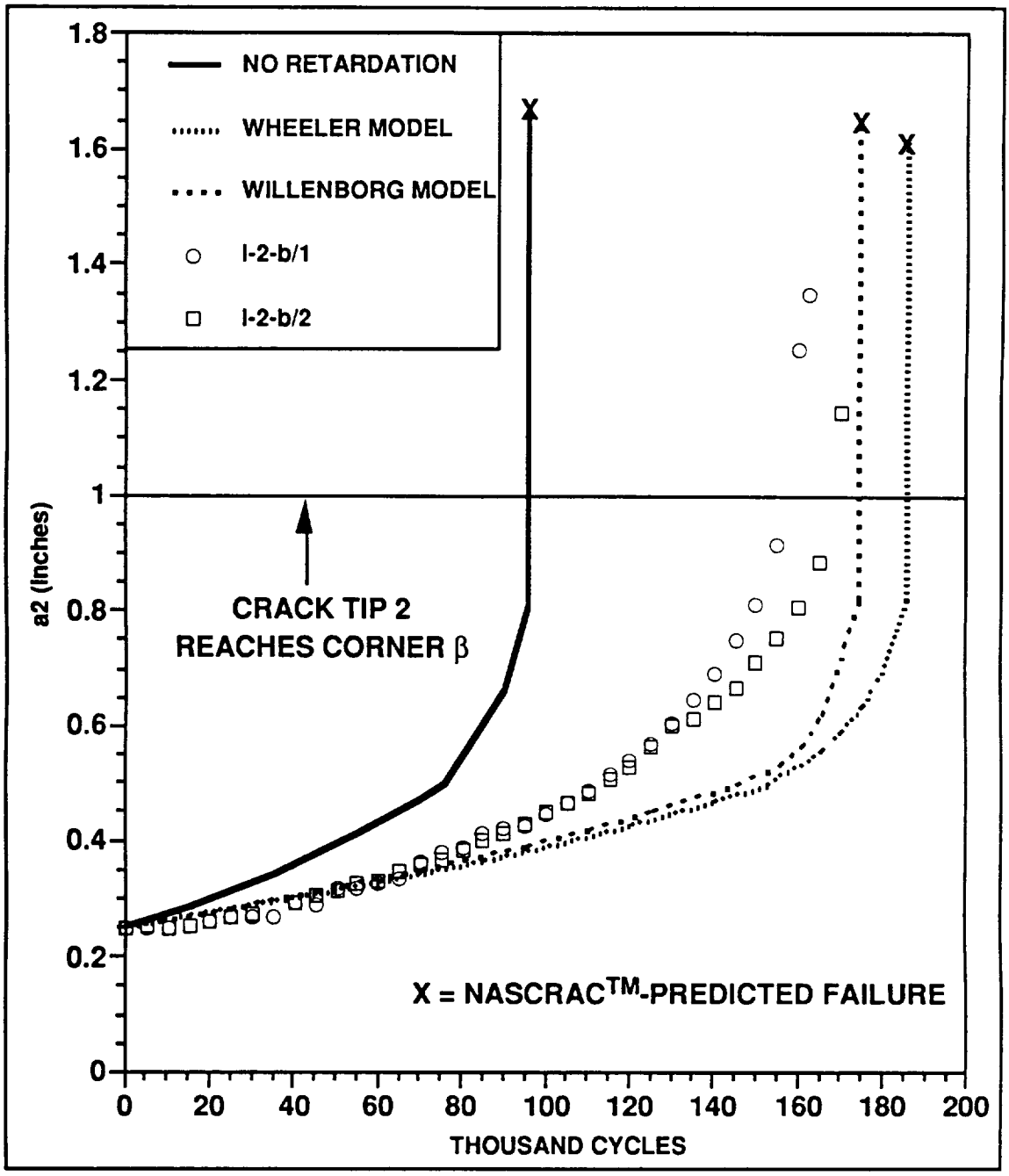

Figure 4.11.2.1-4. Experimentally-Observed and NASCRAC™-Predicted Crack Length *a*2 Versus Cycles for Test Series I-2-b

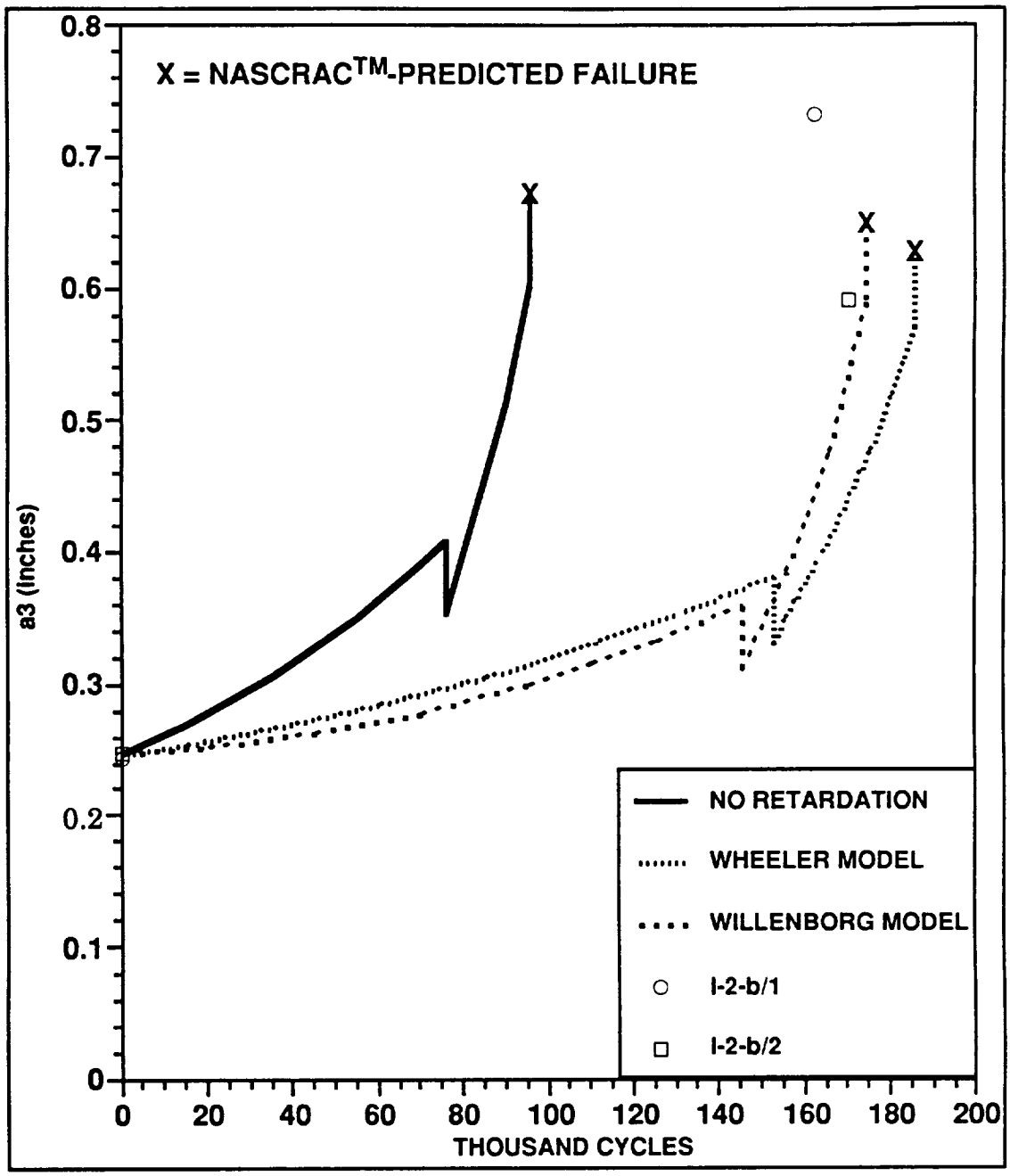

Figure 4.11.2.1-5. Experimentally-Observed and NASCRAC™-Predicted Crack Length *a*3 Versus Cycles for Test Series I-2-b

Except for the overload, this test series is similar to Test Series I-2-a. For a given number of cycles, the crack lengths observed in test series I-2-b were less than the smallest cracks observed in test sereis I-2-a. This observation indicates that crack retardation occurred in test series I-2-b.

The NASCRAC™ analyses that use the Wheeler or Willenborg retardation models are collectively referred to as the retarded NASCRAC™ analyses. The NASCRAC™ analysis that did not incorporate retardation is referred to as the non-retarded NASCRAC™ analysis. The two

retarded NASCRAC™ analyses predict the first transition within 7000 cycles of each other, and the second transition within 11,000 cycles. The two retardation models do not necessarily predict similar crack growth for all spectrum load histories.

The retarded NASCRAC™-predicted crack growth rates are close to the experimentally-observed crack growth rates for the first approximately 60,000 fatigue cycles. As crack tip 1 approaches corner α, as defined in Figure 4.11.2.1-1, the experimentally-observed crack growth rate increases. The retarded NASCRAC™ analyses do not predict this increased crack growth rate. As a result of this discrepancy, the non-retarded NASCRAC™-predicted l_1 is closer to experimentally-observed l_1 than the two retarded NASCRAC™-predicted l_1 are.

Following the second transition, retarded NASCRAC™-predicted crack length a_1 catches up to the experimentally-observed crack length a_1. The closeness of retarded NASCRAC™-predicted and experimentally-observed crack lengths a_1 following the second transition should be considered the result of compensating errors. NASCRAC™ transition methodology is analyzed in Section 4.10.

The effect of yield stress on NASCRAC™-predicted l_2 and l_2 was studied. Except for yield stress, the input for the analyses used in this study were the same as that given in Table 4.11.2.1-1. The NASCRAC™-predicted l_1 and l_2 are shown as functions of yield stress in Figure 4.11.2.1-6. In these analyses, the Willenborg model is more sensitive to changes in yield stress than the Wheeler model.

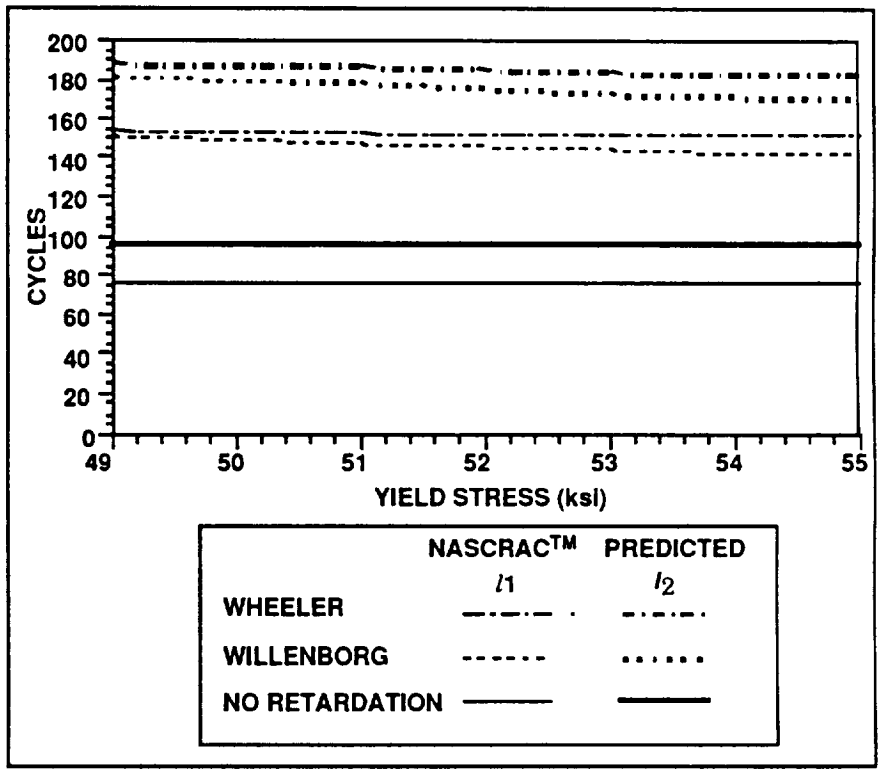

Figure 4.11.2.1-6. Sensitivity of NASCRAC™-Predicted Life to Yield Stress

In summary, the following conclusions regarding these tests can be made:

- Retardation affects the crack growth rate in this test series.

- At some parts of the fatigue life, both the Wheeler and Willenborg models predict crack growth better than the nonretarded crack growth model does.

- Discrepancies between crack growth rates predicted with the Wheeler and Willenborg retardation models and experimentally-observed crack growth rates result in NASCRAC™-predicted number of cycles before the first transition, l_1, approximately 60% greater than the experimentally observed l_1.

4.11.2.2 Single Overload

Test series III was designed to test NASCRAC™ proof test logic. This test series consisted of three stages. Stage I was constant amplitude fatigue loading, and is described in Section 4.5.2.4. Stage II was a near-failure proofload, and is described in Section 4.8. Fatigue crack growth observed in stage 3 is described in this subsection. The tests as a whole are described in section 4.7. The retardation of fatigue crack growth in stage 3 due to the proofload in stage 2 is discussed in this subsection.

The geometry for this test series is given in Figure 4.11.2.2-1. Parameters that define the load history are defined in Figure 4.11.2.2-2. The fatigue loads in stage 3 were applied with the four point bend configuration. In some tests, the proofload was applied in a three point bend configuration. In the remaining tests, the proofload was applied in a four point bend configuration. The magnitude of the applied load, P, varied. The size of the crack when the proofload was applied also varied. For the purposes of this subsection, the most consistant measure of the magnitude of the proofload was assumed to be the NASCRAC™-calculated K at crack tip 2.

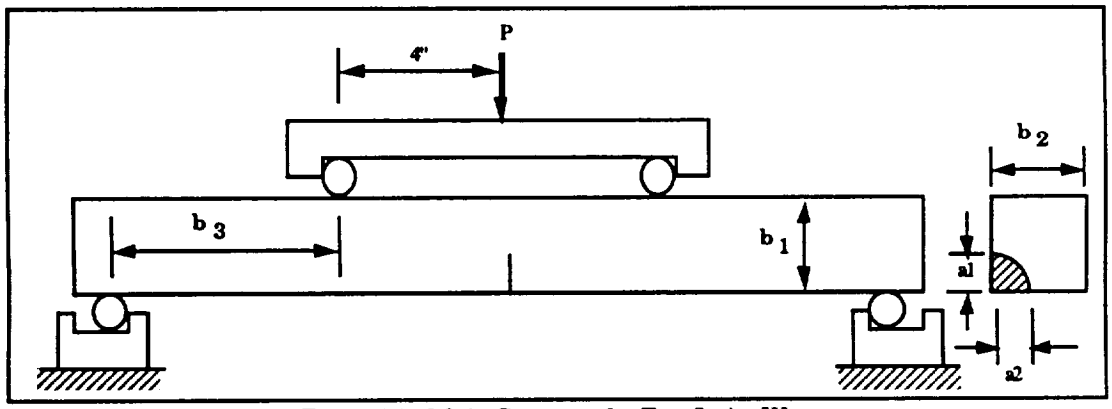

Figure 4.11.2.2-1. Geometry for Test Series III-a

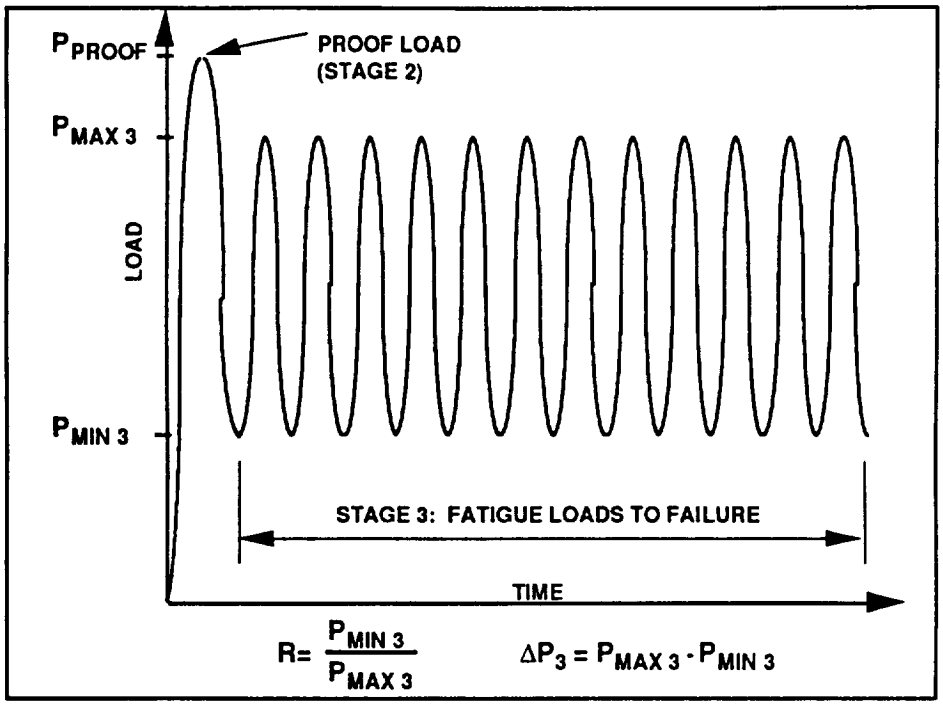

Figure 4.11.2.2-2. Definition of Load History for Stages 2 and 3 of Tests Series III-a

Table 4.11.2.2-1. Average Dimensions for Stages 2 and 3 of Test Series III-a

NUMBER OF TESTS		
DIMENSION	AVERAGE VALUE	UNITS
*a*1(STAGE 2)	0.795	INCHES
*a*2(STAGE 2)	1.160	INCHES
*b*1	3.001	INCHES
*b*2	3.001	INCHES
*b*3	3.001	INCHES
Δp_3	20.89	kips
R-RATIO	0.2294	-

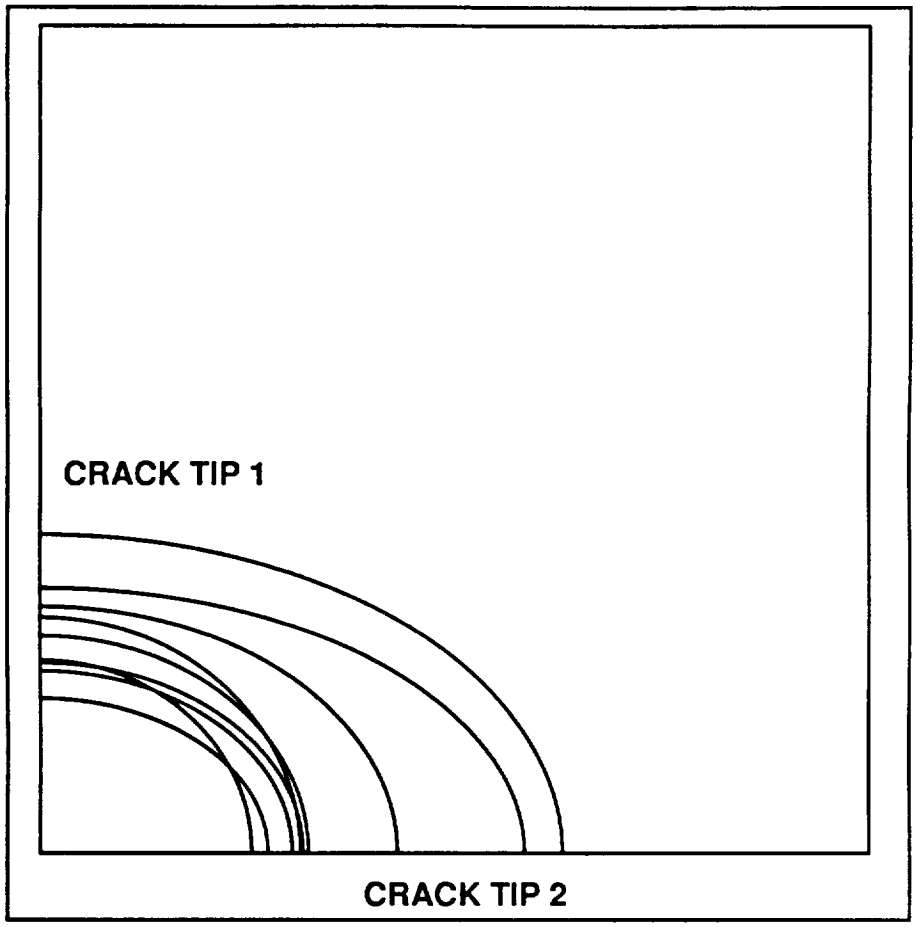

Figure 4.11.2.2-3. Crack Sizes at Beginning of Stage 2 of Test Series III

Because of the large difference in crack size at the beginning of Stage 2, two standard measures of retardation, υ_1 and υ_2, are defined.

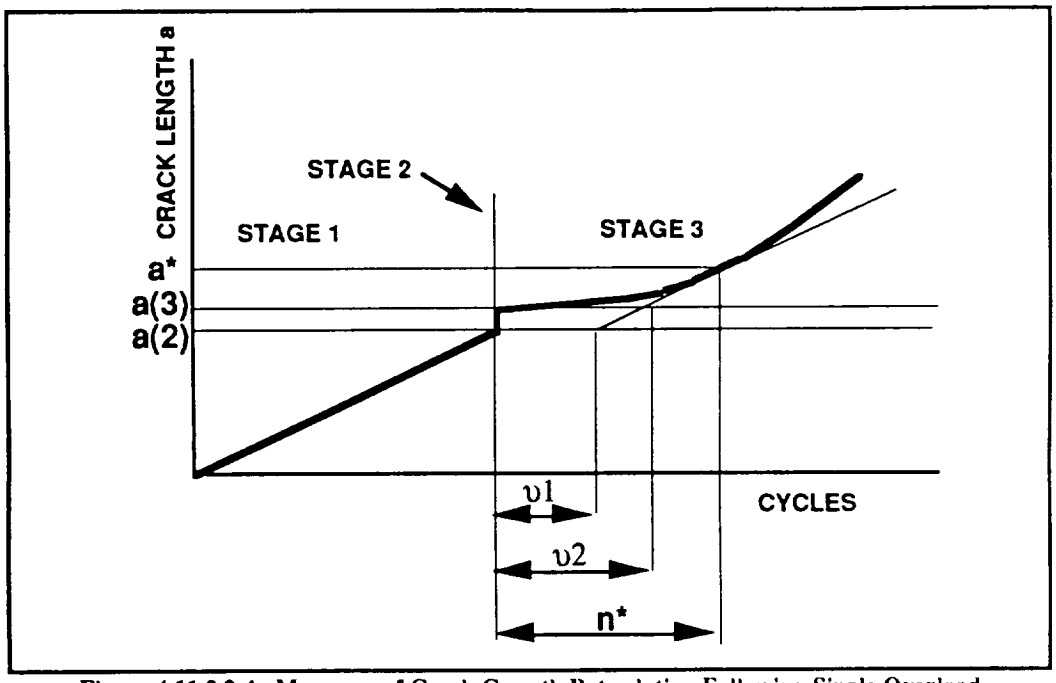

Figure 4.11.2.2-4. Measures of Crack Growth Retardation Following Single Overload

The procedure for calculating the two measures, as shown in Figures 4.11.2.2-3, is as follows:

(1) The number of cycles after the proofload, n*, where the observed crack growth rate of tip 2 equals the crack growth rate observed at tip 2 just prior to the application of the proofload is found. The crack length a_2 at this number of cycles is denoted a^*.

(2) The number of cycles required to grow the crack from the a_2 observed before the proofload, denoted $a(2)$ in Figure 4.11.2.2-3, to a^* at the crack growth rate observed prior to the proofload is calculated. This number is subtracted from n* to obtain υ1.

(4) The number of cycles required to grow the crack from the a_2 observed imediately after the proofload, denoted $a(3)$ in Figure 4.11.2.2-3, to a^*, at the crack growth rate observed prior to the prrofload is calculated. This number is subtracted from n* to obtain υ2.

Other measures of retardation could have been defined. For instance, the same procedure could be followed for crack tip 1. Different definitions of retardation would change the number of cylces of retardation calculated. However, the trends observed for this definition would be similar for many other definitions of retardation.

In this test series, the variation in crack sizes and applied proof loads preclude useful discussion of test averages. Therefore, a NASCRAC™ analysis was performed for each test in this series. These analyses are summarized in Table 4.11.2.2-2. The loading in the analyses

consisted of three components: 1) the last fatigue cycle in stage 1, which was used to calculate the pre-proof load crack growth rate, 2) the proof load applied to the test, and 3) the average stage 3 fatigue loads applied to NASCRAC™-predicted failure.

Table 4.11.2.2-2. Input for NASCRAC™ Analsyses of Retardation in Stage 3 of Test Series III-a

	NASCRAC™ INPUT	VALUE	CORRESPONDING TEST DIMENSION
MODEL	605		III-a
GEOMETRY	a1	VARIED	*a*1
	a2	VARIED	*a*2
	W1	3.001	*b*1
	W2	3.001	*b*2
LOADING	TRANSIENT 1 RANGE: EQ. B R RATIO	1 CYCLE 14.06, -9.37 0.2319	STAGE 1 LOADING
	TRANSIENT 2 MAX: Eq. B R	1 CYCLE VARIED 0	STAGE 2 LOADING FIGURE 4.11.2.2-2
	TRANSIENT 3 RANGE: Eq. B R	5000 CYCLES 14.01, -9.34 0.2294	STAGE 3 LOADING FIGURE 4.11.2.2-2 TABLE 4.11.2.2-1
	BLOCK	1 X TRANSIENT 1 1 X TRANSIENT 2 TRANSIENT 3 REPEATED TO FAILURE	
MATERIAL PROPERTIES	2219-T851 Al L-T, T-L 75F	ALUM3 #104	2219-T851 Al LAB AIR

Due to experimental erors, $\upsilon 1$ and $\upsilon 2$ were not available for all tests in this series. For each test in which $\upsilon 1$ and $\upsilon 2$ were available, experimentally-observed values of $\upsilon 1$ and $\upsilon 2$ were within 7000 cycles of each other and NASCRAC™-predicted values of $\upsilon 1$ and $\upsilon 2$ were within 600 cycles of each other. Therefore, only $\upsilon 1$ will be discussed in the remainder of the section.

In Figure 4.11.2.2-4, the two retardation measures are plotted versus applied proofload in terms of the NASCRAC™ calculated stress intensity factor at tip 2, K(2). The various specimens have different initial crack sizes, which would affect any relationship between applied K and retardation.

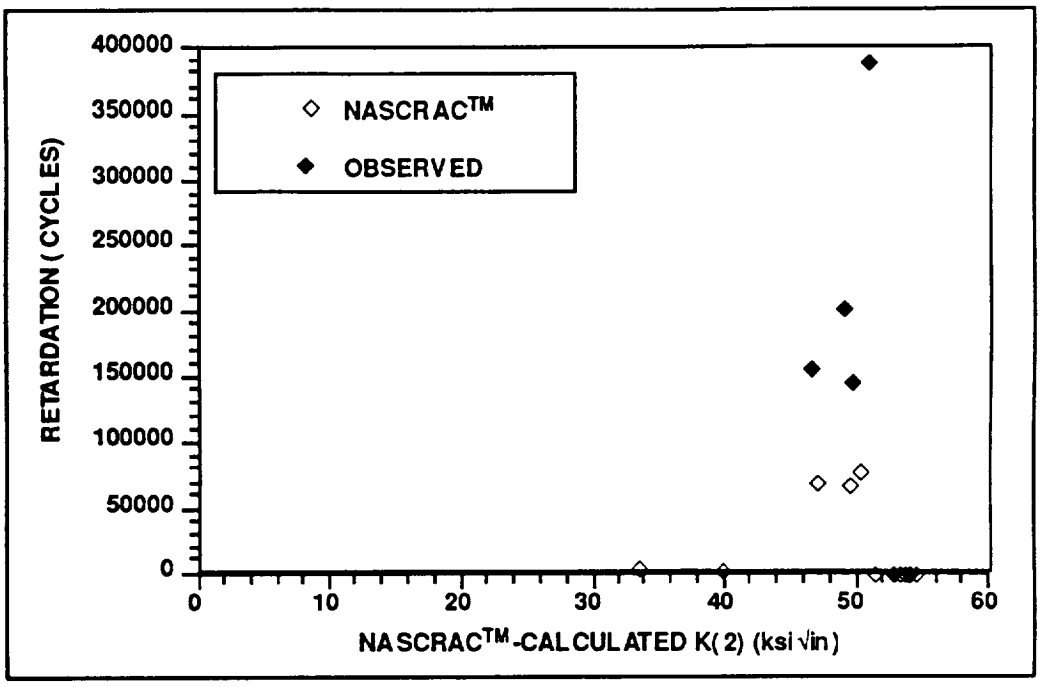

Figure 4.11.2.2-5. Retardation Versus Maximum K_2 Applied During Overload

The proof tests were designed to investigate remaining life following a near-ultimate-capacity-overload. For this geometry, the failure load for the crack sizes tested was near or at the load required for gross section plasticity. Therefore, many of the experimental observations might be out of the range of LEFM. The following conclusions were reached:

- In these tests, a single proofload retards crack growth significantly.
- The Wheeler retardation model underpredicts the retardation observed in test series III-a. It is likely, however, that the proofloads applied in this test series were large enough to invalidate LEFM.

4.11.3 REFERENCES FOR SECTION 4.11

1. *Broek, D., Elementary Engineering Fracture Mechanics, 4th ed, Martinus Nijhoff, Boston, 1986.*
2. *Wheeler, O.E., "Spectrum Loading and Crack Growth," Journal of Basic Engineering, Transactions of ASME, 1972, pp 181-186.*
3. *Schijve, J., "Observations on the Prediction of Fatigue Crack Growth Propagation Under Variable Amplitude Loading," in Fatigue Crack Growth Under Spectrum Loads, ASTM STP 595, ASTM, 1976.*

4.12 ELASTIC PLASTIC STRESS REDISTRIBUTION

This section describes verification and validation testing of the NASCRAC™ modeling capability for elastic-plastic stress redistribution and fatigue crack propagation through the resulting residual stress field.

4.12.1 NASCRAC™ VERIFICATION

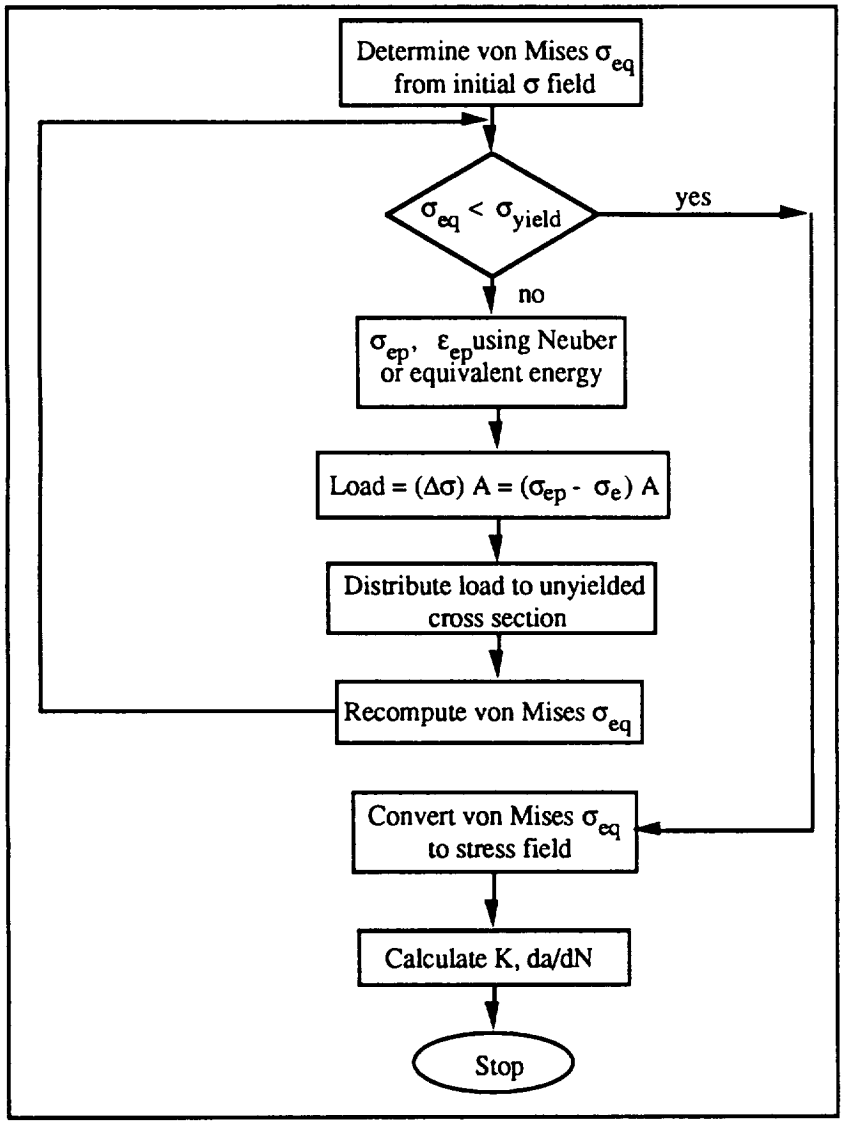

Figure 4.12.1-1. Flow Diagram of the Elastic-Plastic Stress Redistribution Algorithm In NASCRAC™

The NASCRAC™ procedure for elastic-plastic stress redistribution is summarized in Figure 4.12.1-1. Von Mises equivalent stresses are calculated from the known elastic stress field. Then, either the Neuber notch or equivalent energy method is used to find elastic-plastic stresses and strains. The difference between the elastic and the elastic-plastic stress at the most stressed point is multiplied by an area to obtain a load, which is then redistributed to the remaining unyielded cross section. The procedure is repeated until a new von Mises equivalent stress field, which does not exceed the yield stress at any point, is obtained. The equivalent stresses are then converted back to three dimensional stresses. Once the redistributed stress field is found, stress intensity factors due to combined residual stresses and cyclic fatigue loads are calculated, and the fatigue crack propagation algorithm is implemented.

4.12.1.1 Limitation of Algorithm

Stress intensity factor calculation for arbitrary stress fields is essential for modeling crack propagation through a residual stress field. **Therefore, elastic-plastic stress redistribution and crack propagation through a residual stress field in NASCRAC™ may be performed only with models for which weight functions are available.**

The Neuber notch and equivalent energy methods of elastic-plastic stress redistribution were designed for use near notches; therefore, the initial choice of geometry to test the NASCRAC™ stress redistribution capability was a plate containing a hole. The appropriate NASCRAC™ model for this geometry is 208. However, this configuration does not incorporate a weight function. Therefore, a single edge crack in a plate (203) with bending loads was chosen as an alternate geometry.

4.12.1.2 Suggested Change in NASCRAC™ Code

A coding error was found in the subroutines *NEUBER* and *NEUTWO*, which may cause a divide-by-zero during execution of NASCRAC™ This can be avoided by changing the original source code of *NEUBER* shown in Figure 4.12.1.2-2 to a proposed modification shown in Figure 4.12.1.1-3. An equivalent modification should be made to *NEUTWO*.

```
      IF (iway .ne. 1) GO TO 330
c
c  Find root of Neuber-Ramberg-Osgood set of equations
c
      dues = es - ssyi(i) + sy
      IF ((dues .gt. 0.0) .and. (zs .gt. 0.0) GO TO 71
      ps = es
      pss = 0.39*sy
      GO TO 72
 71   CONTINUE
      CALL rfind(pss,dues,sy,xn,xk)
      ps = pss - sy + syyi(i)
 72   CONTINUE
     .
     .
     .
c
c  Using a weighted average of the elastic (nu) and plastic (nuplas)
c  Poisson's ratios, we obtain
c
     nueff = (nu*eel + nuplas*epl)/(eel + epl)
      pmat(8) = nueff
      eplas = (eel+epl)/e
c
```

Figure 4.12.1.1-2. Original Source Code for Subroutine *NEUBER* with Potential Error Highlighted

```
      IF (iway .ne. 1) GO TO 330
c
c  Find root of Neuber-Ramberg-Osgood set of equations
c
      dues = es - ssyi(i) + sy
      IF ((dues .gt. 0.0) .and. (zs .gt. 0.0) GO TO 71
      ps = es
      pss = 0.39*sy
      GO TO 72
 71   CONTINUE
      CALL rfind(pss,dues,sy,xn,xk)
      ps = pss - sy + syyi(i)
 72   CONTINUE
     .
     .
     .
c
c  Using a weighted average of the elastic (nu) and plastic (nuplas)
c  Poisson's ratios, we obtain
c
c  WTR 9/29/93  SET nueff = nu IF TOTAL STRAIN = 0.0
c
      IF ((eel+epl) .eq. 0.0) THEN
        nueff = nu
      ELSE
        nueff = (nu*eel + nuplas*epl)/(eel + epl)
      END IF
       pmat(8) = nueff
       eplas = (eel+epl)/e
c
```

Figure 4.12.1.1-3. Proposed Change in Subroutine *NEUBER* to Prevent Potential Runtime Error

4.12.2 VALIDATION OF THE ELASTIC-PLASTIC STRESS REDISTRIBUTION CAPABILITY

Test series I-3-a was designed to validate NASCRAC™'s *fatigue crack propagation through a residual stress field* capability. Four tests were performed in this test series. The geometry for these tests is shown in Figure 4.12.2-1. The crack length is identified with two different variables (a_1, a_2) because the crack length was not necessarily the same on both faces of the beam during the tests. Proofloads were applied to two of the test specimens in this series before the initial notch was cut. A typical load spectrum for the tests is shown in Figure 4.12.2-2. The proofloads were designed to induce a residual stress field in the beam. The two remaining tests were used as controls. The dimensions for the four tests are summarized in Table 4.12.2-1.

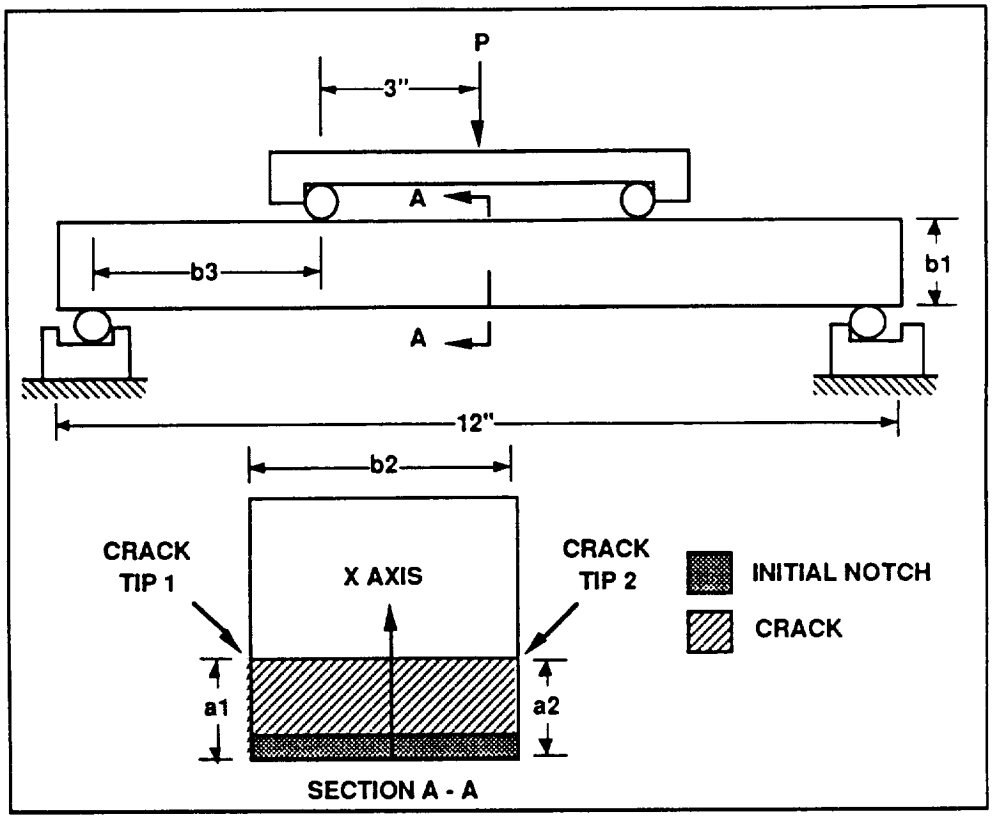

Figure 4.12.2-1. Geometry for Test Series I-3-a

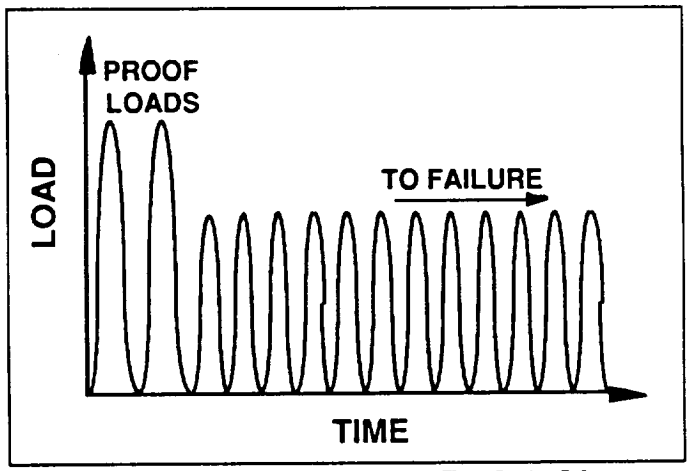

Figure 4.12.2-2. Load History for Test Series I-3-a

Table 4.12.2-1. Parameters for Test Series I-3-a

PARAMETER	I-3-a/1	I-3-a/2	I-3-a/4	I-3-a/6	UNITS
$b1$	1.990	1.991	1.994	2.000	INCHES
$b2$	0.650	0.653	0.656	0.652	INCHES
$b3$	2.397	2.409	2.360	2.407	INCHES
$a1(0)$	0.013	0.018	0.004	0.003	INCHES
$a2(0)$	0.013	0.019	0.003	0.003	INCHES
PROOF	2	0	2	0	CYCLES
LOADS	20	n.a.	21.28	n.a.	kips
Δp_{fat}	6.249	6.258	6.284	6.394	kips
R-RATIO	0.2159	0.2237	0.2109	0.2048	-

Experimentally-observed crack lengths versus cycles for tests I-3-a/1 and I-3-a/2 are shown in Figure 4.12.2-3. Test I-3-a/1 included two proof cycles, as shown in Table 4.12.2-1. No proof cycles were applied to test I-3-a/2. The results of three NASCRAC™ analyses and one NASA/FLAGRO analysis are also shown in Figure 4.12.2-3. The three NASCRAC™ analyses included one where no proof loads were applied; one where two proof cycles were applied and plane strain assumed; and one where two proof cycles were applied and plane stress assumed. Table 4.12.2-2 lists the inputs for the three analyses. The NASA/FLAGRO analysis was performed using input given in Table 4.12.2-3. Proofloads were not considered in the FLAGRO analysis. The NASCRAC™-predicted crack length at failure is shown to be significantly less than that predicted by FLAGRO or experimentally-observed. This is due to the output option used for the NASCRAC™ analyses. Crack length was printed only once every thousand cycles. Near failure, the crack is propagating quickly. Therefore, in the 1000 cycles (or less) between the last output and actual NASCRAC™-predicted failure, the predicted crack can grow significantly but the total number of fatigue cycles before failure would not change by more than 1000 cycles.

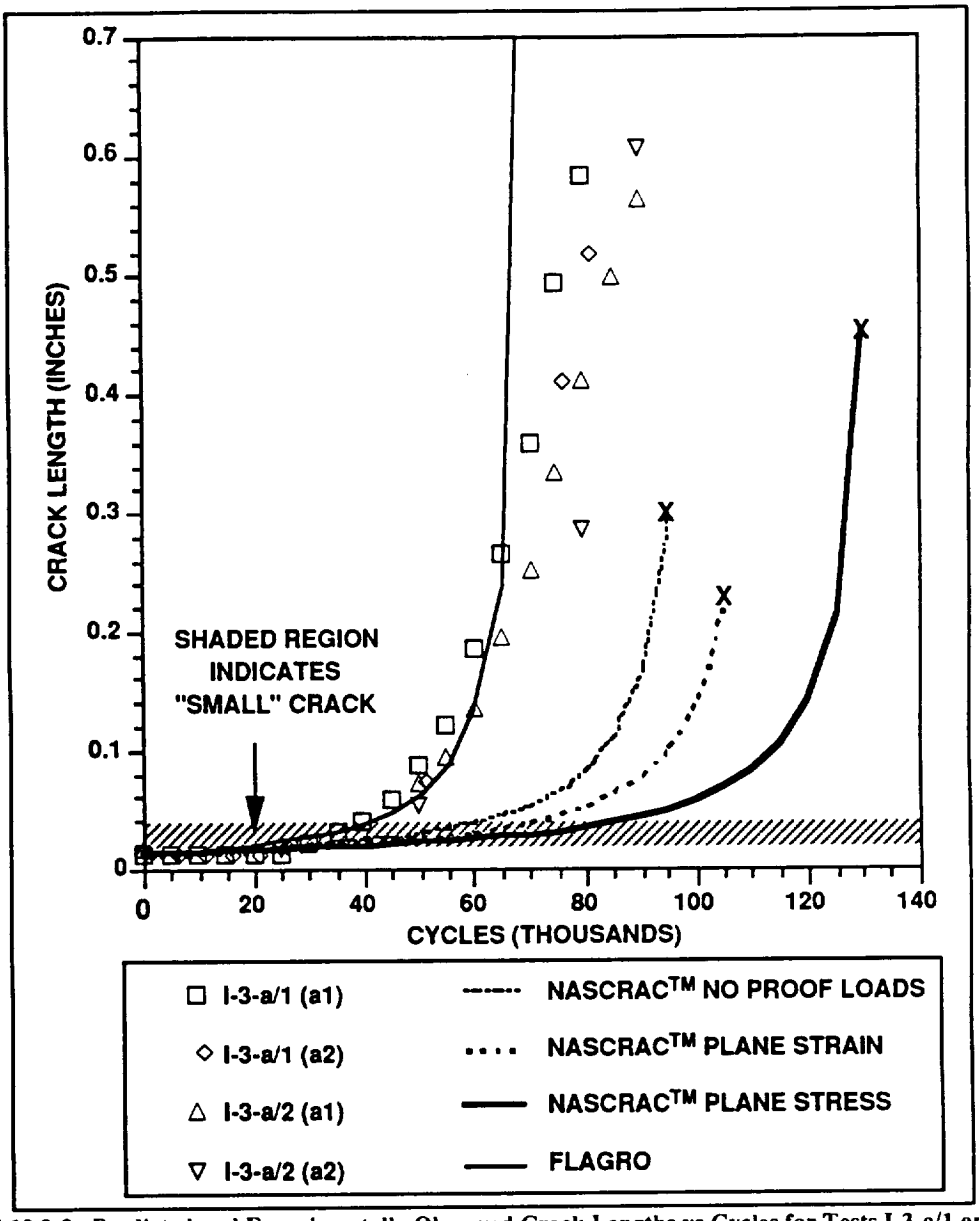

Figure 4.12.2-3. Predicted and Experimentally Observed Crack Lengths vs Cycles for Tests I-3-a/1 and I-3-a/2

Table 4.12.2-2 . NASCRAC Input for Simulation of Test I-3-a/1

	NASCRAC INPUT	VALUE	CORRESPONDING TEST DIMENSION
MODEL	203		I-3-a/1
GEOMETRY	W	1.990	*b*1
	a	0.013	(*a*1(0) + *a*2(0))/2
LOADING	PROOFLOADS max σb elast min σb elast	2 CYCLES 55.87 ksi 0 ksi	PROOFLOADS FIGURE 4.10.3.2-2 TABLE 4.12.2-1
	FATIGUE LOADS max σb elast min σb elast	REPEATED TO FAILURE 22.264 ksi 4.806 ksi	FATIGUE LOADS FIGURE 4.10.3.2-2 TABLE 4.12.2-1
MATERIAL PROPERTIES	2219-T851 Al L-T, T-L 75F	ALUM3 #104	2219-T851 AL LAB AIR
	SIGYS	53	
	YOUNGS	10000	
	POISSN	0.33	
	N	13	
	D	85.48	
ANALYSIS PARAMETERS	*IBOUND*	0	PHYSICS OF E-P STRESS REDISTRIBUTION
	PHEIGHT	0 (default)	
	REDISTRIBUTION METHOD	EQUIVALENT ENERGY	

Table 4.12.2-3. NASA/FLAGRO Input for Simulation of Test I-3-a/1

	FLAGRO INPUT	VALUE	CORRESPONDING TEST DIMENSION
MODEL	TC02		I-3-a/1
GEOMETRY	W	1.99	b1
	t	0.65	b2
	c	0.013	(*a*1(0) + *a*2(0))/2
LOADING	FATIGUE LOADS	REPEATED TO FAILURE	FATIGUE LOADS
	max σb elast	22.46 ksi	FIGURE 4.10.3.2-2
	min σb elast	4.81 ksi	TABLE 4.12.2-1
MATERIAL PROPERTIES	2219-T851 Plt & Sht L-T		2219-T851 Al LAB AIR

Figure 4.12.2-4 shows experimentally-observed and NASCRAC™-predicted crack lengths vs cycles for test I-3-a/4 . Two proofloads were applied to this test specimen. The NASCRAC™ predictions were obtained using the input given in Table 4.12.2-4. No proofloads were applied in the NASCRAC™ simulation. Test I-3-a/6 was similar to test I-3-a/4, except no proofloads were applied. Test I-3-a/6 consisted of 2,600,000 fatigue cycles. The test was stopped before fatigue crack initiation was observed. Because crack initiation had such a significant effect on the fatigue life of test I-3-a/6, it is likely that crack initiation also had a significant effect on the fatigue life of

test I-3-a/4. If crack intiation took a significant number of cycles in test I-3-a/4, the crack propagation would no longer match NASCRAC™ predicions. Given the fatigue life of test I-3-a/6, it appears that the apparently correct NASCRAC™ prediction of test I-3-a/4 is due to offsetting errors caused by ignoring crack intiation and modeling small crack growth incorrectly.

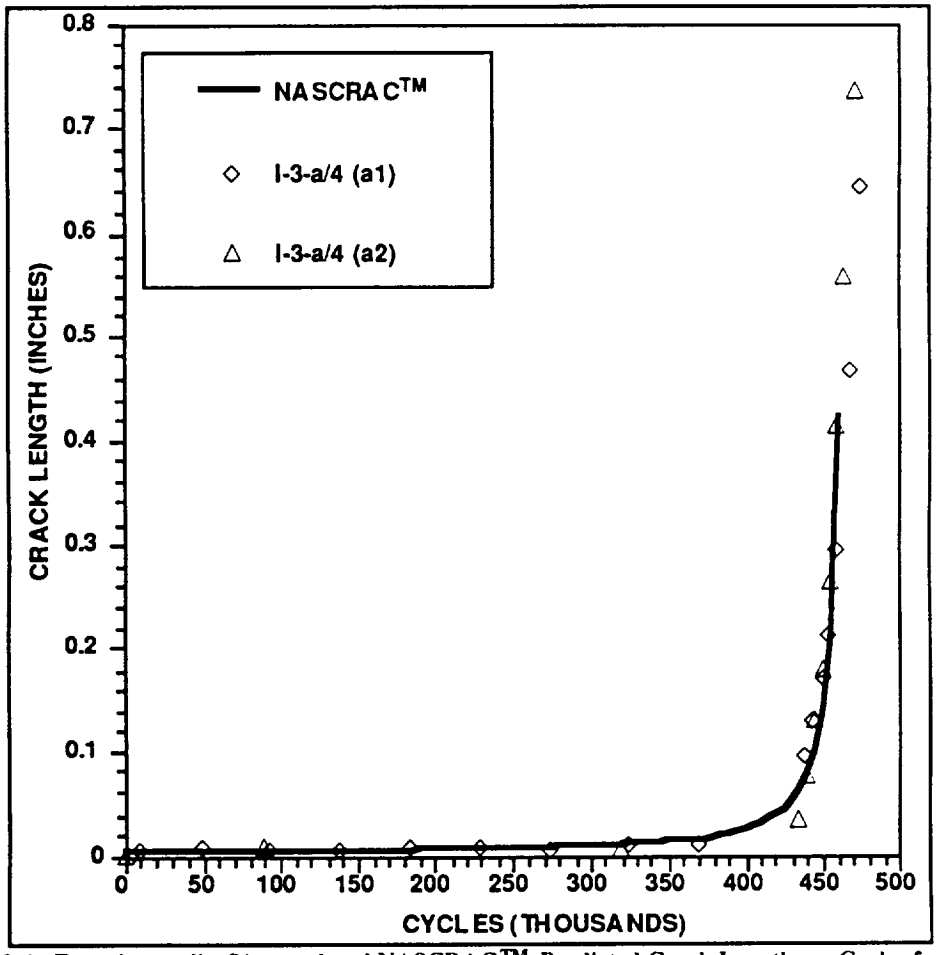

Figure 4.12.2-4. Experimentally-Observed and NASCRAC™-Predicted Crack Lengths vs Cycles for Test I-3-a/4

Table 4.12.2-4. NASCRAC™ Input for Analysis of Test I-3-a/4

	NASCRAC INPUT	VALUE	CORRESPONDING TEST DIMENSION
MODEL	203		I-3-a/4
GEOMETRY	W	1.994 INCHES	b_1
	a	0.0035 INCHES	($a1(0) + a2(0)$)/2
LOADING	FATIGUE LOADS RANGE: EQ. B R-RATIO:	REPEATED TO FAILURE 17.06, -17.11 0.2109	FATIGUE LOADS FIGURE 4.10.3.2-2 TABLE 4.12.2-1
MATERIAL PROPERTIES	2219-T851 Al L-T, T-L 75F	ALUM3 #104	2219-T851 AL LAB AIR

The test results depicted in Figures 4.12.2-3 and 4.12.2-4 highlight several issues associated with the elastic plastic stress redistribution model in NASCRAC™. These issues include:

- Plane stress and plane strain assumptions can have significant effects on predicted stress redistribution and crack growth rates.
- Crack initiation and small crack effects (both ignored by NASCRAC™) might have a significant effect on fatigue life.
- The accuracy of calculated residual stresses might effect the predicted fatigue life.

To quantify these issues sensitivity analyses were conducted. Results from these analyses are reported in the following subsections.

4.12.2.1 Sensitivity of NASCRAC Analyses to Input Parameters

Analyses were performed to determine the sensitivity of NASCRAC™-predicted life to various NASCRAC™ input parameters. The base input for the analyses discussed in this section is given in Table 4.12.2.1-1.

Table 4.12.2.1-1. Base Input for NASCRAC™ Sensitivity Analysis

	NASCRAC INPUT	VALUE
MODEL	203	
GEOMETRY	W	1.990
	a	0.012
LOADING	OVERLOADS	2 CYCLES
	max σb elast	57.66 ksi
	min σb elast	0 ksi
	FATIGUE LOADS	REPEATED TO FAILURE
	Δσb elast	17.760 ksi
	R-ratio	0.204
MATERIAL PROPERTIES	2219-T851 Al L-T, T-L 75F	ALUM3 #104
	SIGYS	50.00
	POISSN	0.33
	N	13.00
	D	85.48
ANALYSIS PARAMETERS	*IBOUND*	0
	PHEIGHT	0 (default)
	REDISTRIBUTION METHOD	EQUIVALENT ENERGY

Both plane strain and plane stress analyses were performed in this study. In test series I-3-a, and in many practical situations, the actual state of stress varies through the depth of the structure, and neither of the two-dimensional constraint conditions describe the state of stress accurately.

The first parameter studied was yield stress. NASCRAC™-predicted fatigue life is plotted as a function of yield stress in Figure 4.12.2.1-1. All other input was the same as that given in Table 4.12.2.1-1. The manufacturer's testing indicates a uniaxial 0.2% offset yield strength that ranges from 49.9 to 55 ksi. With this range of yield stress, the NASCRAC™-predicted life can vary from 78,000 to 110,000 cycles for plane strain and 120,000 to 150,000 cycles for plane stress. A uniaxial yield strength will not necessarily be a sufficient predictor of yielding for a three dimensional stress field. In the region of material where yielding occurs, a complicated, three-dimensional state of stress occurs and redistribution is governed by a multi-axial flow rule, only one parameter of which is the uniaxial yield strength. Furthermore, the actual constraint conditions will vary across the beam, and will likely approach plane stress near the free surfaces and plane strain away from the free surfaces. Considering these uncertainties, it was difficult to determine what the "correct" input should be before comparing NASCRAC™-predictions with experimental observations The variation of NASCRAC™-predicted life within the bounds of reasonable yield stress and planar constraint conditions must be considered when performing NASCRAC™ elastic-plastic stress redistribution calculations.

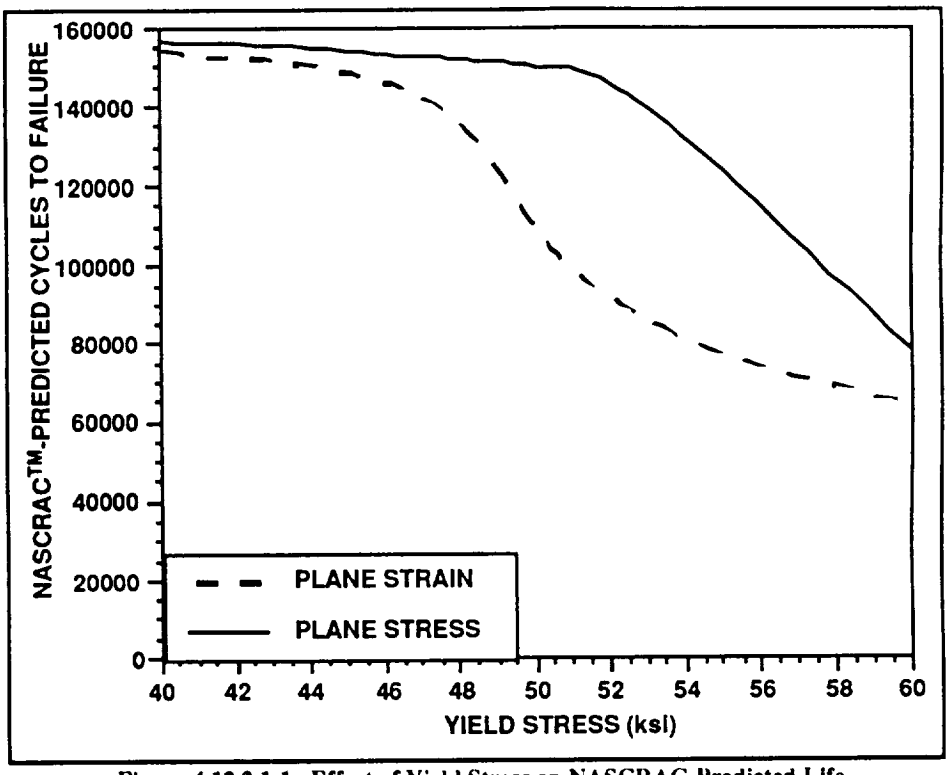

Figure 4.12.2.1-1. Effect of Yield Stress on NASCRAC-Predicted Life

The second sensitivity study forcused on the Ramberg-Osgood parameters. The Ramberg-Osgood equation models the two-dimensional stress-strain relationship of materials. The form of this equation is given in Equation 4.12.2.1-1.

$$\varepsilon = \frac{\sigma}{E} + \left(\frac{\sigma}{D}\right)^{N} \qquad \text{eq. (4.12.2.1-1)}$$

For these analyses, the parameter *D* was a dependent variable. It was adjusted according to the value of *N* to allow for 0.002 plastic strain at yield stress. The results of these analyses are shown in Figure 4.12.2.1-2. In these analyses, the Ramberg-Osgood parameters do not affect the predicted life much for plane stress analyses but do have an affect on plane strain analyses.

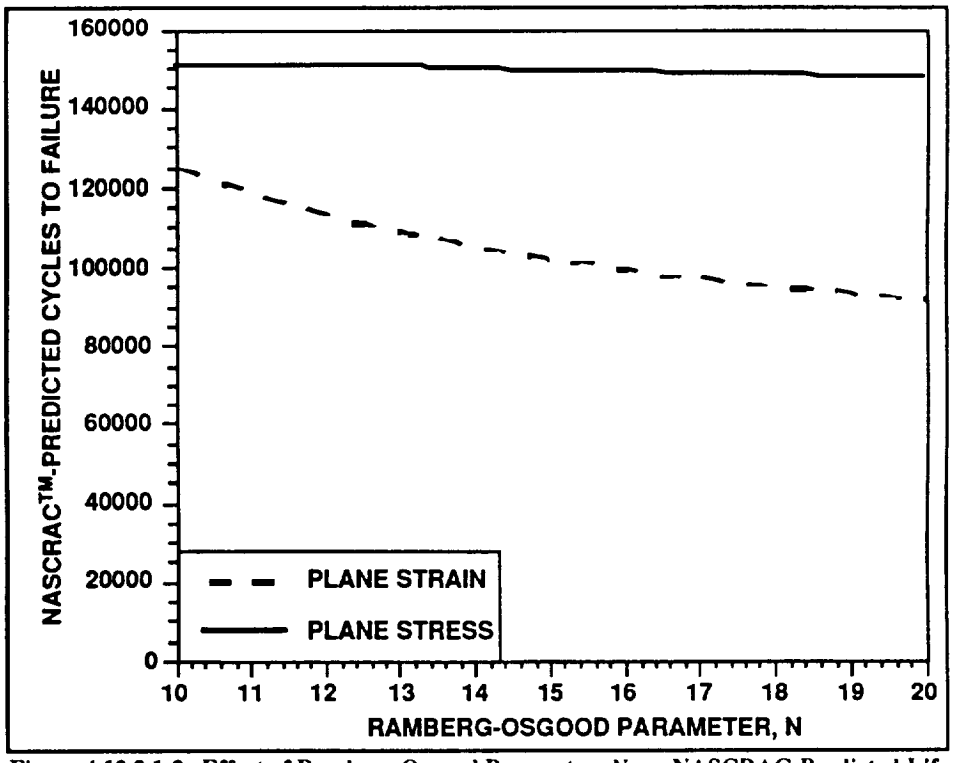

Figure 4.12.2.1-2. Effect of Ramberg-Osgood Parameter, *N*, on NASCRAC-Predicted Life

The final parameter chosen for a sensitivity study was the NASCRAC™ parameter, *PHEIGHT*. This parameter is used to determine the gradient with which stresses are re-distributed. NASCRAC™ redistributes residual stresses based on the stress gradient near the edge of a hypothetical elliptical hole in a plate with far-field uniform stresses. *PHEIGHT* determines the shape of the ellipse used to calculate this stress gradient. The steepest allowable gradient corresponds to the stress gradient near the edge of a circular hole. Therefore, increasing *PHEIGHT* beyond a certain length has no effect on predictions; a circular hole is used instead. Likewise, decreasing *PHEIGHT* below a minimum length has little effect on the predictions. As *PHEIGHT* becomes small, the hypothetical ellipse approaches a slit parallel to the direction of stress. The stress gradient at the edge of this ellipse approaches zero as the ellipse approaches a slit. The analyses in this sensitivity study in which *PHEIGHT* was greater than 0.02 inches predicted a fatigue life within 10% of the life predicted using the default setting for *PHEIGHT*. These results are displayed in Figure 4.12.2.1-3.

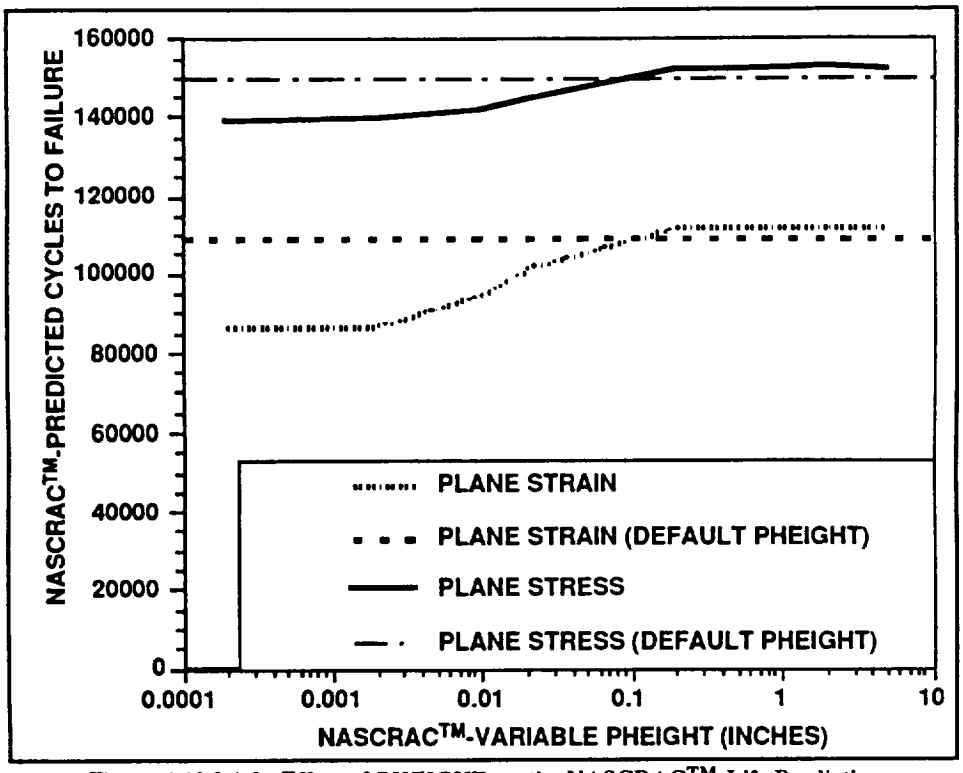

Figure 4.12.2.1-3. Effect of *PHEIGHT* on the NASCRAC™ Life Prediction

4.12.2.2 Predicted vs Observed Fatigue Crack Growth Rates for Small Cracks

The similarity of the crack lengths observed in tests I-3-a/1 and /2 indicates little to no retardation occurred due to the residual stress field in test I-3-a/1. Therefore, this section will compare crack growth rates predicted by NASCRAC™ and NASA/FLAGRO without accounting for retardation. A more thorough analysis of test I-3-a/2 is performed in Section 4.5.

The majority of the difference between crack lengths observed in test I-3-a/2, and those predicted by FLAGRO and NASCRAC™ (without proofloads) can be attributed to the difference between predicted and observed crack growth rates when the crack length is less then 0.034 long. This crack length corresponds to a crack length 0.02 inches longer than the initial notch. This region is shaded in Figure 4.12.2-3. Between 57% and 62% of the NASCRAC™-predicted fatigue life for this test occurs when the crack is less than 0.034 inches long. For tests I-3-a/1 and /2, the crack lengths are within the small crack region for approximately 40% to 50% of the fatigue life. Experimentally observed and NASCRAC predicted crack growth rates appear to coincide well for given crack lengths greater than 0.034 inches.

It has been observed [1] that small cracks can propagate much faster than larger cracks with the same stress intensity factors applied. This is known as the small crack effect. For aluminum, cracks that are less than 0.02 inches beyond an initial notch can be considered small. The small crack effect appears to have a significant effect on the total fatigue life of specimens in this test series.

Two proofloads were applied to test I-3-a/4. It was anticipated that these loads would retard fatigue crack growth. However, the experimentally observed crack lengths matched crack lengths predicted by NASCRAC™ without accounting for the proofloads. Test I-3-a/6, which had no proofloads applied, consisted of 2,600,000 fatigue load cycles. Fatigue crack propagation was not observed during this loading. Therefore, it is concluded that the fatigue life of test I-3-a/4 was dominated by crack initiation, not retardation due to a residual stress field.

4.12.2.3 Residual Stress Field Calculations

The analyses shown in Figures 4.12.2.1-1, through 4.12.2.1-3 illustrate the potential variation in NASCRAC™ predicted life. These figures should put the observations made in this section into perspective; it is possible to predict "answers" that have a large range of values. In light of the variation in predictions, the following analyses should be used to illustrate trends only.

Figure 4.12.2.3-1 shows residual stress fields calculated using NASCRAC™ with the input given in Table 4.12.2-2. Both plane strain and plane stress analyses were considered. The plane stress analysis predicts a larger region of compressive stresses than the plane strain analysis predicts. Furthermore, the magnitude of the predicted compressive residual stresses is greater for the plane stress analysis than the plane strain analysis. It is this difference in the residual stress fields that causes the differences in predicted crack growth illustrated in Figure 4.12.2-3. Strain gage measurements made during application of the proofloads in tests I-3-a/1 and I-3-a/4 indicate the presence of a residual stress field in the region where crack growth was anticipated.

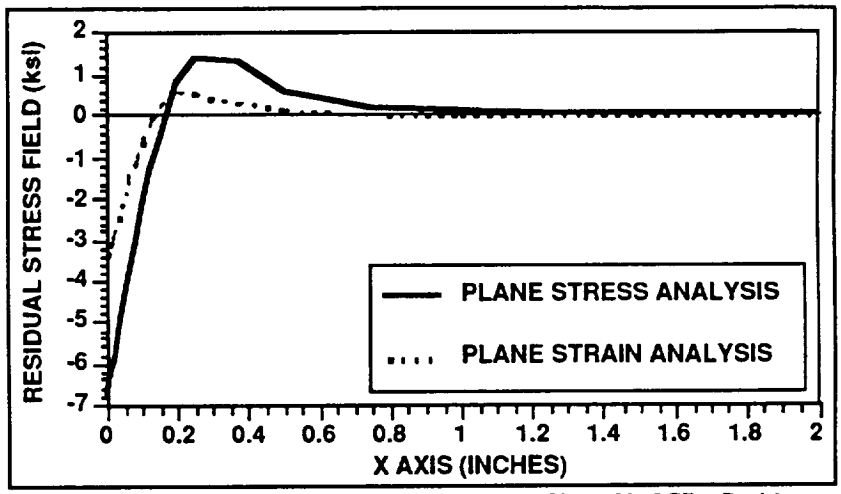

Figure 4.12.2.3-1. Residual Stress Fields Predicted Using NASCRAC with two Different Constraint Assumptions

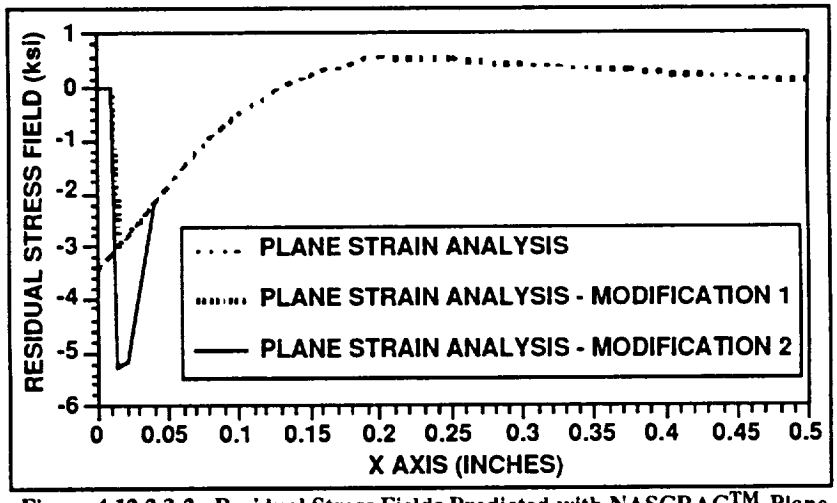

Figure 4.12.2.3-2. Residual Stress Fields Predicted with NASCRAC™ Plane Strain Analysis, with two Modifications to aAccount for Initial Notch

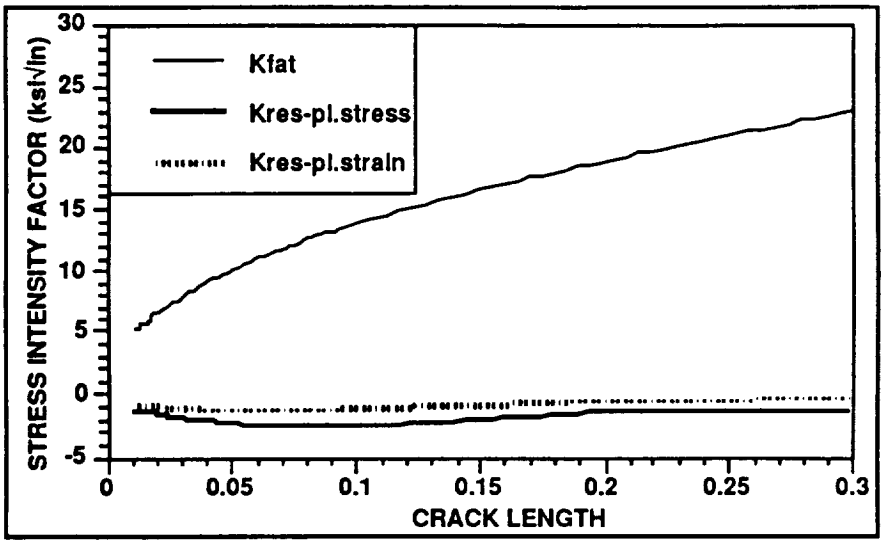

Figure 4.12.2.3-3. NASCRAC-Calculated K_{fat}, $K_{res\text{-}pl.strain}$ and $K_{res\text{-}pl.\ stress}$ vs Crack Length *a*

The notch in test I-3-a/1 was cut after the residual stress field was created. One difference between the NASCRAC™ elastic plastic analyses and the actual test is the effect of this notch. Residual stresses cannot be present where the two crack faces do not touch. Therefore, to some extent, the residual stress fields shown in Figure 4.12.2.3-1 are incorrect because the affect of cutting the notch has not been quantified.

Two modified residual stress fields were used to evaluate the effect that the initial notch might have on calculated stress intensity factors. The modified residual stress fields were based on the residual stress field obtained from a NASCRAC™ plane strain analysis of the input given in Table 4.12.2-2 representing the geometry shown in Figure 4.12.2-1. This residual stress field was chosen for investigation because crack growth predicted by the NASCRAC™ plane strain analysis matched the experimental observations better than crack growth predicted by the NASCRAC™ plane stress analysis.

The modified residual stress fields were input to NASCRAC™ using a table of X coordinates and corresponding stresses. In the first modified field, the stresses at two entries in the table, X = 0.000 inches and X = 0.010 inches, were set to zero. These entries corresponded to the region where the initial notch was cut. All the remaining entries in the table ($X \geq 0.015$ inches) matched the NASCRAC™ plane strain analysis residual stress field. In the second modified stress field, the stresses at X = 0.000 inches and X = 0.010 inches were "relieved" as in the first modified field. However, the relieved load was uniformly redistributed over the next two entries in the table, X = 0.015 and X = 0.020 inches. The remaining entries ($X \geq 0.040$ inches) matched the stress field from the NASCRAC™ plane strain analysis. The residual stresses that were released when the notch was cut had to be re-distributed in some manner to maintain equilibrium. Therefore, the second modified stress field more closely simulated the residual stress field that occurred in test I-3-a. The manner in which the relieved stresses were redistributed for this analysis was not unique. This modified stress field was chosen arbitrarily for the sake of comparison. The plane strain analysis residual stress field, and the two modified residual stress fields are shown in Figure 4.12.2.3-3.

The residual stress fields discussed above would retard fatigue crack growth by reducing the stress intensity factors encountered during fatigue loading. The stress intensity factors caused

by the residual stress fields, $K_{res\text{-}pl.stress}$ and $K_{res\text{-}pl.strain}$, and the stress intensity factors caused by the maximum fatigue load, K_{fat}, are shown in Figure 4.12.2.3-3 as functions of crack length *a*.

Stress intensity factors from the plane strain analysis, $K_{res\text{-}pl.strain}$ and from the two modified residual stress fields, $K_{res\text{-}pl.strain\text{-}mod\ 1}$ and $K_{res\text{-}pl.strain\text{-}mod\ 2}$, are shown in Figure 4.12.2.3-4. These values are shown as a percent of the stress intensity factors due to the maximum fatigue load, K_{fat}, in Figure 4.12.2.3-5. The kinking of the stress intensity factor plots is probably due to the discretization of the load tables. The modified residual stress fields have extreme stress gradients near the notch tip, making the analyses susceptible to discretization errors.

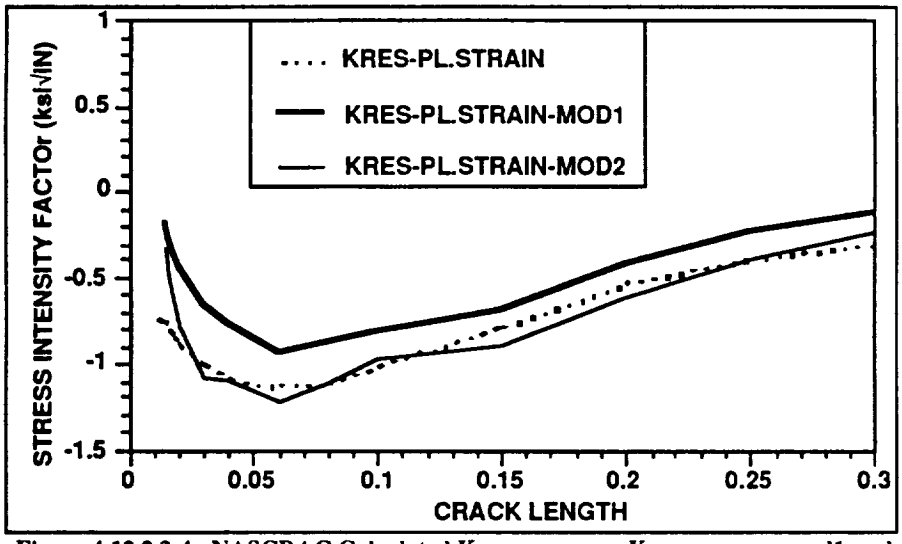

Figure 4.12.2.3-4. NASCRAC Calculated $K_{res\text{-}pl.strain}$, $K_{res\text{-}pl.strain\text{-}mod1}$ and $K_{res\text{-}pl.strain\text{-}mod\ 2}$ vs Crack Length *a*

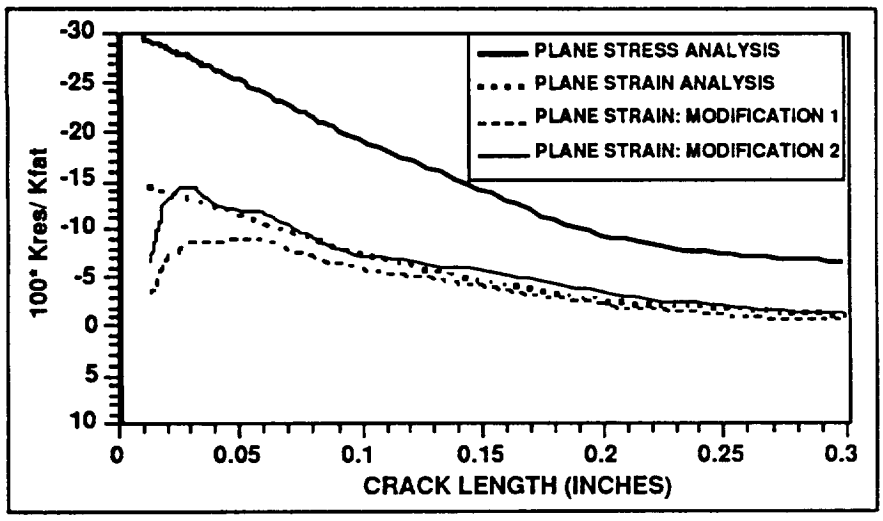

Figure 4.12.2.3-5. K_{res} vs crack length *a* as % of K_{fat}

All the residual stress fields analyzed had both regions of tension and regions of compression. The predicted stress intensity fields became less negative when the crack tip reached the region of tensile residual stresses. The first modified residual stress field had less compressive load than both the second modified field or the plane strain analysis residual stress field. Therefore, the stress intensity factors calculated with the first modified stress field remain less negative than the stress intensity factors calculated with the other two residual stress fields. The stress intensity factors for cracks close to the initial notch size calculated for the second modified residual stress field were less negative than the stress intensity factors calculated for the original plane strain analysis stress field. As the crack grews beyond the region of the initial notch, the two sets of stress intensity factor calculations converged.

An analysis of the second modified residual stress field predicted that the redistribution of the residual stresses when the notch was cut affected crack growth rate in the first 0.01 inches of true fatigue crack propagation. This number is dependent on the way in which the residual stresses were actually redistributed. The effect of the notch might be significant for crack lengths greater than that predicted using the second modified-residual stress field. All of the residual stress fields analyzed small cracks more than large cracks.

4.12.3 CONCLUSIONS

The following conclusions may be drawn regarding the NASCRAC™ crack propagation through a residual stress field and elastic plastic stress redistribution algorithms:

- NASCRAC™-predicted fatigue life is sensitive to the input parameters used. It was observed that a 10% change in the yield stress could double the NASCRAC™-predicted life.

- NASCRAC™-predicted fatigue crack growth retardation for this test series is most significant for small cracks. This is contrary to the experimental results, where no retardation was observed.

- In this test series, the most significant factors affecting the crack growth rates for small cracks were crack initiation and/or the "small crack effect."

Cutting an initial notch prior to the overloads might allow cracks to initiate and to propagate through a residual stress field but have a smaller portion of the fatigue life spent in the small crack region. However, the residual stress field would still have the most significant effect on crack growth rates when the crack was small, and there still would be problems predicting crack growth for small cracks. Furthermore, there are limits to how much of the ligament may yield and still have the elastic-plastic stress redistribution algorithm be applicable. The test specimens in this test were chosen to represent reasonable structural members, but larger test specimens would allow for a larger region of residual stresses, and possibly more noticeable crack growth retardation.

4.12.4 REFERENCES FOR SECTION 4.12

1. Newman, J.C. Jr., Swain, M. H., "An Assesment of the Small-Crack Effect for 2024-T3 Aluminum Alloy", Small Fatigue Cracks, Ritchie, R.O., and Lankford, J., ed.

2. Newman, J.C. Jr., Swain, M.H., Phillips, E.P. "An Assessment of the Small-Crack Effect for 2024-T3 Aluminum Alloy", Small Fatigue Cracks. Proceedings of the Second Engineering Foundation International Conference/Workshop, Santa Barbara, CA. Jan 5-10, 1986 Ritchie, R.O., Lankford, J., ed.

5.0 CONCLUSIONS AND RECOMMENDATIONS

Evaluation of NASCRAC™ version 2.0 for verification and validity has been completed. Several limitations and minor errors were detected and documented in Section 4.0 of this report. Additionally, a few major flaws were observed and are reiterated and discussed in this section. These major flaws are generally due to application of a specific method or theory, not due to programming logic.

The *K vs a, J vs a* and *crack opening area* capabilities in NASCRAC™ were generally found to be valid. Variable thickness *K vs a* solutions were in good agreement with the references when consistent input quantities were included. The *J vs a* and *crack opening area* capabilities in NASCRAC™ were very limited in scope; only eight *J vs a* configurations and five *crack opening area* configurations were available. NASCRAC should not be promoted for these capabilities because of this limited scope.

The K solution for configuration 404, edge crack in a solid circular bar, should be reformulated in future releases of NASCRAC™. The current solution assumes a geometry that is easily described with two variables. This geometry is reasonable for static *K vs a* analyses where *a* is less than the radius of the cylinder; however, during fatigue crack growth, this model would grow the crack in a non-conservative manner.

The use of RMS averaging to calculate K values for three dimensional surface cracks such as configurations 601, 602, 702 and 704 is suspect when high stress gradients are present. NASA/MSFC should develop a consensus on this approach to calculating K's before employing NASCRAC™ computed K's for these configurations when bending or significant stress concentration is present.

The results for configurations 601 and 602 suggest the development of improved solutions which more accurately model these configurations. A parametric finite element analysis is the most viable approach to develop these improved solutions. The analysis should include hole diameter, plate width, plate thickness, and pin load distribution as parameters.

Weight functions for 702, 704, and 705 were derived from the 703 weight function and adjusted for geometry. Application of this function to the 702 and 704 geometry is questionable due to curvature effects, especially at crack tip a_2, which is curved in the case of 703 and 705 but straight in the case of 702 and 704. To increase confidence, NASA should develop independent weight function solutions for 702 and 704 for incorporation into NASCRAC™. It may be possible to derive such independent solutions from the work of Newman and Raju.

The *fatigue crack growth* capability in NASCRAC™ is valid for the Paris equation in situations where the Paris equation is applicable and material parameters are valid. The Walker

and Collipriest equations in NASCRAC™ were verified but not validated because only a limited number of references were found and because these equations are not commonly used. The modified Forman and Hopkins-Rau equations in NASCRAC were found to be invalid due to coding errors. The coded algorithms for both equations diverged from the source algorithms. The differences were not simple typographical errors. In some instances (e.g., R = 0.0), the error in the modified Forman equation did not significantly effect predicted crack growth rates.

An attempt was made to validate the NASCRAC™ *proof test logic* with comparisons of predictions to experimental observations for three dimensional configurations. Observed failure loads were much higher than predicted by NASCRAC™ for the plane strain fracture toughness given in the NASCRAC™ material properties library. This discrepancy resulted in NASCRAC™ underpredicting the largest crack that could survive a given proofload. In the remaining fatigue life calculation, NASCRAC™ neglects retardation following the proofload, which was a significant factor in the test results. Due to these two discrepancies, the guaranteed life predicted by NASCRAC™ did not correlate with test results.

The *tearing instability* capability in NASCRAC™ was evaluated versus results from closed form and graphical solutions. Although the results were in good agreement, the algorithm implemented in NASCRAC™ did not agree with the algorithm described in the NASCRAC™ Theory Manual. In addition, the three-dimensional capability has little applicability to physical problems because criteria for stable tearing cannot be achieved in the available NASCRAC three-dimensional configurations.

The C* *creep crack growth* algorithm implemented in NASCRAC™ is only applicable to a limited number of materials. In particular, the C* model is not valid for predicting creep crack growth rates in aluminum and is not a recommended model in designing aluminum structural members. C* is applicable to type 304 stainless steel; however, the range of crack growth rates reported in the literature is broad. The experimentally-observed and NASCRAC™-predicted creep crack growth rates for 304 stainless steel fell within this reported range; however, because this range was broad, the evaluation of NASCRAC™ creep crack growth validity was inconclusive.

The *crack transitioning* capability in NASCRAC™ predicted conservative results due to the simplistic algorithm implemented. The NASCRAC™ algorithm employs a transition factor f_t to describe the transition from one configuration (e.g., a surface crack) to another configuration (e.g., a corner crack). This implementation missed the cycles required to effect this transition in laboratory tests. In the tests, transition from a surface crack to a corner crack occurred over a finite number of cycles, not a single cycle with a correction factor for area.

Results from the Wheeler and Willenborg *retardation models* in NASCRAC™ were compared to offline algorithms and experimental observations. These comparisons verified of implementation of these models. In general, the NASCRAC™ models predicted the trends of crack growth retardation. However, these models are very simplistic and do a poor job of capturing the physics of crack retardation. In a number of instances, the predicted crack growth

rates were non-conservative compared to tests; therefore, the models can only be considered marginally valid

The NASCRAC™ *elastic-plastic stress redistribution* results were very sensitive to material properties and constraint conditions. This sensitivity renders this capability impractical for engineering calculations since small perturbations in inputs result in large variations in predicted crack growth rates.

In conclusion, several minor errors and a few major flaws were observed during in NASCRAC™ version 2.0. These flaws result in the following general conclusion: *NASCRAC™ is an acceptable fracture tool for K solutions of simplified geometries, an acceptable but limited tool for J solutions and crack opening areas, and an acceptable tool for fatigue crack propagation with the Paris equation and constant amplitude loads when the Paris equation is applicable.*

APPENDIX A
Recommended Limits on K, J, and Crack Opening Area Solutions

This appendix provides the recommended limits on the input variables for the NASCRAC K, J, and crack opening area solutions. The limits were derived from the NASCRAC documentation, the literature, and analytical results.

K SOLUTIONS

Configuration 101
- $2 \leq W/B \leq 4$ where W = plate width and B = plate thickness.
- $0.2 \leq a/W < 1.0$

Configuration 102
- $2 \leq W/B \leq 4$ where W = disk width and B = disk thickness.
- $0.2 \leq a/W < 1.0$

Configuration 103
- $2 \leq W/B \leq 4$ where W = arc width and B = arc thickness.
- $0.3 \leq a/W < 1.0$

Configuration 104
- $2 \leq W/B \leq 4$ where W = beam depth and B = beam thickness.
- $L = 2W$ where 2L = span length.

Configuration 201
- Variable thickness option requires load/unit width inputs.

Configuration 202
- Variable thickness option requires load/unit width inputs.
- Loads assumed to be symmetric about panel centerline.

Configuration 203
- Variable thickness option requires stress inputs.

Configuration 204
- Variable thickness option requires load/unit width inputs.
- Loads assumed to be symmetric about plate centerline.

Configuration 205

- $a/W < 0.99$
- Variable thickness option requires stress inputs. Option has littlepractical use.
- $r/W \leq 20$ for uniform tension solution.
- Weight function coded only for $r/W = 1, 5, 10$ where r = inner cylinder radius and W = cylinder wall thickness. NASCRAC™ will accept other ratios but always reverts to a coded ratio.

Configuration 206

- Variable thickness option requires stress inputs.

Configuration 207

- Variable thickness option requires stress inputs. Option has little practical use.
- $r/W = 1$ where r = inner cylinder radius and W = cylinder wall thickness. NASCRAC™ will accept other ratios but always reverts to the coded ratio.

Configuration 208

- $H/W \geq 2$. Marginally acceptable for $1 \leq H/W < 2$ where H is plate height and W = plate width.

Configuration 209

- None known.

Configuration 301

- Thin shell theory, i.e., $R/t \geq 10$ where R = sphere radius and t = wall thickness.
- $\lambda \leq 3$ where $\lambda = a/\sqrt{tR}$

Configuration 302

- Thin shell theory, i.e., $R/t \geq 10$ where R = cylinder radius and t = wall thickness.
- $0 < \lambda \leq 10$ where $\lambda = a/\sqrt{tR}$

Configuration 303

- Thin shell theory, i.e., $R/t \geq 10$ where R = cylinder radius and t = wall thickness.

Configuration 401

- $0.1 \leq r/(r+t) \leq 0.9$ where r = inner cylinder radius and t = wall thickness.
- $0.11 \leq r/t \leq 20$ for uniform tension solution.
- Weight function coded for $r/t = 5, 10$. For $r/t \leq 7.5$ NASCRAC™ reverts to $r/t = 5$ and for $r/t > 7.5$ NASCRAC™ reverts to $r/t = 10$.

Configuration 402

- None known.

Configuration 403

- $0.1 \leq r/(r+t) \leq 0.9$ where r = inner cylinder radius and t = wall thickness.

Configuration 404

- $a/R \leq 0.5$

Configuration 502

- None known.

Configuration 601

- Solution is non-conservative due to RMS averaging. Users should understand the consequences of RMS averaging.

Configuration 602

- Solution is non-conservative due to RMS averaging. Users should understand the consequences of RMS averaging.

Configuration 605

- None known.

Configuration 702

- $1 \leq (a_2+a_3)/2a_1 \leq 20$
- Solution is non-conservative for high stress gradients (e.g., bending loads) due to RMS averaging. Users should understand the consequences of RMS averaging.

Configuration 703

- $1 \leq (a_2+a_3)/2a_1 \leq 20$

Configuration 704

- $1 \leq (a_2+a_3)/2a_1 \leq 20$
- Solution is non-conservative for high stress gradients (e.g., bending loads) due to RMS averaging. Users should understand the consequences of RMS averaging.

Configuration 705

- $1 \leq (a_2+a_3)/2a_1 \leq 20$

J SOLUTIONS

Configuration 101

- $0.25 \leq a/W \leq 1.0$
- $1 \leq n \leq 20$

Configuration 104

- $0.125 \leq a/W \leq 0.875$
- $1 \leq n \leq 20$

Configuration 202

- $0.0 \leq a/W \leq 0.875$
- $1 \leq n \leq 20$

Configuration 203

- $0.0 \leq a/W \leq 0.875$
- $1 \leq n \leq 20$
- Avoid plane strain analyses for elastic-plastic and plastic conditions.

Configuration 204

- $0.125 \leq a/W \leq 0.875$ for plane stress.
- $0.125 \leq a/W \leq 0.75$ for plane strain.
- $1 \leq n \leq 20$

Configuration 205

- $0.125 \leq a/W \leq 0.75$
- $1 \leq n \leq 10$

Configuration 303

- Invalid due to two coding errors. If coding errors are corrected, solution limits become $0.25 \leq a/W \leq 1.0$ and $1 \leq n \leq 20$

Configuration 401

- $0.25 \leq a/W \leq 1.0$
- $1 \leq n \leq 20$

CRACK OPENING AREA SOLUTIONS

Configuration 201

- Valid for plane strain.
- Underestimates plane stress COA by $(1-\nu^2)$ where ν is Poisson's ratio.

Configuration 202

- Valid for plane strain.
- Underestimates plane stress COA by $(1-\nu^2)$ where ν is Poisson's ratio.

Configuration 301

- $0 < \lambda \leq 3$ where $\lambda = a/\sqrt{tR}$

Configuration 302

- $0 < \lambda \leq 5$ where $\lambda = a/\sqrt{tR}$

Configuration 303

- $0 < \lambda \leq 1$ where $\lambda = a/\sqrt{tR}$
- Coding error invalidates solution for $1 < \lambda \leq 5$

INDEX

Synthesized Results

Advanced Capabilities

Experiments

NASA
National Aeronautics and Space Administration

Report Documentation Page

1. Report No.	2. Government Accession No.	3. Recipient's Catalog No.

4. Title and Subtitle

Final Report
NASA Contract NAS8-38103

5. Report Date
14 September 1994

6. Performing Organization Code

7. Author(s)

J. A. Favenesi
T. G. Clemmons
W. T. Riddell
A. R. Ingraffea
P. A. Wawrzynek

8. Performing Organization Report No.

10. Work Unit No.

9. Performing Organization Name and Address

Nichols Research Corporation
4040 So. Memorial Pkwy.
Huntsville, AL 35802

11. Contract or Grant No.
NAS8-38103

13. Type of Report and Period Covered
Final, 1 Sept 91 - 12 Sept 94

12. Sponsoring Agency Name and Address

George C. Marshall Space Flight Center
National Aeronautics and Space Administration
Marshall Space Flight Center, Huntsville, AL

14. Sponsoring Agency Code

15. Supplementary Notes

16. Abstract

Final report documenting results of the evaluation of NASCRAC™ for verification and validity.

17. Key Words (Suggested by Author(s))	18. Distribution Statement
NASCRAC™, verification, validation, fracture, fracture mechanics software, fracture testing	

19. Security Classification (of this report)	20. Security Classification (of this page)	21. No. of pages	22. Price
Unclassified	Unclassified	270	

NASA FORM 1626 OCT 86